Towards visualizing translation by single-molecule imaging of nascent peptides within hyphae of *Ustilago maydis*

Inaugural-Dissertation

Zur Erlangung des Doktorgrades
der Mathematisch-Naturwissenschaftlichen Fakultät
der Heinrich-Heine-Universität Düsseldorf

vorgelegt von

Kira Müntjes
aus Bremerhaven

Düsseldorf, Juni 2020

aus dem Institut für Mikrobiologie
der Heinrich-Heine-Universität Düsseldorf

Gedruckt mit der Genehmigung der
Mathematisch-Naturwissenschaftlichen Fakultät der
Heinrich-Heine-Universität Düsseldorf

Berichterstatter:

1. Prof. Dr. Michael Feldbrügge

2. Prof. Dr. Lutz Schmitt

Tag der mündlichen Prüfung: 07.08.2020

Eidesstattliche Erklärung

Ich versichere an Eides Statt, dass die Dissertation von mir aus selbstständig und ohne unzulässige fremde Hilfe unter der Beachtung der „Grundsätze zur Sicherung guter wissenschaftlicher Praxis an der Heinrich-Heine-Universität Düsseldorf“ erstellt worden ist. Die Dissertation wurde in ihrer jetzigen oder ähnlichen Form noch bei keiner anderen Hochschule eingereicht. Ich habe zuvor keine erfolglosen Promotionsversuche unternommen.

Ort, Datum	Kira Müntjes

Die Untersuchungen zur vorliegenden Arbeit wurden von November 2015 bis Juli 2020 in Düsseldorf an der Heinrich-Heine-Universität am Institut für Mikrobiologie unter der Betreuung von Herrn Prof. Dr. Michael Feldbrügge durchgeführt.

Teile dieser Arbeit wurden veröffentlicht in:

Kira Müntjes, Magnus Philipp, Lisa Hüsemann, Nicole Heucken, Stefanie Weidtkamp-Peters, Kerstin Schipper, Matias D. Zurbriggen, Michael Feldbrügge (2020), Frontiers in Microbiology (Volume 11; DOI: 10.3389/fmicb.2020.01384)

Establishing polycistronic expression in the model microorganism *Ustilago maydis*

Summary

Polar growth of cells depends on the spatiotemporal regulation of expression. Active transport of mRNAs along the cytoskeleton ensures a defined localization of encoded proteins and is an important regulatory mechanism for asymmetric cell division and cell migration. The polar growth of the phytopathogenic basidiomycete *Ustilago maydis* is based on the long-distance transport of mRNAs along the microtubule cytoskeleton. For transport, the key RNA-binding protein Rrm4 is crucial which is part of messenger ribonucleic particle complexes. Here, different mRNAs, for example septin mRNAs, are hitchhiking on endosomes and transported by molecular motors. Because of an accumulation of translational products of transported mRNAs on endosomes and the mRNA binding of Rrm4 not only in the 3´UTR but also at landmark sites of translation, the hypothesis of translationally active transport units was postulated. To verify this hypothesis, this project was focused on the establishment of an antibody-based method to visualize nascent peptides for the analyzation of translational processes on endosomes as well as the role of Rrm4 in translation. The method can sense translation by encoding a tag sequence within a reporter mRNA that, once translation started, is recognized by an antibody fused to superfolder Gfp. Another RNA-tag within the reporter allows simultaneous mRNA detection. For the visualization of local translation in hyphae of *U. maydis*, a red fluorescence protein for labeling of mRNAs, an antibody, a degron sequence and a so-called 2A peptide should be established. For the labeling of mRNAs within their 3´UTR, the red fluorescence protein mKate2 was successfully investigated. In addition, it was discovered that the analyzed antibodies GCN4-scFv, BC2-Nb and Moontag-Nb shuttled bidirectionally with Rab5a-positive endosomes in a microtubule-dependent manner through hyphae. Deletion of the potential interacting protein UMAG_00933, which was detected by LC-MS/MS analysis, abolished unspecific shuttling of GCN4-scFv and BC2-Nb. Furthermore, GCN4-scFv interacted with its cognate peptide epitope *in vivo*. Therefore, this antibody can potentially be used to label a nascent peptide chain. It has been confirmed that for full functionality, a degron sequence from mouse ornithine-decarboxylase has to be located at the C-terminus of a protein. To maintain the equilibrium of proteins encoded by analyzed mRNAs, the 2A peptide P2A was successfully established to separate two open reading frames with separation efficiencies of nearly 100%. This enables a degradation of the expressed peptide epitope to which GCN4-scFv binds to without degrading synthesized proteins encoded by analyzed mRNAs.

Zusammenfassung

Das polare Wachstum von Zellen hängt von der räumlichen und zeitlichen Regulation der Expression ab. Der aktive Transport von mRNAs entlang des Zytoskeletts, gewährleistet eine definierte Lokalisierung kodierter Proteine. Das polare Wachstum des phytopathogenen Basidomyceten *Ustilago maydis* basiert auf dem Mikrotubuli-abhängigen Langstreckentransport von mRNAs. Für dieses ist das Schlüssel-RNA-bindende Protein Rrm4 entscheidend, welches Teil von *messenger* Ribonukleoproteinkomplexen ist. Hier werden verschiedene mRNAs mit Rab5a-positiven Endosomen und molekularen Motorproteinen transportiert. Aufgrund einer Lokalisation von Translationsprodukten der transportierten mRNAs auf Endosomen und der mRNA-Bindung von Rrm4, welche nicht nur in der 3'UTR, sondern auch an Start- und Stopp-Codons der Transkripte erfolgt, wird vermutet, dass translational aktive Einheiten transportiert werden. Dieses Projekt konzentrierte sich auf die Etablierung einer Methode zur Visualisierung der Translation, um translationale Prozesse auf Endosomen sowie die Rolle von Rrm4 bei der Translation zu analysieren. Die Expression eines Peptid-Epitops innerhalb einer Reporter-mRNA ermöglicht die Visualisierung der naszierenden Peptidkette durch die Bindung eines Fluoreszenz-markierten Antikörpers an dieses Peptid-Epitop. Ein weiterer Reporter innerhalb der 3´UTR der Reporter-mRNA ermöglicht eine simultane mRNA-Detektion. Für die Visualisierung der lokalen Translation in Hyphen von *U. maydis* sollten ein rotes Fluoreszenzprotein zur Markierung der mRNAs, ein Antikörper, eine Degron-Sequenz und ein sogenanntes 2A-Peptid etabliert werden. Für die Markierung der mRNAs innerhalb ihrer 3'UTR wurde das rot fluoreszierende Protein mKate2 etabliert. Darüber hinaus wurde festgestellt, dass sich die analysierten Antikörper GCN4-scFv, BC2-Nb und Moontag-Nb bidirektional in Abhängigkeit von Rab5a-positiven Endosomen und des Mikrotubuli-Zytoskeletts durch Hyphen bewegen. Die Deletion des potentiell interagierenden Proteins UMAG_00933, welches durch eine LC-MS/MS-Analyse gefunden wurde, hob diese Lokalisation auf. Darüber hinaus konnte gezeigt werden, dass GCN4-scFv *in vivo* mit dem zugehörigen Peptid-Epitop interagierte. Daher kann dieser Antikörper potenziell zur Markierung einer naszierenden Peptidkette verwendet werden. Es konnte nachgewiesen werden, dass eine Degron-Sequenz der Ornithindecarboxylase aus der Maus für die volle Funktionalität am C-Terminus eines Proteins lokalisiert sein muss. P2A wurde mit einer Separationseffizienz von nahezu 100 % etabliert, um eine Degradation des translatierten Peptid-Epitops ohne den vollständigen Abbau der Reporter-mRNA zu ermöglichen.

List of Abbreviations

µl	Microliter	mODC	Mouse ornithine decarboxylase
°C	Degree centigrade	mRNA	Messenger RNA
a-	Anti-	mRNPs	Messenger ribonucleotide particle
aa	Amino acid	MS	Mass spectrometry
add.	Fill up to end volume	MS2	Bacteriophage MS2
AHA	Azidohomoalanine	MT	Microtubules
AID	Auxin inducable degron	N-	Amino-
Amp	Ampicillin	NAA	Aaphthaleneacetic acid
APS	Ammonium persulfate	Nat	Nourseothricin
Ara	Arabinose	Nb	Nanobody
BirA	Biotin ligase	NEB	New England Biolabs
boxB	RNA stem-loops recognized by ln protein	ng	Nanogram
bp	Base pairs	NLS	Nuclear localization signal
C-terminal	Carboxy-terminal	NM	Nitrate medium
CBB	Coomassie Brilliant Blue	nm	Nanometer
Cbx	Carboxin	nt	Nucleotides
CHX	Cyclohexamide	N-terminal	Amino terminal
CM	Complete medium	OD	Optical density
ddH2O	De-mineralized water	ORF	Open reading frame
DF	Downstream flank	ORFoi	Open reading frame of interest
DIC	Differential interference contrast	PAM2	PABC interacting motif
DIG	Digoxigenin	PCR	Polymerase chain reaction
DNA	Desoxyribonucleic acid	P_{crg}	Crg promoter
EDTA	Ethylenediaminetetraacetic acid	PEST	Degron sequence
ESCRT	Endosomal sorting complex required for transport	Phleo	Phleomycin
et al.	And others	P_{otef}	Otef promoter
FUNCAT	Fluorescent noncanonical amino acid tagging	PP7	Bacteriophage PP7
$GCN4^{24}$	24 repeats of binding site of GCN4-scFv	P_{tef}	Tef promoter
gDNA	Genomic DNA	RBP	RNA-binding protein
Gfp	Green fluorescence protein	Rfp	Red fluorescence protein
Glc	Glucose	RNA	Ribonucleic acid
GTP	Guanosine triphosphate	RNA-FISH	RNA fluorescence in situ hybridization
h	Hours	RNA-seq	RNA sequencing
h.p.i	Hours post induction	rpm	Rounds per minute
HA	Hemagglutinin	RRM	RNA recognition motif
HCR	Hybridization chain reactions	RT	Room temperature
HF	High Fidelity	scFv	Single chain variable fragment
Hyg	Hygromycin	s	Second
iCLIP	Individual-nucleotide resolution UV crosslinking and immunoprecipitation	sfGfp	Fast folding variant of Gfp
Ig	Immunoglobulin	sm-FISH	Single-molecule RNA fluorescence in situ hybridization
in situ	Examination of a phenomenon exactly in the place where it occurs	TE	Tris-EDTA
in vitro	Independent of a living organism	TEMED	Tetramethylethylenediamin
in vivo	In a living organism	T_{nos}	Terminator of the nopaline synthase gene of *Agrobacterium tumefaciens*
ip^{s}	Iron-sulfur subunit of the succinate dehydrogenase	TRICK	Translating RNA Imaging by Coat Protein Kick off
IRES	Internal ribosome entry site	Ub	Ubiquitin
kb	Kilobase	UF	Upstream flank
kDa	Kilodalton	UPS	Ubiquitin-proteasome system
L	Liter	UTR	Untranslated region
M	mol/L	UV	Ultraviolet

Table of contents

1 Introduction

1.1 mRNA transport and local translation

The expression of genes can be divided into two processes, beginning with the transcription and biogenesis of an mRNA, followed by the translation of this mRNA into a protein by ribosomes. One of the most intriguing questions is to understand how cells sort mRNAs for localization, storage and/or translation. mRNAs are always associated with several proteins, interacting directly and indirectly to form messenger ribonucleic particles (mRNPs) that play a crucial role in mRNA stability, degradation and regulatory processes (Dreyfuss et al., 2002; Langdon and Gladfelter, 2018). The composition of mRNPs differs at specific phases of the mRNA lifetime from synthesis, over maturation until translation and contributes to the organization of these steps (Neriec and Percipalle, 2018). Importantly, a minor number of mRNAs incorporated into mRNPs are directly translated after nuclear export (Neriec and Percipalle, 2018). A large subset of mRNAs localizes to specific subcellular sites where they are stored inactively, or are translated on site (Neriec and Percipalle, 2018). Thus, specific mRNA localization patterns occur within cells. The phenomenon of patterned mRNA localization is evolutionary conserved from *Escherichia coli* to human cells (Valencia-Burton et al., 2007; Weatheritt et al., 2014). Already in bacteria, the spatial localization of mRNAs affects gene expression and post-transcriptional regulation (Fei and Sharma, 2018). In the developmental stages of *Drosophila melanogaster*, up to 70% of expressed mRNAs are located in distinct spatial patterns (Lecuyer et al., 2007). The asymmetric distribution of mRNAs is thought to be more energy-efficient than transporting translational products because fewer mRNA molecules need to be mobilized for a local enrichment of proteins at a defined subcellular site (Weatheritt et al., 2014). Furthermore, the asymmetric distribution of mRNAs allows cells to build up local proteomes (Holt et al., 2019). This holds especially true for highly polarized cells, such as neurons or long hyphae of filamentous fungi (Langdon and Gladfelter, 2018). In hippocampal pyramidal neurons, 2,500 mRNAs were found to be localized in dendrites and axons (Cajigas et al., 2012). In filamentous fungi, it was shown that mRNA localization and subsequent local translation supports the complex formation of macromolecules (Zander et al., 2016). Furthermore, RNA localization is a key determining factor for localized proteins of the neuronal-enriched proteome (Zappulo et al., 2017). This underlines that both, mRNA localization and localized translation are important regulatory mechanisms for asymmetric cell division, cell migration and neuronal morphogenesis.

Spatial localization can be achieved by diffusion or active transport along the cytoskeleton (Martin and Ephrussi, 2009). Active transport of mRNAs along the cytoskeleton ensure a defined localization of mRNAs and encoded proteins and a spatiotemporal regulation of expression (Becalska and Gavis, 2009; Holt and Bullock, 2009). Key factors of mRNA transport are RNA-binding proteins (RBPs) which bind to so-called zipcodes mostly located within the 3´ untranslated region (UTR) of mRNAs (Andreassi and Riccio, 2009). Furthermore, zipcodes for the binding of RBPs can also be found in the 5´UTR and in the open reading frame (ORF) of mRNAs (Jambhekar and Derisi, 2007). It was shown that some mRNAs are attached to either cytoskeleton motor or adaptor proteins which ensures active transport through the cell (Czaplinski, 2014; Mofatteh and Bullock, 2017; McClintock et al., 2018; Baumann et al., 2020). Cytoskeleton motor proteins can be divided into three families: dyneins, kinesins and myosins (Bullock, 2007). Dyneins and kinesins mediate the movement along microtubules towards the minus- and plus-ends, respectively. Motor proteins belonging to the myosin family move along actin filaments (Bullock, 2007).

1.1.1 Actin- and microtubule-dependent transport of mRNAs

One of the best studied examples for the active transport of mRNAs along the actin cytoskeleton is the transport of the *ASH1* mRNA in the yeast *Saccharomyces cerevisiae* (Figure 1.1 A; Bertrand et al., 1998). In *S. cerevisiae*, the mother cell switches the mating type after each division, allowing newly formed sister cells to mate after maturation (Rusche and Rine, 2010). The mating type switch is based on an endonuclease encoded from the *HO* gene which is expressed exclusively in the mother cell (Herskowitz, 1988). It was found out that the transcription factor Ash1p represses the expression of the *HO* gene specifically in the daughter cell and thereby prevents its mating type switch (Sil and Herskowitz, 1996). To allow exclusive expression of Ash1p in the daughter cell, the *ASH1* mRNA is actively transported into the daughter cell during division. This transport is based on the actin cytoskeleton and the interaction with the RBP She2p, which binds to zipcodes within the 3´UTR and the ORF of *ASH1* mRNA (Figure 1.1 A; Long et al., 2000). She2p interacts with She3p which forms a complex with the myosin motor protein Myo4p. The assembled mRNP is transported to the daughter cell where the *ASH1* mRNA is anchored afterwards (Figure 1.1 A; Gonsalvez et al., 2004). Importantly, translation of *ASH1* mRNA is repressed during transport to ensure exclusive expression of Ash1p within the daughter cell (Gu et al., 2004). Interestingly, the transport of mRNAs mediated by the RBP Shep2p, the adaptor protein She3p and myosin Myo4p could be shown for at least 24 mRNAs, of which several are involved in stress response as well as cell wall maintenance (Shepard et al., 2003).

Thus, the transport of mRNAs seems to play an important role for different cellular processes.

Transport along the microtubule cytoskeleton plays a crucial role during oogenesis, embryogenesis and neuronal processes in higher eukaryotes as well as for filamentously growing fungi (Baumann et al., 2012). In the oocyte of *D. melanogaster*, the transport and localization of mRNAs is essential for the establishment of the body axis (St Johnston, 2005; Kugler and Lasko, 2009). Prominent examples for spatial localization of mRNAs in the later stages of oogenesis in the oocyte are *oskar*, *bicoid* and *gurken* mRNA (Figure 1.1 B). Within the oocyte the localization of the *oskar* mRNA defines where the abdomen and germ cells are formed in the embryo. The active transport of *oskar* mRNA is based on the microtubule plus-end directed motor kinesin (Zimyanin et al., 2008). In the later stages of oogenesis the mRNA is transported in all directions with a bias towards the posterior cell pole (Figure 1.1 B; Zimyanin et al., 2008). The transport along the microtubule cytoskeleton also directs *bicoid* mRNA to the oocyte anterior, and *gurken* mRNA to the dorsal/anterior corner, respectively (Figure 1.1 B; Weil et al., 2006; Jaramillo et al., 2008). The localization of *bicoid* mRNA is essential to produce the Bicoid protein gradient that forms the anterior-posterior axis (Figure 1.1 B). The Gurken protein establishes dorsal cell fates in lateral follicle cells. The localization of both mRNAs is dependent on the minus-end directed motor protein dynein (Weil et al., 2006; Jaramillo et al., 2008). The localization of *gurken* and *oskar* mRNAs is dependent on RBPs. While Squid is required for the movement as well as for the anchoring and translation of *gurken* mRNA (Norvell et al., 2005), the localization of *oskar* mRNA depends on the exon-junction complex as well as the RBP Staufen (Yano et al., 2004). For the localization and anchoring of *bicoid* mRNA, several RBPs seem to play an important role (Macdonald et al., 1991; Ferrandon et al., 1994; Pokrywka et al., 2004). Interestingly, *bicoid* mRNA anchoring also requires specific binding of an endosomal sorting complex (Irion and St Johnston, 2007). Importantly, the translation of spatially localized mRNAs is silenced during transport by RBPs like Bruno or Pumilio (Flora et al., 2018).

The spatiotemporal regulation of translation of mRNAs also plays an important role in the rapid and dynamic activity of highly polarized neurons (Glock et al., 2017). In the mammalian brain, numerous transported mRNAs were identified which encode structural proteins like β-actin, receptors and signaling molecules like the CaMKIIα subunit of Ca^{2+}/Calmodulin kinase II (Rook et al., 2000; Tiruchinapalli et al., 2003; Grooms et al., 2006). In both dendrites and axons, mRNPs are actively transported along the microtubule cytoskeleton (Figure 1.1 C; Das et al., 2019). It was shown that increased neuronal activity enhances the anterograde movement of mRNAs for more

efficient localization in dendrites (Buxbaum et al., 2015). Moreover, stimulation of neurons increased the transport of zipcode containing mRNAs (Bauer et al., 2019). The mRNPs which are transported in axons and dendrites share common features (Figure 1.1 C; Das et al., 2019). However, the key components that regulate the transport of mRNAs in neurons are still unknown (Baumann et al., 2020). It is thought that kinesin as well as dynein mediates this transport, but so far this has not been proven *in vivo* (Kanai et al., 2004; Hirokawa, 2006). A common assumption is that RBPs which bind to mRNAs play an crucial role for the localization of mRNAs. Importantly, it is still not clear how RBPs interact with motor proteins. There are two putative ways in which RBPs can interact with motor proteins: via direct interaction or protein-based interaction. A potentially direct interaction of the RBP Fragile X mental retardation protein (FMRP) with a kinesin (Kif3C) was discovered in a yeast two-hybrid screen (Davidovic et al., 2007). It was further shown that FMRP binds to several mRNAs such as CaMKIIα and it is assumed to be involved in their transport (Darnell et al., 2011; Kao et al., 2010; Pilaz et al., 2016). The best studied localized mRNA in neurons is the β-actin mRNA. It is associated with the RBP zipcode binding protein 1 (ZBP1) and ribosomes in a translationally repressed mRNP (Buxbaum et al., 2014). Upon stimulation, β-actin mRNA and ribosomes are released from the complex for activation of translation (Buxbaum et al., 2014). In an *in vitro* reconstitution it was further shown that the RBP adenomatous polyposis coli (APC) also interacts with β-actin mRNAs and forms stable complexes, which are connected to a kinesin-2 via a cargo adapter (Baumann et al., 2020).

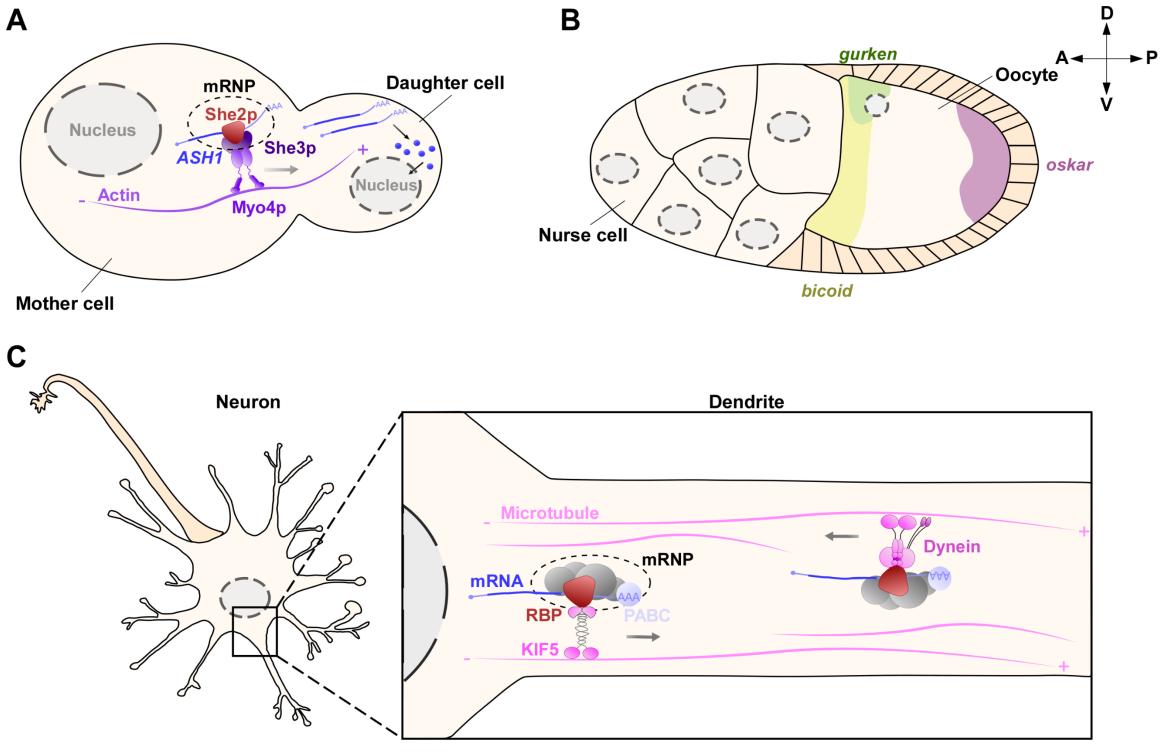

Figure 1.1: mRNA localization in different eukaryotic organisms. **(A)** Schematic representation of the *ASH1* mRNA (blue) transport along the actin (light purple) cytoskeleton during budding in *S. cerevisiae*. The mRNA is bound by the RBPs She2p (red) and She3p (dark purple). The motor protein Myo4p (purple) is responsible for the transport. Translation of *ASH1* mRNA takes place in the daughter cell and Ash1p (blue) is transported into the nucleus (Figure modified according to Niessing et al., 2018). **(B)** Localization of mRNAs in *D. melanogaster* oogenesis (middle stage). The *oscar* mRNA (rose) localizes at the posterior pole (P) and the *bicoid* mRNA (yellow) at the anterior pole (A) of the oocyte. The *gurken* mRNA (green) is located in the dorso (D)-anterior (A) region near the nucleus. The figure was modified according to Morris and Lehmann, 1999. **(C)** The mRNA transport along the microtubule cytoskeleton (light pink) in the dendrites of mammalian neurons is mediated by the motor proteins dynein and the kinesin KIF5 (pink). mRNAs (blue) are bound by the PABC protein (light blue), RBP (red) and several other proteins (gray) forming an mRNP complex (Figure modified according to Song et al., 2018).

1.1.2 Recruitment of mRNAs for organelle-coupled translation

The spatial localization of mRNAs plays a crucial role in developmental and neuronal processes (Glock et al., 2017). In addition, the localization at defined subcellular sites is particularly important within eukaryotic cells for the delivery of proteins to membrane-bound organelles (Bethune et al., 2019). Such organelles, like the endoplasmic reticulum (ER), mitochondria and endosomes, serve as platforms for membrane-coupled translation. The mechanism of membrane-coupled translation orchestrates the formation and assembly of macromolecule-complexes and efficient import of organelle-targeted proteins (Ricart et al., 1997; Zander et al., 2016).

The most prominent example, is the membrane-coupled translation of secreted and integral membrane proteins at the ER (Lesnik et al., 2015). In general, for ER-coupled translation, the complex of nascent peptide chains, ribosomes and mRNAs is targeted to the ER membrane via the so-called translocon complex. For this, the signal recognition particle (SRP) recognizes hydrophobic N-terminal signal peptides as well as transmembrane domains and targets the mRNP to the SRP receptor, which is localized in the ER membrane (Bethune et al., 2019). In addition to the classical way of how mRNAs associate to the ER, it was shown in metazoans that mRNAs can be targeted to the ER independently of ribosomes and translation (Cui et al., 2012). This is achieved by a membrane-bound mRNA receptor which recruits mRNAs to the ER membrane (Cui et al., 2012). Interestingly, a co-migration of mRNPs with tubular ER structures was shown in *S. cerevisiae*. The association seemed to be dependent on Myo4p as well as the adaptor protein She3p (Schmid et al., 2006).

Another example for organelle-coupled translation processes has been discovered for localized mRNAs that encode mitochondrial proteins. It was shown that 99% of mitochondrial proteins in *S. cerevisiae* are nuclear encoded and have to be transported to mitochondria (Elstner et al., 2009). The F1β mRNA encoding the β subunit of mitochondrial H^+-ATP synthase in rat hepatocytes localizes in electron-dense clusters, often in close proximity to mitochondria. Further experiments proved that the F1β mRNA

is translated, either freely or attached to mitochondria (Egea et al., 1997; Ricart et al., 1997). With the help of a proximity-specific ribosome profiling method, a lot of mRNAs (87% of the enriched genes) that encode mitochondrial proteins were identified to localize near the mitochondrial outer membrane (Williams et al., 2014). In addition, it was shown that many mRNAs encoding mitochondrial inner-membrane proteins are translated by mitochondria-associated ribosomes (Williams et al., 2014). For the localization of mRNAs encoding mitochondrial proteins, the 3´UTR as well as RBPs seems to play a crucial role. For the β subunit of the mitochondrial F_1F_0 ATP synthase Atp2p in *S. cerevisiae* it was shown that the 3´UTR promotes its mitochondrial localization (Margeot et al., 2002). The RBP Puf3p from *S. cerevisiae* preferentially binds mRNAs that encode mitochondrial proteins. In addition, it is associated with the mitochondrial outer membrane, and deletion affected the localization of many mRNAs at the mitochondria (Garcia-Rodriguez et al., 2007; Saint-Georges et al., 2008). The advantage of mRNA localization and local translation in close proximity to mitochondria relies on the linkage between translation and the import process. Furthermore, it can contribute to the proper assembly of protein complexes, e.g. ATP-synthase or cytochrome C oxidase, since components of both are translated in close proximity of mitochondria (Lesnik et al., 2015).

Other examples of membrane-bound and organelle-coupled translation are endosomes and lysosomes. In eukaryotic cells, membrane trafficking relies on endosomes which carry macromolecules for targeted delivery (Wideman et al., 2014). Using the endosomal pathway, cargo from the cell surface is internalized and storage, recycling or degradation within lysosomes is coordinated (Huotari and Helenius, 2011). In addition to this, endosomes function as cellular platforms where intracellular signaling cascades can be activated (Villasenor et al., 2016). These processes are mediated by early and late endosomes which can be distinguished by their associated Rab guanosine triphosphatases (GTPases; Stenmark, 2009). The endocytosis and fusion of early endosomes is organized by Rab5a, while Rab7a regulates the transport and maturation of late endosomes (Luzio et al., 2009). Furthermore, Rab7a controls the fusion of late endosomes to lysosomes. Inside the latter, extracellular as well as intracellular components are collected for degradation (Luzio et al., 2009). In the axons of retinal ganglion cells of *Xenopus laevis* (clawed frog), it was shown that mRNPs associate with Rab7a-positive endosomes (Cioni et al., 2019). These endosomes shuttle with a slight bias towards anterograde. Furthermore, ribosomes are associated with transported mRNPs and translational activity was shown during the transport. Interestingly, the translationally active mRNPs transported together with Rab7a-positive endosomes are often in physical contact with mitochondria and mRNAs, which encode

proteins for mitochondrial function. This shows that late endosome-coupled translation can potentially supply mitochondrial proteins to maintain axonal mitochondrial function (Cioni et al., 2019). Upon heat stress, mRNPs hitchhike on lysosomes for long-distance trafficking in dependency of the microtubule cytoskeleton in mammalian neuronal cells (Liao et al., 2019). It was shown that the protein ANXA11, which can be associated with the neurodegenerative disorder Amyotrophic lateral sclerosis (ALS), binds to mRNA and lysosomes (Liao et al., 2019). Furthermore, it was shown that this binding might be regulated by the release of Ca^{2+}, enabling a precise spatiotemporal recruitment as well as release of mRNPs (Liao et al., 2019). The authors reported that minor changes in the mRNA transport could lead to widespread disruption of neuronal homeostasis and potential deregulation of synaptic activity since ANXA11 knockdown reduced axonal mRNP transport. Very recently it was shown that mRNAs were co-transported with Rab5a-positive endosomes in rice endosperm cells (Tian et al., 2020). One of the first examples in which endosome-coupled translation could be identified was in hyphae of the phytopathogenic fungus *Ustilago maydis* (Baumann et al., 2012; Baumann et al., 2014). Here, translation of septin-encoding mRNAs on fast moving early endosomes is crucial for the formation of septin complexes (Baumann et al., 2014; Zander et al., 2016). In contrast to the view that localized mRNAs are translationally silenced during their transport (Besse and Ephrussi, 2008), these findings underline that transported mRNPs are not always translationally silenced. This can be advantageous to distribute equal amounts of some translated proteins within highly polarized cells such as neurons and hyphae of filamentous fungi. In addition, the translation on transportation platforms enables the supply of proteins to specific subcellular sites like mitochondria, which can be more efficient than solely transporting mRNAs or translational products.

1.2 Local translation of mRNAs on early endosomes in *U. maydis*

1.2.1 The eukaryotic model organism *U. maydis*

The phytopathogenic hemibasidiomycete *U. maydis* belongs to the subsection of *Ustilaginomycotina* and is a well-established microbial model for signaling pathways, regulation of the cell cycle, membrane trafficking, DNA recombination and repair, as well as for transcriptional and post-translational regulation or modification in eukaryotes (Bölker, 2001; Feldbrügge et al., 2008; Vollmeister et al., 2012; Langner et al., 2015; Langner and Göhre, 2016). In addition, it is tested for a putative industrial production of proteins, such as antibodies as well as the synthesis of metabolites (Bölker et al., 2008; Sarkari et al., 2014; Terfrüchte et al., 2014; Terfrüchte et al., 2017; Stoffels et al., 2020).

The biphasic lifecycle of *U. maydis* consists of a saprophytic and a biotrophic phase and ensures a developmental switch from haploid cigar-shaped sporidia to

unipolarly growing diploid hyphae which is important for infection of *Zea mays* and *Zea mays ssp. parviglumis* (teosinte; Figure 1.2 A and B; Lanver et al., 2017). The developmental switch is achieved by the fusion of two sporidia that comprises compatible mating types. Two different mating type loci, the biallelic *a* locus and the multiallelic *b* locus, mediate the control of cell fusion as well as the establishment of pathogenicity (Gillissen et al., 1992; Bölker, 2001). The recognition and fusion of two sporidia is based on a pheromone/pheromone receptor system, encoded by the *a* locus (Garcia-Muse et al., 2003). Pheromone recognition activates a signaling pathway containing a pheromone-responsive mitogen-activated protein kinase (MAPK) module, resulting in the formation of so-called conjugation tubes and a cell cycle arrest in the G2 phase. The conjugation tubes grow towards each other along a pheromone gradient and subsequently fuse after cell-cell contact (Figure 1.2 A; Spellig et al., 1994). After plasmogamy, which is typically separated from karyogamy in basidiomycetes (Kruzel and Hull, 2010), the *b* locus is crucial for the formation of a dikaryotic hypha. This locus, which has a large genetic diversity with approximately 25 different alleles (Schulz et al., 1990; Gillissen et al., 1992), encodes a pair of unrelated homeodomain proteins (*bE* and *bW*) that form a heterodimeric complex when both proteins derive from different alleles (Kamper et al., 1995). The formation of a dikaryotic hypha only takes place if mating partners have different alleles of the multiallelic *b* mating type locus. Based on this, a stable heterodimer is formed, activating gene cascades which are necessary for stability of pathogenicity and the formation of the dikaryotic hypha (Figure 1.2 A; Gillissen et al., 1992; Brachmann et al., 2004). During hyphal growth, the cells elongate towards the apical pole, while septa are built at the basal pole which represents barriers to separate the growing hypha from areas that do not contain cytoplasm (Figure 1.2 B). By forming several septa at regular intervals, the cell is able to maintain unipolar growth without the need for *de novo* generation of cytoplasm (Steinberg et al., 1998; Freitag et al., 2011). The mechanism of the *b*-dependent regulation of hyphae formation was used for the construction of the *U. maydis* lab strain AB33 (Figure 1.2 B). This strain contains compatible *b*-alleles under control of the nitrogen-inducible P_{nar} promoter (P_{nar}:bW2bE1). A switch from ammonium to nitrate as nitrogen source induces expression of these compatible *b*-alleles, which leads to the formation of an active *b*- heterodimer (Brachmann et al., 2001). This strain is widely used to study biological processes in hyphae of *U. maydis*.

If the hypha recognizes certain chemical and physical signals on the surface of the host, an appressorium-like structure is formed (Figure 1.2 A). With the help of the secretion of plant cell wall degrading enzymes, the hypha is able to enter its host plants (Kolattukudy et al., 1995; Lanver et al., 2010). Once inside, the fungus proliferates and

forms branched hyphae. At later stages of infection, tumor formation takes place (Figure 1.2 A). During maturation of tumors, hyphal cells differentiate and form teliospores which are then released into the environment (Figure 1.2 A). Under appropriate environmental conditions, the teliospores germinate and undergo meiosis on the host surface, giving rise to haploid sporidia and the lifecycle begins anew (Vollmeister et al., 2012).

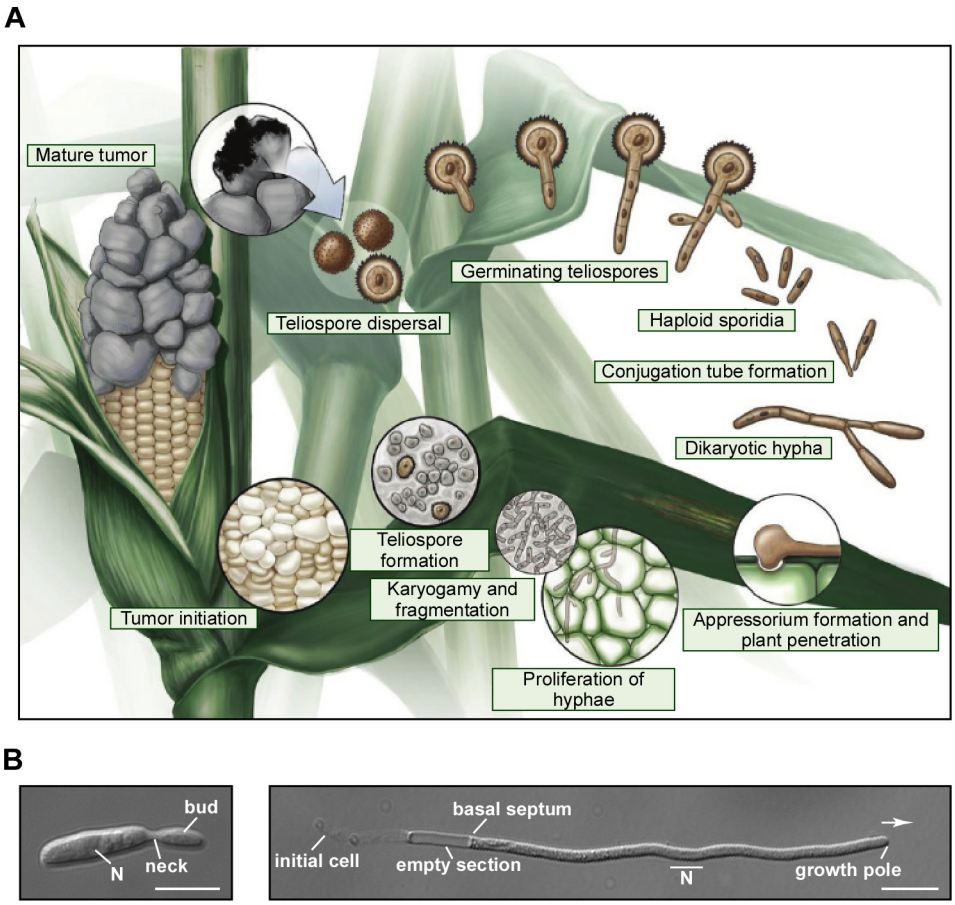

Figure 1.2: The lifecycle of *U. maydis*. (A) When *U. maydis* tumors burst, diploid teliospores are released into the environment. Under appropriate environmental conditions, the teliospores germinate and undergo meiosis on the host surface, giving rise to haploid sporidia. When haploid sporidia of different mating types recognize each other via a pheromone/pheromone receptor system, they form conjugation tubes which fuse at their tips. After the formation of an infectious dikaryotic hypha, an appressorium is formed and *U. maydis* enters the plant. Subsequently proliferation, karyogamy and fragmentation as well as tumor formation occurs and the cycle begins again (modified according to Saville, 2012). **(B)** Morphology of sporidia and hyphal cells of the laboratory strain AB33 (N, nucleus; scale bar 10 µm; for hyphal cells: 6 h.p.i.; growth direction is indicated by arrow).

1.2.2 Microtubule-dependent mRNA transport in *U. maydis*

The microtubule cytoskeleton plays a crucial role during the hyphal growth of *U. maydis*. Without microtubules (MT), growing hyphae reach only approximately 50-60 µm in length and they start to grow in a bipolar manner compared to normal unipolar growth (Fuchs et al., 2005). Thus, the microtubule cytoskeleton is crucial for the morphology of hyphae and determines cell polarity (Steinberg et al., 2001). The MTs span the entire hyphae in an anti-parallel orientation. At the cell peripheries, the MTs are arranged in a

parallel fashion whereby the plus ends are orientated towards the cell poles (Lenz et al., 2006; Egan et al., 2012). Early endosomes are transported along the microtubule cytoskeleton through hyphae of *U. maydis*. Here, dynein (split dynein Dyn1/2) and kinesin Kin3 mediate the long-distance transport towards the minus- and plus-ends, respectively (Wedlich-Söldner et al., 2002; Lenz et al., 2006). Kin3 is in permanent contact to the endosomes while dynein only interacts transiently during the transport to the minus-ends (Schuster et al., 2011). The kinesin Kin1, which moves like Kin3 to the plus-ends of the microtubule bundles, is responsible for returning dynein from the minus- to the plus-ends (Vollmeister et al., 2012). This is important to ensure a bidirectional movement of endosomes through hyphae of *U. maydis*. A so-called hook protein, Hok1, coordinates the binding of Kin3 and dynein to early endosomes (Bielska et al., 2014). Besides the motor proteins, the endosomal sorting complex required for transport (ESCRT) plays a crucial role since it is a key component of endosomal maturation (Teis et al., 2009). A previous study shows, that an ESCRT complex regulating protein, Did2, plays an important role in the coordination of endosomal transport. Deletion of *did2* results in reduced endosomal association of the molecular motor proteins and a decrease of processive long-distance transport (Haag et al., 2017). Thus, the ESCRT complex is crucial for efficient endosomal long-distance transport.

The first examples of mRNPs hitchhiking on endosomes has been demonstrated in hyphae of *U. maydis* (Baumann et al., 2012). Within these transported mRNPs, two important RBPs were identified: the poly(A)-binding protein Pab1 and the ELAV-type RNA recognition motif (RRM) protein Rrm4. The latter is the key RBP, which contains three amino-terminal (N-terminal) RRM domains for RNA binding and two carboxy-terminal (C-terminal) MLLE domains for protein-protein interactions (previously known as PABC domain; (Becht et al., 2005; Kozlov et al., 2010). It was shown that Rrm4 is essential for the polarity of hyphae since its deletion increases the number of bipolar growing hyphae and causes a reduction in the formation of retraction septa (Figure 1.3 A; Becht et al., 2006). With the help of a fusion to a green fluorescence protein (Gfp), it could be shown that Rrm4 localizes almost exclusively on shuttling Rab5a-positive endosomes and moves bidirectional on microtubules through the hyphae (Figure 1.3 B and C; Becht et al., 2006; König et al., 2009; Baumann et al., 2012). Pab1 interacts with the poly(A)-tail of cytoplasmic occurring mRNAs and co-localizes to Rrm4-positive endosomes (Figure 1.3 C; Hogan et al., 2008; König et al., 2009).

The first identified cargo mRNAs of Rrm4-dependent endosomal transport were the *ubi1* mRNA, encoding a natural fusion protein consisting of ubiquitin and the ribosomal protein Rpl40, the *rho3* mRNA which encodes a small G protein, the *cdc3* mRNA encoding the septin Cdc3 as well as the *cts1* mRNA which encodes a chitinase

(König et al., 2009; Koepke et al., 2011). The latter is an unconventionally secreted enzyme which plays an important role in cell wall degradation during cell separation (Langner et al., 2015). The loss of Rrm4 results in a reduced export of Cts1 in fungal hyphae (Koepke et al., 2011). Septins are conserved GTP-binding proteins that are found in fungi, animals and microsporidia but are absent in higher plants (Lindsey and Momany, 2006; Estey et al., 2011). In general, septins assemble into filaments and higher-order structures. They are functionally active during polar growth and cytokinesis in fungi (Weirich et al., 2008). The genome of *U. maydis* encodes four septins (Cdc3, Cdc10, Cdc11 and Cdc12) and deletion of individual septin genes led to bipolarly growing hyphae at early stages of hyphal growth which were delayed in the formation of retraction septa (Baumann et al., 2014; Zander et al., 2016). The subcellular localization of all septin mRNAs was analyzed *in vivo*. They shuttled through hyphae in a Rrm4-dependent manner together with Rab5a-positive endosomes (Baumann et al., 2014; Zander et al., 2016). On average, two directed septin mRNA particles were observed per 100 µm of hyphae of *U. maydis* (Baumann et al., 2014; Zander et al., 2016). Interestingly, an mRNA-dependent accumulation of septin proteins on endosomes was observed. Hence, both the mRNAs as well as the encoded proteins shuttled in a microtubule-dependent manner through hyphae (Figure 1.3 C; Baumann et al., 2014; Zander et al., 2016). This led to the hypothesis that local translation of transported mRNAs takes place on endosomes (Baumann et al., 2014). Local translation of the septin mRNAs during the transport seemed to facilitate the assembly and delivery of septins (Zander et al., 2016). The hypothesis was strengthened by the finding that also translational active ribosomes associate in mRNPs and that the association of ribosomal proteins was dependent on the presence of mRNAs (Baumann et al., 2014; Higuchi et al., 2014). To get a transcriptome-wide view of Rrm4 targets, an individual-nucleotide resolution UV crosslinking and immunoprecipitation (iCLIP) experiment was performed (Olgeiser et al., 2019). Here, around 3,000 mRNAs were identified to be bound by Rrm4. In addition, it was found out that Rrm4 binds to the motif 5´-UAUG-3´ within its target mRNAs using its third RRM domain (Olgeiser et al., 2019). Rrm4 predominantly binds within the 3´UTR of target mRNAs. However, precise binding was also observed at start and stop codons, representing landmark sites of translation, which suggests a close connection of Rrm4-dependent mRNA transport and translation (Olgeiser et al., 2019).

In addition to the two already described RBPs Rrm4 and Pab1, other proteins were found to be associated within the microtubule-dependent and endosome-coupled mRNPs. The FYVE zinc finger domain protein Upa1 was found to interact with endosomal lipids as well as with the MLLE domains of Rrm4 and Pab1 via so-called PAM2 (P) and PAM2-like (PL) motifs (Figure 1.3 C; Pohlmann et al., 2015). Thus, Upa1

serves as an adaptor protein which couples the mRNP to endosomes (Pohlmann et al., 2015). Another PAM2 motif containing protein which was identified to be associated within the mRNP is Upa2 (Jankowski et al., 2019). Upa2 contains four PAM2 motifs, a coiled-coil domain, which is presumably important for a dimerization process, and a C-terminal GWW domain, which is important for protein-protein interactions and maintenance of endosomal localization (Figure 1.3 C; Jankowski et al., 2019). It acts as a scaffolding protein and potentially stabilizes the mRNP complex by the interaction to Pab1 (Jankowski et al., 2019). However, an interacting protein which is responsible to couple Upa2 via its GWW domain to endosomes still remains unknown. With the help of a co-immunoprecipitation method, the RBP Grp1 was identified (Figure 1.3 C). This glycine-rich protein is alternatively spliced and both isoforms shuttle on endosomes in a Rrm4-dependent manner. In addition to this, Grp1 binds predominantly in the 3´UTRs of transported mRNAs, often in close proximity to Rrm4 (Olgeiser et al., 2019).

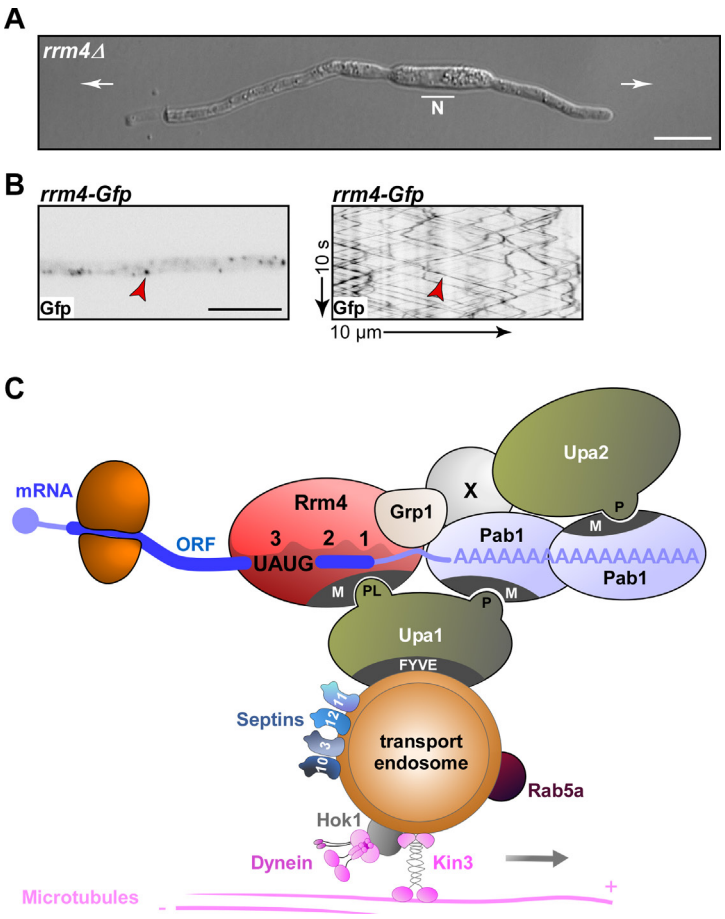

Figure 1.3: Microtubule-dependent mRNA transport in *U. maydis*. (A) Morphology of *rrm4*Δ hyphae growing bipolar (N, nucleus; scale bar 10 µm; 6 h.p.i.; growth direction is indicated by arrow). **(B)** Micrograph and kymograph of hypha expressing Rrm4-Gfp. Dotted localization as well as shuttling trough the hyphae is indicated by red arrowhead (6 h.p.i.; inverted pictures; arrow length on the left and bottom of kymograph indicate time and distance). **(C)** Schematic representation of transported mRNP along the microtubule cytoskeleton in *U. maydis*: motor proteins kinesin Kin3 and dynein (pink) mediate transport along the microtubule cytoskeleton (light pink); the hook protein (Hok1, gray) coordinates binding of Kin3 and dynein to early endosomes; small GTPase Rab5a (purple) marks early endosomes; transport endosome (orange);

Upa1 (khaki) binds endosomes as well as Rrm4 and Pab1; RNA-binding proteins Rrm4 (red) and Grp1 (beige) binding mRNAs (blue line with poly(A)-tail) predominantly in 3´UTR; poly(A)-binding protein (Pab1, light blue) binds poly(A)-tail of mRNAs; Upa2 (khaki) binds Pab1 and an unknown interaction partner (X); ribosomes (dark orange); septin proteins which are assembled on the endosome (shades of blue; modified depiction; originally designed by Markus Tulinski).

1.3 Methods to visualize the subcellular localization of mRNAs

To better understand the mechanics of mRNA transport, it is crucial to visualize mRNAs and associated processes. Several methods were developed which allow the visualization of the subcellular localization of mRNAs (Buxbaum et al., 2015). With RNA fluorescence *in situ* hybridization (RNA-FISH) or single-molecule FISH (smFISH) it is possible to detect endogenous mRNAs with the usage of fluorescently labeled oligonucleotides (Paradies and Steward, 1997; Femino et al., 1998). Much of the knowledge about the subcellular localization of mRNA was gained by using FISH methodology. However, these methods only provides a static picture of mRNA localization at the time where the cells were fixed (Tyagi, 2009).

In contrast to this, live-cell imaging of mRNAs provides dynamic temporal and spatial information. To visualize the localization of mRNAs *in vivo*, RBPs fused to fluorescence proteins can be used which bind specifically to unique RNA hairpins integrated into the 3´UTR of an mRNA of interest (Figure 1.4 A; Buxbaum et al., 2015). Three systems deriving from bacteriophages are mainly used to visualize mRNAs in living cells: the MS2 (Bertrand et al., 1998), PP7 (Larson et al., 2011) and λN system (Daigle and Ellenberg, 2007). All systems utilize the RNA binding capacities of specific phage proteins. The original RBP (λN) deriving from the bacteriophage lambda binds to RNA stem-loops termed boxB. It was first optimized for better visualizing mRNAs and later on to stabilize the binding to its cognate RNA stem-loops *in vivo* (new version named as λN*; Austin et al., 2002). The detection of shuttling mRNAs in hyphae of *U. maydis* was performed with the help of the λN system (Figure 1.4 B and C). Here, the modified λN* peptide was fused to a double Gfp (Baumann et al., 2014). 16 boxB RNA hairpins ($boxB^{16}$) were integrated into the 3´UTR of the *cdc3* mRNA to analyze the localization (Figure 1.4 C). For the RBP deriving from the bacteriophage MS2 it was shown that its usage impairs mRNA degradation in *S. cerevisiae* leading to 3´ decay fragments which are visualized with the MS2 system (Garcia and Parker, 2015; Garcia and Parker, 2016; Heinrich et al., 2017). Thus, an improved version of the MS2 binding sites was investigated which showed a reduced affinity for the MS2 coat protein (Tutucci et al., 2018). This clearly indicates that the integration of several copies of RNA hairpins within the 3´UTR of an mRNA of interest which are each bound by an RBP fused to a fluorescence protein can alter mRNA processing. Another possibility of labeling mRNAs

in vivo is based on the integration of artificial RNA motifs (aptamers) into the UTRs of mRNAs of interest. These aptamers can stably bind to small, cell-permeable and non-fluorescent dyes. Upon binding, the dyes become fluorescent (Swetha et al., 2020). Several aptamers were investigated to analyze the localization of mRNAs in living cells including the early developed malachite green (Grate and Wilson, 1999) and later ones such as Spinach (Kikuchi and Kolpashchikov, 2016), Broccoli (Braselmann et al., 2018) and Pepper (Chen et al., 2019). RNA aptamers exhibit high brightness, a small size and almost background-free labeling of mRNAs. However, imaging of mRNAs within living cells using aptamers is still at early stages. Thus, the MS2, PP7 and λN systems are the state-of-the-art methods to analyze subcellular localizations of mRNAs *in vivo*.

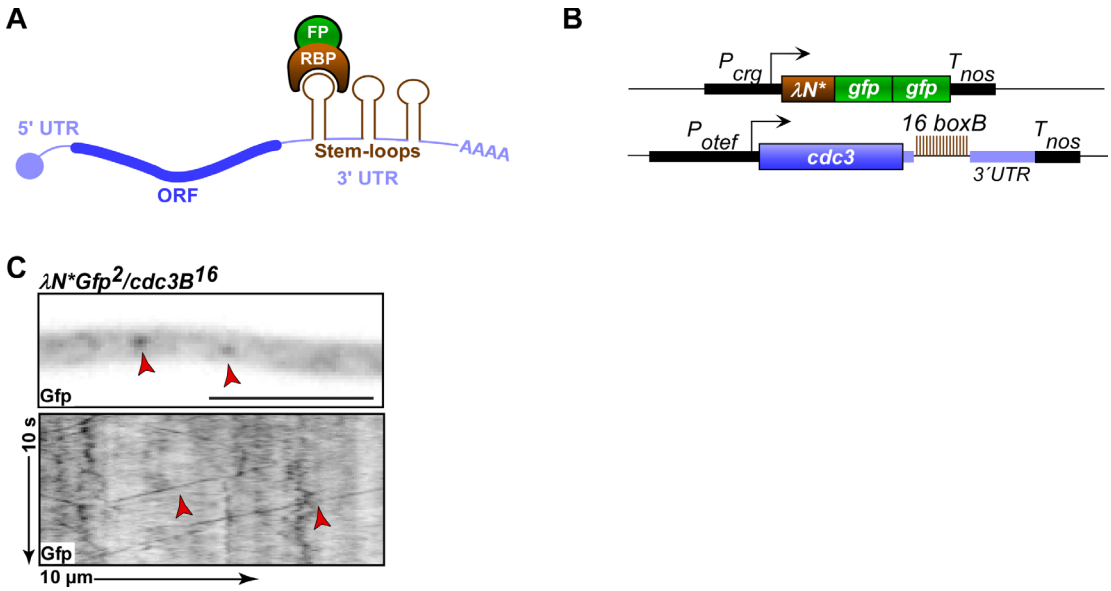

Figure 1.4: RNA live imaging of *cdc3* mRNA in *U. maydis*. (A) RNA live imaging is based on the binding of heterologous RNA binding proteins to a unique RNA hairpin sequence which is integrated in the 3´UTR of defined mRNAs. A fusion of RBPs with Gfp allows the visualization and tracking of mRNAs (modified according to Zander et al., 2018). **(B)** Components of the RNA live imaging in *U. maydis*. A modified λN* peptide fused to a double Gfp and an arabinose-regulated promoter (P_{crg}) as well as a heterologous transcriptional terminator (T_{nos}) were used. 16 boxB RNA hairpins (B^{16}) were integrated in the 3´UTR of cdc3 mRNA modified according to (modified according to Zander et al., 2018). **(C)** Micrograph and kymograph of hypha expressing λN*Gfp^2/*cdc3*B^{16}. Dotted localization of *cdc3* mRNA as well as moving mRNAs are indicated by red arrowhead (6 h.p.i.; inverted pictures; arrow length on the left and bottom of kymograph indicate time and distance; modified according to Zander et al., 2018).

1.4 Methods to quantify and visualize translational sites within cells

The spatiotemporal regulation of translation is a fundamental biological process. Together with a defined localization of mRNAs, the tight regulation of translation is crucial to control protein levels and allow cells to orchestrate the synthesis of proteins in a spatiotemporal manner (Chekulaeva and Landthaler, 2016). In addition to the knowledge of the mechanism of translation obtained by biochemical and structural

studies, there has been growing interest to study the dynamics of translation in a cellular context. Expression of mRNA reporters encoding fluorescence proteins could not answer questions towards translational dynamics since fluorescent signals were detected after completion of protein synthesis and proper folding. Several techniques have been developed to measure translational efficiency and to visualize translation in the cellular context. Methods which use either RNA sequencing (RNA-seq) or mass spectrometry (MS) technology enable a transcriptome-wide view on translation. MS-based methods rely on the labeling of newly synthesized proteins which are enriched, purified and subsequently quantified in MS. For this, either labeled amino acids (Schwanhausser et al., 2009), amino acid analogs (Dieterich et al., 2006; Howden et al., 2013) or puromycin (Aviner et al., 2013) are incorporated into newly synthesized proteins. The most common example for the usage of RNA-seq is the ribosome profiling method. Here, ribosome-protected mRNAs from nuclease digestion are sequenced which allows an identification of translated mRNAs under different growth conditions (Ingolia et al., 2009). Proximity-specific ribosome profiling makes use of labeling ribosomes with biotin and allows the analysis of translation at defined subcellular localizations (Jan et al., 2014; Williams et al., 2014). Importantly, RNA-seq as well as MS-based methods do not offer spatiotemporal information on localized mRNA translation. In addition, a detection of translational heterogeneities within a cell population is not feasible (Glock et al., 2017).

In contrast to this, imaging-based methods enable the analysis of subcellular localization of translation and monitoring of individual mRNA molecules (Chekulaeva and Landthaler, 2016). For visualizing and identifying newly synthesized proteins, several methods were established. For this, again either amino acid analogs or (Dieterich et al., 2010; Tom Dieck et al., 2012) puromycin (Schmidt et al., 2009) are incorporated into newly synthesized proteins. Both can subsequently be visualized by fluorescently labeled antibodies. In addition to visualizing newly synthesized proteins, methods which enable a simultaneous detection of mRNAs as well as a nascent peptide chain are coming into focus. The first published method which enables a synchronized detection is based on the integration of RNA stem-loops into mRNAs (Halstead et al., 2015). By integrating PP7 and MS2 RNA stem-loops upstream and downstream of the stop codon of an mRNA of interest, labeling of the ORF as well as the 3´UTR is possible. For this, the equivalent RBPs PP7 and MS2 were expressed in fusion to Gfp or a red fluorescent protein (Rfp), respectively. Thus, untranslated mRNAs appear yellow by labeling with both, green and red fluorophores. Upon the first round of translation, the ribosomes remove all RBPs interacting with sequences within the ORF of mRNAs. Hence, the RBP PP7, which binds inside the ORF, is displaced from the transcript and a shift in the detectable fluorescence from yellow to red indicates translation of the labeled mRNA

(Halstead et al., 2015). Because of the displacement of the coat protein which binds to the ORF, the method is called "**T**ranslating **R**NA **I**maging by **C**oat Protein **K**ick-off" (TRICK). The main disadvantage of this method is that the fluorophore labeling the ORF is displaced after the first round of translation. Thus, visualization of several rounds of translation or translational dynamics cannot be monitored. To overcome this problem, novel reporter systems were developed in which antibodies are fused to fluorescence proteins to label a nascent peptide (Morisaki et al., 2016; Wang et al., 2016; Wu et al., 2016; Yan et al., 2016).

1.4.1 Labeling of nascent peptide chains with antibodies to visualize translational sites *in vivo*

The two core detection elements of the aforementioned novel reporter systems are peptide- and mRNA labeling tags. The MS2 or PP7 RNA stem-loops were integrated in the 3´UTR to label the mRNA transcript with the RBPs MS2 or PP7 fused to fluorescence proteins (Wang et al., 2016; Wu et al., 2016; Yan et al., 2016). In addition to the mRNA labeling, a nascent peptide chain is marked with the SunTag method (Tanenbaum et al., 2014). In this, a peptide epitope tag is specifically recognized by an fluorescently-labeled antibody. Thus, this experimental composition allows the simultaneous detection of mRNA molecules and their corresponding nascent peptides.

In the SunTag method, a repeating peptide array is fused to an ORF, which can recruit a fluorescently labeled single-chain variable antibody fragment (Figure 1.5 A; scFv; for further description see section 1.4.1.1; Tanenbaum et al., 2014). By this, long-term imaging of single protein molecules is possible in mammalian cells. For the SunTag method, the GCN4-scFv and 24 copies of its cognate peptide epitope ($GCN4^{24}$) were used (Figure 1.5 A). GCN4-scFv was previously optimized for an intracellular expression and originally binds to endogenous Gcn4p in *S. cerevisiae* with high affinity (Worn et al., 2000). Gcn4p is a transcription factor which controls the transcription of many genes involved in amino acid synthesis (Albrecht et al., 1998). By expressing GCN4-scFv fused to Gfp, protein aggregates were observed in human cells at high expression levels. To overcome this, GCN4-scFv was fused to superfolder-Gfp (fast folding variant of Gfp, sfGfp; Figure 1.5 A), which almost completely eliminated protein aggregation (Tanenbaum et al., 2014). Subsequently, for establishing methods to label a nascent peptide chain, GCN4-scFv-sfGfp was used. The great advantage of the SunTag method is that the antibody fused to sfGfp is expressed independently from the protein which will be labeled. Thus, the fluorophore is already matured and is able to bind to the cognate peptide epitope as soon as it emerges from the ribosome. In addition, several copies of

the peptide epitope fused to an ORF increase the number of bound sfGfp molecules and subsequently the quantifiable intensity during fluorescence microscopy.

For the application of the SunTag method in mammalian cells, GCN4^{24} was fused N-terminally to the ORF of interest (ORFoi; Figure 1.5 B; Wang et al., 2016; Yan et al., 2016; Cioni et al., 2019). Simultaneously, GCN4-scFv was expressed in fusion to sfGfp. To label the mRNAs, 24 copies of the PP7 RNA stem-loops were integrated in the 3´UTR and the corresponding RBP protein was fused to Rfp (Figure 1.5 B; Rfps; mCherry or tdTomato). Thus, translationally active transcripts were labeled with both, red and green fluorescence proteins, and appeared as yellow dots during live cell fluorescence microscopy. In order to prove whether the overlap of mRNA and nascent peptide chain fluorescence signals are referable to translational active transcripts, cells were treated with the translational inhibitor cycloheximide (CHX) which blocks ribosome elongation and prevents synthesis of new SunTag peptides. The translational sites detected with GCN4-scFv-sfGfp did not increase after CHX treatment, underlining translational specific binding of GCN4-scFv-sfGfp to GCN4^{24} (Wang et al., 2016; Yan et al., 2016). Thus, antibody-based labeling of a nascent peptide chain in combination with RNA live imaging offers an excellent and robust way to track translational sites of a single mRNA *in vivo*. However, GCN4-scFv-sfGfp binds to nascent peptide chains and keeps attached to the synthesized proteins after translation is completed. Hence, the number of labeled proteins increases within the cell over time. To overcome this problem, the auxin-inducible degron was used (AID;(Nishimura et al., 2009); for further description see section 1.4.1.2) to remove completely synthesized proteins. For this, in addition to the N-terminally GCN4^{24}, the AID was C-terminally fused to the ORFoi (Wang et al., 2016).

The labeling of mRNAs as well as their corresponding nascent peptides provides a direct quantitative readout of initiation, elongation and localization of translation (Chekulaeva and Landthaler, 2016). The approach enabled a simultaneous detection of movement of mRNA and the nascent peptide chain produced from this mRNA (Morisaki et al., 2016). In addition, measurements of diffusion rates of translated and untranslated mRNAs (Wu et al., 2016), as well as initiation and elongation rates (Wang et al., 2016; Yan et al., 2016) were possible.

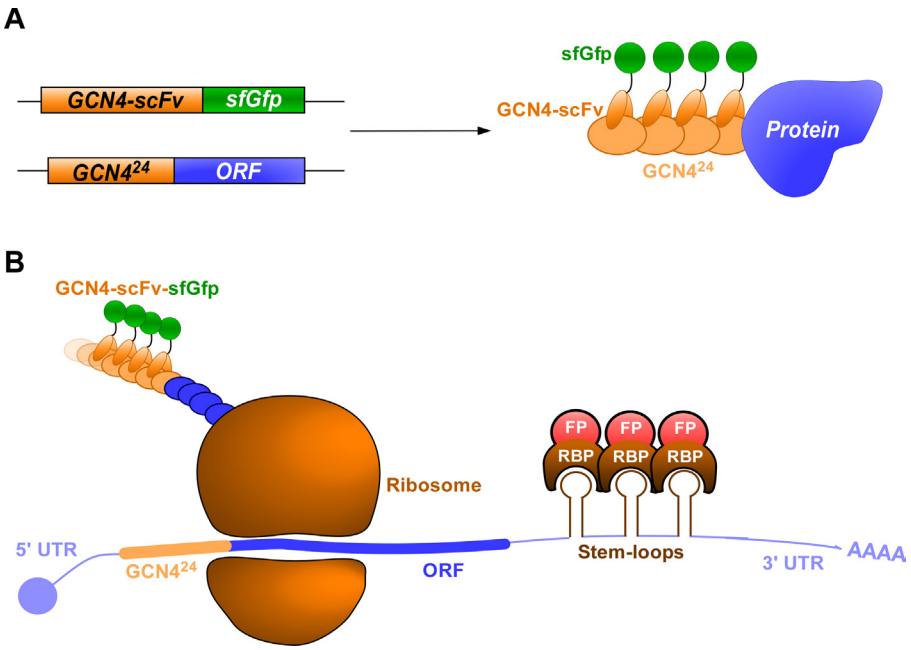

Figure 1.5: Schematic representation of the SunTag method and its application to label a nascent peptide chain. (A) The SunTag method is based on the binding of the GCN4-scFv (orange) to its cognate peptide sequence (light orange; GCN4^{24}). Repeating arrays of GCN4^{24} are fused to the ORF of a protein of interest (blue) which can recruit multiple GCN4-scFv fused to sfGfp (green) for long-term imaging of single proteins. The antibody fused to sfGfp is independently expressed from the ORF fused to GCN4^{24}. **(B)** Methodology in which the nascent peptide chain is visualized by using the SunTag peptide epitope (light orange) which is bound by GCN4-scFv-sfGfp (orange/green). The mRNA (blue) is visualized by RNA stem-loops (brown), integrated into the 3´UTR, which are recognized by an RNA-binding protein (RBP, brown) fused to a red fluorescence protein (FP, red). The dual labeling of mRNA and the nascent peptide chain enables the visualization of translational sites *in vivo*.

1.4.1.1 Composition of antibodies

Antibodies are immunoglobulin (Ig) molecules which specifically recognize their target molecule (antigen) with high affinity (Joosten et al., 2003). In addition to their function of recognizing antigens of pathogens during immune response, they are also used in medical and scientific research due to their specific binding to antigens. Immunoglobulin G (IgG) are class G antibodies, which have a characteristic tertiary structure of identical polypeptide chains comprising a light- (L) and heavy-chain (H) which are connected by disulfide bridges (Figure 1.6 A; Narciso, 2012). Each chain can be divided into variable (heavy and light chain variable domain ,V_H and V_L) and constant parts (C_H1-$_H3$ and C_L). The unique antigen-binding site consists of the V_H and V_L domains (fragment antigen binding, Fab fragment). The non-antigen binding part (fragment crystallizable region, Fc fragment) is not essential for therapeutic applications, but mediates binding to receptors and has other immunological functions (Joosten et al., 2003). Because most of the whole IgG antibodies have a size of approximately 160 kDa, many recombinant antibody fragments were developed in which the non-antigen binding part is removed (Holliger and Hudson, 2005). These include so-called single-chain variable fragments (scFvs) in which a flexible amino acid linker or disulfide bond connects the V_H and V_L parts (Figure

1.6 A; Glockshuber et al., 1990). scFvs show antigen affinities which are comparable to whole antibodies and can easily be produced in heterologous systems e.g. *E. coli* (Griffiths and Duncan, 1998; Ahmad et al., 2012). The smallest antigen-binding antibody fragment is the so-called nanobody (Nb; Figure 1.6 B). It is based on antibodies which are found in *Camelidae* or cartilaginous fish (Hamers-Casterman et al., 1993). These antibodies lack the light chains and the antigen-binding site only consists of the heavy-chain variable domains (V_{HH};Figure 1.6 B; Muyldermans and Lauwereys, 1999). Because of the small size, the V_{HH} domain has superior body distribution properties. In addition, Nbs are highly resistant to denaturation, exhibit high aqueous solubility and are functionally expressed in standard microbial expression systems (Doshi et al., 2014).

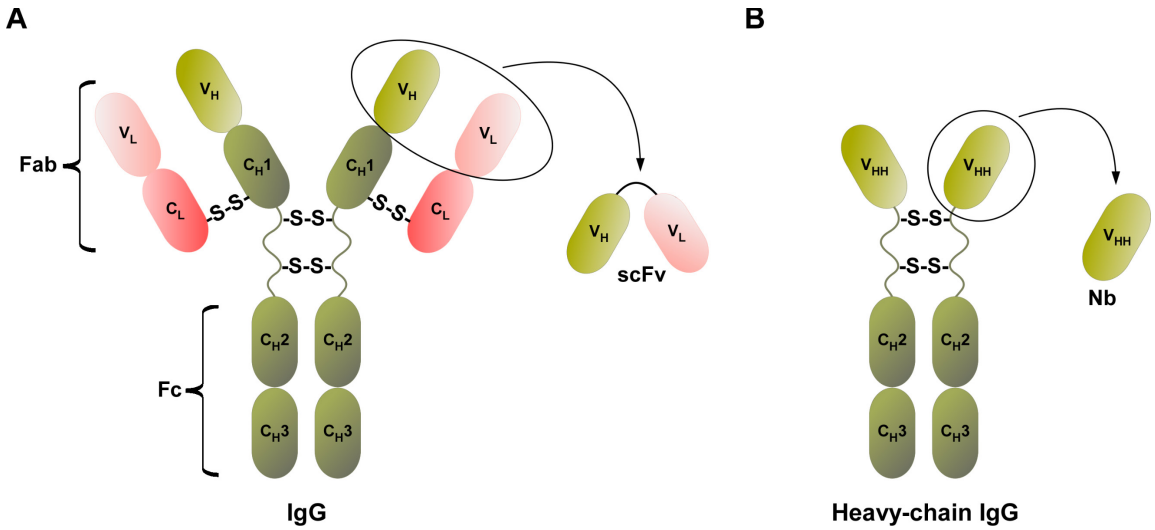

Figure 1.6: Schematic representation of IgG antibodies and antibody fragments. (A) Complete IgG antibody consisting of two identical heavy chains (H, khaki) and light chains (L, rose). Heavy chains are composed of three constant (C_H1, C_H2, C_H3) and one variable (V_H) part. The light chain contains one constant (C_L) and one variable (V_L) domain. The antigen-binding site consists of the V_H and V_L domain (Fab fragment) while the non-antigen binding part comprises C_H2 and C_H3 (Fc fragment). Via hydrolysis of the Fc fragment, a single chain variable fragment (scFv) consisting of V_H and V_L linked by a flexible amino acid linker or disulfide bond is formed. **(B)** Complete camelid type heavy-chain IgG antibody. It consists of two identical chains where each contain a variable (V_{HH}) and two constant (C_H2, C_H3) domains. The isolation of V_{HH} domains lead to the discovery of nanobodies (Nb).

1.4.1.2 Methods to degrade synthesized proteins

Organisms must tightly control the levels of intracellular proteins in order to adapt to changing environmental conditions (Balch et al., 2008). Rapid removal of misfolded proteins by the proteasome is crucial for the proper function of a cell´s health (Amm et al., 2014). However, the proteasome is also responsible for the rapid turnover of regulatory proteins (Bhattacharyya et al., 2014). Several sequences and modifications target proteins for proteolysis and play a key role in regulating the degradation of proteins (Chassin et al., 2019). One example of a modifying target is ubiquitin (Ub), which is covalently linked to lysine residues of proteins that are targeted for degradation

in the proteasome (Bailey-Elkin et al., 2017). For a rapid and specific degradation of proteins, several Ub-based systems were developed. One of these systems is the auxin-inducible degron (AID;(Nishimura et al., 2009). This system is based on the auxin-dependent degradation pathway of plants, which was implemented in other eukaryotic cells. Addition of the synthetic auxin 1-naphthaleneacetic acid (NAA) induces poly-ubiquitinated of proteins fused to the AID degron (Nishimura et al., 2009).

Most of the cellular proteins are poly-ubiquitinated and targeted to the proteasome for degradation. However, some proteins are also degraded by the proteasome independently of Ub. Short intrinsic amino acid sequences, which are called degron sequences were found to be involved in this degradation pathway. Such small peptide motifs are for example PEST motifs. In general, PEST sequences are hydrophilic stretches, which are not interrupted by positively charged residues. They begin and end with positively charged amino acids like lysine, arginine or histidine and are rich in proline (P), glutamate (E), serine (S) and threonine (T; Rogers et al., 1986). The proteasome-mediated turnover of PEST motif containing proteins is often based on phosphorylation (Rechsteiner, 1991). PEST sequences are present in key metabolic enzymes, transcription factors, protein kinases, phosphatase and cyclins (Rechsteiner and Rogers, 1996). They are often present as C-terminal extensions but some proteins also contain multiple PEST regions within their amino acid sequence. The activation of degradation varies from exposure to light (Phytochrome; Rechsteiner, 1990), phosphorylation (G1 cyclin; Rechsteiner, 1990) to ligand binding (Shumway et al., 1999). One of the well-studied PEST sequences is located C-terminally within the mouse ornithine decarboxylase (mODC). This sequence is conserved and induces rapid proteasomal proteolysis (Murakami et al., 1992). The mODC degron was already successfully used for heterologous destabilization of proteins in *S. cerevisiae* (Hoyt et al., 2003) and mammalian cells (Li and Coffino, 1993).

1.4.1.3 2A peptides for the generation of polycistronic mRNAs in eukaryotes

Genes can be found clustered in so-called operons in which they are transcribed coherently to form one mRNA (polycistronic mRNA), or separated from each other resulting in mRNAs encoding for one protein (monocistronic mRNA). In bacteria and archaea, the gene expression is often organized in operons resulting in polycistronic mRNAs (Kozak, 1983). In eukaryotes, most of the mRNAs are monocistronic. However, some polycistronic precursor mRNAs, which are cleaved at the polyadenylation site and trans-spliced are also found in eukaryotes (Spieth et al., 1993). For genetic and metabolic engineering, polycistronic mRNAs are beneficial because they allow the co-regulation of expression of different proteins. One possibility to generate polycistronic

mRNAs in eukaryotes is the use of internal ribosome entry site (IRES) sequences. It was shown that ORFs combined by IRES sequences are often not expressed at the same level leading to different protein levels (Szymczak et al., 2004). In addition, the usage of multiple IRES sequences can lead to a competition for translational factors (Wang et al., 1996), and it was shown that the expression of proteins can be significantly lower compared to monocistronic expression (Mizuguchi et al., 2000).

Another approach which circumvents the emerging limitations using IRES sequences is the usage of viral 2A peptides (Szymczak et al., 2004). The name “2A” refers to a specific region in the viral genome and is attributable to the gene numbering scheme of viruses (Liu et al., 2017). 2A peptides, which contain a characteristic C-terminally DXEXNPGP motif were first discovered in the foot-and-mouth disease virus (FMDV, F2A peptide; Ryan et al., 1991). In a so-called ‘stop and carry on‘ (Sharma et al., 2012) or ’stop and go‘ (Atkins et al., 2007) mechanism, the ribosome pauses the translation at the glycine within the characteristic motif (Figure 1.7 (2)). It is thought that the 2A peptide sequence interacts with the exit tunnel of the ribosome, causing a sterically restricted C-terminus of the 2A peptide within the peptidyl-transferase center (P site). Thus, nucleophilic attack of the ester linkage of the glycyl-tRNA by the prolyl-tRNA is inhibited (Roulston et al., 2016). Several subsequent scenarios are conceivable: termination of translation at this point, resumption of translation or release of the nascent peptide and resuming of translation with proline as first amino acid (Roulston et al., 2016). For the latter, the eukaryotic release factors are proposed to release the nascent protein from the ribosome (Figure 1.7 (3); Roulston et al., 2016). Because of the failure of forming a peptide bond, the prolyl-tRNA is released from the ribosome. The translational release factors eRF1 and eRF3 enter the ribosome and disassociate the nascent peptide chain (Roulston et al., 2016). Subsequently, the prolyl-tRNA enters the ribosome and translation is resumed (Figure 1.7 (4)). The ratio of the different potential scenarios is dependent on the separation efficiency of the 2A peptide in the organism in which it is applied. Different 2A peptides deriving from different viruses were already successfully used in fungal model organisms for the production of carotenoids in *S. cerevisiae* (Beekwilder et al., 2014) or fungal toxins in *Aspergillus niger* (Schuetze and Meyer, 2017).

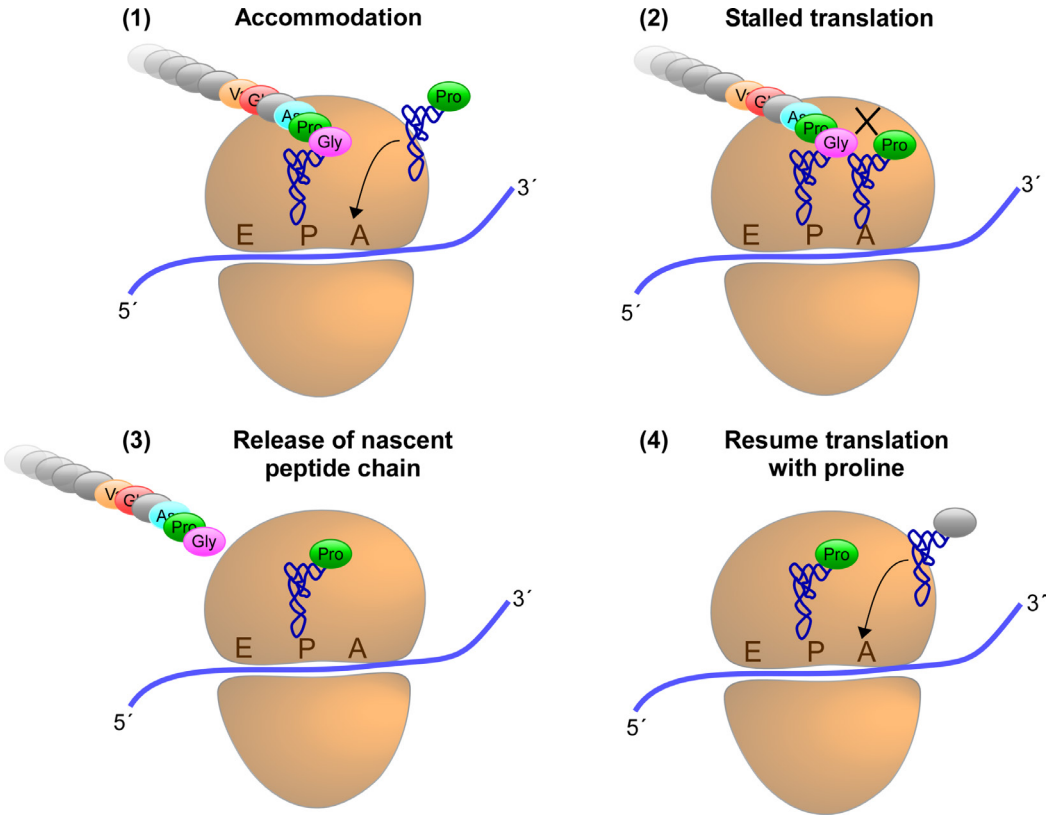

Figure 1.7: 2A peptide mediated 'stop and carry on' mechanism. The nascent peptide upstream of the 2A peptide sequences is emerging from the ribosome and translational accommodation and translocation takes place. When the prolyl-tRNA (blue/green) enters the accommodation site of the ribosome (A-site, step 1), the nascent 2A peptide interacts with the exit tunnel of the ribosome causing a sterically restricted C-terminus of the 2A peptide within the peptidyl-transferase center (P-site, step 2). The nucleophilic attack of the ester linkage of the glycyl-tRNA by the prolyl-tRNA is inhibited and the nascent peptide chain is released from the ribosome (step 3). To overcome ribosomal stalling, the prolyl-tRNA enters the ribosome and translation is resumed (step 4).

1.5 Aim of this thesis

In the past it was already successfully shown, that mRNAs bound by Rrm4 are transported through hyphae of *U. maydis* together with early endosomes. Furthermore, the accumulation of translational products of transported mRNAs on endosomes was observed. Together with the observation that active ribosomes are also part of the mRNP and that the association of ribosomal proteins in mRNPs is mRNA-dependent, the mentioned observations led to the hypothesis that local translation of transported mRNAs takes place on the endosomal surface (Baumann et al., 2014; Higuchi et al., 2014). In addition to this, a potential regulatory role of Rrm4 during translation was hypothesized because Rrm4 binds mRNA not only in the 3´UTR but also at landmark sites of translation (Olgeiser et al., 2019). The observation of translational sites of an mRNA *in vivo* enables better insides in both the translation on endosomes as well as in the regulatory role of Rrm4 during translation. Hence, this project focused on the

establishment of an antibody-based method to visualize the nascent peptide chain to analyze translational processes on endosomes as well as the role of Rrm4 in translation. On the one hand, the SunTag method should be applied in *U. maydis* to label a nascent peptide chain. For this, the GCN4-scFv had to be stably expressed in fusion to sfGfp (Figure 1.8 A). In addition to the labeling of a nascent peptide chain with GCN4-scFv-sfGfp, the analyzed mRNA should be fluorescently marked within its 3´UTR. At the beginning of this project, mRNAs were labeled within their 3´UTR with the λN system in which λN* was fused to double Gfp (Baumann et al., 2014). Because of a simultaneous visualization of a nascent peptide chain and the corresponding mRNA, the mRNA has to be labeled with a Rfp. A proper candidate for the λN system should be identified in this project (Figure 1.8 B).

On the other hand, various tools should be established that allow an optimal visualization of translation by fusion to the ORFoi. First of all, the interaction of GCN4-scFv-sfGfp to its cognate peptide epitope ($GCN4^{24}$) should be analyzed *in vivo*. Besides, a reliable degron sequence should be combined with the 2A peptide (Figure 1.8 C). The degron should enable a background-reduced fluorescence microscopy since completely translated $GCN4^{24}$ will be degraded. To maintain the equilibrium of proteins encoded by analyzed mRNAs by the integration of a degron, the 2A peptide downstream of the degron sequence and upstream of the ORFoi should enable the independent expression of $GCN4^{24}$ fused to a degron and the ORFoi from one mRNA (Figure 1.8 C).

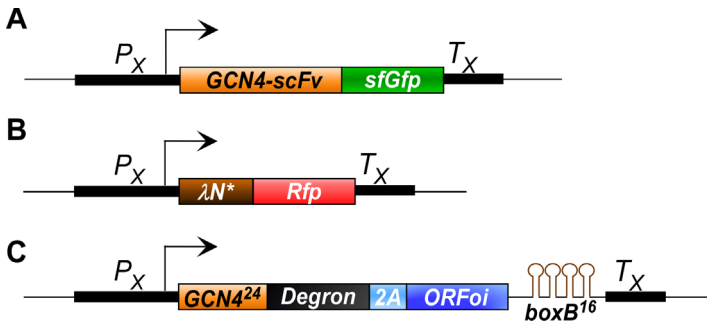

Figure 1.8: Schematic representation of desired constructs. (A) The GCN4-scFv antibody (orange) which was used in the SunTag method in fusion with sfGfp (green) to label the nascent peptide chain. **(B)** The RNA-binding protein λN* (brown) in fusion with a red fluorescence protein (Rfp, red) to fluorescently label mRNAs within their 3´UTR. **(C)** The final fusion construct of the ORF of interest (ORFoi, blue) to which upstream the peptide epitope of the GCN4-scFv antibody (GCN424, orange), a degron sequence (black) and the 2A peptide (light blue) is fused, respectively. 16 RNA stem-loops (boxB16, brown) should be integrated into the 3´UTR of the mRNA to ensure binding of λN* protein.

2 Results

2.1 Establishing of red fluorescence proteins as a marker to label mRNAs *in vivo*

To visualize local translation of mRNAs in hyphae of *U. maydis in vivo*, various building blocks of a detection system had to be established. At the beginning of this study, mRNAs in *U. maydis* were labeled with Gfp. As only sfGfp was used to label nascent peptide chains, the establishment of labeling mRNAs with a Rfp by binding to the 3´UTR was the first crucial step towards analyzing local translation of mRNAs *in vivo*. In the context of establishing TRICK in *U. maydis*, the capability of mCherry and TagRfp to label the 3´UTR of *cdc3* mRNA was already tested (Müntjes, 2015). RNA live imaging with mCherry or TagRfp was not feasible because both fluorescence proteins were visible in vacuoles due to their high stability in acidic environments. *U. maydis* tends to have a lot of vacuoles and the visible accumulations outshined moving mRNAs. For this reason, two other Rfps, mKate2 and mOrange2, were established and tested for their ability to label mRNAs *in vivo*. mKate2 and mOrange2 have the same molecular weight as Gfp and therefore should not influence the efficiency of RNA live imaging. mKate2 is a monomeric Rfp which is an optimized version of mKate (Shcherbo et al., 2009). mKate itself was produced by site-specific and random mutagenesis from TurboRfp deriving from the sea anemone *Entacmaea quadricolor* (Shcherbo et al., 2007). mOrange2 is further developed from the orange fluorescence protein mOrange (Shaner et al., 2008). mOrange is an derivate of DsRed, which originally was found in *Discosoma sp.* (Shaner et al., 2004). The excitation and emission maxima of mKate2 (588 nm/630 nm) do not differ much compared to mCherry (587 nm/610 nm). This should enable the detection with a laser operating at a wavelength of 561 nm of the given fluorescence microscopy set-up. Contrary to this, the excitation and emission of mOrange2, as the name already indicates, are more shifted to the orange spectral range of visible light (549 nm/565 nm) which could probably not be detected in full efficiency with the given fluorescence microscopy filter set. Importantly, both fluorescence proteins have a low stability in acidic environments compared to mCherry and TagRfp which could avoid visible accumulation in vacuoles (Day and Davidson, 2009).

2.1.1 Determining the expression levels of mKate2 and mOrange2 in *U. maydis*

To examine mKate2 and mOrange2, it was first necessary to analyze expression levels and intensities of both fluorescent proteins *in vivo*. To this end, the protein sequences of mKate2 and mOrange2 were fused to Rrm4 (Zhou et al., 2018). Plasmids encoding the fusion proteins were integrated at the native locus of *rrm4* by homologous recombination

in the genetic background of AB33 (Brachmann, 2001). Correct transformants were verified by PCR and by Southern blot analysis and used for further studies. To compare the intensities of mKate2 and mOrange2 with already existing Rfps, fluorescence microscopy and line scan measurements were performed in hyphae (Figure 2.1 A-D). The signals of moving Rrm4-mKate2 particles (Figure 2.1 D) appeared to be brighter than Rrm4-mCherry (Figure 2.1 A) and were comparable to those of Rrm4-TagRfp (Figure 2.1 B). In contrast to this, the signal of Rrm4-mOrange2 was barely visible (Figure 2.1 C, note the scale of the y-axis). This can be referred to a non-optimal excitation with a laser operating at a wavelength of 561 nm. The differences in the signal intensities of the Rfps were visualized and quantified using line scans, where the different absolute gray levels were directly comparable. Note that the fluorescence pictures were taken with the same laser power and without an autocorrected signal intensity. Thus, the absolute intensities are comparable. For the line scans, a background value of 100 (average value of the background fluorescence measured in 10 pictures) of each fluorescence microscopy picture was subtracted and the intensities of distinct particles (gray level) were measured. The intensities of Rrm4-TagRfp and Rrm4-mKate2 were comparable with peaks at values around 1,200-1,300. The maximum intensity of Rrm4-mCherry was determined to be around 600 (Figure 2.1 A). This underlines the first impression of an increased brightness of TagRfp and mKate2 (Figure 2.1 B and D) compared to mCherry and mOrange2 (Figure 2.1 A and C). The maximum absolute gray level of mOrange2 was around 220. For quantification, line scans of 45 hyphae from three independent experiments were conducted. For better comparison, all measured intensities were normalized to the maximum intensity of TagRfp (brightest red fluorescence protein) which was set to 100%. As indicated in Figure 2.1 E, the Rrm4 particles that were detected with TagRfp and mKate2 showed significantly increased intensities compared to mCherry. Normalized to TagRfp, the intensities of mCherry and mKate2 were determined to be around 60% and 99%, respectively (Figure 2.1 E). A normalized intensity of 7% was determined for mOrange2. Thus, mOrange2 was not further investigated because it cannot be used to visualize mRNAs with the given microscopy set-up.

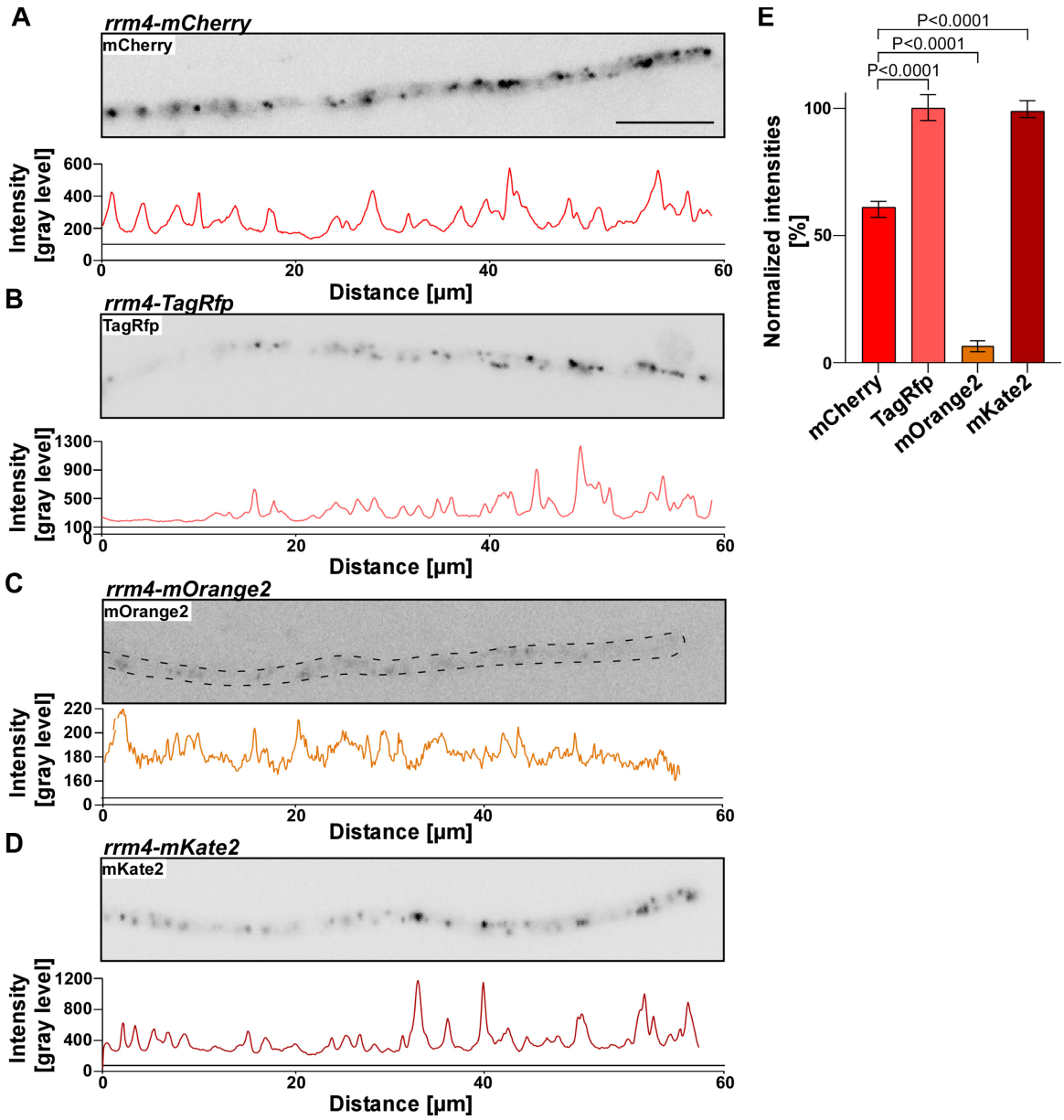

Figure 2.1: Comparison of fluorescence intensities of mCherry, TagRfp, mKate2 and mOrange2 fused to Rrm4. (A-D) Fluorescence microscopy and line scans of hyphae expressing different red fluorescence proteins fused to Rrm4. The fluorescence microscopy pictures show distribution of Rrm4-mCherry **(A)**, Rrm4-TagRfp **(B)**, Rrm4-mOrange2 **(C)** and Rrm4-mKate2 **(D)** signals. The corresponding line scans below the fluorescence microscopy pictures show an intensity profile given as gray levels. (6 h.p.i.; inverted pictures; scale bar 10 µm). **(E)** Quantification of fluorescence intensity scans through hyphae. Intensities of mCherry, mOrange2 and mKate2 tagged Rrm4 particles narmalized to the maximum intensity of TagRfp which was set to 100%. Intensity peaks below 100 were excluded for the analysis (n>30 in 3 independent experiments; error bars, SEM; unpaired two-tailed t-test; α<0.05).

In order to determine the photostability of mKate2 in comparison to mCherry and TagRfp, the shuttling of Rrm4 through hyphae was analyzed by recording movies for 75 s with a constant excitation of the fluorophore (Figure 2.2 A). In the kymograph recorded from Rrm4-mKate2, defined signals of shuttling Rrm4 particles were visualized for the whole period of time (red arrowheads). Comparatively, the shuttling of Rrm4-mCherry and Rrm4-TagRfp was also visible but the signal intensity decreases over a period of 75 s (Figure 2.2 A). Note that the signals disappeared much faster for TagRfp

than for mCherry. With mCherry, it was possible to detect moving particles for the whole period of time but the number seemed to be decreased. However, mKate2 seemed to be more photostable than TagRfp and mCherry which allows a detailed analysis of subcellular localization of fusion proteins over an extended period of time. Because of the fact that the pH stability of mCherry and TagRfp results in strong fluorescence in vacuoles and that this causes difficulties in quantification and the detection of cognate fusion proteins, mKate2 was analyzed with respect to the visibility in vacuoles. To analyze the accumulation in vacuoles, strains capable of cytosolic expression of mCherry, TagRfp or mKate2 were investigated. Plasmids were integrated at the *ip*^{S} locus (see 2.2.1 for further information) via homologous recombination in the genetic background of AB33. Single insertion strains, which were confirmed by PCR and Southern blot analysis, were used for further studies. For co-localization experiments, hyphae expressing different fluorescence proteins were labeled with CellTracker™ Blue (CMAC) which is a fluorescent chloromethyl derivate that stains vacuolar membranes. Due to high fluctuation of the vacuolar system, images of CMAC staining were taken in close successions to green or red fluorescence pictures. As control, a strain with cytosolic expression of Gfp (eGfp, enhanced version of Gfp) was used, because a visible accumulation of Gfp in vacuoles of hyphae of *U. maydis* was not observed before. In addition, Gfp exhibits low pH stabilities *in vitro* (Ishii et al., 2007). As indicated by red arrowheads in Figure 2.2 B and E, the Gfp and mKate2 fluorescence were not visible in vacuolar structures. Both fluorescence signals seemed to lose their ability to emit a signal upon excitation under acidic conditions. Contrary to this, TagRfp (Figure 2.2 C) as well as mCherry (Figure 2.2 D) were visible in the whole cell including vacuolar structures.

In summary, these results show that mKate2 is a bright fluorescence protein possessing high photostability compared to mCherry and TagRfp in *U. maydis*. In addition, it is presumably not stable at low pH values because no visible accumulation in vacuoles was detected. To analyze whether mKate2 can be used to visualize the localization of mRNAs *in vivo*, RNA live imaging was conducted.

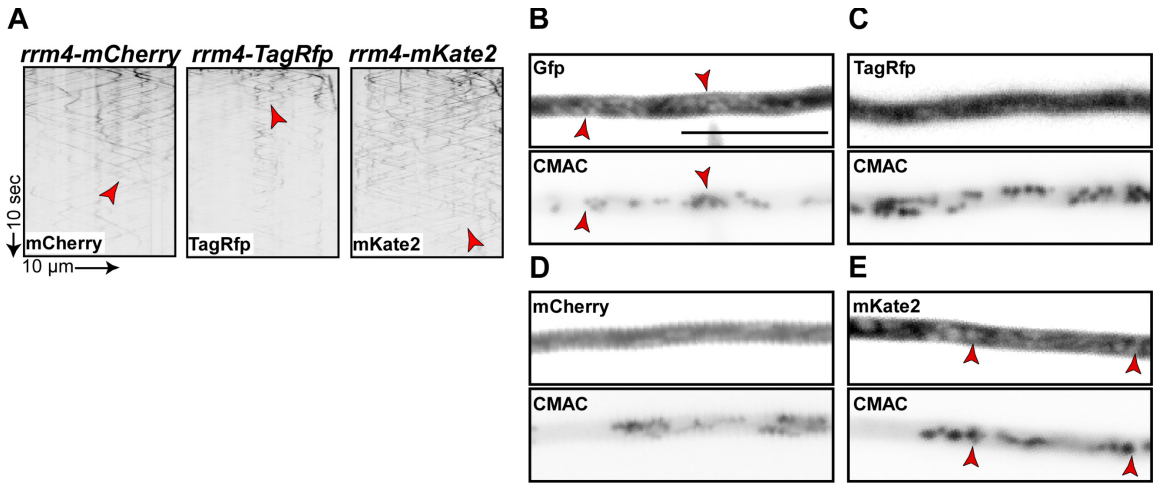

Figure 2.2: Analysis of mCherry, TagRfp and mKate2 expressed in hyphae of *U. maydis* regarding their photo and pH stability. (A) Kymographs of hyphae expressing different Rrm4 fusions to red fluorescence proteins (6 h.p.i.; arrow length on the left and bottom indicates time and distance; inverted pictures). Bidirectional movement is indicated by red arrowheads. **(B-E)** Micrographs of hyphae capable of cytosolic expression of Gfp (**B**, top), TagRfp (**C**, top), mCherry (**D**, top) and mKate2 (**E**, top) and the corresponding CMAC staining (bottom) to analyze accumulation of fluorescent proteins in vacuolar structures (6 h.p.i.; inverted pictures; scale bar 10 µm). Red arrowheads in **(B)** and **(E)** indicate vacuoles stained with CMAC.

2.1.2 Usage of mKate2 to visualize movement of *cdc3* mRNA

RNA live imaging was carried out by labeling the well-studied *cdc3* mRNA (Baumann et al., 2014; Zander et al., 2016) with mKate2 by using defined RNA hairpins within its 3´UTR. By using a comparable integration construct design, this enabled a direct comparison to the published system which uses λN* fused to two copies of Gfp (Baumann et al., 2014). For this, the RNA-binding protein λN* was fused to two copies of mKate2 (λN*mKate2^2) under the control of the inducible promoter from the arabinase gene *crg1* which is active in the presence of arabinose and inactive in the presence of glucose (P_{crg}; Bottin et al., 1996; Brachmann, 2001). The plasmid expressing the fusion protein was integrated into the *ip^S* locus via homologous recombination in the genetic background of AB33 and harbors 16 copies of boxB binding sites (B^{16}) integrated into the 3´UTR of *cdc3* (AB33-*cdc3*B^{16}). After identifying positive recombination events by Southern blot analysis, RNA live imaging was conducted with the strain AB33-λN*mKate2^2/*cdc3*B^{16} and AB33-λN*Gfp^2/*cdc3*B^{16} as control. By analyzing the movement of *cdc3* mRNAs in AB33-λN*Gfp^2/*cdc3*B^{16}, cytoplasmic green fluorescence was observed. Due to this high background noise, the movement of *cdc3* mRNAs was barely visible (Figure 2.3 A, indicated by red arrowheads). In comparison, the background noise was reduced when detecting signals of *cdc3* mRNA with λN*mKate2^2 (Figure 2.3. B). Hence, shuttling of *cdc3* mRNA was clearly visible as indicated in the kymograph by red arrowheads (Figure 2.3. B). In addition to weaker *cdc3* mRNAs, shuttling signals with

higher fluorescence intensities were observed (yellow arrowhead; Figure 2.3 B). To verify whether these particles were mRNA-dependent, the λN*mKate2^2 fusion protein was integrated at the *ip^S* locus by homologous recombination in the genetic background of AB33. After Southern blot analysis for the verification of correct transformants, fluorescence microscopy of AB33-λN*mKate2^2 was conducted. Because of the fact that B^{16} was not integrated in a 3´UTR of an mRNA, no binding sites for λN*mKate2^2 were present. Thus, signals of moving particles should not be attributed to mRNA shuttling. In comparison to AB33-λN*mKate2^2/*cdc3*B^{16}, no shuttling particles were detectable in the strain only expressing λN*mKate2^2 (Figure 2.3 C). Due to this, it can be assumed that the shuttling signals with higher fluorescence intensities were mRNA-dependent.

In summary, these experiments show that mKate2 can be used to label mRNAs *in vivo*. The low fluorescence background enabled a noise-reduced detection of mRNAs. The visible and moving fluorescence accumulations will probably not interfere with further experiments and seemed to be mRNA-dependent.

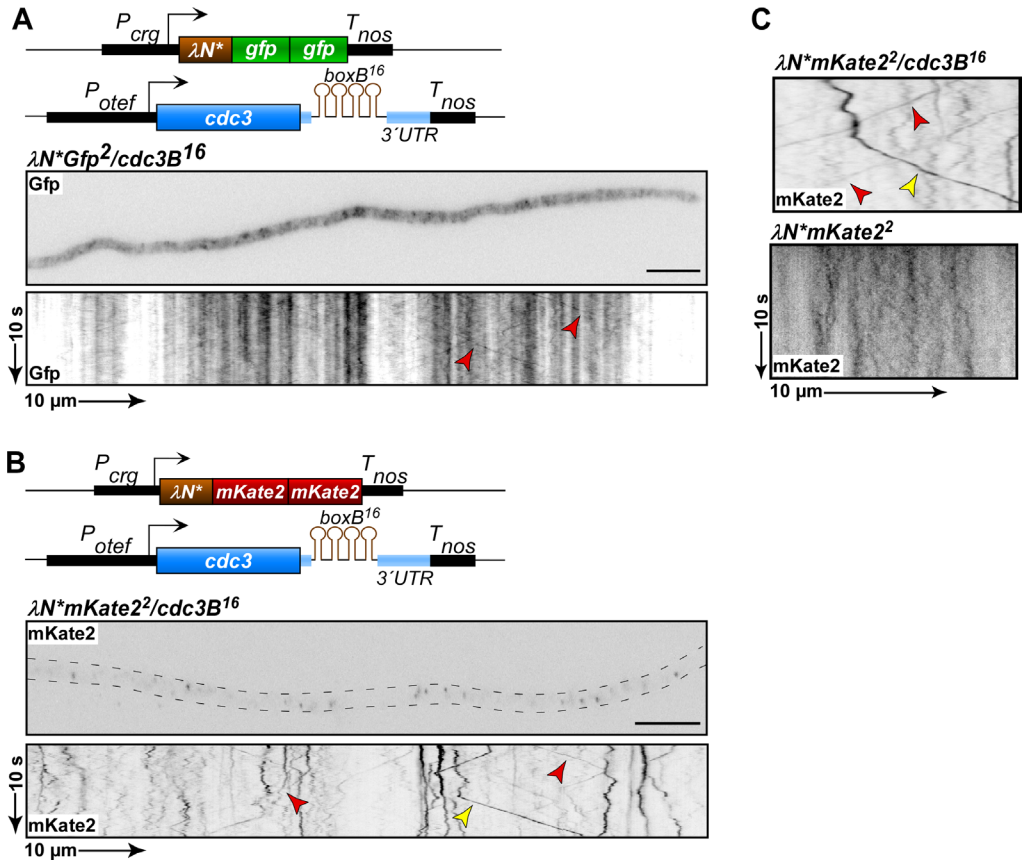

Figure 2.3: RNA live imaging with mKate2 to visualize movement of *cdc3* mRNA. (A-B) Top: Schematic representation of constructs necessary for RNA live imaging: RNA binding protein λN* (brown) fused to two copies of Gfp (green, Gfp^2) or two copies of mKate2 (red, mKate2^2), inducible promoter P$_{crg}$ and terminator T$_{nos}$ (both black). 16 copies of boxB RNA hairpins (brown, B^{16}) were integrated into the 3´UTR of *cdc3* mRNA (blue). Bottom: Fluorescence microscopy and kymographs of hyphae of an AB33 derivative expressing the λN* system to label the *cdc3* mRNA. Moving mRNAs are indicated by red arrowheads. Shuttling signals with higher fluorescence intensities are indicated by yellow arrowheads (6 h.p.i.; arrow length on the left and bottom of kymograph indicates time and distance; inverted pictures; scale bar 10 µm).

(C) Kymographs of hyphae of AB33 derivatives expressing the λN* system to label the *cdc3* mRNA (top) or λN* fused to mKate2[2] only (bottom). Moving mRNAs are indicated by red arrowheads. Brighter moving fluorescence protein accumulations are indicated by yellow arrowheads (6 h.p.i.; arrow length on the left and bottom of kymograph indicates time and distance; inverted pictures).

2.2 Expression of heterologous antibodies for the labeling of nascent peptide chains

In order to establish a system to visualize local translation in hyphae of *U. maydis*, the expression of a heterologous antibody for the labeling of nascent peptide chains was the most crucial part since the detection of a nascent peptide chain is based on a fluorescently labeled antibody. In a previous study in which a scFv was fused to different N- and C-terminal fusion proteins, it was found that sfGfp almost completely eliminated protein aggregation (Tanenbaum et al., 2014). Thus, for labeling nascent peptides, the expressed antibodies were fused to sfGfp. For the expression of heterologous antibodies, first of all, a suitable locus had to be found because the well-studied ip^S locus is needed for the expression of the fluorescently labeled RBP to mark the mRNA. For this, two protease loci were analyzed regarding their capability of a homogeneous distribution of expression within the population. Afterwards, different single chain variable fragments (scFv) as well as nanobodies (Nb) were expressed in *U. maydis* and examined for their expression levels and localization.

2.2.1 Establishment of aspartic protease *upp3* locus to express heterologous proteins

The so-called ip^S locus is the best known and most widely used locus to express heterologous proteins in *U. maydis*. The ip^S gene expresses the succinate dehydrogenase iron-sulfur protein subunit SDH2 (UMAG_00844). Insertion of a mutant version (ip^R), in which two point mutations are inserted, mediates resistance against carboxin (Keon et al., 1991). Due to the fact that the RNA-binding protein λN*, which is needed to label the 3´UTR of the mRNA of interest will be expressed in this locus, another genomic locus was needed for the expression of an antibody. In a previous study, several protease genes were deleted to increase the yield of secreted proteins in *U. maydis* (Sarkari et al., 2014). The deletion of the genes *pep4* (UMAG_04926), *upp2* (UMAG_00064), *upp3* (UMAG_11908) and *prb1* (UMAG_04400) had no effect on the growth of sporidial cells. As protease deletions tend to have no severe effects on the phenotype in *U. maydis*, the respective genomic regions are potential loci to express heterologous proteins. The *pep4* locus was already used to express heterologous proteins. However, the expression of Gfp seemed to be heterogeneous (data not shown). This effect could not be observed for the ip^S locus. Because of this, the *upp2*

and *upp3* protease deletion mutants were analyzed. First of all, single deletion strains were generated in the genetic background of AB33 (AB33-*upp3*Δ; AB33-*upp2*Δ) and the morphology of sporidia as well as of hyphae was analyzed. Both growth forms did not show any morphological differences compared to the wild type strain (data not shown). Because there was no apparent effect of the deletion, Gfp was integrated into the genetic regions of *upp2* and *upp3* by homologous recombination into the genetic background of AB33-*upp3*Δ and AB33-*upp2*Δ strains, respectively. This was done to analyze the distribution of expression within the population. A huge advantage of using single protease deletions was that a counter-selection procedure was feasible to accelerate strain generation. The deletion of the genes was achieved by introducing a hygromycin resistance cassette as marker, while Gfp was inserted in the same locus with a nourseothricin resistance cassette as marker afterwards. Potential positive transformants lose their resistance against hygromycin and gain nourseothricin resistance. This can be tested easily with a plate assay. After verifying correct transformants by Southern blot analysis, fluorescence microscopy was performed. As indicated in Figure 2.4 A, no high variation of expression could be observed for Gfp integrated into the ip^S and the *upp3* locus. Contrary to this, the Gfp expression level was heterogeneous in the *pep4* and the *upp2* locus in which hyphae with a reduced Gfp expression were observed (Figure 2.4 A). To quantify this effect, the numbers of hyphae showing a reduced Gfp fluorescence (dim expressing cells) from the protease loci were compared to the ip^S locus (Figure 2.4 B). Importantly, dim expressing cells were visible in all strains. However, no significant difference was visible between the dim expressing cells of the ip^S and the *upp3* locus, contrary to the *pep4* and the *upp2* locus. In the latter, 55% or 84% dim expressing cells were detected, respectively (Figure 2.4 B). Importantly, the measured RFUs did not differ significantly between the ip^S and the *upp3* locus (Figure 2.4 C). In both strains RFU values of approximately 20,000 were measured.

In summary, these results show that the *upp3* locus can be used to express heterologous proteins in *U. maydis* with a homogeneous expression within the population and expression rates which are comparable to the ip^S locus. In addition, this locus enables rapid strain generation via counter-selection.

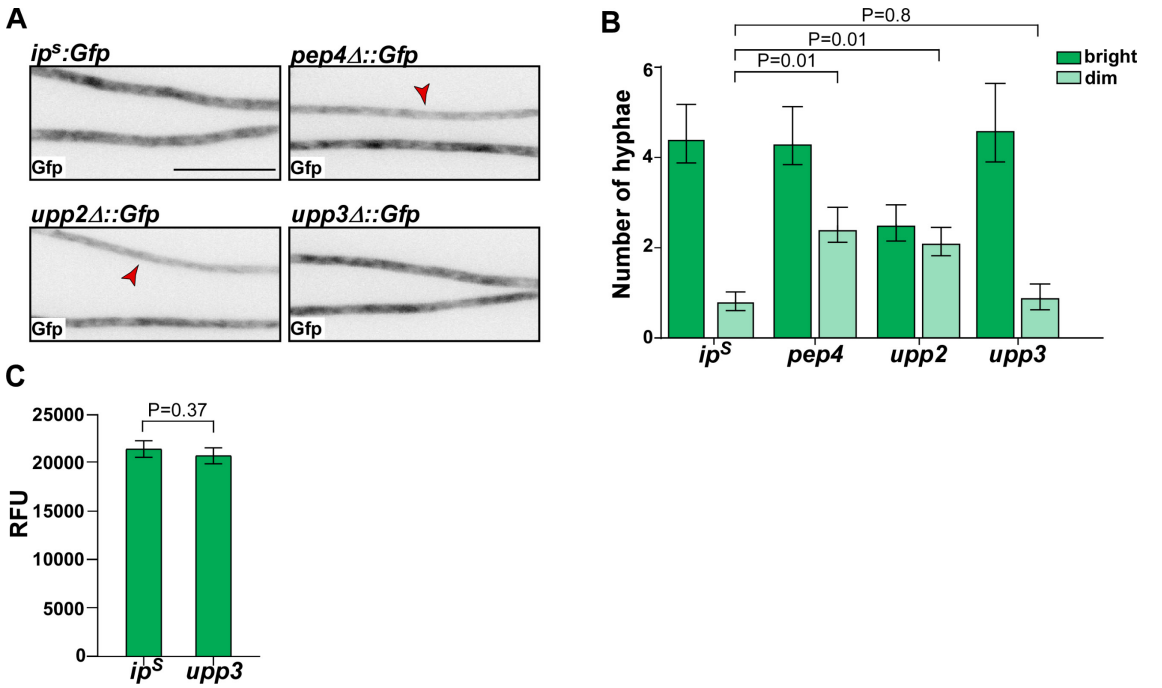

Figure 2.4: **Analysis of the distribution of Gfp expression from different loci within the population of hyphal growing cells. (A)** Micrographs of hyphae of AB33 derivates expressing Gfp from different loci. Hyphae showing lower expression of Gfp are marked with red arrowheads (6 h.p.i.; inverted pictures; scale bar 10 µm). **(B)** Quantification of bright and dim Gfp expressing cells in different loci (n>10 in 3 independent experiments; error bars, SEM; unpaired two-tailed t-test; α<0.05). **(C)** Comparison of Gfp expression in the *ip*^{S} and the *upp3* locus (3 independent experiments; RFU: relative fluorescence units; error bars, SEM; unpaired two-tailed t-test; α<0.05).

2.2.2 Expression of heterologous antibodies in *U. maydis*

2.2.2.1 Expression of Myc-scFv, Bot-Nb and GCN4-scFv in hyphae of *U. maydis*

The usage of an antibody to label the nascent peptide chain is crucial. Thus, different antibodies were fused to sfGfp and the expression level in hyphae was analyzed. The first two antibodies that were investigated for their capability to label a nascent peptide chain, a scFv against the myc epitope (Myc-scFv) and a nanobody against the botulinum toxin (Bot-Nb), were already expressed in fusion to the chitinase Cts1 in sporidia of *U. maydis* (Sarkari et al., 2014; Terfrüchte et al., 2017). To analyze the expression levels of both antibodies in the context of labeling a nascent peptide chain, they were fused to sfGfp (Figure 2.5 A). The transcription of the construct was controlled by the constitutive *tef* promoter (P_{tef}) from the elongation factor 1 of *U. maydis* (Figure 2.5 A; Spellig et al., 1996). The constructs expressing the fusion proteins were transformed into the genetic background of AB33-*upp3*Δ via homologous recombination, and positive candidates were identified via counter-selection. After verifying positive recombination events by Southern blot analysis, the expression of the encoded constructs was analyzed by Western blot experiments. The Western blot analysis of whole cell lysate of positive clones in sporidial and hyphal cells confirmed that the expression of the Myc-scFv-sfGfp

construct was reduced in hyphae compared to sporidia (Figure 2.5 B). In hyphae, only a faint band of the full length protein was visible. The expression of Bot-Nb-sfGfp was barely visible in both growth forms. Here, only hardly visible bands for the full-length protein were detectable by Western blot analysis using an α-Gfp antibody (Figure 2.5 C). Because the intended application of the antibodies is needed in hyphae, these antibody candidates were not further investigated.

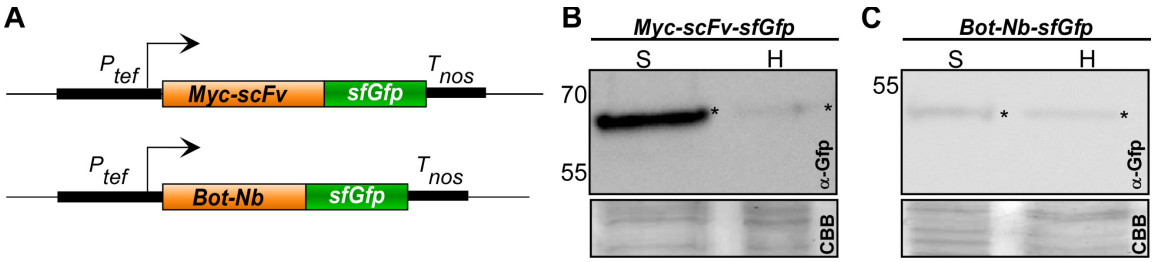

Figure 2.5: Expression of Myc-scFv-sfGfp and Bot-Nb-sfGfp in sporidia and hyphae of *U. maydis*. (A) Schematic representation of the fusion constructs of Myc-scFv and Bot-Nb (orange) fused to sfGfp (green). The constructs are expressed under control of P_{tef} (black) and terminated with T_{nos} (black). **(B/C)** Western blot analysis of the expression of Myc-scFv-sfGfp **(B)** and Bot-Nb-sfGfp **(C)** in sporidial (S) and hyphal (H) cells 6 h.p.i. 5 µg of whole cell extracts were subjected to SDS-PAGE and Western blot analysis. Both antibodies were detected via sfGfp and the membrane was stained with Coomassie brilliant blue after detection (CBB). Bands representing full-length protein of both antibodies are marked with asterisks.

The next antibody which was analyzed was the scFv against the transcriptional master regulator GCN4 (GCN4-scFv) from *S. cerevisiae*, which was originally used for signal amplification in gene expression and fluorescence imaging (Tanenbaum et al., 2014). This antibody was already successfully used to label a nascent peptide chain in mammalian cells (Pichon et al., 2016; Wang et al., 2016; Wu et al., 2016; Yan et al., 2016). Note that neither the GCN4 protein nor homologous proteins are present in *U. maydis*. The fusion protein was integrated in the genetic background of AB33-*upp3*Δ. A Western blot analysis of whole cell lysates of positive clones in sporidial and hyphal cells confirmed that the GCN4-scFv-sfGfp was expressed in equal amounts in both growth forms (Figure 2.6 B). Fluorescence microscopy was conducted to analyze the subcellular localization in a strain lacking a cognate peptide epitope of GCN4-scFv-sfGfp. Because of this genetic background, a cytosolic distribution of the Gfp fluorescence signal was expected. However, fluorescence microscopy revealed that the GCN4-scFv-sfGfp fusion protein localized in a manner reminiscing of microtubule-like structures within hyphae of *U. maydis*. In addition to this, recording a movie and generating a kymograph revealed shuttling of GCN4-scFv-sfGfp through the hyphae along stained tracks (red arrowheads; Figure 2.6 C). Because this shuttling resembled the movement of mRNP components which shuttle on the endosomal surface, a co-localization study using FM4-64 was performed. The styryl dye FM4-64 visualizes endocytic pathway components like early and late endosomes and multivesicular bodies.

The localization analysis of GCN4-scFv-sfGfp and FM4-64 revealed a co-localization of both fluorescence signals, as indicated by red arrowheads in Figure 2.6 D. Thus, the GCN4-scFv-sfGfp seemed to localize to endocytic compartments. To further characterize whether the shuttling of GCN4-scFv-sfGfp with endocytic compartments is dependent on microtubules, hyphae were treated with benomyl. Benomyl is a benzimidazole fungicide which binds to microtubules and inhibits polymerization and thus shuttling of endosomes. As indicated in Figure 2.6 E, GCN4-scFv-sfGfp stopped shuttling through hyphae after benomyl treatment. Thereby, the shuttling of GCN4-scFv-sfGfp appeared to be dependent on the endocytic compartment as well as on microtubules. To finally characterize the specificity of the shuttling signals, co-localization studies with different endosomal marker proteins were performed. For this, Rab5a-mKate2 and Rab7-mKate2 fusion proteins were integrated in the genetic background of AB33-GCN4-scFv-sfGfp. Rab5a mainly localizes to early and Rab7 mainly to late endosomes, respectively. Note, that Rab7 does not shuttle as extensively within the hyphae as Rab5a (Haag et al., 2017). Analyzing the strains expressing GCN4-scFv-sfGfp and either Rab5a-mKate2 or Rab7-mKate2 revealed a co-localization of GCN4-scFv-sfGfp to Rab5a-positive endosomes, but not to Rab7-positive endosomes (Figure 2.6 F and G). Thereby, GCN4-scFv-sfGfp seemed to specifically localize to early endosomes.

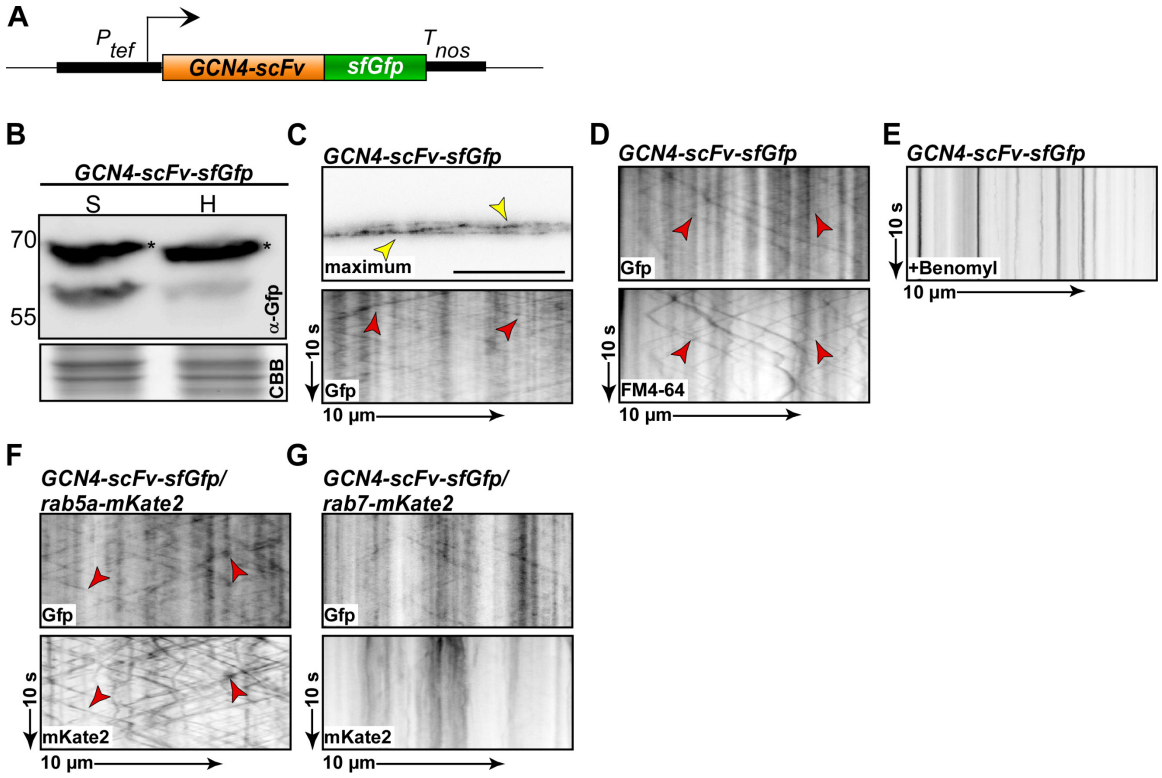

Figure 2.6: Analysis of the expression and localization of the GCN4-scFv in *U. maydis*. (A) Schematic representation of the fusion construct of the GCN4-scFv (orange) fused to sfGfp (green). The construct is expressed under control of P_{tef} (black) and terminated with T_{nos} (black). **(B)** Western blot analysis of the

expression of GCN4-scFv-sfGfp in sporidial (S) and hyphal (H) cells 6 h.p.i. 5 µg of whole cell extracts were subjected to SDS-PAGE and Western blot analysis. GCN4-scFv-sfGfp was detected via sfGfp and the membrane was stained with Coomassie brilliant blue after detection (CBB). Bands representing full-length protein of GCN4-scFv-sfGfp are marked with asterisks. **(C)** Micrograph and kymograph of an hypha of AB33 derivative expressing GCN4-scFv-sfGfp in *upp3* locus. Staining of microtubule-like structure is indicated by yellow arrowheads. Shuttling particles are indicated by red arrowheads. **(D)** Kymographs of GCN4-scFv-sfGfp expressing hypha showing the Gfp signal and staining with FM4-64. Co-localization events are indicated by red arrowheads. **(E)** Kymograph of GCN4-scFv-sfGfp expressing hypha treated with benomyl for two hours. **(F)** Kymographs of GCN4-scFv-sfGfp/Rab5a-mKate2 expressing hypha showing the Gfp and the mKate2 signal. Co-localization events are indicated by red arrowheads. **(G)** Kymographs of GCN4-scFv-sfGfp/Rab7-mKate2 expressing hypha showing Gfp and mKate2 signals (**D-G**: 6 h.p.i.; inverted pictures; arrow length on the left and bottom of kymograph indicate time and distance).

The GCN4-scFv binds to a 19 amino acid peptide epitope with the amino acid sequence EELLSKNYHLENEVARLKK. Because of the unspecific shuttling of GCN4-scFv-sfGfp, a sequence comparison of the epitope against the whole proteome of *U. maydis* was performed. By this, proteins which have a comparable sequence were identified. Because of the shortness of the peptide epitope, more than 100 proteins were identified containing a sequence which is comparable, including Kinesin-7a (UMAG_00896) and Tea1 (UMAG_15019). In both proteins, several amino acid stretches were found sharing up to 80% identity with the peptide epitope of GCN4-scFv. Kinesin-7a is a CENP-E-like motor protein without any defect in cell morphology after deletion in *U. maydis* and is thought to play a role in membrane trafficking or mitosis/meiosis (Schuchardt et al., 2005). Note that Kinesin-7a was initially published as Kinesin-1 (Lehmler et al., 1997). Tea1 is a kelch domain protein, which is involved in marking cell poles and sites of growth (Tatebe et al., 2005). The microtubule cytoskeleton and microtubule-associated proteins are crucial for the localization of Tea1 (Mata and Nurse, 1997; Busch et al., 2004). In *U. maydis*, Tea1 is a multidomain protein necessary for establishing the axis of polarity, septum positioning and cell wall integrity (Woraratanadharm et al., 2018). Because both proteins seem to be directly or indirectly involved in transport processes on microtubules, deletions of both proteins should be investigated in the genetic background of GCN4-scFv-sfGfp to analyze if one of these proteins is actually bound and visualized by this antibody fusion. In the context of this project, it was not possible to delete *tea1*. Tea1 fused to Gfp localized to the growing pole of sporidia and hyphae. Shuttling of Tea1-Gfp could not be observed in hyphae of *U. maydis* (data not shown). This decreases the probability that GCN4-scFv-sfGfp interacts with Tea1 which would result in shuttling signals. The deletion of *kin7a* was feasible in the strain expressing GCN4-scFv-sfGfp, but did not inhibit the movement of GCN4-scFv-sfGfp within hyphae of *U. maydis* (Figure 2.7 A). By quantifying the number of particles per 10 µm of hyphae, no significant difference was detected between the GCN4-scFV-sfGfp and GCN4-scFv-sfGfp/*kin7a*Δ strains (Figure 2.7 B). Thus, both proteins found by sequence comparison seemed not to be responsible for the unspecific shuttling of GCN4-scFv.

In summary, these experiments showed that the expression of heterologous antibodies were differed between the two growth forms of *U. maydis*. Unexpectedly, GCN4-scFv-sfGfp, which was expressed in sporidia as well as in hyphae, shuttled through hyphae of *U. maydis*. GCN4-scFv-sfGfp seemed to localize to early endosomes and the shuttling was dependent on microtubules. The analysis of potential interacting proteins did not reveal a direct interaction partner which is responsible for the unspecific shuttling. In conclusion, GCN4-scFv-sfGfp seemed to be unsuitable to label a nascent peptide chain. Therefore, other heterologous antibodies were tested and their expression profile as well as their localization within the cell were analyzed.

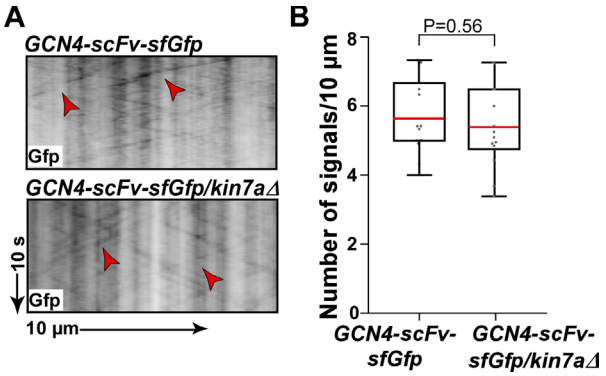

Figure 2.7: Effect of *kinesin-7a* deletion on shuttling GCN4-scFv-sfGfp units . (A) Kymographs of cells expressing GCN4-scFv-sfGfp without (top) and with (bottom) deletion of *kin7a*. Shuttling particles are indicated by red arrowheads (6 h.p.i.; inverted pictures; arrow length on the left and bottom of kymograph indicate time and distance). **(B)** The number of particles per 10 µm of hyphae was quantified with respect to the effect of the deletion of *kin7a* (Box and whisker plot with median shown in red; n>30 in 3 independent experiments; unpaired two-tailed t-test; $\alpha<0.05$).

2.2.2.2 BC2-Nb and Moontag-Nb

Because of the unspecific shuttling of GCN4-scFv, two additional antibodies were expressed and analyzed with respect to their localization in *U. maydis*. The first antibody, BC2-Nb, was originally generated against β-catenin and binds to its peptide epitope with a very high affinity (Braun et al., 2016). In addition, the interaction relies on sequence-independent backbone interactions. Therefore, the chance of an unspecific binding of BC2-Nb to other sequences was considered small. The Nb was already successfully used to tag proteins specifically in direct stochastic optical reconstruction microscopy (dSTORM) in mammalian and yeast cells, respectively (Virant et al., 2018). The second antibody, Moontag-Nb, binds a 15 amino acid long peptide from the HIV envelope protein complex subunit gp41 (Lutje Hulsik et al., 2013). It was used to study translational heterogeneity in mammalian cells in combination with the GCN4-scFv (Boersma et al., 2019). The sequences from both antibodies were optimized for dicodon usage in *U. maydis* and plasmids expressing fusion proteins to sfGfp were generated

(Figure 2.8 A). After verifying correct insertion at the *upp3* locus via homologous recombination in the genetic background of AB33-*upp3*Δ, Western blot analysis as well as fluorescence microscopy were performed. As indicated in Figure 2.8 B and F, both nanobodies were expressed in sporidia as well as in hyphae. The expression level of BC2-Nb seemed to be decreased in sporidia compared to hyphae. This should not interfere with further applications because the translation of mRNAs should be analyzed in hyphae. Surprisingly, both nanobodies shuttled throughout the whole hyphae and stained a microtubule-like structure (Figure 2.8 C and G; red and yellow arrowheads). On the basis that GCN4-scFv-sfGfp showed the same localization, both strains expressing the nanobodies were stained with FM4-64 and treated with benomyl, respectively. In fact, both nanobodies co-localized to FM4-64 shuttling particles in a microtubule-dependent manner (Figure 2.8 D, H, E and I). In consequence of the fact that three antibodies shuttled through hyphae of *U. maydis*, sfGfp was analyzed in more detail. For this, a construct in which the antibody sequence was removed from the original construct was generated (Figure 2.8 A). By this, the possibility of an interaction of the different construct components to early endosomes or microtubules could be excluded. As indicated in Figure 2.8 J, within the strain expressing sfGfp in the *upp3* locus, no shuttling particles could be observed. Thus, the previously observed shuttling of the different antibodies seemed to be antibody-specific.

In summary, these results show that three antibodies, GCN4-scFv, BC2-Nb and Moontag-Nb, shuttled bidirectionally through hyphae of *U. maydis*, most likely coupled to early endosomes, in a microtubule-dependent manner. To characterize the shuttling behavior, the next important step was to analyze whether the shuttling could be referred to a direct protein-protein interaction and consequently an accidental recruitment of antibodies to endosomes.

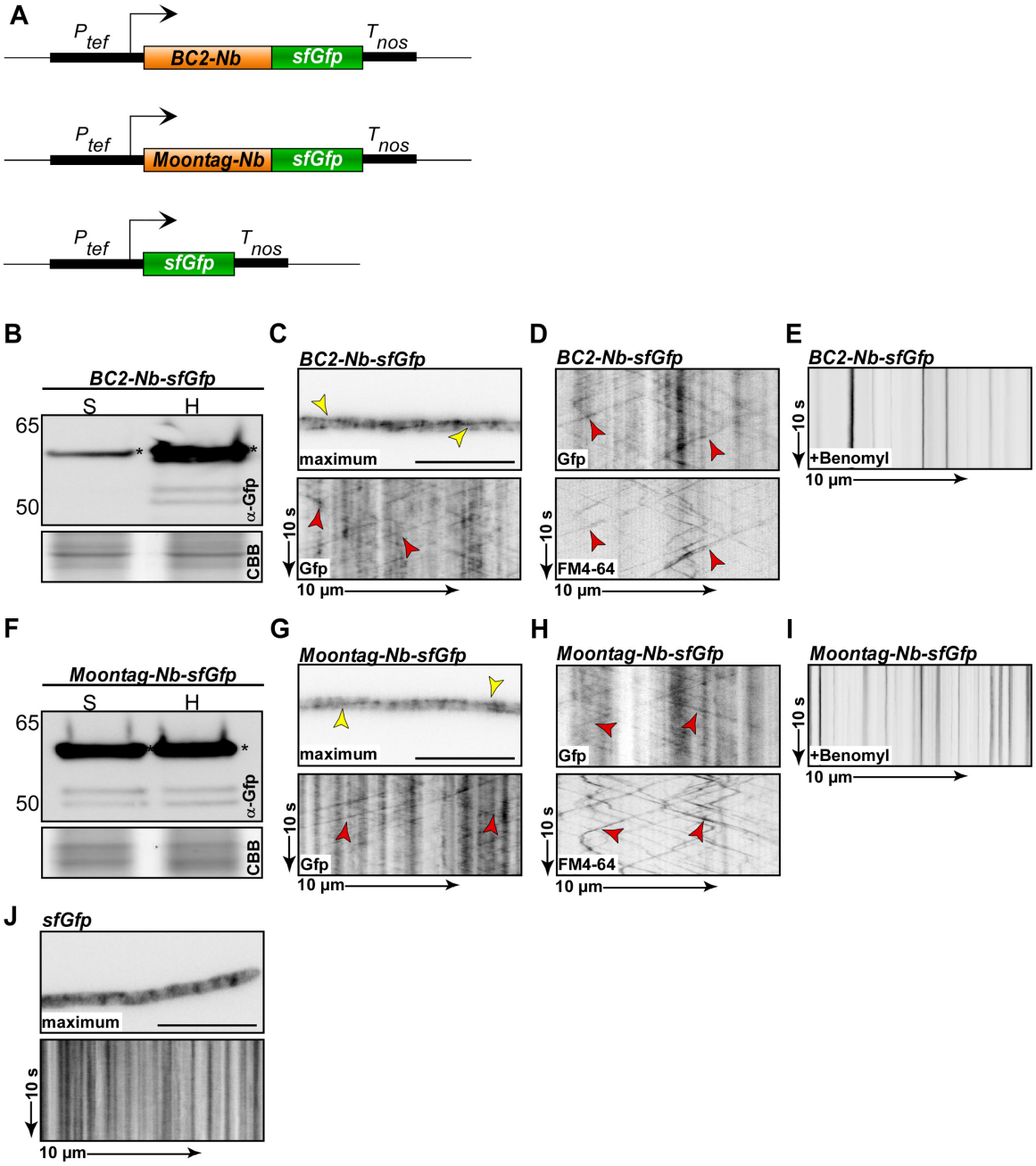

Figure 2.8: Analysis of the expression and localization of BC2-Nb and Moontag-Nb in *U. maydis*. (A) Schematic representation of the fusion constructs of the antibodies (orange) fused to sfGfp (green). All constructs are expressed with P_{tef} (black) and terminated with T_{nos} (black). **(B/F)** Western blot analysis of the expression levels of antibodies in sporidial (S) and hyphal (H) cells 6 h.p.i. 5 µg of whole cell extracts were subjected to SDS-PAGE and Western blot analysis. BC2-Nb-sfGfp and Moontag-Nb-sfGfp were detected via sfGfp and the membranes were stained with Coomassie brilliant blue after detection (CBB). Bands representing full-length proteins are marked with asterisks. **(C/G)** Micrograph and kymograph of hypha expressing different antibodies. Staining of microtubule-like structures is indicated by yellow arrowheads. Shuttling particles are indicated by red arrowheads. **(D/H)** Kymographs of hyphae stained with FM4-64 expressing different antibodies fused to sfGfp. Co-localization events are indicated by red arrowheads. **(E/I)** Kymograph of hypha expressing BC2-Nb or Moontag-Nb treated with benomyl for two hours. **(J)** Kymograph of hypha expressing sfGfp in the *upp3* locus. (**C-J**: inverted pictures; arrow length on the left and bottom of kymograph indicate time and distance).

2.2.3 Analysis of direct protein-protein interactions

To analyze whether the shuttling of antibodies is referable to a direct protein-protein interaction, a so-called Far-Western blot experiment was performed (Hall, 2004). For this, cell extracts of hyphal wild type cells, a Gfp expressing strain (AB33-Gfp) as well as a strain expressing Pab1-mCherry (AB33-Pab1-mCherry) were generated and 10 µg of total cell extract were used for SDS-Page followed by Western blotting. The membrane-bound cell extract of AB33-Gfp was used as an internal control. Two identical blotting-membranes were generated which were subsequently treated differently. The first membrane (membrane A) was incubated with natively obtained cell extracts of sfGfp expressing sporidia. The second membrane (membrane B) was incubated with natively obtained cell extracts of GCN4-scFv-sfGfp expressing sporidia. After incubation of the membranes with native cell extracts, signal detection was performed using an α-Gfp antibody directed against the sfGfp of both cell extracts as well as the membrane-bound Gfp from AB33-Gfp. Subsequently, incubation with the secondary α-mouse HRP antibody enabled final detection (Figure 2.9 A). By this, a potential interaction of GCN4-scFv-sfGfp to proteins should be visible because it serves as primary antibody in this method. As indicated in Figure 2.9 B on membrane A, no protein bands except the membrane-bound Gfp with a size of 28 kDa were detected. On membrane B, which was incubated with native cell extracts from sporidia expressing GCN4-scFv-sfGfp, different protein bands were visible with a size of 70-130 kDa (Figure 2.9 B). A strong band was detectable at the size of 130 kDa. The bands occurred in all three blotted cell extracts at the same height emphasizing a strain-independent result. It can be claimed that GCN4-scFv-sfGfp seemed to be able to interact with proteins of *U. maydis*. The unknown interacting proteins appeared at the size of around 130 kDa.

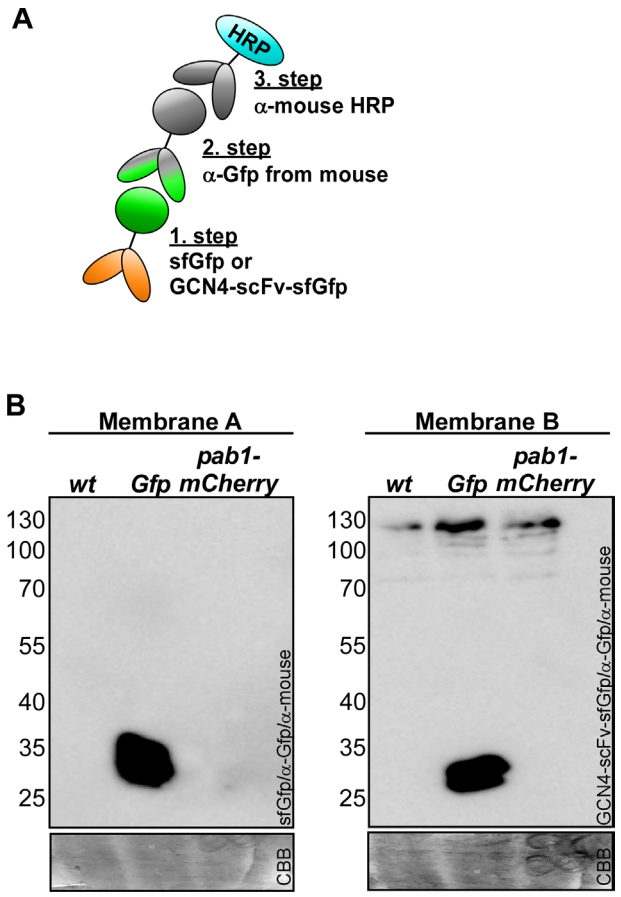

Figure 2.9: Western blot analysis to confirm protein-protein interaction of GCN4-scFv to an unknown protein partner. (A) Schematic representation of Far-Western blots with GCN4-scFv (orange) fused to sfGfp (green), α-Gfp antibody (green/gray) and α-mouse HRP (gray/blue). **(B)** Western blot membranes incubated with native purified sfGfp (membrane A) or GCN4-scFv-sfGfp (membrane B). 10 µg of whole cell extracts of wild type (wt), AB33-Gfp or AB33-Pab1-mCherry strains were subjected to Western blot analysis with three-step antibody system. Interacting GCN4-scFv-sfGfp was detected as shown in A. Membranes were stained with Coomassie brilliant blue (CBB) after detection.

There are three possible ways in which an interaction between the antibodies and an unknown protein could take place. The first one is based on the peptide epitope, the second one is sequence- and the third one is structure-based, respectively. The three peptide epitopes recognized by GCN4-scFV, BC2-Nb and Moontag-Nb were compared and studied concerning analogous sequences. First of all, it became clear that the three peptide epitopes differ in the recognized amino acid numbers. Whereas GCN4-scFv recognizes 19 amino acids, BC2-Nb and Moontag-Nb recognize peptide epitopes with a length of 12 and 15 amino acids, respectively. The sequence comparison showed a low similarity between the three peptide epitopes without any consensus amino acid stretch (Figure 2.10 A). Similar amino acids in all three peptide epitopes are highlighted in black, similarities in two epitopes are marked in gray, respectively. Only some amino acids, marked in gray in Figure 2.10 A, were similar. Therefore, the possibility of an interaction based on the binding of an unknown protein to all peptide epitopes was low. To test whether a sequence-based interaction could be possible, the amino acid sequences of

GCN4-scFv, BC2-Nb and Moontag-Nb were compared. GCN4-scFv consists of 256 amino acids, whereas BC2-Nb and Moontag-Nb comprise of 123 amino acids (Figure 2.10 B). For the comparison, the V_H region of GCN4-scFv was aligned to BC2-Nb and Moontag-Nb. The sequence similarity was expected to be higher in this area, since Nb only consists of a variable heavy chain region (V_{HH}). Similar amino acids in all antibodies are marked in black, similarities in two antibodies are marked in gray, respectively. As indicated in Figure 2.10 B, areas with a high level of coincidence in the sequence were found. Especially the N-termini of all antibodies showed a high level of consistency. The Moontag-Nb and the GCN4-scFv showed a higher similarity than GCN4-scFV to BC2-Nb (Figure 2.10 B). Based on this sequence alignment, an interaction of an unknown protein with the N-termini of all antibodies could be possible.

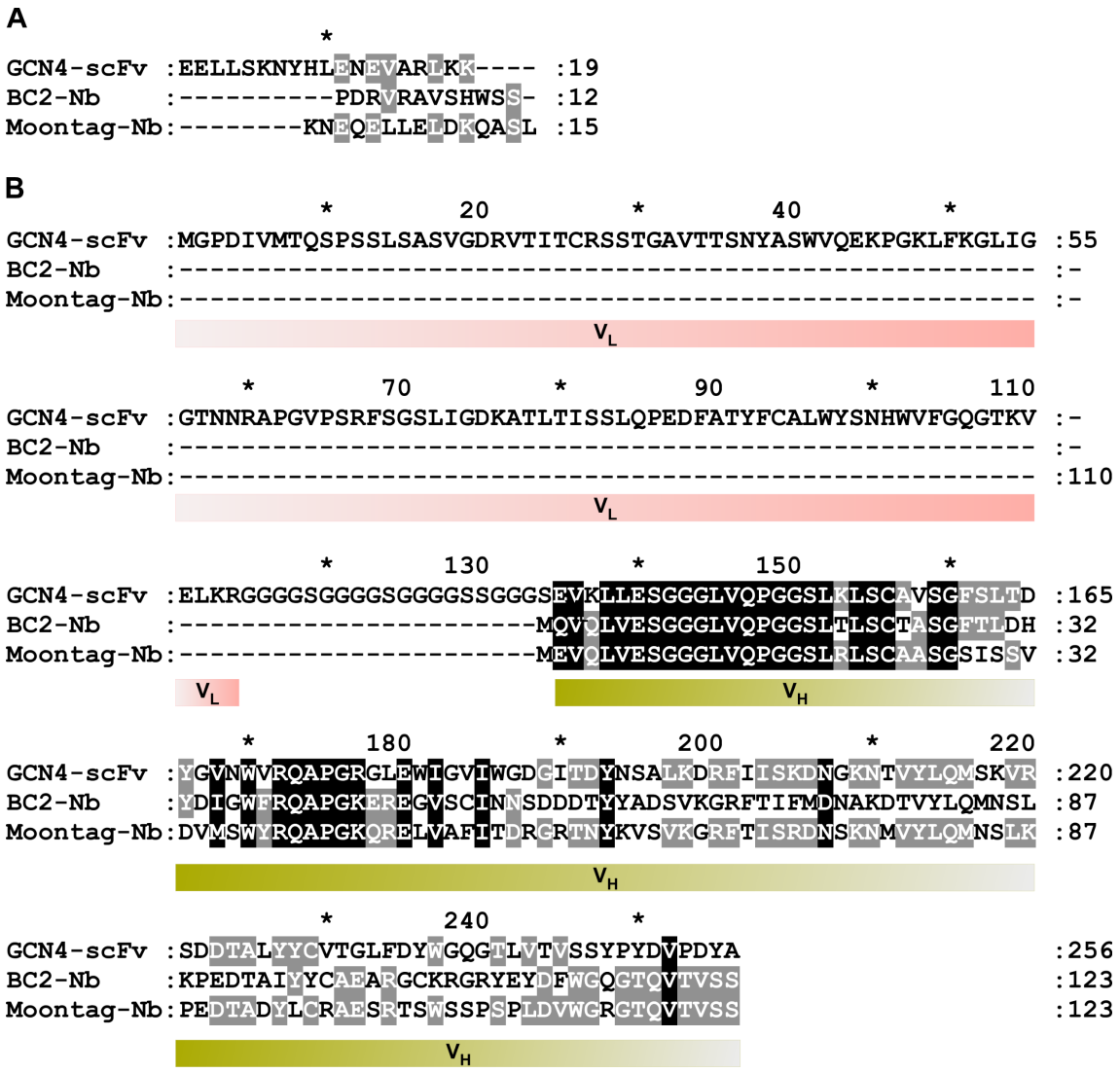

Figure 2.10: Sequence alignments of GCN4-scFV, BC2-Nb and Moontag-Nb. Sequence comparison of **(A)** peptide epitopes recognized by and **(B)** amino acid sequences of GCN4-scFv, BC2-Nb and Moontag-Nb. Sequence alignments were conducted using ClustalW. Similar amino acids in all peptide epitopes or antibodies are marked in black, similar amino acids in two epitopes or antibodies are marked in gray.

Variable part of light chain (V_L, rose) and variable part of heavy chain (V_H, khaki) of GCN4-scFv are indicated by boxes below the sequence comparison.

The final possibility of an interaction to an unknown protein could be based on the structure of antibodies. These were obtained from the Protein Data Bank (PDB) advanced sequence search (PDB, n.d.). For the structures of GCN4-scFv and Moontag-Nb, other previously solved structures of an α-acetyl antibody from mouse (C6-scFv) and an antibody against HIV-1 glycoprotein gp41 (GP41-Nb) showing high PDB validation rates for the deposited sequences were used (GCN4-scFv, Nishiguchi et al., 2019; Moontag-Nb, Lutje Hulsik et al., 2013). The structure of BC2-Nb is already solved and available on PDB and was used for this analysis (Braun et al., 2016). With the help of Prof. Dr. Lutz Schmitt (Head of Biochemistry I, Heinrich Heine University, Düsseldorf), the structures of the antibodies were aligned with the coot tool (Tool, n.d.) and the alignment was visualized using pymol (Pymol, n.d.). As indicated in Figure 2.11 C, the structure of BC2-Nb (orange) and Moontag-Nb (yellow) showed a high similarity. In addition, GCN4-scFv (blue) showed a comparable structure. This became more clearly visible in the overlay of all structures. Here, the structures of BC2-Nb and Moontag-Nb corresponded to the C-terminus of GCN4-scFv (Figure 2.11 C). Thus, a potential protein-protein interaction could be based on the structure of the antibodies.

In summary, GCN4-scFv seemed to be able to interact to an unknown protein since an potential interaction was visible in the Far-Western Blot experiment. The protein-protein interaction could possibly base on the primary and tertiary structure of antibodies since peptide epitope alignments did not show high similarities between the three tested antibodies. The unspecific shuttling which is possibly based on protein-protein interactions made the usage of an antibody to label a nascent peptide chain impossible unless the interaction partner is found. In addition, it was crucial to characterize whether the shuttling is dependent on known proteins which are present on the early endosomal surface.

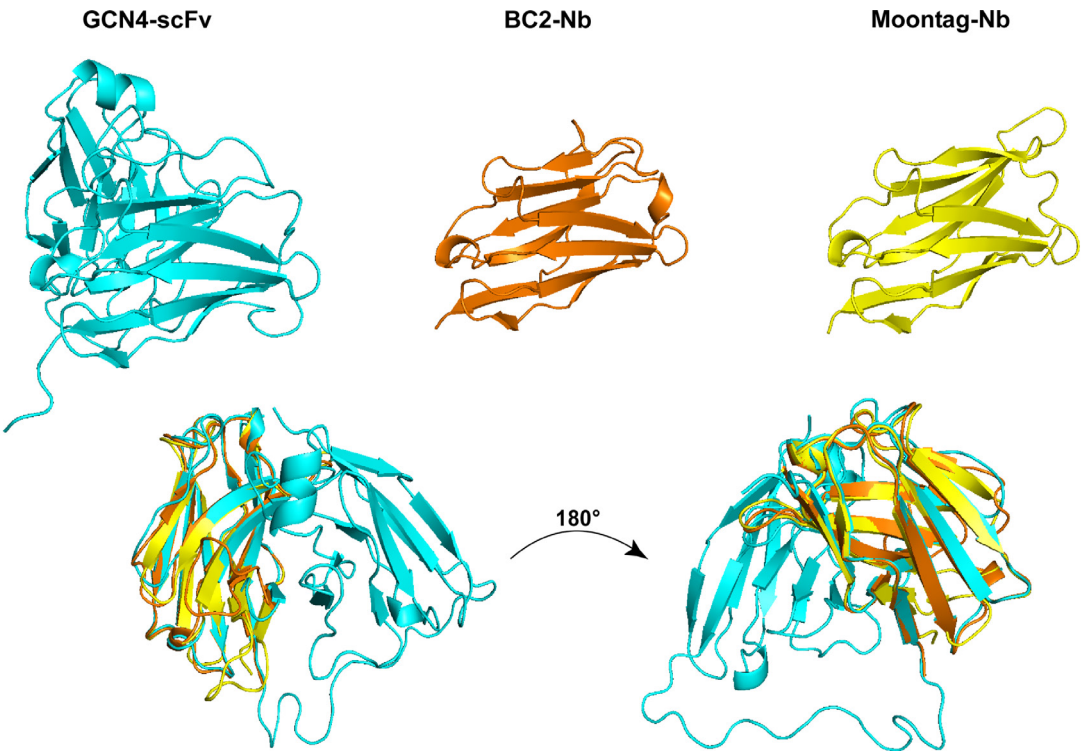

Figure 2.11: Structure alignments of GCN4-scFV, BC2-Nb and Moontag-Nb. Tertiary structures of GCN4-scFv (blue), BC2-Nb (orange) and Moontag-Nb (yellow) obtained from Protein Data Base (PDB). The structures of GCN4-scFv and Moontag-Nb were compared to other known structures and best PDB validated structures were chosen. The structure of BC2-Nb is solved and was used for the analysis. Alignment of secondary structures was obtained using coot tool. Visualization was conducted with pymol.

2.2.4 Dependency of shuttling antibodies on mRNP components

Known proteins which are part of the mRNP complex in *U. maydis* show the same subcellular localization as it was observed for antibodies. They all shuttle in a bidirectional manner through the hyphae, co-localize with FM4-64 and the early endosomal marker protein Rab5a, and the shuttling is dependent on microtubules. Notably, the velocities of observed shuttling particles of the antibodies were comparable to mRNP complex proteins (data not shown). It was important to verify that the antibodies did not interact with known proteins of the mRNP complex because a potential interaction partner has to be deleted to be able to use antibodies to label a nascent peptide chain. To investigate whether the shuttling of antibodies in hyphae of *U. maydis* is due to an interaction to known early endosomal proteins from the mRNP complex, different core proteins were deleted. Because of the fact that all antibodies behave the same way, GCN4-scFv-sfGfp was chosen as a proof of principle for the analysis. All of the analyzed mRNP proteins are crucial for efficient endosomal mRNA transport and deletions lead to an increasing number of bipolar growing hyphae. In addition, they show interdependency to each other and deletion of one protein of the mRNP complex leads to the loss of different proteins. The following genes were deleted

in the genetic background of GCN4-scFv-sfGfp: *upa2*, *rrm4*, *upa1* and *kinesin-3* (*kin3*). The deletion of all four genes led to bipolar growth of hyphae (Figure 2.12 A-D). As shown with yellow arrowheads in Figure 2.12 A to D, a stained microtubule-like structure was visible in all hyphae. Note that the background signal of Gfp seemed to be increased in the *kin3*Δ strain. GCN4-scFv-sfGfp shuttled in the *upa1*Δ, *rrm4*Δ and *upa2*Δ strains bidirectionally through the hyphae. The number of shuttling signals seemed to be decreased in the strain in which *kin3* was deleted (Figure 2.12 D). This led to the hypothesis of a Kin3-dependent shuttling of GCN4-scFv-sfGfp. To quantify whether the deletion of *upa1*, *rrm4*, *upa2* and *kin3* had a significant effect on the shuttling of GCN4-scFv-sfGfp, the traveled distance, the velocity and the number of particles per 10 µm of hypha were analyzed. Within the traveled distance of the shuttling particles, no significant differences could be observed between the strain expressing GCN4-scFv-sfGfp and the generated deletion strains (Figure 2.12 E). The velocities of the moving particles changed significantly between the strain expressing GCN4-scFv-sfGfp and the strains GCN4-scFv-sfGfp/*rrm4*Δ and GCN4-scFv-sfGfp/*kin3*Δ, respectively. While the velocity in the strain expressing GCN4-scFv-sfGfp was around 2 µm/s, it increased up to 2.4 µm/s in GCN4-scFv-sfGfp/*rrm4*Δ. Contrary to this, there was a reduction of the velocity of moving particles to 1.5 µm/s in GCN4-scFv-sfGfp/*kin3*Δ (Figure 2.12 F). The number of detectable moving particles per 10 µm of hypha did not differ significantly between the strain expressing GCN4-scFv-sfGfp and the deletion strains of *upa2*, *rrm4* and u*pa1*, as in all cases approximately 5 particles per 10 µm of hypha were observed. In the *kin3* deletion strain, the number of moving GCN4-scFv-sfGfp particles was significantly decreased to 1.6 particles per 10 µm of hypha (Figure 2.12 G).

In summary, the deletion of *kin3* seemed to have an influence on the shuttling behavior of GCN4-scFv-sfGfp. Nevertheless, there were still moving particles detectable which indicated that there seemed to be another protein which transports antibodies. Besides, an interaction to the mRNP proteins Upa2, Rrm4 and Upa1 could be excluded. Thus, it was important to find the unknown interaction partner and test whether a deletion would abolish the shuttling of the antibodies without affecting any relevant process like mRNA transport and endosomal transport.

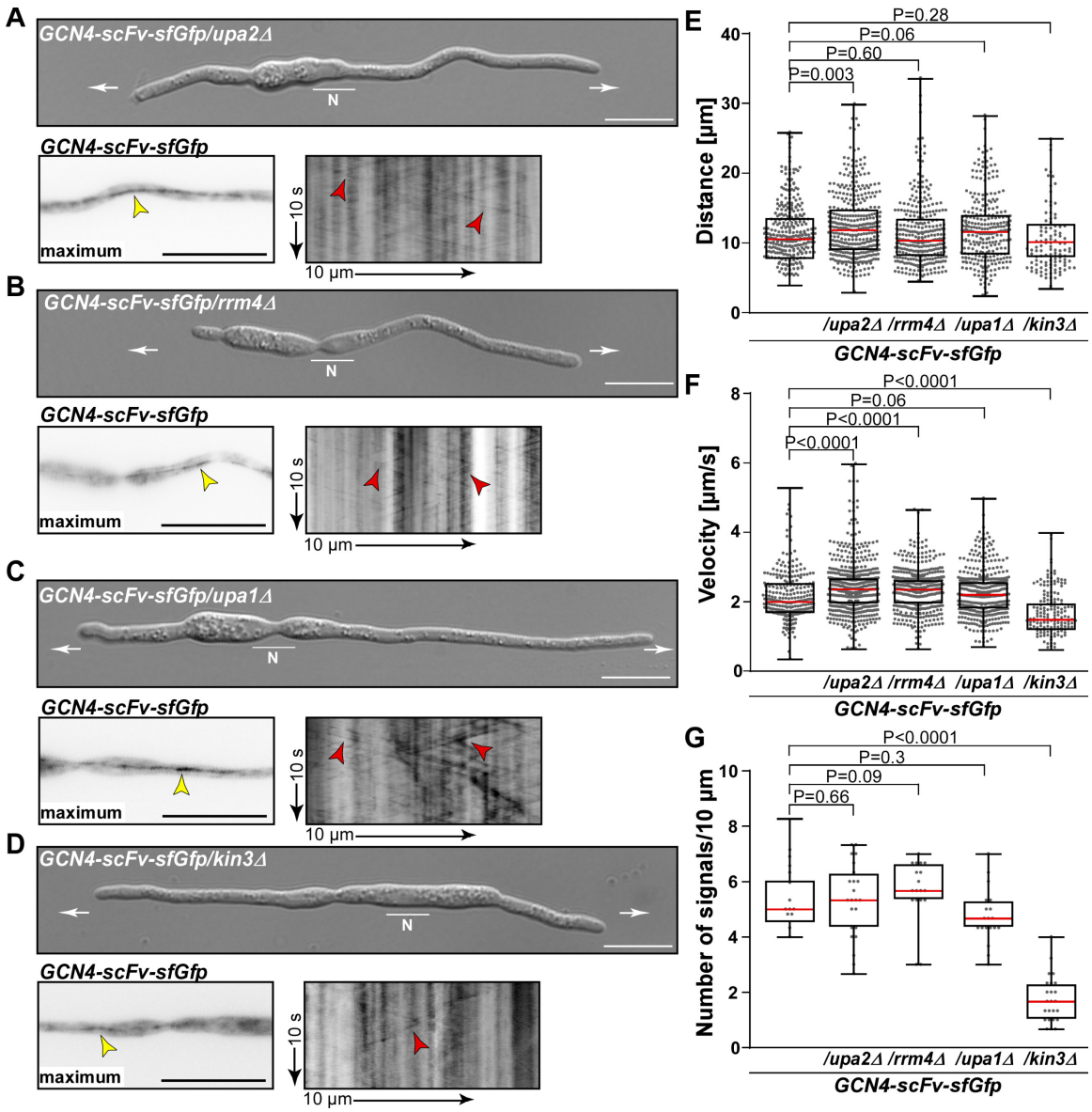

Figure 2.12: Impact of the deletion of mRNP proteins on the shuttling of GCN4-scFv-sfGfp. (A-D) DIC microscopy, micrographs and kymographs of hyphae expressing GCN4-scFv-sfGfp in combination with different deletions of mRNP proteins (6 h.p.i.). Yellow arrowheads indicate stained microtubule-like structures. Moving particles are indicated by red arrowheads (micrographs show maximum projection; inverted picture; scale bar 10 µm; arrow length on the left and bottom of kymograph indicates time and distance). **(E-G)** The distance of shuttling particles of GCN4-scFv-sfGfp **(E)**, the particle velocity **(F)** and the number of particles per 10 µm of hypha **(G)** were quantified in respect to the effect of the deletion of different mRNP proteins (box and whisker plot shows median (red) and min and max values; n>30 in 3 independent experiments; shuttling particles with a distance <5 µm were excluded from the analysis; unpaired two-tailed t-test; α<0.05).

2.2.5 LC-MS/MS analysis for the identification of potential interaction partners

To enrich proteins which potentially interact with the expressed antibodies, an immunoprecipitation (IP) was performed (Bonifacino et al., 2016). For this, total cell extracts of hyphae expressing GCN4-scFv-sfGfp or BC2-Nb-sfGfp were mixed with magnetic agarose beads coated with α-Gfp antibodies. This enabled a specific purification of interacting proteins. As a control, cell extracts of a strain expressing sfGfp

and AB33-*upp3*Δ were included. In total, three replicates of each IP were analyzed by liquid chromatography coupled to mass spectrometric analysis (LC-MS/MS), which was performed in collaboration with the Molecular Proteomics Laboratory (MPL, BMFZ, Heinrich Heine University Düsseldorf, Dr. Gereon Poschmann and Prof. Dr. Kai Stühler). Raw data was further processed using MaxQuant software environment with standard parameters (Dr. G. Poschmann). Due to a higher quality of the data, GCN4-scFv-sfGfp was chosen for further analysis. To identify proteins which were significantly enriched in the GCN4-scFv-sfGfp strain, sfGfp was chosen as negative control for further analysis since the difference between the identified proteins of the strains AB33-*upp3*Δ and sfGfp was minor (data not shown). In total, 292 proteins were identified by LC-MS/MS analysis. A plot of paired student's t-test p-values (Y-axis, $-Log_{10}$[p-value]) against the protein's fold change, (X-axis, difference of log_2 [mean intensity]), showed that 37 proteins are significantly enriched in GCN4-scFv-sfGfp in comparison to sfGfp (Figure 2.13 A; student's t-test p-value < 0.1, fold change > 2; red dots). 251 Proteins did not show a significant enrichment (Fig.2.10 A, gray dots), four proteins were significantly enriched in the control group and therefore false positive (Figure 2.13 A, light blue dots). Eleven out of 37 enriched proteins were enriched at least fivefold including known proteins like Cdc11 and Cdc12 (Figure 2.13 B; green dots). Interestingly, also Tea1 was significantly enriched in GCN4-scFv-sfGfp which was already found by sequence comparison analysis (see 2.2.2.1). Besides, different potential subunits of the pyruvate dehydrogenase were found (Pdr1, Pda1 and Pdb1; Figure 2.13 B). Surprisingly, a related protein of myosin-1 isoform heavy chain (MYO1), which is part of myosin-1 belonging to the type II myosin transporter, was also highly enriched in GCN4-scFv-sfGfp. The most abundant protein was UMAG_00933 (Figure 2.13 B). By analyzing the three replicates from all strains, it became clear that UMAG_00933 was highly abundant in all three replicates of GCN4-scFv-sfGfp and totally absent in the control strains (Figure 2.13 C).

In summary, the LC-MS/MS analysis showed that the uncharacterized protein UMAG_00933 was highly enriched in the IP sample of GCN4-scFv-sfGfp. Interestingly, also Tea1, which was already found by sequence comparison of the epitope of GCN4-scFv against the whole proteome of *U. maydis*, was enriched. However, Tea1 could be excluded to be responsible for the recruitment of antibodies to shuttling units. Thus, UMAG_00933 could possibly be the interacting protein which recruits the antibodies to shuttling units within hyphae of *U. maydis*. To prove this hypothesis, *UMAG_00933* was studied further.

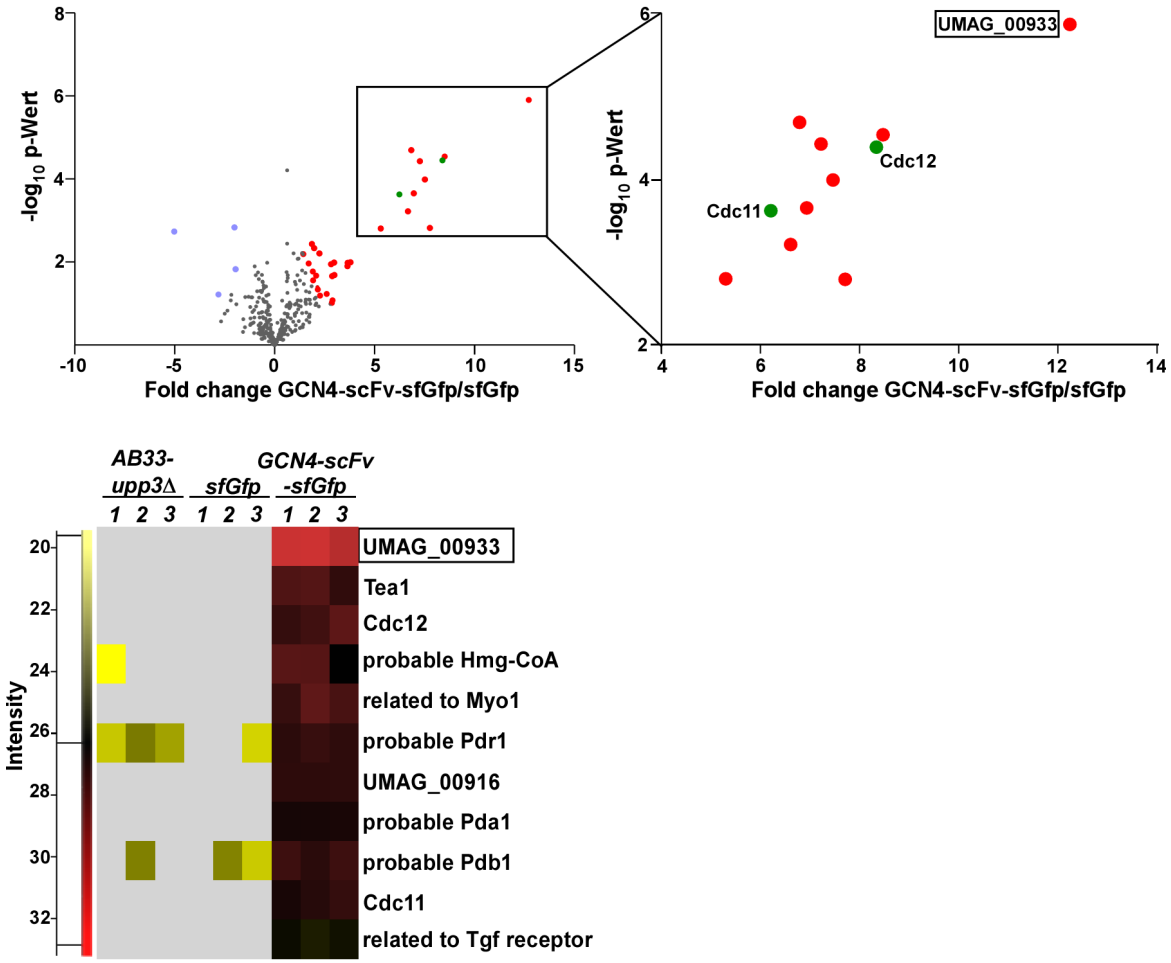

Figure 2.13: Liquid chromatography coupled to mass spectrometric analysis of GCN4-scFv-sfGfp. (A) Volcano blot of GCN4-scFv-sfGfp versus sfGfp. Significantly enriched proteins within GCN4-scFv-sfGfp are marked in red, within sfGfp are marked in light blue. Non-significant proteins are marked in gray (X-axis, fold change between GCN4-scFv-sfGfp and sfGfp, difference of $\log_2$ normalized intensities; Y-axis, $-\log_{10}$ of p value of unpaired t-test of GCN4-scFv-sfGfp and sfGfp). **(B)** Close-up of volcano blot showing the eleven most enriched proteins. Known proteins are marked in green. The most abundant protein is framed. **(C)** Heat map showing $\log_2$ normalized intensities of the eleven highly enriched proteins in three replicates of analyzed AB33-*upp3*Δ, sfGfp and GCN4-scFv-sfGfp expressing strains (Intensities ranging from low (yellow) to red (high)).

2.2.6 Analysis of UMAG_00933 as potential interaction partner

2.2.6.1 Bioinformatical analysis of UMAG_00933

Figure 2.14: Schematic representation of the domain architecture of UMAG_00933. UMAG_00933 consists of 1290 amino acids and has two predicted domains; CTD-domain (blue) and SMC-domain (purple; predicted domains obtained from the SMART website: http://smart.embl-heidelberg.de).

With an IP of GCN4-scFv-sfGfp followed by a LC-MS/MS run, UMAG_00933 was significantly enriched in comparison to the control strains. Due to this, UMAG_00933 could be a possible interaction partner of antibodies within *U. maydis*. UMAG_00933 is

annotated as hypothetical protein consisting of 1290 amino acids and has a molecular size of 136 kDa. It contains a predicted CTD-domain at the C-terminus which can also be found at the C-terminus of Spt5 from *Schizosaccharomyces pombe* and representatives of the division of Basidiomycota (Figure 2.14). Spt5 interacts with Spt4 and forms a complex (Spt5-Spt4) which regulates early transcription elongation by RNA polymerase II (Schwer et al., 2009). Note that UMAG_00933 and Stp5 from *S. pombe* and representatives of the division of Basidiomycota share only minimal overall identities in the protein sequences. Another domain which was found in UMAG_00933 is a SMC-domain (Figure 2.14). This domain can be found in several proteins which play a role in chromosome segregation, and this domain seems to be conserved in all kingdoms. A very low conserved SMC domain was found in Upa2, a member of the mRNP complex in *U. maydis*. Note that the conservation of this domain was also very low in UMAG_00933. Both domains might indicate that this protein has the capability of nucleic acid binding. Overall, 110 orthologs of UMAG_00933 could be found by a protein sequence search in fungal species and all of them were found in Basidiomycota. In addition, no orthologs were found in mammalian species. This indicated that the protein seems to be specific for Basidiomycota. A previous study analyzed the conservation of core components of the mRNP complex in *U. maydis* to other representatives of the fungal kingdom (Müller et al., 2019). Orthologs of Upa1, Rrm4 and Upa2 are present in most analyzed Basidiomycota, e.g. *Sporisorium reilianum* (*S. reilianum*), *Coprinopsis cinerea* (*C. cinerea*) and *Microbotryum lychnidis-dioicae* (*M. lynchnidis-dioicae*), but absent in *Malassezia globosa* (*M. globosa*). Furthermore, Upa1 and Rrm4 orthologous are also found in Mycoromycota but are most likely absent in Ascomycota. To analyze a potential link of UMAG_00933 to the mRNP complex, a search for orthologs in selected organisms was performed. An UMAG_00933 ortholog was found in *S. reilianum* and *C. cinerea.* Interestingly, no apparent ortholog was found in *M. lynchnidis-dioicae* and *M. globosa.* This indicated that the presence of UMAG_00933 seemed to be independent of the presence of core components of the mRNP complex from *U. maydis*.

In summary, UMAG_00933 is a hypothetical protein which seemed to be specific to Basidiomycota. The occurrence in other organisms was independent of the presence of core components of the mRNP complex. To examine the interaction with antibodies *in vivo*, a deletion strain was generated in the genetic background of expressed antibodies. First of all, the effect of deleting *UMAG_00933* was analyzed in sporidia as well as in hyphae to investigate the role of UMAG_00933 in cellular processes.

2.2.6.2 Impact of the *UMAG_00933* deletion on sporidia and hyphae of *U. maydis*

To be able to use the deletion of *UMAG_00933* in combination with the antibodies to label a nascent peptide chain, it was important to analyze the impact of the deletion in more detail. First of all, the morphology of sporidia and hyphal cells was studied. For this, the strains GCN4-scFv-sfGfp/*UMAG_00933*Δ and BC2-Nb-sfGfp/*UMAG_00933*Δ were compared to GCN4-scFv-sfGfp, BC2-Nb-sfGfp and wild type (wt). As indicated in Figure 2.15 A, in comparison to the antibody expressing cells and wt no morphological changes could be observed for the strains in which *UMAG_00933* was deleted. Sporidial cells were cigar shaped, and hyphae grew unipolar while inserting septa at the basal site. To analyze whether an impact on the hyphal growth would be visible on plates, the GCN4-scFv-sfGfp/*UMAG_00933*Δ and BC2-Nb-sfGfp/*UMAG_00933*Δ strains were spotted on nitrate medium plates containing charcoal, on which the hyphal growth is induced. If a strain is able to form hyphae, a fuzzy area surrounding the dropped colony is visible. Note that a colony is visible on the plate because the cell cycle is not arrested directly upon dropping cells on the plates. In comparison to the wt, GCN4-scFv-sfGfp/*UMAG_00933*Δ and BC2-Nb-sfGfp/*UMAG_00933*Δ strains showed a slight reduction of the hyphal growth (Figure 2.15 B). Nonetheless, the deletion strains were in general able to grow unipolar which was detectable by the minor fuzzy areas surrounding the growing colonies on the plate (Figure 2.15 B). Secondly, the doubling time of sporidia in which *UMAG_00933* was deleted was determined. For this, the growth was monitored in the BioLector, in which the OD_{600} was measured every 30 min. All strains were diluted to the same starting OD_{600} of 0.1 and growth was monitored for 24 h. Note that the BioLector measures the scattered light in contrast to the transmitted light which is measured with spectrophotometry. As indicated in Figure 2.15 C and D, a slight difference could be observed in the growing behavior of sporidial cells harboring a deletion of *UMAG_00933* in comparison to the wt and the progenitor strains. The doubling time of strains harboring GCN4-scFv-sfGfp and BC2-Nb-sfGfp was 1.76 h and 1.81 h, respectively. In comparison to this, the doubling time of GCN4-scFv-sfGfp/*UMAG_00933*Δ and BC2-Nb-sfGfp/*UMAG_00933*Δ decreases about 10-20% to 1.56 h and 1.44 h, respectively. This indicated that even though no difference was found in the morphology of the sporidia, the GCN4-scFv-sfGfp/*UMAG_00933*Δ and BC2-Nb-sfGfp/*UMAG_00933*Δ strains seem to grow more slowly. Third, the growth of hyphal cells was quantified to finally exclude an impact of the deletion of *UMAG_00933* since a slight decrease of fuzziness of growing hyphae on plates was observed. No significant difference between the progenitor strains, the wild type and the strains harboring a deletion of *UMAG_00933* could be observed (Figure 2.15 E). A slight decrease from

90% to 70% of unipolar growing cells which formed at minimum one septum at the basal site of the hyphae was already observable in the strain expressing GCN4-scFv-sfGfp or BC2-Nb-sfGfp. Between the strains expressing the antibodies and strains harboring the deletion in addition, a difference of 5% of unipolar growing cells with a septum was quantified (Figure 2.15 E). Note that no bipolar growth of cells was observed in all analyzed strains. To exclude slower growing hyphae in the deletion strains, the length of the hyphal growing cells was quantified since there was a slight decrease in the number of unipolar growing cells which inserted at least one septum. As shown in Figure 2.15 E, the length of the hyphae of the wild type, GCN4-scFv-sfGfp, GCN4-scFv-sfGfp/*UMAG_00933*Δ and BC2-Nb-sfGfp/*UMAG_00933*Δ did not differ significantly. The hyphae showed an average length of 75-90 µm. Thus, the deletion of *UMAG_00933* seemed to have no severe influence on the growth of hyphal cells, even though a slight reduction of hyphal growth could be observed on plates containing charcoal.

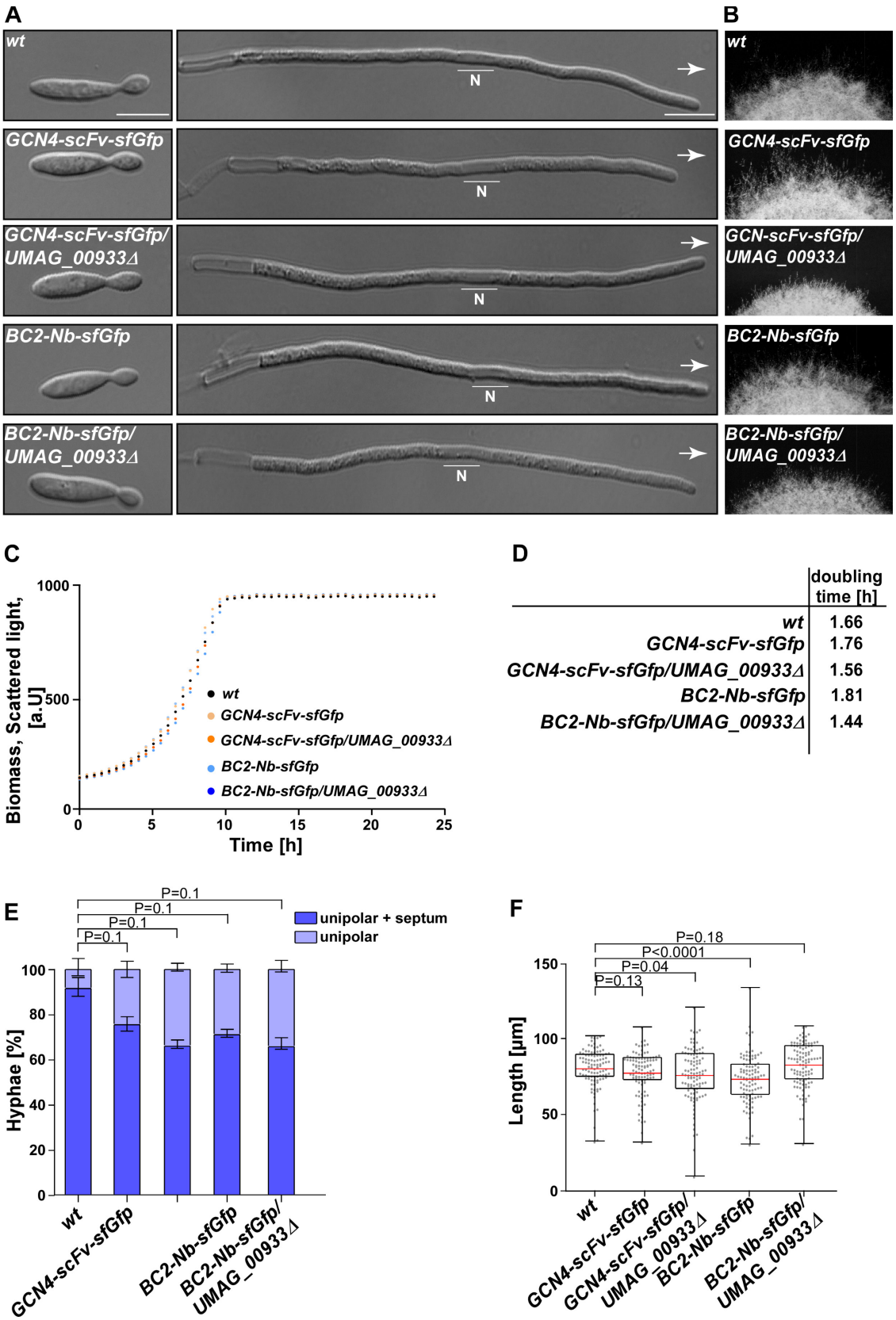

Figure 2.15: Analysis of the impact of the *UMAG_00933* deletion on sporidia and hyphae of *U. maydis*. **(A)** DIC microscopy of sporidia and hyphal cells expressing GCN4-scFv-sfGfp, BC2-Nb-sfGfp, GCN4-scFv-sfGfp/*UMAG_00933*Δ, BC2-Nb-sfGfp/*UMAG_00933*Δ and wild type. The growth direction of hyphae is indicated by arrows, the nucleus of hyphae is indicated with N (6 h.p.i.; scale bar 10 µm). **(B)** Hyphal growing plate assay on nitrate minimum medium plates containing charcoal. **(C)** Growth curves of sporidia expressing GCN4-scFv-sfGfp, BC2-Nb-sfGfp, GCN4-scFv-sfGfp/*UMAG_00933*Δ, BC2-Nb-

sfGfp/*UMAG_00933*Δ and wild type (starting OD_{600}, 0.1; measured every 30 minutes for 24 hours; biomass indicated in scattered light). **(D)** Calculated doubling times of growth curves obtained in B. **(E)** Quantification of unipolar growing hyphae (light blue) and unipolar growing hyphae which inserted at least one septum (dark blue) expressing GCN4-scFv-sfGfp, BC2-Nb-sfGfp, GCN4-scFv-sfGfp/*UMAG_00933*Δ, BC2-Nb-sfGfp/*UMAG_00933*Δ and wild type (n>30 in 3 independent experiments; unpaired two-tailed t-test; α<0.05). **(F)** Quantification of length of hyphal cells expressing GCN4-scFv-sfGfp, BC2-Nb-sfGfp, GCN4-scFv-sfGfp/*UMAG_00933*Δ, BC2-Nb-sfGfp/*UMAG_00933*Δ and wild type (box and whisker plot shows median (red) and min and max values; n>30 in 3 independent experiments; unpaired two-tailed t-test; α<0.05).

Finally, stress tests were conducted with the cells harboring a deletion of *UMAG_00933* to exclude a crucial role of UMAG_00933 in cellular processes. The cells were on the one hand spotted on plates in serial dilutions and incubated at 16, 28 and 37 °C for up to four days. For this, sporidial cells of the strains GCN4-scFv-sfGfp/*UMAG_00933*Δ and BC2-Nb-sfGfp/*UMAG_00933*Δ were compared to GCN4-scFv-sfGfp, BC2-Nb-sfGfp, *rrm4*Δ, *grp1*Δ and wild type. The deletions of *rrm4* and *grp1* served as controls because both deletions show growth defects. *rrm4*Δ hyphae grow in a bipolar manner in contrast to unipolar growing wild type cells. *grp1*Δ results in slower proliferation, an increased cell length of hyphae as well as in a decreased tolerance towards lower temperatures (Olgeiser et al., 2019). Note that 28 °C is the optimal growth temperature for *U. maydis*. At 16 °C, all strains grew in a comparable way except the *grp1* deletion strain which exhibited altered colony morphology and a strongly reduced growth (Figure 2.16 A). The altered colony morphology was also observed on plates which were incubated at 28 °C in contrast to the other tested strains which grew in a comparable way to the wild type strain. At 37 °C it seemed that the BC2-Nb-sfGfp as well as BC2-Nb-sfGfp/*UMAG_00933*Δ strains had an increased tolerance towards higher temperatures since both colonies exhibited stronger growth (Figure 2.16 A). Importantly, the deletion of *UMAG_00933* seemed to have no influence on the temperature stress tolerance of *U. maydis*. On the other hand, sporidial cells were plated out and an agar diffusion test with different stress inducing agents was performed. For this test, filter paper was soaked with different stress inducing agents and placed on the plates. After two days, zones of growth inhibition (halo formation) were analyzed and compared between the different strains. Here, sporidial cells of the strain GCN4-scFv-sfGfp/*UMAG_00933*Δ were compared to GCN4-scFv-sfGfp, *rrm4*Δ and wild type. As a positive control for induced growth inhibition, H_2O_2 was chosen, because its toxic effect on *U. maydis* is already known (Molina and Kahmann, 2007). Upon treatment with H_2O_2, reactive oxygen species (ROS) accumulate within the cell which has to be detoxicated. Pure H_2O and DMSO were used as solvent controls, because the tested agents were solved in one of these two media. Here, no reaction of *U. maydis* was expected, otherwise the test would be inconclusive. The first reagent that was tested was SDS. SDS is a detergent that denatures proteins and thus alters the stability of membranes. The second reagent

targeted the ATPase Complex V within the mitochondrial membrane. Olegomycin A inhibits the proton channel which is necessary for oxidative phosphorylation of ADP to ATP (Jastroch et al., 2010). The third reagent was Tunicamycin. It is an antibiotic which is commonly used to induce endoplasmic reticulum (ER) stress by inhibiting the first steps of glycoprotein biosynthesis. This results in the accumulation of misfolded proteins and a strong induction of the unfolded protein response (UPR; Guha et al., 2017). The fourth reagent was Benomyl which was already used to treat hyphae to analyze microtubule-dependent shuttling processes. The fifth reagent targets the translation of eukaryotes. Cycloheximide (CHX) is an antibiotic which blocks the translocation step in elongation of translation resulting in cell growth arrest and cell death (Schneider-Poetsch et al., 2010). To arrest the cell cycle by inhibiting the formation of deoxyribose nucleoside triphosphate (dNTPs) and therefore stalling of replication forks, Hydroxyurea (HU) was used as sixth reagent. It targets class I ribonucleotide reductase, the enzyme that catalyzes the formation of dNTPs (Jordan and Reichard, 1998). The seventh reagent tested was Latrunculin A. It disrupts actin cytoskeleton organization by binding to monomeric G-actin (Mailfert et al., 2017). The last reagent tested was Calcofluor White (CW). It interferes with the cell wall assembly by binding to chitin and thereby induces a stress response of the cell wall (Ram and Klis, 2006). In all tested reagents, no enormous difference between the control strains (see appendix Figure 6.1), GCN4-scFv-sfGfp and GCN4-scFv-sfGfp/*UMAG_00933*Δ was detectable. Sporidia of all strains formed comparable halos under all tested conditions (Figure 2.16 B). One exception was the *rrm4*Δ strain which exhibited higher tolerance towards Benomyl which was expected because it prevents polymerization of microtubules. Because of the deletion of *rrm4*, the long distance transport of mRNAs and corresponding translational products was already altered. Hence, Benomyl seemed to have a minor effect on the cells compared to the wild type. Note that exactly the same result was visible for tested hyphal growing cells (data not shown). No huge difference between the control strains, GCN4-scFv-sfGfp and GCN4-scFv-sfGfp/*UMAG_00933*Δ regarding halo formation was observed. Thus, deletion of *UMAG_00933* seemed to have no influence on the tested cellular processes.

In this study, no severe effect of *UMAG_00933*Δ to the morphology of sporidia as well as hyphal cells was observed. Besides, UMAG_00933 seemed to have no crucial role in tested cellular processes. To investigate the subcellular localization of UMAG_00933, a Gfp fusion was analyzed. In addition the localization of GCN4-scFv-sfGfp as well as BC2-Nb was analyzed in *UMAG_00933* deficient hyphae.

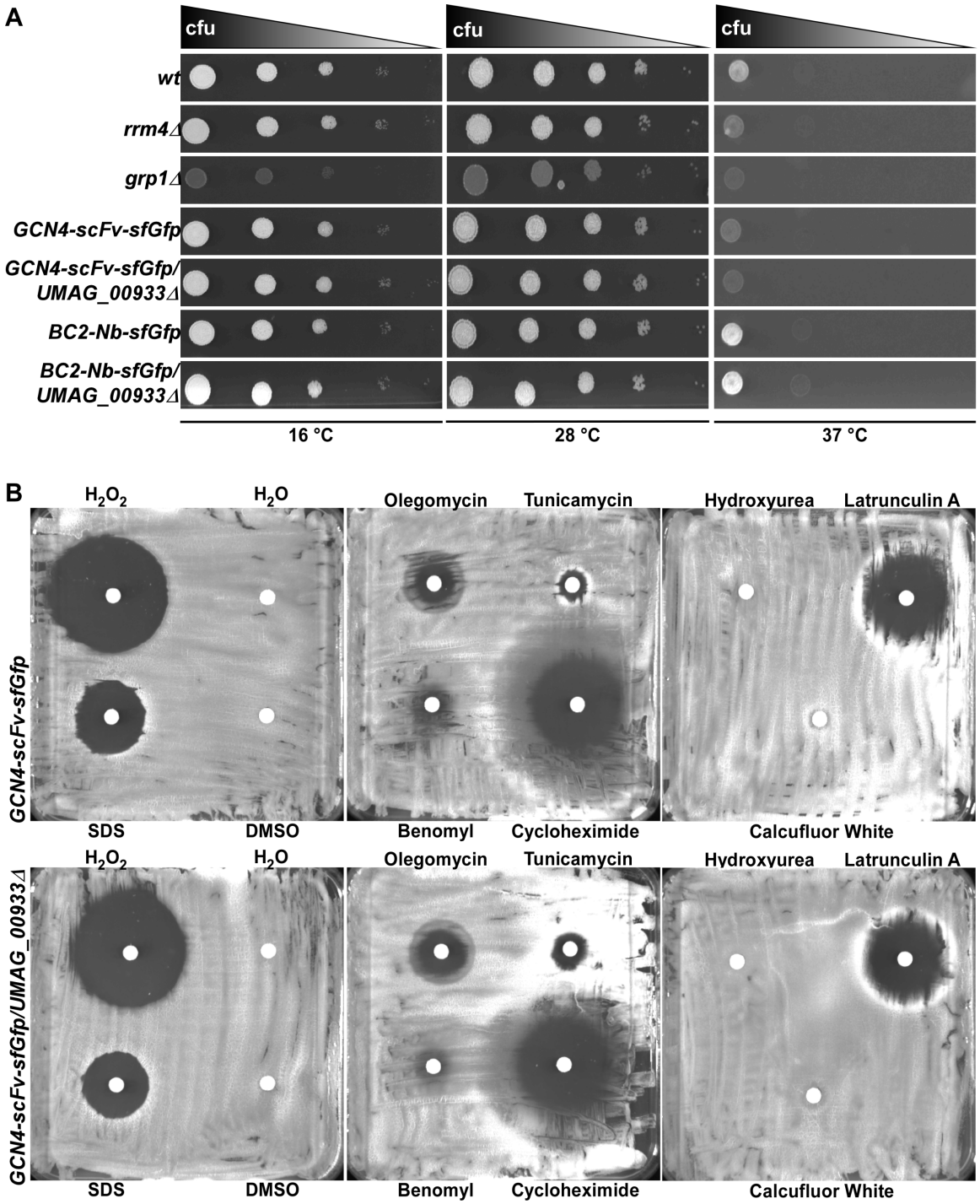

Figure 2.16: Testing of sporidial growth of *UMAG_00933*Δ strain under stress conditions. (A) Plate assay to analyze growth behavior of different strains at 16, 28 and 37 °C. Serial dilutions of sporidial cells were dropped on CM plates containing glucose (cfu, colony forming units; 10^1-10^5; colony formation was analyzed after 48 hours of incubation). **(B)** Halo plate assay to study the role of UMAG_00933 in different cellular processes. For agar diffusion test, filter paper was soaked with different stress inducing reagents. The deletion strain GCN4-scFv-sfGfp/*UMAG_00933*Δ was compared to its progenitor strain. Halo formation was analyzed after 48 hours of incubation.

2.2.6.3 Analysis of the impact of an *UMAG_00933* deletion on shuttling of antibodies *in vivo*

To analyze the subcellular localization of UMAG_00933, a Gfp fusion construct was generated. The construct was integrated into the native locus of *UMAG_00933* in the genetic background of AB33 and transcription was under the control of the native promoter. After verifying correct transformants by Southern blot analysis, the localization in hyphae was analyzed with fluorescence microscopy. As indicated by yellow arrowheads in Figure 2.17 A, a stained microtubule-like structure was visible. In addition, UMAG_00933 shuttled bidirectional through hyphae (red arrowheads). A co-localization analysis with FM4-64 revealed that UMAG_00933 seemed to co-localize to endocytic compartments (Figure 2.17 B). The shuttling of UMAG_00933 through hyphae was dependent on the microtubule cytoskeleton since the shuttling units were no longer detectable after benomyl treatment (Figure 2.17 C). The localization of UMAG_00933 was equal to the localization of the investigated antibodies which increased the possibility that this protein could be responsible for their shuttling. To be able to verify this hypothesis, a deletion of *UMAG_00933* was realized in the genetic background of strains expressing either GCN4-scFv-sfGfp or BC2-Nb-sfGfp. After verifying the deletion strains with Southern blot analysis, the shuttling behavior of GCN4-scFv-sfGfp and BC2-Nb-sfGfp was analyzed. As it can be seen in Figure 2.17 D, the stained microtubule-like structure was no longer visible in fluorescence microscopy of the GCN4-scFv-sfGfp/*UMAG_00933*Δ strain. In addition, no shuttling particles were detected. To prove whether GCN4-scFv-sfGfp is still expressed, a Western blot experiment was performed. Here, a full-length protein band of the fusion of GCN4-scFv to sfGfp could be detected in sporidia as well as in hyphae (Figure 2.17 D). The same result was observed for the BC2-Nb-sfGfp/*UMAG_00933*Δ strain. No shuttling of BC2-Nb-sfGfp was visible even though the antibody was expressed in both growth forms (Figure 2.17 E). Thus, UMAG_00933 seemed to interact with antibodies and is responsible for the unspecific shuttling.

In summary, this result show that UMAG_00933 seemed to interact with heterologous expressed antibodies in *U. maydis*. It could be proven that deletion of *UMAG_00933* abolished shuttling of GCN4-scFv-sfGfp as well as BC2-Nb-sfGfp. Consequently, antibodies could potentially be used to label a nascent peptide chain for visualizing local translation together with the deletion of *UMAG_00933*. Ultimately, it was necessary to analyze the direct interaction of antibodies to their peptide epitopes *in vivo*. This was the last important step to demonstrate that the usage of an antibody to label the nascent peptide chain is possible.

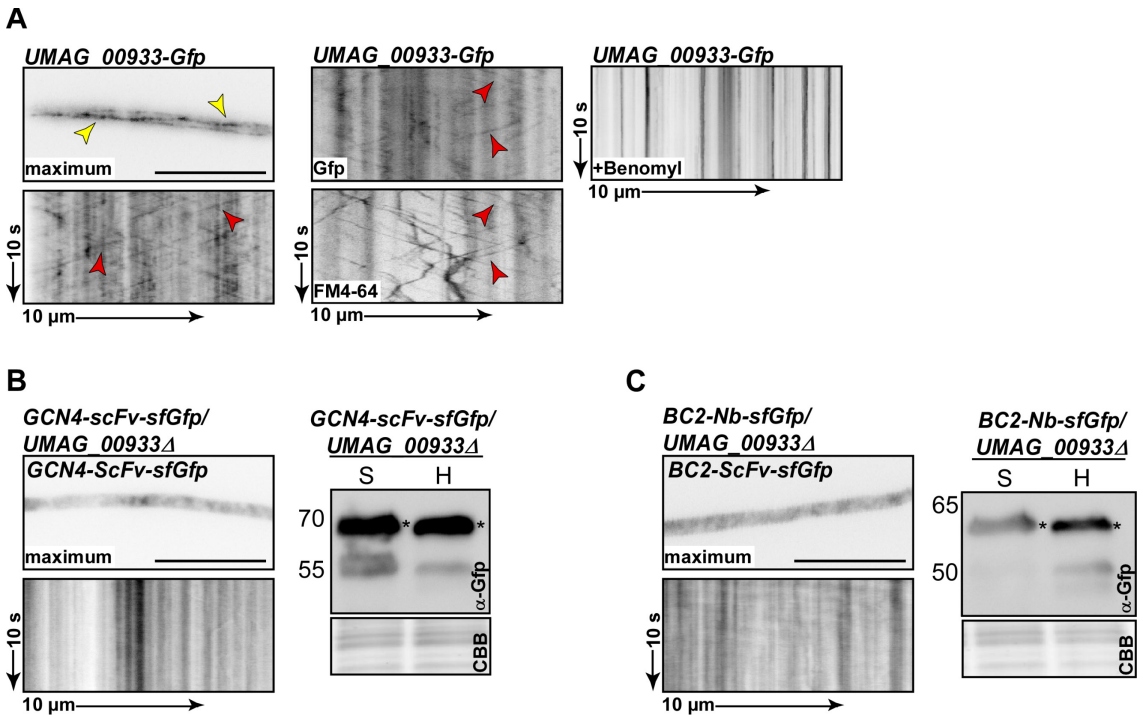

Figure 2.17: Analysis of the subcellular localization of UMAG_00933 and its impact on shuttling antibodies. **(A**) Micrograph and kymograph of hypha expressing UMAG_00933-Gfp. Staining of microtubule-like structure is indicated by yellow arrowhead. Shuttling particles are indicated by red arrowheads (6 h.p.i.; maximum projection; inverted picture; scale bar 10 µm; arrow length on the left and bottom of kymograph indicates time and distance). **(B)** Kymographs of hyphae stained with FM4-64 expressing UMAG_00933-Gfp. Co-localization events are indicated by red arrowheads (6 h.p.i.; inverted pictures; arrow length on the left and bottom of kymograph indicates time and distance). **(C)** Kymograph of hypha expressing UMAG_00933 fused to Gfp after treatment with benomyl for two hours (inverted pictures; arrow length on the left and bottom of kymograph indicates time and distance). **(D/E)** Micrograph and kymograph of hypha expressing GCN4-scFv-sfGfp/*UMAG_00933*Δ or BC2-Nb-sfGfp/*UMAG_00933*Δ and Western blot analysis of the expression levels of antibodies in sporidial (S) and hyphal (H) cells 6 h.p.i. 5 µg of whole cell extracts were subjected to SDS-PAGE and Western blot analysis. GCN4-scFv-sfGfp and BC2-Nb-sfGfp were detected via the sfGfp and the membrane was stained with Coomassie brilliant blue after detection (CBB). Bands representing full-length proteins are marked with asterisks (maximum projection; inverted picture; scale bar 10 µm; arrow length on the left and bottom of kymograph indicate time and distance).

2.2.7 Analysis of interaction of antibodies to corresponding peptide epitope *in vivo*

In order to investigate the interaction of GCN4-scFv-sfGfp and BC2-Nb-sfGfp with their corresponding peptide epitopes, fusion constructs of the peptide epitopes to a so-called phox domain and mKate2 were generated. This domain originates from the t-SNARE protein Yup1 from *U. maydis* (Wedlich-Soldner et al., 2000). The phox-domain is able to interact with phosphoinositides and can bind to the surface of early endosomes. Thus, expressed peptide epitopes fused to the phox-domain and mKate2 were recruited to the endosomal surface und shuttle through hyphae. The peptide epitopes of GCN4-scFv and BC2-Nb were optimized for dicodon usage in *U. maydis* and were multimerized up to 24 copies. For the GCN4-scFv, 24 copies of the peptide epitope ($GCN4^{24}$) were fused

N-terminally to mKate2 and the phox-domain, because 24 copies of the epitope were previously proven to be sufficient for visible interaction (Figure 2.18 A; Tanenbaum et al., 2014). For the BC2-Nb, 12 ($BC2^{12}$) as well as 24 ($BC2^{24}$) copies were tested (Figure 2.18 A). Transcription was driven by the constitutive derivative of the promoter from the translational elongation factor 1 of *U. maydis*, in which 14 tetracycline operator sequences were integrated (Spellig et al., 1996). The fusion constructs were integrated into the genetic background of the corresponding antibodies in either GCN4-scFv-sfGfp/*UMAG_00933*Δ or BC2-Nb-sfGfp/*UMAG_00933*Δ strains at the ip^S locus, respectively. Observable shuttling of GCN4-scFv-sfGfp and BC2-Nb-sfGfp would now indicate an interaction to the expressed peptide epitopes since deletion of *UMAG_00933* abolished unspecific shuttling. Correct transformants were verified by Southern blot analysis and fluorescence microscopy was conducted. As indicated in Figure 2.18 B, shuttling of GCN4-scFv-sfGfp was observed. In addition a co-localization of GCN4-scFv-sfGfp and phox-mKate2-$GCN4^{24}$ was visible. Thus, GCN4-scFv-sfGfp seemed to interact with the corresponding peptide epitope *in vivo*. In contrast to this, no shuttling could be observed for BC2-Nb-sfGfp independently of the number of integrated peptide epitopes (Figure 2.18 C). Neither the antibody nor the peptide epitope shuttled through hyphae. This indicated that the peptide epitope expression could be too low to analyze shuttling of both BC2-Nb-sfGfp and the corresponding peptide epitope.

In summary these results show that GCN4-scFv-sfGfp interacted to its cognate peptide epitope *in vivo*. Contrary to this, BC2-Nb interaction to the corresponding peptide epitope was not observed probably due to low expression of the peptide epitope. Conclusively, in combination with *UMAG_00933*Δ, GCN4-scFv-sfGfp can possibly be used to label the nascent peptide chain to visualize sites of translation of mRNAs *in vivo*.

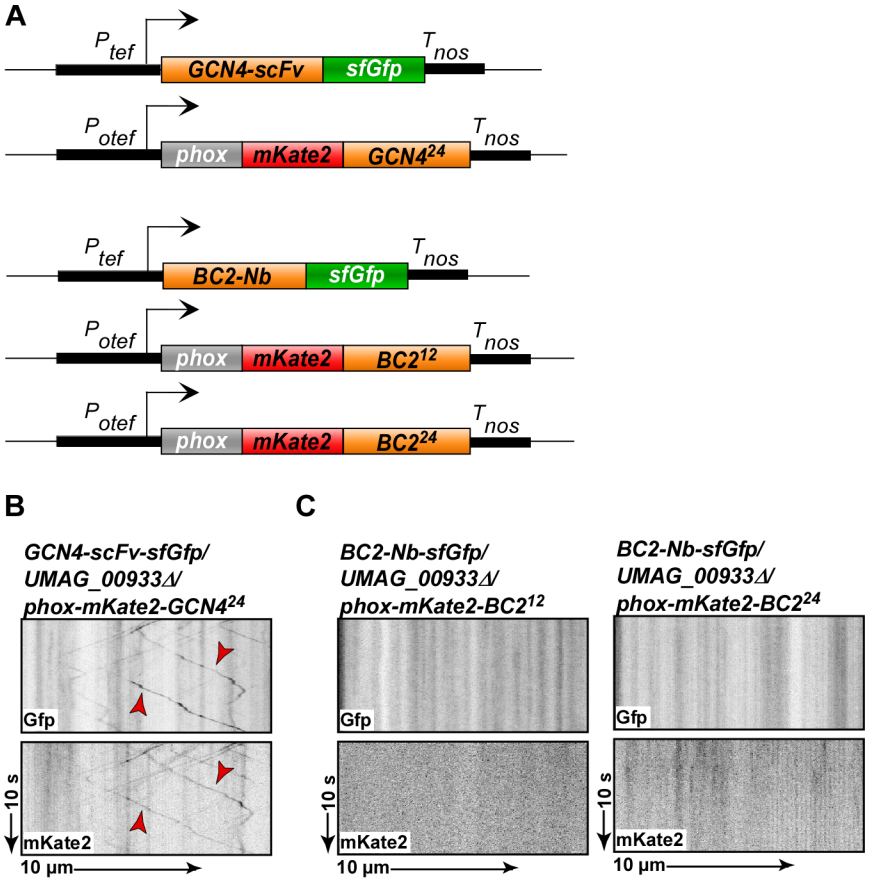

Figure 2.18: *In vivo* interaction of GCN4-scFv-sfGfp and BC2-Nb with their cognate peptide epitopes. **(A)** Schematic representation of constructs generated for *in vivo* interaction studies of expressed antibodies and their cognate peptide epitopes. 24 copies of GCN4-scFv epitope ($GCN4^{24}$) or BC2-Nb (BC^{24}) and 12 copies of BC2-Nb peptide epitope (BC^{12}) were N-terminally fused to mKate2 (red) and a phox-domain (gray) from Yup1 of *U. maydis*. Expression was driven by constitutive P_{otef} promoter and terminated with T_{nos} (black). **(B)** Kymographs of hyphae expressing GCN4-scFv-sfGfp/*UMAG_00933*Δ/phox-mKate2-$GCN4^{24}$. Co-localization events of GCN4-scFv-sfGfp and phox-mKate2-$GCN4^{24}$ are indicated by red arrowheads (6 h.p.i.; inverted pictures; arrow length on the left and bottom of kymograph indicates time and distance). **(C)** Kymographs of hyphae expressing BC2-Nb-sfGfp/*UMAG_00933*Δ/phox-mKate2-$BC2^{12}$ or BC2-Nb-sfGfp/*UMAG_00933*Δ/phox-mKate2-$BC2^{24}$ (6 h.p.i.; inverted pictures; arrow length on the left and bottom of kymograph indicates time and distance).

2.3 Establishment of 2A peptides and degron sequences

Another important step towards analyzing the site of translation of mRNAs *in vivo* was the reduction of the background fluorescence to increase signal to noise ratios of labeled nascent peptide chains and mRNAs. Once GCN4-scFv-sfGfp binds to $GCN4^{24}$ during translation, the synthesized fusion protein of $GCN4^{24}$-ORF is constantly labeled with sfGfp. To achieve a low fluorescence background, degradation of synthesized $GCN4^{24}$ bound by GCN4-scFv-sfGfp should be realized by fusing degron sequences to $GCN4^{24}$ which induces fast degradation. Degron sequences are features of proteins that make them short-lived *in vivo*. Two versions of the so-called PEST sequence from mouse ornithine-decarboxylase (mODC) were already successfully implemented in *U. maydis* by fusing them C-terminally to Gfp (Brachmann, 2001). The first one, d2, was the original

sequence which can be found at the very C-terminus of mODC and provides a half-live of two hours of the protein to which it is fused to. Within the second one, d1, three glutamic acids were exchanged to alanines. By this, the half-live of fused proteins was decreased to approximately one hour (Brachmann, 2001). The amount of proteins within a cell is controlled by equilibrium of synthesis and degradation. By integrating a PEST sequence into a construct, the amount of resulting proteins within the cell is decreased since protein degradation rates raise while synthesis rates still remain equal. For the application of visualizing local translation it was important to maintain the equilibrium of proteins encoded by analyzed mRNAs. For this reason, it was important to separate the translated protein from GCN4[24]. An elegant way to already separate them during translation is provided by the use of so-called 2A peptides. During translation, the ribosome skips formation of the peptide bound in between the C-terminal amino acids glycine and proline within 2A peptides. Thus, a polycistronic-like mRNA is formed in eukaryotes since translation of one mRNA leads to two separately folded proteins (de Felipe et al., 2006). Therefore degron sequences were combined with 2A peptides which were tested in *U. maydis*.

2.3.1 Combination of d1 PEST sequence and F2A peptide

For the first test of PEST sequences in combination with the 2A peptides, the d1 from mODC was used. In addition, the F2A peptide deriving from the foot-and-mouth disease virus was chosen for the first test since it was already well established in the cooperating lab of Prof. Dr. Matias Zurbriggen (Head of Synthetic Biology, Heinrich Heine University, Düsseldorf; personal communication; Ryan et al., 1991). To test the activity of PEST and F2A in *U. maydis*, a reporter construct was designed. This construct contained the constitutively active P_{otef}, mKate2 fused to an HA tag ($mKate2^{HA}$), d1 mODC, F2A and Gfp (eGFP, enhanced version of Gfp, Clontech) fused to a nuclear localization signal (Gfp^{NLS}; Kalderon et al., 1984). Hence, two different peptides should be synthesized: $mKate2^{HA}$-d1-F2A and Gfp^{NLS} which could be examined by Western blot experiments using α-HA and α-Gfp antibodies (Figure 2.19 A). In addition, an active 2A peptide would result in increased cytoplasmic red fluorescence while green fluorescence will be located to the nucleus because of the NLS. This can be analyzed by fluorescence microscopy (Figure 2.20 B). Note that due to the fusion of d1 mODC to $mKate2^{HA}$ this fusion protein should be degraded, initiated by the d1 sequence. The construct was integrated into the genetic background of AB33-*upp3*Δ in the *upp3* locus. After verifying correct integration of the construct by Southern blot analysis, fluorescence microscopy as well as Western blot experiments with α-HA and α-Gfp antibodies were conducted to analyze separation efficiency and expression levels of both parts of the construct. By analyzing hyphal cells

with fluorescence microscopy, it could be seen that mKate2 and Gfp were located in the nucleus. In addition, both fluorescence proteins seemed to be expressed in equal amounts (data not shown). To analyze the separation efficiency in more detail, total cell extracts of sporidia were subjected to SDS-PAGE and Western blot analysis. The Western blots showed a separation of mKate2^{HA}-d1-F2A and Gfp^{NLS} (Figure 2.19 C). In both blots, protein bands representing mKate2^{HA}-d1-F2A and Gfp^{NLS} were detected at sizes of 36 and 30 kDa, respectively. Thus, the F2A peptide seemed to work in *U. maydis*. However, strong bands at 70 kDa for the unseparated full length protein of mKate2^{HA}-d1-2A-Gfp^{NLS} were detectable in the blots incubated with α-HA antibody as well as with α-Gfp antibody. This indicated that the ratio of separated to unseparated protein was approximately 50%. Hence, the separation efficiency could be improved. Surprisingly, the band of 36 kDa representing the mKate2^{HA}-d1-F2A protein was detectable on the blot incubated with α-HA antibody (Figure 2.19 C). Thus, the construct was not degraded accordingly to previously generated results of d1 fused C-terminally to Gfp (Brachmann, 2001). Due to the fact that the separation of both proteins takes place in the last two C-terminal amino acids of the F2A peptide, the upstream 22 amino acids still remain at the C-terminus of the d1 sequence. The mODC PEST sequence is originally located at the end of the C-terminus. For mODC, conformational change and exposure of the hydrophilic PEST domain within the C-terminus is crucial for direct proteasomal degradation (Murakami et al., 1992). Therefore, embedment of the d1 sequence within a protein instead of at the end of the C-terminus prevent its exposure, leading to a reduction or loss of the signal for degradation in *U. maydis*.

In summary, these results indicated that the 2A peptide seemed to work in *U. maydis*. However, the separation efficiency within F2A was low and not sufficient for the application of visualizing local translation since the equilibrium of proteins encoded by analyzed mRNAs should be unchanged. To avoid degradation of 50% of the generated constructs, the separation efficiency had to be improved. For this, a linker study was conducted and several 2A peptides were tested. The tested d1 from mODC lost its activity as a degrading sequence. To prove that the tested PEST sequence has to be located at the end of the C-terminus of a protein, constructs with and without a short linker sequence were generated. Furthermore, another PEST sequence which is located within in a protein was tested. With this, the capability of destabilizing Gfp was tested.

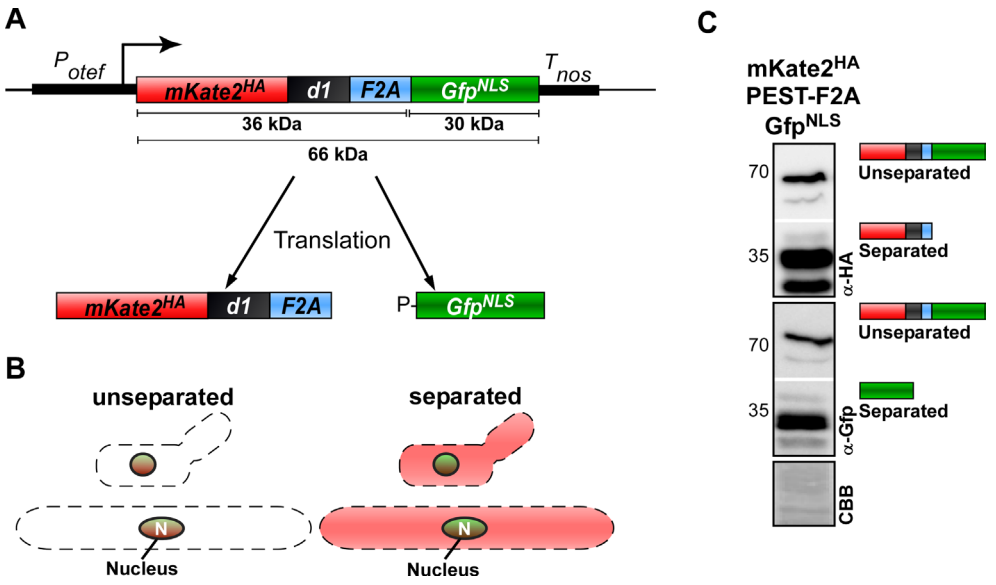

Figure 2.19: Analysis of combined action of d1 PEST sequence and F2A peptide. (A) Schematic representation of construct to analyze action of PEST and F2A peptide and the resulting proteins after translation due to F2A peptide separation: constitutively active promoter (P_{otef}), ORF encoding mKate2 fused to an HA tag (red, $mKate2^{HA}$), F2A (blue) and Gfp fused to a nuclear localization sequence (green, Gfp^{NLS}), transcriptional terminator (T_{nos}). **(B)** Scheme of fluorescent protein localization within yeast-like and hyphal cell of *U. maydis* displaying an inactive 2A peptide (left) or an active version (right) (modified according to (Müntjes et al., 2020; Figure 1). **(C)** Western blot analysis showing ratio of unseparated to separated proteins. 5 µg of whole cell extracts were subjected to SDS-PAGE and Western blot analysis. The proteins were detected with α-HA and α-Gfp antibodies and the membrane was stained with Coomassie brilliant blue after detection (CBB; Western blot membranes were cropped for better visualization).

2.3.2 Testing the role of linker sequences for the function of PEST sequences

To prove the hypothesis that the loss of the signal for degradation of the tested d1 PEST sequence of mODC was due to embedment within a protein instead of a localization at the end of the C-terminus, constructs of different PEST sequences fused downstream to Gfp and an eight amino acid C-terminal extension (linker, L) were generated (Figure 2.20 A). This linker was slightly hydrophobic which was consistent with a study analyzing naturally occurring linkers. Longer naturally occurring linkers were more hydrophilic (George and Heringa, 2002). The C-terminal extension was optimized for dicodon usage in *U. maydis*. For the analysis, both versions of mODC PEST sequence, d1 and d2, were used. In addition, a potential PEST sequence of the G1 cyclin Cln1 (UMAG_04791) of *U. maydis* was tested (G1; Castillo-Lluva and Perez-Martin, 2005). Unlike mODC PEST, this PEST sequence is not located at the end of the C-terminal of Cln1. This increases the probability that this PEST sequence works independently of a direct position at the C-terminus. This is further supported by the fact that in *S. cerevisiae* no direct conformational change induces the degradation of Cln1p, as serine and threonine residues are phosphorylated within the PEST sequence, which causes them to be recognized and processed by the ubiquitin-proteasome pathway (Lanker et al., 1996). The fusion constructs of Gfp and different PEST sequences were constitutively

expressed with P_{otef}. After verifying the correct integration of the constructs via Southern blot analysis, the internal protein levels were measured by Gfp fluorescence. As control, a strain expressing cytosolic Gfp (AB33-Gfp) was used. As indicated in Figure 2.20 B, the relative fluorescence units (RFUs) of AB33-Gfp revealed values of approximately 23,000. In comparison to this, all strains harboring a fusion of Gfp to PEST sequences showed a decreased Gfp fluorescence. The efficiency of degradation ranged from d1 with 1,300 RFUs over d2 with 3,600 RFUs to G1 with 13,800 RFUs, respectively (Figure 2.20 B). Thus, the efficiency of degradation can be scored as followed: d1 > d2 > G1. The linker (L) downstream of the PEST sequence increased the measured Gfp fluorescence for d1 and d2 significantly by the factor 3.8 for d1 and 2.8 for d2. This confirmed that the mODC PEST has to be placed at the end of the C-terminus of a protein to efficiently act as a degron sequence. The degron efficiency of G1 PEST was unaffected by the linker (Figure 2.20 B). Nevertheless, compared to d1 and d2, G1 PEST showed minor degradation efficiency. Here, in comparison to the control strain, 58% of the Gfp fluorescence was measured. It can be claimed that the G1 PEST sequence is not sufficient for needed level of protein degradation.

In summary, these results indicate that the two versions of mODC have to be placed at the end of the C-terminus of a fusion protein to act efficiently as degron sequence in *U. maydis* since a C-terminal linker consisting of eight amino acids already decreased the efficiency of degradation. In addition, it could be shown that the PEST sequence of G1 cyclin Cln1 from *U. maydis* can be used to degrade up to 60% of a protein to which the sequence is fused to. However, for a degradation of almost 100% of the fusion protein this sequence seemed to be not suitable. For the application of degrading synthesized peptide epitopes to which GCN4-scFv binds to, another degron sequence or degron system has to be found which obtains almost 100% degradation even though it is located within the fusion protein.

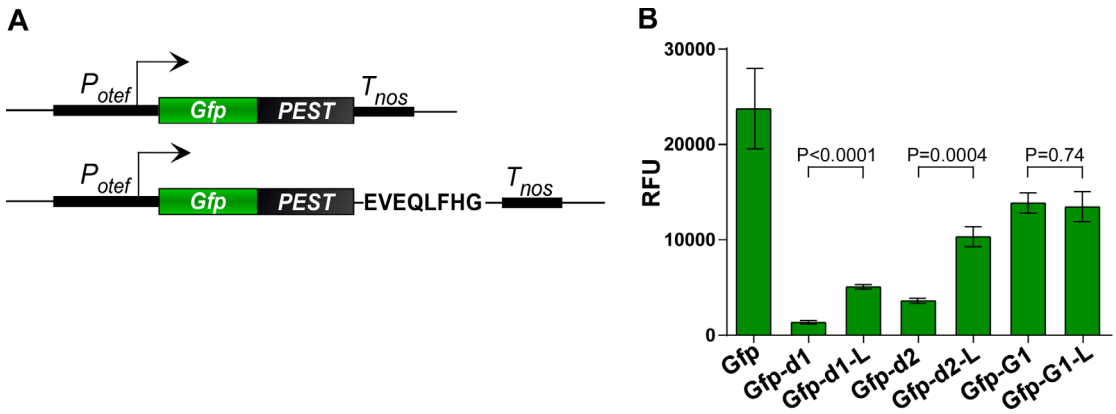

Figure 2.20: Testing the role of linker sequences for the function of PEST sequences. (A) Schematic representation of constructs with and without linker to analyze the influence of downstream linker sequences for degrading efficiency of PEST sequences: constitutively active promoter (P_{otef}), Gfp (green) fused to

different PEST sequences (gray), transcriptional terminator (T_{nos}). **(B)** Measurement of relative fluorescence units (RFU) of reporters expressed in hyphal cells of the following strains: AB33-Gfp (Gfp), two mODC PEST versions with (Gfp-d1-L and Gfp-d2-L) and without (Gfp-d1 and Gfp-d2) linker and G1 cylcin PEST sequence of *U. maydis* with (G1-Gfp-L) and without (G1-Gfp) linker (3 independent experiments with 3 technical replicates each; unpaired two-tailed t-test; $\alpha<0.05$).

2.3.3 Testing of linkers to enhance separation efficiency within F2A

To increase the separation efficiency of 2A peptides, the already established reporter construct containing the constitutively active P_{otef}, mKate2 fused to an HA tag (mKate2^{HA}) and Gfp fused to a nuclear localization signal (Gfp^{NLS}; Figure 2.21 A; Kalderon et al., 1984) was used. In contrast to the previous work, the d1 mODC sequence was removed from the construct, and different linkers upstream of F2A were tested since it was known from other organisms that linker sequences influence the expression of proteins connected by 2A peptides and ensure complete separation (Holst et al., 2006). For this, constructs without linker (no linker; NL) were compared to those having a short GSG linker sequence (L1) and a longer 18 amino acids linker (L2; Figure 2.21 B). Note that efficient separation in within F2A lead to two different proteins: mKate2^{HA}-F2A and Gfp^{NLS}. As a control, the same constructs without the C-terminal proline within the F2A were generated (F2AΔP) since this amino acid has been previously shown to be essential for separation (Ryan et al., 1991). The linker sequences were optimized for dicodon usage in *U. maydis* and the constructs were integrated into the *upp3* locus in the genetic background of AB33-*upp3*Δ via counter selection. After identifying positive recombination events by Southern blot analysis, the separation efficiencies within F2A with the different used linkers were analyzed by Western blot experiments. For this, total cell extracts of sporidia were subjected to SDS-PAGE followed by Western blot analysis in which proteins were detected with α-HA and α-Gfp antibodies (Figure 2.21 C). Expectedly, for the constructs containing F2AΔP no separation of mKate2^{HA}-F2AΔP and Gfp^{NLS} was observed. Independent of the used linker a signal with a size of around 70 kDa was detected on both Western blots. As indicated in Figure 2.21 C, low expression levels of the constructs without a linker were detectable compared to constructs containing the linkers L1 or L2. In addition, the expression level increased with the length of the linker sequence. Thus, L2 seemed to be suitable to enhance the expression level of proteins fused to 2A peptides. Only low separation efficiencies within F2A could be observed in all constructs (Figure 2.21 C). A strong band representing a fusion of mKate2^{HA}-F2A-Gfp^{NLS} was detectable at 70 kDa. Nevertheless, barely visible bands for Gfp^{NLS} around 35 kDa were also detected. Even though separation of two ORFs seemed to work with F2A, only minor separation efficiencies could be achieved in *U. maydis*.

In summary, linker sequences enhance the expression level of proteins separated by 2A peptides. It can be concluded that the expression level increases with the length of the linker. Because of this, L2 was chosen for further experiments. The separation efficiency of F2A appeared to be low. Thus, different 2A peptides had to be tested and analyzed towards their separation efficiencies.

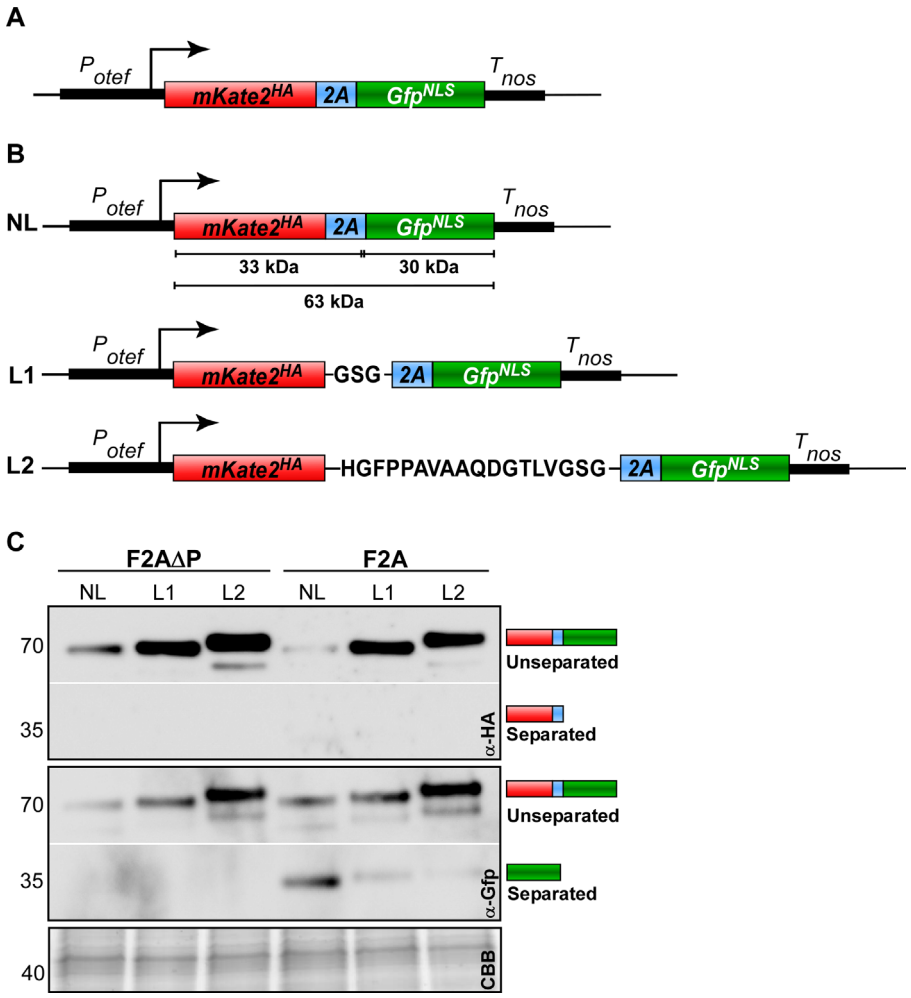

Figure 2.21: Reporter system for screening the activity of 2A peptides. (A) Schematic representation of reporter construct to analyze 2A peptides in *U. maydis* containing constitutively active P_{otef}, ORF encoding mKate2 fused to an HA tag (red, $mKate2^{HA}$), 2A peptide of interest (blue) and Gfp fused to a nuclear localization sequence (green, Gfp^{NLS}), transcriptional terminator T_{nos}. **(B)** Schematic representation of linker constructs for 2A peptide analysis: constitutively active promoter (P_{otef}), $mKate2^{HA}$ (red), F2A (blue), Gfp fused to NLS (green), transcriptional terminator (T_{nos}); no linker (NL), GSG linker (L1), 18 amino acid linker (L2). **(C)** Western blot analysis showing ratio of unseparated to separated proteins. 5 µg of whole cell extracts from sporidia were subjected to SDS-PAGE and Western blot analysis. The proteins were detected with α-HA and α-Gfp antibodies and the membrane was stained with Coomassie brilliant blue after detection (CBB; Western blot membranes were cropped for better visualization; modified according to (Müntjes et al., 2020; Figure 1).

2.3.4 Testing different 2A peptides regarding their cleavage efficiency

It has been previously demonstrated that 2A peptides from various viruses showed varying activities in different organisms (Kim et al., 2011; Souza-Moreira et al., 2018). In order to identify a 2A peptide which exhibits high separation efficiencies in *U. maydis*,

five different 2A peptides were analyzed. For this, P2A from Porcine teschovirus-1 (PTV), T2A from *Thosea asigna* virus (TaV), E2A from *Equine rhinitis* A virus (ERAV) and the already tested F2A from Foot-and-mouth-disease virus (FMDV) were chosen. In addition, Po2A from porcine rotavirus C (PoRV) was analysed which was not previously studied in other organisms. The 2A peptides have a size of 30 amino acids except F2A which comprises 23 amino acids. They all contain the characteristic C-terminal DXEXNPGP motif but differ in the rest of the amino acid sequence (Figure 2.22 A). The 2A peptides were inserted downstream of the L2 linker and the constructs were integrated into the *upp3* locus of AB33-*upp3*Δ. Note that efficient separation between the different 2A peptides leads to two different proteins: mKate2^{HA}-L2-2A and Gfp^{NLS} (Figure 2.22 A). After verification of correct transformants by Southern blot analysis, total cell extracts of sporidial cells were studied by Western blot analysis to investigate the different 2A peptide separation efficiencies (Figure 2.22 B). The separation efficiencies of the different 2A peptides were qualitatively evaluated from the ratio of unseparated versus separated variants of mKate2^{HA}-L2-2A and Gfp^{NLS}. As indicated in Figure 2.22 C, F2A and Po2A were barely active. Only the band representing the fusion of mKate2^{HA}-L2-2A-Gfp^{NLS} was detected at 70 kDa in both Western blots. Increased separation efficiencies were observed for E2A, T2A and P2A and the latter showed the highest efficiency since only bands for the two separated proteins were detected (Figure 2.22 B). Thus, P2A seemed to be the best performing 2A peptide in *U. maydis*.

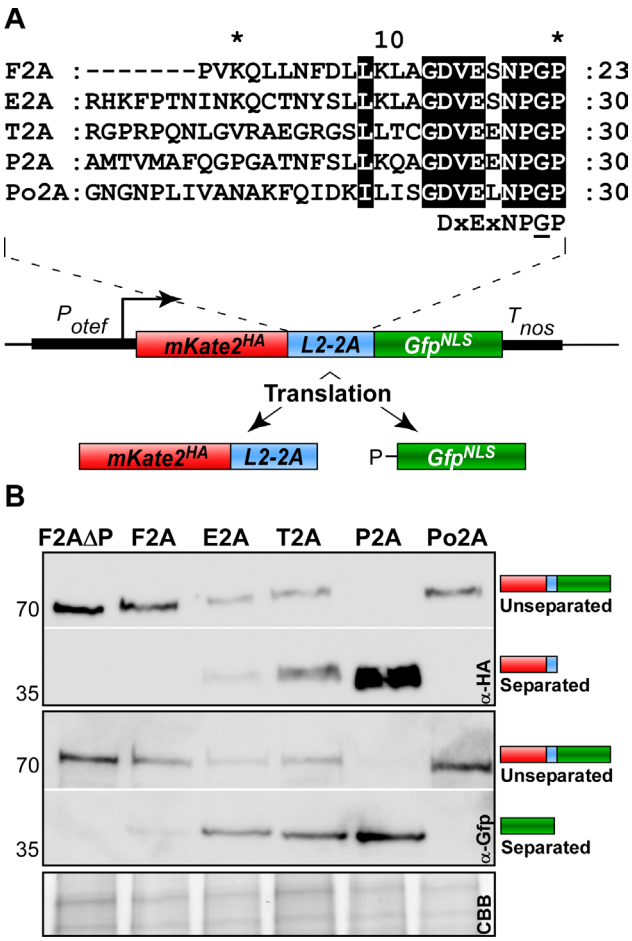

Figure 2.22: Separation efficiencies of 2A peptides (A) Top: Sequence comparison of 2A peptides (highlighted in black: conserved and important amino acids; arrow indicates point of peptide separation; consensus sequence below). Bottom: Schematic representation of reporter construct and the resulting proteins after translation due to 2A peptide separation: constitutively active promoter (P_{otef}), mKate2^{HA} (red), L2 linker upstream of the 2A peptide of interest (blue), Gfp^{NLS} (green), transcriptional terminator (T_{nos}). (**B**) Western blot analysis showing ratio of unseparated to separated proteins for the different tested 2A peptides. 5 µg of whole cell extracts were subjected to SDS-PAGE and Western blot analysis. The proteins were detected with α-HA and α-Gfp antibodies and the membrane was stained with Coomassie brilliant blue after detection (CBB; Western blot membranes were cropped for better visualization; modified according to (Müntjes et al., 2020; Figure 2).

Because of the fusion of Gfp to an NLS sequence, the separation efficiency was in an additional experiment analyzed by fluorescence microscopy. If the separation efficiency within a 2A peptide is high, separated mKate2^{HA}-L2-2A is expected to localize in the cytoplasm in contrast to Gfp^{NLS}, which should mainly localize to the nucleus (Figure 2.19 B). For the fluorescence microcopy, sporidial cells as well as hyphal cells were analyzed. The fluorescence microscopy revealed that the 2A peptides at the N- and C-termini did not interfere with the fluorescence of mKate2 and Gfp. Besides, a strong fluorescence signal of mKate2 and Gfp was detectable in the nucleus of sporidial as well as hyphal cells (Figure 2.23 A and B; Figure 6.2). P2A was an exception to this because mKate2 fluorescence was also visible in the cytoplasm (red arrowheads; Figure 2.23 A; Figure 6.2). This underlines the impression already gained by Western blot analysis that P2A

seemed to have very high separation efficiency in *U. maydis*. To quantify the separation efficiencies, fluorescence resonance energy transfer (FRET) measurements between the reporters Gfp and mKate2 were conducted in sporidial cells. The phenomenon of FRET can only occur if the donor fluorophore (Gfp^{NLS}) is in very close proximity (below 10 nm) to the acceptor ($mKate2^{HA}$-L2-2A;Lakowicz, 2006). FRET is decreasing with an increasing distance between the two fluorescence proteins. Thus, FRET experiments conducted in the nucleus showed the amount of unseparated reporter proteins (Figure 2.23 C), because the fusion protein $mKate^{HA}$-L2-2A-Gfp^{NLS} accumulated in the nucleus due to its NLS. Note that $mKate^{HA}$-L2-2A itself is able to enter the nucleus due to its small size even in the absence of an NLS (Figure 2.23 A; Figure 6.1). However, a so-called “bystander FRET” effect (unspecific FRET due to crowding of non-interacting donor and acceptor) is only likely at very high concentrations of proteins (King et al., 2014). Thus, the small amount of free mKate2 protein in the nucleus which was observed with fluorescence microscopy (Figure 2.23 A) should not interfere with the measurement. With the experimental set-up, minor but very stable apparent FRET efficiencies ($FRET_{app}$) were measured. The highest $FRET_{app}$ efficiency was observed in the nucleus of cells expressing the unseparated negative control F2AΔP, contrary to reduced $FRET_{app}$ efficiencies within cells expressing constructs with the different 2A peptides (Figure 2.23 C). The highest $FRET_{app}$ efficiency of the different 2A peptides was observed for F2A, followed by Po2A, T2A, E2A and P2A in descending order. P2A showed $FRET_{app}$ efficiencies comparable to the control strain only expressing Gfp. Therefore, P2A had a nearly 100% separation rate determined *in vivo*. This is consistent with the results obtained by the Western blot analysis (Figure 2.22 B) and the live cell fluorescence microscopy (Figure 2.23 A; Figure 6.2). Note that the negative values of $FRET_{app}$ were due to slight acquisition bleaching of Gfp. The other tested 2A peptides had separation rates of 20% for F2A, 30% for Po2A, 40% for T2A and 60% for E2A (Figure 2.23 C). Thus, FRET measurements were suitable and sensitive enough for making a quantitative statement about the separation efficiencies of different 2A peptides.

In summary, these experiments showed that the activity of different tested 2A peptides ranged from 20-100% in *U. maydis*. The 2A peptide exhibiting the highest separation efficiency was P2A from porcine teschovirus. After identification of another suitable degron sequence or system, this can be combined with P2A to separate $GCN4^{24}$ and the synthesized protein from the analyzed mRNA for the application of visualizing local translation. By this, the background fluorescence will be decreased without affecting the equilibrium of synthesized proteins. To illustrate the applicability of P2A, it was used to monitor regulated gene expression. For this, the induction of a

promoter over time as well as protein degradation was quantified using a straight forward reporter enzyme activity assay.

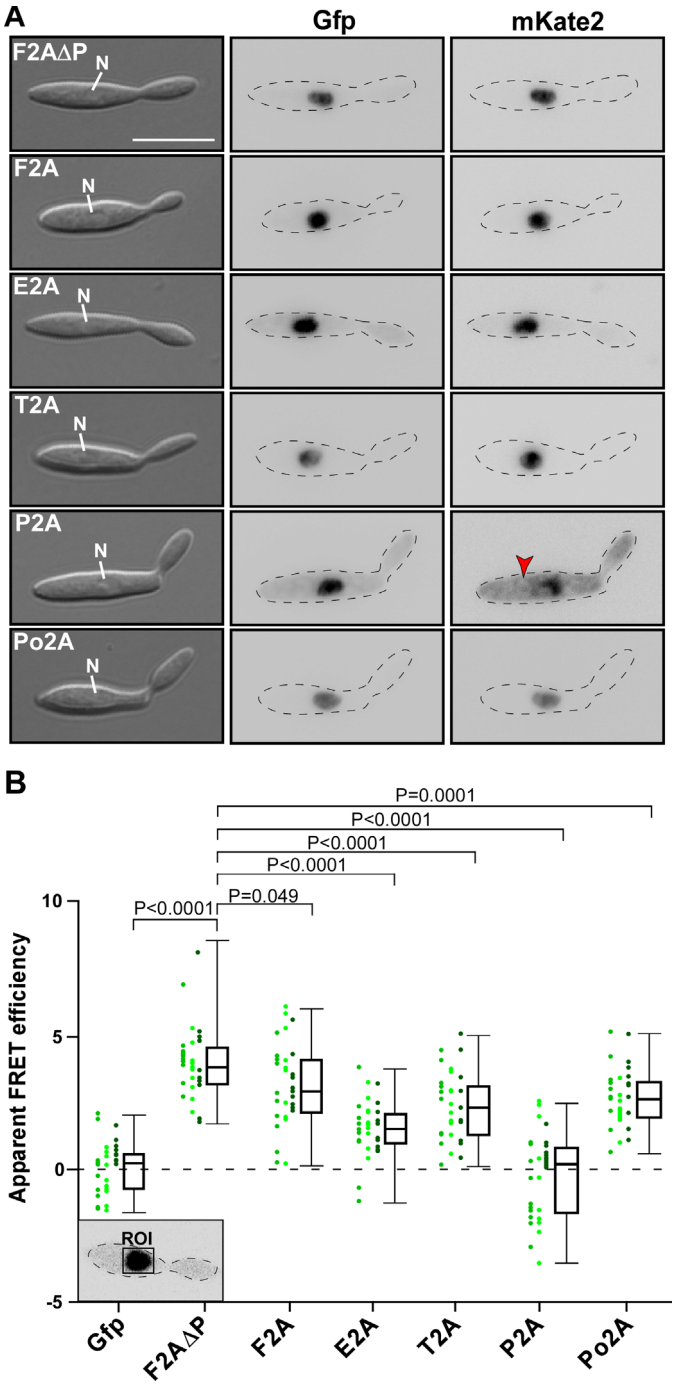

Figure 2.23: Separation efficiencies of 2A peptides analyzed *in vivo*. **(A)** Morphology and fluorescence microscopy of sporidial cells expressing reporter construct for analysis of 2A peptide separation efficiency (inverted picture; N, nucleus; strong fluorescence signal in cytoplasm is indicated by red arrowhead; scale bar 10 µm; for hyphal cells: 6 h.p.i.; growth direction is indicated by arrow). **(B)** Apparent FRET efficiencies of tested 2A peptides determined within nucleus (ROI, region of interest; green dots show apparent FRET efficiencies in individually measured cells; each shade of green represents an independent experiment, (n = 3), box and whisker plot shows median and min and max values; for each experiment > 10 yeast cells were analyzed; unpaired, two-tailed t-test, $\alpha<0.05$; modified according to (Müntjes et al., 2020; Figure 3).

2.3.5 Quantification of Rrm4 protein amounts within the cell using P2A peptide

To monitor regulated gene expression, the *Photinus pyralis* firefly luciferase fused to an HA tag ($FLuc^{HA}$; L. Hüsemann et al., manuscript in preparation) was combined with Rrm4-Gfp using L2-P2A (Figure 2.24 A). A luciferase was already successfully implemented to determine the activity of P2A in *A. niger* (Schuetze and Meyer, 2017). The FLuc activity enabled a straight forward read-out of protein levels within the cell since the converted substrate luciferin is able to pass the cell wall of *U. maydis*. The main advantage of measuring FLuc activities in comparison to Gfp fluorescence is that there is almost no background luminescence in this measurement. The transcription of the desired construct was under the control of the inducible promoter from the arabinase gene *crg1* which is active in the presence of arabinose and inactive in the sole presence of glucose (Figure 2.24 A; Bottin et al., 1996; Brachmann, 2001). The construct was integrated at the ip^S locus via homologous recombination in the genetic background of AB33-*rrm4*Δ. The resulting strain will be referred to as follows: AB33-P_{crg}-Rrm4-Gfp-P2A-$FLuc^{HA}$. After identifying positive recombination events by Southern blot analysis, a Western blot experiment of hyphae growing under uninduced and induced conditions was performed to analyze the protein expression level. As indicated in Figure 2.24 B, FLuc as well as Rrm4-Gfp were expressed in medium containing arabinose and both were fully separated by P2A. The analysis of the morphology of hyphae grown in arabinose or glucose revealed that only hyphae grown in medium containing glucose grew in a bipolar mode (Figure 2.24 C). Note that this growth is characteristic for loss of key components of the mRNP complex in *U. maydis*. Importantly, hyphae grew in a unipolar manner in medium containing arabinose, indicating the expression of a functional version of Rrm4 (Figure 2.24 C). To analyze the subcellular localization, fluorescence microscopy of Rrm4-Gfp was conducted in hyphae which grew in medium containing arabinose or glucose. As control, a strain expressing Rrm4-Gfp with its native promoter was included (AB33-P_{rrm4}Rrm4-Gfp). In this strain, no influence of the carbon source on the dynamic subcellular localization of Rrm4 could be observed. Under both conditions Rrm4 shuttled bidirectionally through hyphae of *U. maydis* (red arrowheads; Figure 2.24 D). The same localization of Rrm4 was visible in AB33-P_{crg}-Rrm4-Gfp-P2A-$FLuc^{HA}$ grown in arabinose. However, no fluorescence signal was detectable in the presence of glucose indicating that the promoter was switched off (Figure 2.24 D).

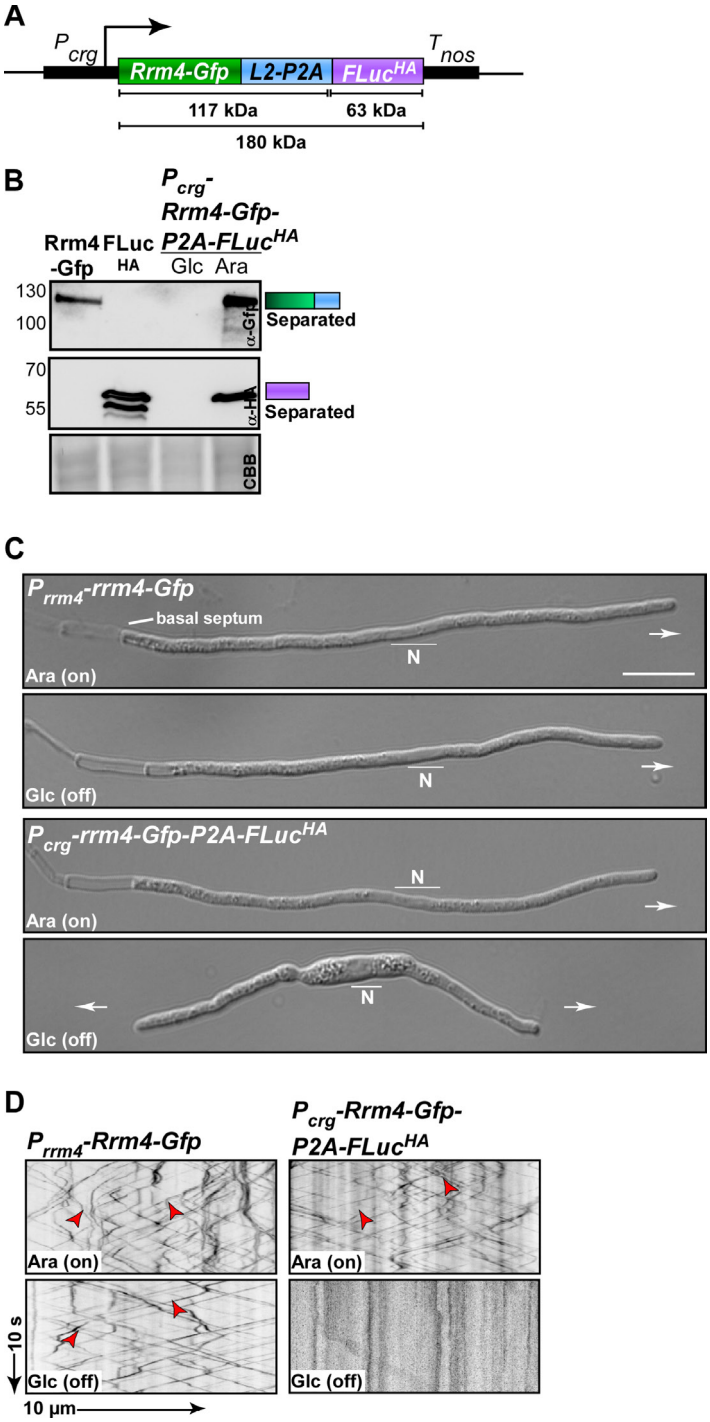

Figure 2.24: Morphology of strain expressing arabinose-inducible Rrm4-Gfp. (A) Schematic representation of a construct to analyze regulated gene expression: arabinose-inducible promoter (P_{crg}), Rrm4 fused to Gfp (green), L2 linker fused to P2A (blue), firefly luciferase fused to HA tag ($FLuc^{HA}$; purple), transcriptional terminator (T_{nos}). **(B)** Western blot analysis of strain expressing construct explained in A in induced and uninduced conditions. 5 µg of whole cell extracts were subjected to SDS-PAGE and Western blot analysis. The proteins were detected with α-HA and α-Gfp antibodies and the membranes were stained with Coomassie brilliant blue after detection (CBB; Glc: Glucose; Ara: Arabinose). **(C)** Morphology of growing hyphae expressing Rrm4-Gfp and $FLuc^{HA}$ separated by P2A in induced and uninduced conditions (6 h.p.i.; Glc: Glucose, Ara: Arabinose; growth direction is indicated by arrow; N, nucleus; scale bar 10 µm). **(D)** Kymographs of hyphae expressing Rrm4-Gfp and $FLuc^{HA}$ separated by P2A in induced and uninduced conditions (6 h.p.i.; Glc: Glucose; Ara: Arabinose; arrow length on the left and bottom indicates time and distance). Bidirectional movement is indicated with red arrowheads (modified according to (Müntjes et al., 2020; Figure 4).

To analyze the induction of the P_{crg} promoter in the presence of arabinose, sporidial cells were initially grown in the presence of glucose. After switching the cells to hyphal growth, the cells were still grown in the presence of glucose (t = 0; Figure 2.25 A). At different time points, 1 h (T1), 2 h (T2) and 3 h (T3) post induction of hyphal growth, hyphae were transferred into medium containing arabinose, and FLuc activity (relative luminescence units; RLU) as well as the fluorescence signal of Rrm4-Gfp were analyzed. As positive and negative control, AB33-P_{crg}-Rrm4-Gfp-P2A-$FLuc^{HA}$ was kept constantly in medium containing arabinose or glucose, respectively, to analyze the background luminescence as well as maximum FLuc activity rates. As indicated in Figure 2.25 A, FLuc activity increased after shifting to medium containing arabinose, indicating an activation of the P_{crg} promoter. A slightly delayed induction in T1 was visible, since the fold change of 300 in FLuc activity was decreased in contrast to 500-600 in T2 and T3. After two hours, fold changes of FLuc activity of around 2,000 were measured in T1, T2 and T3, respectively. Thus, the induction rates of the P_{crg} promoter did not differ in between the samples (Figure 2.25 A). In contrast to the arabinose control, in which a maximum FLuc activity of 650,000 RLU was measured, maximum values of 300,000 RLU, 360,000 RLU and 380,000 RLU for T1, T2 and T3 were measured six hours post induction of hyphal growth (Figure 2.25 A). Hence, AB33-P_{crg}-Rrm4-Gfp-P2A-$FLuc^{HA}$ in T1, T2 and T3 did not reach the maximum FLuc activity measured in the control after six hours. In addition, the maximum FLuc activity measured in T1 was lower compared to T2 and T3. Together with the delayed induction, it can be claimed that a subsequent induction of hyphal growth and the P_{crg} enlarged the stress level in the cells and therefore a lower FLuc activity was measured. Under all conditions, shuttling of Rrm4-Gfp was visible after two hours of inducing P_{crg} which was consistent with increased fold change rates of FLuc activity after two hours (Figure 2.25 B). After six hours, the signal intensities were comparable to a strain expressing Rrm4-Gfp under the control of the native promoter (red arrowheads; Figure 2.25 B). Importantly, no shuttling of Rrm4-Gfp was observed in AB33-P_{crg}-Rrm4-Gfp-P2A-$FLuc^{HA}$ constantly kept in glucose.

In summary, these results show that the usage of 2A peptides enabled simple and reliable quantification of gene expression. This approach can be used to investigate other aspects like mRNA stability, protein turnover or degradation.

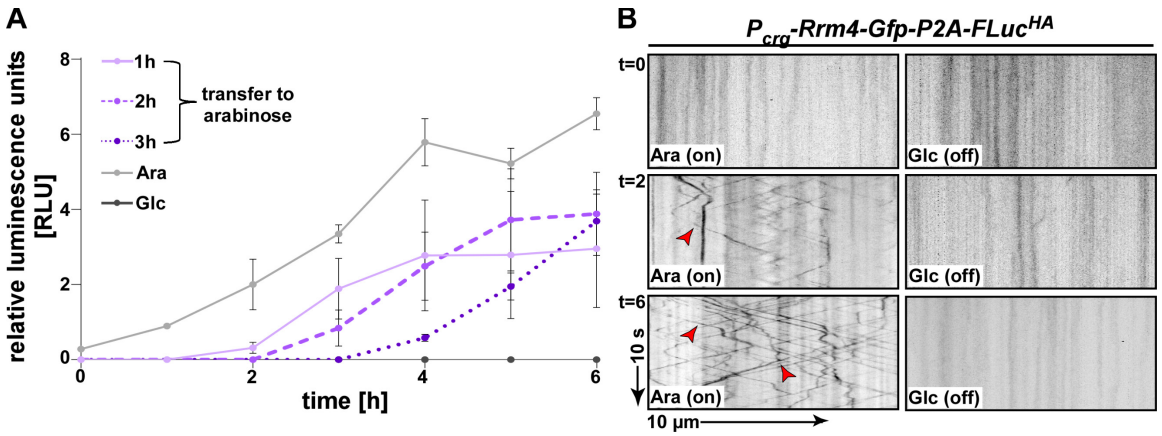

Figure 2.25: Monitoring the induction and turn-off of P_{crg} promoter driving the expression of Rrm4-Gfp and $FLuc^{HA}$ separated by P2A. (A) FLuc activity measured in a strain expressing Rrm4-Gfp-P2A-$FLuc^{HA}$ shifted to hyphal growth at time point 0. After 1, 2 or 3 h cells were transferred to medium containing arabinose (purple variants). As control, FLuc activities were measured in the same strain grown in glucose (black) or arabinose (gray) for the whole time period of the experiment (error bars, SEM; n = 3 independent experiments, relative luminescence units are given). **(B)** Kymographs of hyphae containing the construct P_{crg}-Rrm4-Gfp-P2A-$FLuc^{HA}$ after different time points of switching to medium containing arabinose (Glc: Glucose; Ara: Arabinose; arrow length on the left and bottom indicates time and distance; bidirectional movement is indicated with red arrowheads; modified according to (Müntjes et al., 2020; Figure 4).

3 Discussion

The spatiotemporal regulation of protein expression plays a crucial role for asymmetric cell division, cell migration and neuronal morphogenesis. An important process in this regulation is the active transport of mRNAs along the cytoskeleton. In previous studies, *U. maydis* served as an excellent model organism to study the long distance co-transport of mRNAs and endosomes along microtubules. Here, the key RBP Rrm4 binds mRNAs and hitchhikes on Rab5a-positive endosomes for bidirectional movement through hyphae (Becht et al., 2006; König et al., 2009; Baumann et al., 2012). Due to results obtained in co-localization studies, it is assumed that local translation of transported mRNAs takes place on endosomes (Baumann et al., 2014). This seems to be particularly important for the assembly and delivery of septin complexes (Zander et al., 2016). Recent studies showed that Rrm4 binds predominantly within the 3´UTR of target mRNAs but also to landmark sites of translation (Olgeiser et al., 2019). This further suggests a close connection between Rrm4-dependent mRNA transport and translational processes. However, the technical means to study the sites of translation of single mRNAs *in vivo* had not been established. Thus, this project was focused on the establishment of an antibody-based method to simultaneously visualize a nascent peptide chain and the corresponding mRNA *in vivo*. This technique should lead to better insights in translational processes on endosomes as well as the role of Rrm4 in translation. To visualize local translation of mRNAs in hyphae of *U. maydis in vivo*, various building blocks for labeling both the mRNA and their cognate peptide chain had to be established. For labeling of mRNAs within their 3´UTR, the Rfp mKate2 was successfully established. In addition, it was discovered that the analyzed antibodies GCN4-scFv, BC2-Nb and Moontag-Nb, which were fused to sfGfp, shuttled bidirectionally on Rab5a-positive endosomes in a microtubule-dependent manner through hyphae. Deletion of the potential interacting protein UMAG_00933, which was identified by LC-MS/MS analysis, abolished unspecific shuttling of GCN4-scFv and BC2-Nb. Furthermore, GCN4-scFv-sfGfp interacted with its cognate peptide epitope *in vivo*. Therefore, this antibody can potentially be used to label a nascent peptide chain. It was confirmed that for full functionality, a degron sequence (PEST) derive from mODC has to be located at the C-terminus of a protein. To maintain the equilibrium of proteins encoded by analyzed mRNAs, P2A was successfully established to separate two ORFs with separation efficiencies of nearly 100%. This enables the degradation of the expressed peptide epitope bound by GCN4-scFv-sfGfp without degrading synthesized proteins encoded by analyzed mRNAs.

3.1 mKate2 is a suitable Rfp to label mRNAs in *U. maydis in vivo*

At the beginning of this project, mRNAs were labeled within their 3´UTR with the λN system in which λN* was fused to double Gfp (Baumann et al., 2014). For simultaneous labeling of a nascent peptide chain and the corresponding mRNA, the mRNA has to be labeled with a Rfp since the nascent peptide chain is tagged by sfGfp. In previous studies, the Rfps mCherry and TagRfp were tested regarding their ability to label the 3´UTRs of mRNAs (Müntjes, 2015). Here, the two Rfps accumulated in vacuoles and outshined moving mRNAs. A fusion of mCherry or TagRfp to an NLS did not abolish these accumulations (Müntjes, 2015). This kind of accumulations were not observed with Gfp and can be explained with the high sensitivity of Gfp to low pH values. pH sensitivity is attributed to the protonation of the electron-rich, light-absorbing part of the chromophore, which occurs at lower pH (Roberts et al., 2016). This phenomenon can be referred to the pKa values of the different fluorescence proteins. The pKa values of Gfp, mCherry and TagRfp are 6, <4.5 and <4.0, respectively (Merzlyak et al., 2007; Ma et al., 2014). Thus, compared to Gfp, mCherry and TagRfp have sufficient acidic resistance to allow the emission of a fluorescence signal upon excitation under acidic conditions. Due to this, an alternative Rfp was required, which is not able to emit at low pH. For this, mKate2 and mOrange2 were chosen as potential Rfps. mKate2 has a relative brightness of 74% as compared to Gfp and a pKa value of 5.4 (Day and Davidson, 2009). Thus, it is described to show moderate acid sensitivity (Shcherbo et al., 2009). mOrange2 has a pKa value of 6.5 and it is described to show a high acid sensitivity (Shaner et al., 2008). Furthermore, mOrange2 has a relative brightness of 104% as in comparison to Gfp (Day and Davidson, 2009).

mKate2 and mOrange2 were analyzed in a fusion with Rrm4 and compared to the already established Rfps mCherry and TagRfp. The fusion of Rrm4 to mKate2 and mOrange2 were fully functional resulting in unipolar growing hyphae, whereas the loss of Rrm4 increases the number of bipolar growing hyphae (Becht et al., 2006). Bidirectional movement of Rrm4 through hyphae could be observed with mCherry, TagRfp and mKate2 (Figure 2.1 A-D). The signal of Rrm4-mOrange2 was barely visible (Figure 2.1 C). Note, that mOrange2 fluorescence emission was measured with optimal excitation in a plate reader. Hence, mOrange2 can in general be used to label proteins in *U. maydis* if detection is conducted with a different microscopy set-up. In mammalian cells, the brightness of mKate2 and TagRfp was higher compared to mCherry (Day and Davidson, 2009). Using line scan measurements, it turned out that TagRfp was the brightest Rfp, followed by mKate2, mCherry and mOrange2 (Figure 2.1). In addition, the brightness of mKate2 was significantly increased compared to mCherry, whereas it was significantly decreased for mOrange2. Except for mOrange2, the ratios of the brightness of the

individual Rfps correspond to already measured ratios in mammalian cells (Day and Davidson, 2009; Piatkevich et al., 2010).

In *U. maydis*, the shuttling of Rrm4 visualized with mKate2 and mCherry was visible for 75 s even though in direct comparison more moving particles were detected with mKate2 (Figure 2.2). Contrary to this, Rrm4-TagRfp signals disappeared rapidly. This corresponds to the photostabilities of mCherry, TagRfp and mKate2 measured in mammalian cells where mKate2 is slightly more photostable than mCherry (Bindels et al., 2017). The ability of mKate2 to emit a fluorescence signal under acidic conditions and thus the visible accumulation in vacuoles was analyzed in hyphae. In accordance to the literature and the pKa value, Gfp was not visible in vacuoles of U*. maydis* (Figure 2.2 B). The cellular fluorescence signal of mKate2 was interrupted by structures stained with a vacuolar dye (Figure 2.2 E). This indicated that mKate2 seemed to be unable to emit a fluorescence signal under acidic conditions. Thus, mKate2 probably exhibits high or moderate acidic sensitivity, which was observed before in mammalian cells (Shcherbo et al., 2009).

In RNA live imaging experiments using λN*-mKate2[2], the movement of *cdc3* mRNAs was visible. In contrast to the fusion of λN* to a double Gfp, which was used before to analyze the localization of *cdc3* mRNA in *U. maydis* (Baumann et al., 2014; Zander et al., 2016), a background-reduced fluorescence imaging was possible. However, in addition to weaker *cdc3* mRNA signals, shuttling signals with higher fluorescence intensities were observed (Figure 2.3 B). An explanation could be a potential dimerization of mKate2. mKate2 showed a monomeric character at high concentrations in mammalian cells (Shcherbo et al., 2009). However, high-pressure liquid chromatography (HPLC) analysis revealed the presence of an equilibrium of monomer-dimer fractions of mKate2 (Lin et al., 2009). Even though this equilibrium is most probably due to very high protein concentrations during HPLC, the dimerization events could explain shuttling of brighter fluorescence signals in RNA live imaging experiments with λN*-mKate2[2]. Importantly, these accumulations were mRNA-dependent (Figure 2.3 C) and would probably not interfere with further experiments. In addition, the usage of mKate2 in fusion with proteins seems to cause no apparent difficulties in *U. maydis* as it is now frequently used in other experiments. However, the potential of a slight dimerization of mKate2 should be considered for further applications. In recent years, a new class of Rfps has been developed, which show no dimerization tendency. They vary in their pKa values and usually have a lower brightness compared to Gfp (Wannier et al., 2018). Whether one of these fluorescent proteins is suitable for the visualization of mRNAs in *U. maydis* without the formation of any brighter accumulations could be tested in the future. In summary, it can be concluded that

mKate2 was established as another Rfp for the visualization of proteins in *U. maydis*. It exhibits better photostability than the previous used Rfps and is unable to emit light under acidic conditions. Therefore, it can be used to label mRNAs *in vivo*.

3.2 Recruitment of antibodies to early endosomes via UMAG_00933

3.2.1 Single chain variable fragments and nanobodies shuttle unspecifically through hyphae of *U. maydis*

Besides visualizing the subcellular localization of translation *in vivo*, co-tracking of a nascent peptide chain and the corresponding mRNA enabled the analysis of translation initiation as well as the elongation (Wang et al., 2016; Wu et al., 2016). The analysis of translation in real time revealed moving polysomes in dendrites (Wang et al., 2016; Wu et al., 2016), which coincides with the assumption that the transport of mRNAs is accompanied by their translation in *U. maydis* (Baumann et al., 2014). The measured elongation rates between three and ten amino acids per second were comparable to previously measured rates by pulse-chase experiments (Bostrom et al., 1986; Wang et al., 2016; Wu et al., 2016; Yan et al., 2016). This underlines the preciseness and strength of this approach. Moreover, the direct interaction of polysomes with membranous structures like the ER, mitochondria and late endosomes was observed (Wang et al., 2016; Wu et al., 2016; Cioni et al., 2019). This further supports the assumption that the association of mRNA transport and their translation on membranous structures, which was initially discovered in *U. maydis* by co-localization studies (Baumann et al., 2014), seems to be conserved.

To label a nascent peptide chain, an antibody has to be expressed which binds its cognate peptide epitope *in vivo*. For this, the *upp3* locus was successfully established with comparable expression rates measured in the well-studied ip^S locus (Figure 2.4). Upp3 is a protease whose deletion had no severe effect on the morphology of *U. maydis* (Sarkari et al., 2014). The first two antibodies which were tested regarding their ability to label nascent peptides were already successfully expressed in fusion to the chitinase Cts1 in sporidia of *U. maydis* (Sarkari et al., 2014; Terfrüchte et al., 2017). Myc-scFv against the myc-epitope and Bot-Nb against the botulinum toxin were expressed in fusion to sfGfp in the *upp3* locus. The expression of Myc-scFv-sfGfp was reduced in hyphae compared to sporidia (Figure 2.5 B). The reasons for a lower expression of the Myc-scFv-sfGfp in hyphae compared to sporidia was not further investigated in this project. It can only be assumed that the construct seems to be degraded or is potentially unstable in hyphae. In the above-mentioned study, in which Myc-scFv was fused to Cts1, only the expression in sporidia was analyzed (Sarkari et al., 2014). The expression

of Bot-Nb-sfGfp was low in both growth forms (Figure 2.5 C). The protein amount of Bot-Nb analyzed in whole cell extracts of AB33 sporidia was already described to be diminished in fusion to Cts1 (Terfrüchte et al., 2017). Nevertheless, the expression of Bot-Nb-sfGfp was investigated, since a different composition of the construct and the usage of a different promoter compared to the previous experiments could have led to a different expression rate. However, because the intended application of the antibodies is needed in hyphae, other antibodies were tested regarding their expression. In mammalian cells, the SunTag antibody GCN4-scFv, which was originally established in *S. cerevisiae* was used to label a nascent peptide chain (Wang et al., 2016; Wu et al., 2016; Yan et al., 2016; Cioni et al., 2019). GCN4-scFv-sfGfp was detected in sporidial as well as hyphal cells. GCN4-scFv-sfGfp shuttled microtubule-dependent in a bidirectional manner on early endosomes through hyphae (Figure 2.6). This unexpected endosomal localization was neither described in mammalian cells nor in *S. cerevisiae* (Worn et al., 2000; Tanenbaum et al., 2014). Because of the unspecific shuttling of GCN4-scFv-sfGfp, two additional nanobodies, BC2-Nb and Moontag-Nb, were expressed and analyzed with respect to their localization in *U. maydis*. Both antibodies resembled the same localization as GCN4-scFv-sfGfp. Importantly, the shuttling can be directly attributed to the antibodies, since the expression of the same construct without an antibody did not lead to any shuttling particles (Figure 2.8). In summary, the antibodies investigated in this project showed an unexpected cellular localization that could not be resolved by deleting possible interaction partners.

The obtained results suggest that there could be a protein that can interact with antibodies, even if the origin of scFv and Nb is different. Using Far-Western blot methodology, a strong interaction of GCN4-scFv-sfGfp with a protein which has a molecular size of approximately 130 kDa was detected (Figure 2.9). This result confirmed that GCN4-scFv-sfGfp interacts with an unknown protein. Based on the same cellular localization of all antibodies, it can be concluded that they probably interact with this protein. A possible interaction can be explained by comparable peptide epitope sequences recognized by the different antibodies, a similar amino acid sequences of the antibodies themselves or a comparable tertiary structure. No homologous regions were found within the amino acid sequences of the recognized peptide epitopes (Figure 2.10 A). Furthermore, the recognition of BC2-Nb relies on sequence-independent backbone interactions (Braun et al., 2016). Thus, an interaction to an unknown protein based on comparable peptide epitope sequences which are recognized by the different antibodies can be excluded. Within the amino acid sequences of the analyzed antibodies, areas with a high level of coincidence were found. Especially the N-termini of BC2-Nb and Moontag-Nb showed a high degree of sequence homology with the N-terminus of the V_H

domain of GCN4-scFv (Figure 2.10 B). In general, the sequence diversity between different scFv is higher than in Nbs. This can be referred to the origin of scFv from many different IgG antibodies from different species compared to the smaller number of genes that are used to produce the majority of Nbs (Mitchell and Colwell, 2018). However, the V_H domain of scFvs and Nbs, show a high degree of amino acid sequence identity (Muyldermans et al., 2001). The amino acid sequence similarity found in the antibodies analyzed in this project is therefore consistent with the data sets which are already described. Based on the amino acid sequence alignment, an interaction of an unknown protein with the N-termini of all antibodies could be possible. The tertiary structure of the three analyzed antibodies showed a high structural identity within the V_H domain of GCN4-scFv and the whole sequence of BC2-Nb and Moontag-Nb. This phenomenon was already described in an earlier report in which Nbs adopt the typical IgG fold and cover perfectly the structure of V_H domains of full IgGs or scFv (Muyldermans et al., 2001). Thus, an interaction to an unknown protein based on a similar tertiary structure of the V_H domain of GCN4-scFv and BC2-Nb as well as Moontag-Nb is also conceivable.

The shuttling behavior of GCN4-scFv-sfGfp, BC2-Nb-sfGfp and Moontag-Nb-sfGfp resembled the movement of mRNP components which shuttle on the endosomal surface (König et al., 2009; Baumann et al., 2012; Pohlmann et al., 2015; Jankowski et al., 2019). Hence, it was particularly important to find out whether the protein which seemed to be responsible for the recruitment of antibodies to early endosomes is directly involved in the long-distance transport of mRNAs. Note, that not all proteins involved in the transport of mRNAs are already known. Therefore, only the core components *upa2*, *rrm4*, *upa1* and *kin3* of the mRNA transport were deleted, because the loss of these proteins causes other proteins to lose their association to mRNPs. The deletion of *upa2*, for example, leads to a reduced shuttling of Pab1 and thus mRNAs, but does not affect the localization of the RBP Rrm4 (Jankowski et al., 2019). On the other hand, the deletion of *rrm4* causes Upa2 to be no longer associated in to mRNP complexes (Jankowski et al., 2019). The deletion of *rrm4* does not affect the localization of Upa1 (Pohlmann et al., 2015). Deletion of *kin3*, the plus-end directed microtubule motor protein, influences the shuttling of all analyzed components of the mRNP complex (Baumann et al., 2012; Pohlmann et al., 2015). This clearly shows the hierarchical interdependencies of the individual proteins of mRNP complexes and illustrates that the deletion of important components of the mRNP complex can lead to the loss of further proteins. In accordance to the literature, the deletion of the core mRNP proteins led to a bipolar growth of analyzed hyphae. However, deletion of *upa2*, *rrm4* and *upa1* did not influence the cellular localization of GCN4-scFv-sfGfp (Figure 2.12). Notably, the velocity of moving particles of GCN4-scFv-sfGfp was significantly increased in the *upa2* and *rrm4*

deletion strains. This phenomenon was observed before for moving Rrm4-Gfp signals in *upa2* depleted hyphae suggesting that the absence of Upa2 and Rrm4 in mRNP complexes has an influence on transporting endosomes in general (Jankowski et al., 2019). Therefore, it can be assumed that GCN4-scFv-sfGfp and thus all tested antibodies co-traffic with early endosomes which also transport mRNPs. Interestingly, significantly less moving particles of GCN4-scFv-sfGfp were observed in the *kin3*Δ strain. However, some moving particles were detected in *kin3* depleted hyphae which possessed a significantly reduced velocity but unaltered travelled distance. This underlines that Kin3 is important for the trafficking of an unknown protein which seems to recruit antibodies to early endosomes. However, this protein also appears to be transported by an alternative motor protein. Three motor proteins (Kin1, Kin3 and Dyn1/2) were described to be involved in the transport of early endosomes in *U. maydis*. The deletion of *kin1* (previously named *kin2*; Lehmler et al., 1997) and *kin3* led to bipolar growing cells as well as drastically reduced movement of Rrm4 (Becht et al., 2006; Baumann et al., 2012). Nevertheless, residual movement of Upa1 was observed in *kin3* depleted hypha (Pohlmann et al., 2015). This movement might be due to the transport of mRNP complexes with dynein and could also be the reason why still moving GCN4-scFV-sfGfp particles were observed. In a strain that carries a temperature-sensitive allele of *dyn2* which causes inactivation of dynein at restrictive temperatures, no residual movement of mRNP complexes were detected (Baumann et al., 2012). To analyze whether Dyn1/2 is responsible for the remaining moving particles of GCN4-scFV-sfGfp in *kin3* depleted cells, the temperature sensitive allele of *dyn2* could be integrated in GCN4-scFv-sfGfp expressing cells. If no more moving particles are detectable in this strain, it can be concluded that dynein could possibly be responsible for the movement. Furthermore, deletion of *kin1* could be carried out in GCN4-scFV-sfGfp expressing cells to analyze whether Kin1 is involved in the residual movement of GCN4-scFV-sfGfp. It is important to mention that it cannot be excluded that the unknown protein is in direct contact with a motor protein transporting early endosomes. Hok1 for example is a protein which directly interacts with dynein and is crucial for its association to early endosomes (Bielska et al., 2014).

3.2.2 UMAG_00933 as potential interaction partner of single chain variable fragments as well as nanobodies

For the identification of potential antibody-interacting proteins, an immunoprecipitation of GCN4-scFv-sfGfp followed by LC-MS/MS was performed. In this, eleven high abundant proteins were identified in comparison to the control sfGfp, including UMAG_00933 (Figure 2.13). In addition, Cdc11 and Cdc12 were detected, which are described to be

associated with mRNP complexes (Zander et al., 2016). UMAG_00933 is annotated as a hypothetical protein and has a molecular size of 136 kDa. Interestingly, in a Far-Western blot using GCN4-scFv-sfGfp as an antibody, a strong interaction to a protein, which has a size of approximately 130 kDa was visible (Figure 2.9). This shows, that the identification of UMAG_00933 using LC-MS/MS analysis seems to coincide with the Far-Western blot result.

To characterize UMAG_00933, deletion strains as well as a strain harboring a Gfp fusion protein were generated. The analysis of the deletion was particularly important: if UMAG_00933 interacts with antibodies, a deletion of *UMAG_00933* could enable the usage of antibodies to label a nascent peptide chain, assuming that this deletion has no effect on the growth of *U. maydis*. *UMAG_00933* deficient sporidia and hyphae neither showed a severe phenotype nor a change in the response to temperature stress or different stress inducing reagents tested in this project (Figure 2.14, Figure 2.15, Figure 2.16, Figure 6.1.). Surprisingly, UMAG_00933 showed the same cellular localization as the analyzed antibodies (Figure 2.17). Therefore, a connection between the localization of UMAG_00933 and the antibodies being tested was conceivable. Due to the fact that by deleting *UMAG_00933* no bipolar hyphae could be observed, UMAG_00933 cannot play an important role in the long-distance transport of mRNAs, since deletion of important core components leads to an increase in bipolar growing hyphae (Becht et al., 2006; Pohlmann et al., 2015; Jankowski et al., 2019). This is consistent with the results obtained in the analysis of the influence of mRNP complex proteins on the shuttling of GCN4-scFv-sfGfp. No direct influence of core components was observed. In fact, the shuttling was only influenced by the deletion of *kin3*. However, deletion of core components of the mRNP complex had an influence on the velocity of shuttling GCN4-scFv-sfGfp which indicated co-trafficking. The small glycine-rich protein Grp1 is part of the mRNPs in *U. maydis*. Deletion of *grp1* did not influence the movement of Rrm4 whereas it had an effect on the temperature stress tolerance as well as on the response towards cell wall stress (Olgeiser et al., 2019). Although the deletion of *UMAG_00933* had no observable effect on the stress stimuli tested in this project, it could be possible that a protein can still be part of the mRNP complex without being essential for the transport of mRNAs.

The analysis of the deletion of *UMAG_00933* in hyphae expressing GCN4-scFv-sfGfp or BC2-Nb revealed that the deletion prevents shuttling of both antibodies (Figure 2.17). In addition, the stained microtubule-like structure was absent in these strains. Consequently, UMAG_00933 is responsible for the subcellular localization of the tested antibodies and seems to interact with them. Importantly, in *UMAG_00933* deficient sporidia and hyphae, GCN4-scFv-sfGfp as well as BC2-Nb-sfGfp were still expressed in

full-length. It can be concluded that the interaction partner of the tested antibodies was successful identified by LC-MS/MS analysis. UMAG_00933 seems to be a protein that is transported through hyphae together with mRNP complexes without having an essential role in this transport. These results are an important step towards visualizing translation by single-molecule imaging of nascent peptides within hyphae of *U. maydis*.

3.2.3 Interaction of UMAG_00933 to antibodies and its own endosomal localization

Due to the different origin and structure of scFvs and Nbs, UMAG_00933 seems to be able to recognize either the secondary structure of the antibodies (Figure 2.11) or a conserved amino acid sequence (Figure 2.10) within the V_H and V_{HH} domains. Several proteins were described in the last years which exhibit an antibody-binding capacity. The first described antibody-binding protein was protein A, which is a small cell wall protein isolated from *Staphylococcus aureus* (Forsgren and Sjoquist, 1966). Protein A primarily binds to the Fc region of antibodies between the C_H2 and C_H3 domain (Deisenhofer, 1981; Moks et al., 1986). A second protein from *Streptococci*, named protein G, recognizes structures in the Fc-region of IgG antibodies (Kronvall, 1973). Interestingly, in addition to the recognition of the Fc regions, both proteins can also bind to the Fab region. Protein G recognizes the first constant domain (C_H1) from the heavy chain within the Fab region (Derrick and Wigley, 1992). Protein A interacts with the V_H domain of the heavy chain (Inganäs, 1981). The sequence recognized within the domain is only present in the V_H3 family (Graille et al., 2000). Based on nucleic acid sequence homology, the V_H genes in humans have been grouped into seven families. Among these families, the V_H3 family is the largest consisting of 22 functional genes (Cook and Tomlinson, 1995). Importantly, V_{HH} domains have a high sequence and structural identity with human V_H3 domains. However, only some of them were recognized by protein A (Crauwels et al., 2020). This can be referred to the fact, that important amino acids to which protein A binds to in V_H3 domains are mostly substituted in V_{HH} domains (Frenken et al., 2000; Graille et al., 2000). However, this shows that it is generally possible for a protein to bind both the V_H domain of scFv and the V_{HH} of which Nbs consist. Other Fab-region binding proteins are protein L from *Peptostreptococcus magnus*, which predominantly binds to the V_L domain and protein P, isolated from *Clostridium perfringens*, which is thought to bind to both the V_H and V_L chain (Björck, 1988; Lindahl and Kronvall, 1988; Nilson et al., 1992). However, nothing is known about these proteins to have the capability to bind to V_{HH} Nbs. Another protein, called protein Fv (previously named protein F) recognizes V_H domains (Bouvet et al., 1990). It was shown that protein Fv binds to the V_H3 domain of various antibody types with high

affinity (Bouvet et al., 1991; Silverman et al., 1995). However, it is not reported whether there is the possibility that protein Fv binds to V_{HH} domains. Due to the fact that the Fv protein is able to bind V_H3 domains which show a similarity to V_{HH} of the Nbs, it is conceivable that the protein could also recognize Nbs. In general, these examples clearly indicate that it cannot be excluded that a protein is able to interact with the V_H domain of scFvs and the V_{HH} of Nbs. UMAG_00933 showed no amino acid sequence similarities to protein A or the other reported antibody-binding proteins. In general, it can be said that the amino acid sequences of the different antibody-binding proteins do not show a high degree of similarity. The amino acid composition of protein G, for example, was found to be different from protein A (Akerström and Bjorck, 1986). Therefore, a sequence-based prediction of antibody-binding proteins is particularly difficult. In any case, it is essential to verify whether UMAG_00933 is generally capable of binding antibodies. It is important to mention that there is the possibility that only the antibodies examined in this project could be recruited to early endosomes by UMAG_00933, but other antibodies do not show any interaction. This could be investigated, for example, by the expression of other antibodies (e.g. the nanobody against Gfp), which have already been successfully expressed in sporidia of *U. maydis*, but no analysis of the cellular localization was conducted (Terfrüchte et al., 2017).

The less conserved CTD and SMC domains, which are found in the amino acid sequence of UMAG_00933 are not described to directly interact with endosomal lipids or to be involved in the association of proteins to endosomes. However, it could be shown that UMAG_00933 seems to localize to early endosomes (see 3.2.2). The CTD domain found in UMAG_00933 shows homology to the CTD domain found in the C-terminus of the transcription elongation factor Stp5 in *S. pombe*. This domain is crucial for the interaction with another protein which acts as a functional complex and regulates early transcription elongation (Schwer et al., 2009). Furthermore, this complex might be involved in pre-mRNA processing since it associates with mRNA capping enzymes. Thus, the CTD domain facilitates binding of Stp5 to other proteins (Schwer et al., 2009). Whether this domain is important for the endosomal localization of UMAG_00933 could be investigated by deleting this region followed by the analysis of the cellular localization. Proteins containing a SMC domain are capable of binding nucleic acid since they drive conformational changes in DNA topology (Hassler et al., 2018). Therefore, it could also be assumed that this domain is capable of binding RNA. mRNAs are bound by Rrm4 and this binding is essential for their localization in mRNP complexes (König et al., 2009). The association of mRNAs in mRNPs is further stabilized by Upa2 (Jankowski et al., 2019). When Upa2 or Rrm4 are deleted, the localization of mRNAs on endosomes is reduced or completely abolished (König et al., 2009; Jankowski et al., 2019). Due to

the unchanged localization of GCN4-scFv-sfGfp in hyphae carrying a deletion of *rrm4* or *upa2*, and the fact that UMAG_00933 is responsible for this localization, it can be assumed that UMAG_00933 does not attach to endosomes through binding of mRNA. Note, that a low conserved SMC domain was also found in Upa2, a member of the mRNP complex in *U. maydis*. In the context of Upa2, Gfp fusion experiments showed that the SMC domain was insufficient for endosomal localization (personal communication Dr. Silke Jankowski). In addition, it was shown that a C-terminal GWW motif is important for the specific endosomal localization of Upa2 (Jankowski et al., 2019). It is thought that Upa2 interacts via its GWW domain to an up to now unknown protein which is associated to the mRNP complex and recruits Upa2 to endosomes (Jankowski et al., 2019). Importantly, no GWW motif could be identified in UMAG_00933. The recent identification of the GWW motif demonstrates that the association of proteins to early endosomes can also be achieved through small motifs which were previously unknown. Therefore, it is possible that UMAG_00933 is recruited onto early endosomes by interacting with a yet unknown protein of the mRNP complex. Furthermore, there is also the general possibility that it interacts with proteins on the endosomal surface. In order to determine the region within UMAG_00933 that is responsible for the endosomal localization, truncations of the protein could be investigated. By analyzing the cellular localization of UMAG_00933-Gfp, the truncations can then be used to precisely determine the region that is involved in shuttling through the hyphae of *U. maydis*. This technique was already successfully used to uncover the GWW motif within Upa2 which is responsible for the endosomal localization (Jankowski et al., 2019).

3.2.4 Usage of antibodies to label the nascent peptide chain in *U. maydis*

The unspecific localization of the analyzed antibodies was prevented by the deletion of *UMAG_00933*. Furthermore, the interaction of the antibodies to their cognate peptide epitopes is crucial. To test the interaction of GCN4-scFv-sfGfp and BC2-Nb-sfGfp with their peptide epitopes, several copies of these peptide epitopes were fused C-terminally to mKate2, which was itself fused to a phox domain. The phox domain recruits the whole construct to the surface of early endosomes (Wedlich-Soldner et al., 2000). Thus, the interaction of the antibodies to their peptide epitopes was analyzed *in vivo* by co-localization of both sfGfp and mKate2 in hyphae. For the GCN4-scFv-sfGfp, 24 copies of the peptide epitope ($GCN4^{24}$) were used, because 24 copies of the epitope were previously proven to be sufficient for visible interaction (Tanenbaum et al., 2014). For the BC2-Nb, 12 ($BC2^{12}$) as well as 24 ($BC2^{24}$) copies were tested. For dSTORM microscopy in mammalian cells, only one copy of the peptide epitope was sufficient for a detectable

binding of BC2-Nb labeled with fluorescent dyes (Virant et al., 2018). However, it was thought that an increased copy number of the peptide epitope would increase the probability of detectable signals. The generated constructs were integrated in strains that carry a deletion of *UMAG_00933* and express either GCN4-scFv-sfGfp or BC2-Nb-sfGfp. For BC2-Nb-sfGfp, no interaction to its cognate peptide epitope was detectable (Figure 2.18 C). This could be due to the absence of an mKate2 signal in fluorescence microscopy. Whether the expression of the reporter constructs mKate2-BC2^{12} and mKate2-BC2^{24} was too low for a visible detection or whether the constructs were not expressed at all could not be further investigated within the framework of this project. Interestingly, the interaction of the BC2-Nb to its cognate peptide epitope was further developed by industry and is now commercially available as Spot-Tag (Chromotek, 2018). For this, four amino acids were exchanged in the BC2 epitope, which results in a significantly higher affinity to the antibody. It is not reported if this replacement decreases potential expression problems in other model systems than mammalian cells. Fortunately, shuttling was observed for GCN4-scFv-sfGfp as well as for mKate2-GCN4^{24} (Figure 2.18 B). Furthermore, co-localization of both fluorescence proteins was observed which is attributable to an interaction of GCN4-scFv-sfGfp with the related peptide epitope. Since GCN4-scFv-sfGfp has already been successfully used in mammalian cells, this observation is consistent with the literature (Tanenbaum et al., 2014; Wu et al., 2016). In summary, the investigation of the interaction of GCN4-scFv-sfGfp to its cognate peptide epitope in *UMAG_00933* depleted hyphae was a major step towards simultaneous detection of mRNAs and the associated nascent polypeptide chains.

3.3 Combination of degron and 2A peptide

3.3.1 PEST sequence from mouse ornithine-decarboxylase cannot be used together with 2A peptide

GCN4-scFv-sfGfp, which could probably be used to label a nascent peptide chain binds constantly to its cognate peptide epitope. Thus, it will also bind to fully translated proteins and not only to nascent peptides which results in an increased number of labeled proteins. To overcome this problem, a degron can be used to remove fully synthesized proteins. For this, a degradation inducing sequence is fused C-terminally to GCN4^{24}. The auxin-inducible degron (AID) was already successfully used in combination with GCN4-scFv-sfGfp and GCN4^{24} in mammalian cells (Wang et al., 2016). This system is based on the auxin-dependent degradation pathway of plants which was implemented in other eukaryotic cells such as *S. cerevisiae* (Nishimura et al., 2009). Addition of the synthetic auxin 1-naphthaleneacetic acid (NAA) induces polyubiquitination of proteins which are fused to the AID degron. The polyubiquitination is mediated by the interaction

of an F-box protein (TIR1) to the E3 ubiquitin ligase enzyme (Nishimura et al., 2009). The establishment of AID has already been tried in the past in *U. maydis* (Master thesis, Christine Höwner). Unfortunately, the expression of TIR1 was not possible in the framework of this master thesis. In addition, it is important to mention that *U. maydis* itself is able to produce auxin (Reineke et al., 2008). Whether the cellular amount would be sufficient to activate the degron without addition of NAA is questionable.

As the preliminary results already showed that the establishment of AID seems to be difficult, this project concentrated on the application of so-called PEST sequences, because these have already been used successfully to degrade Gfp in *U. maydis* (Brachmann, 2001). PEST sequences are present in key metabolic enzymes as well as cell cycle regulating proteins (Rechsteiner and Rogers, 1996). The PEST sequences which were already applied in *U. maydis* derive from the mODC. Two different versions were already used which provide different half-lives (d1, one hour; d2, two hours)(Brachmann, 2001). The amount of proteins within a cell is controlled by an equilibrium of synthesis and degradation. Because of the usage of a degron sequence to degrade fully synthesized GCN4^{24}, also the protein to which GCN4^{24} is fused to will be degraded. Thus, the amount of resulting proteins within the cell is decreased since protein degradation rates raise while synthesis rates still remain equal. To visualize local translation, it is important to maintain the equilibrium of proteins encoded by analyzed mRNAs. Because of this, it was essential to separate the translated protein from GCN4^{24}. For this, a 2A peptide should be used in *U. maydis*. During translation, the ribosome skips formation of the peptide bound in between the C-terminal amino acids glycine and proline within 2A peptides. Thus, a polycistronic-like mRNA is formed in eukaryotes since translation of one mRNA leads to two separately folded proteins (de Felipe et al., 2006). It is important to mention that the amino acids upstream from the ribosomal skipping site within 2A peptides remain on the protein which is N-terminally fused to them. For the combination of PEST sequences and the 2A peptide, a reporter construct was designed in which mKate2 fused to an HA-tag and the d1 from mODC (mKate2^{HA}-d1) and Gfp fused to an NLS (Gfp^{NLS}) should be separated by the well-studied F2A (Figure 2.19 A). Because of the fusion of d1 to mKate2^{HA}, it should be rapidly degraded by the proteasome after translation. It could be shown that the separation of mKate2^{HA} and Gfp^{NLS} was successful using F2A (further characterization, 3.3.2). However, the mKate2^{HA} was still detected on Western blot membranes and therefore not degraded by d1 (Figure 2.19 C). This was referable to the C-terminal extension of the d1 sequence by the N-terminus of the 2A peptide since the integration of an eight amino acid long linker influences the degradation efficiency of d1 as well as of d2 (Figure 2.20). Two elements are crucial for the destabilization activity of mODC.

The first one is a cysteine-alanine motif, which is important for the association with the proteasome. The other one is an unstructured region which flanks the cysteine-alanine motif (Takeuchi et al., 2008). It is known that for an efficient degradation of mODC, conformational change and exposure of the hydrophilic PEST domain within the C-terminus are crucial (Murakami et al., 1992). It was further reported that blocking of the C-terminus with antibodies prevents degradation (Li and Coffino, 1993). Therefore, it is not surprising that both versions of the mODC degron show a reduced activity when they were combined with F2A. For this reason, another PEST sequence from the G1 cyclin Cln1 from *U. maydis* was analyzed with respect to its ability to mediate protein degradation even when it is integrated in the middle of an amino acid sequence. Cyclins are constitutively unstable and their expression is tightly regulated and dependent on the cell cycle (Rahman and Kipreos, 2010). The PEST sequence of Cln1 (G1) is located in the middle of the protein (Castillo-Lluva and Perez-Martin, 2005). In *S. cerevisiae* it was shown that the degradation of the two G1 cyclins Cln1p and Cln2p is dependent on their PEST sequences and ubiquitin ligases (Quilis and Igual, 2017). Furthermore, it was found out that no direct conformational change induces the degradation of Cln1p in *S. cerevisiae* and that phosphorylation within the PEST sequence causes the recognition by the proteasome pathway (Lanker et al., 1996). Cln1p and Cln2p had a half-live of around 10 minutes measured in translational shut-off assays (Quilis and Igual, 2017). Unfortunately, the role of the PEST sequence in Cln1 was not investigated in *U. maydis* (Castillo-Lluva and Perez-Martin, 2005; Heimel et al., 2010). However, it was shown that *cln1* from *U. maydis* moderately functions in *S. cerevisiae* and partially complemented *cln1* and *cln2* deletion mutants (Castillo-Lluva and Perez-Martin, 2005). Therefore it was assumed that the PEST sequence of the Cln1 protein from *U. maydis* has a short half-life and a high degradation efficiency. Compared to the d1 and d2 PEST sequence of mODC, the G1 PEST sequence exhibited a significantly reduced efficiency of degradation (Figure 2.20). Interestingly, C-terminal extension of the fusion construct did not influence the degradation efficiency of the G1 PEST sequence. This is referable to the fact that this PEST sequence is naturally embedded in the Cln1 protein. However, the G1 PEST sequence of the Cln1 protein from *U. maydis* cannot be used to degrade GCN4^{24} because 50% of the peptide epitope would remain which can lead to false results as they indicate potential translation sites although the protein is already translated. For an efficient degradation of GCN4^{24}, the degradation of mODC PEST sequences has to be optimized, or another degron sequence or system has to be found. In *S. cerevisiae*, the mODC PEST sequence was C-terminally fused to a TEV protease cleavage site to create a bidirectional degron in combination with a dormant N-degron. Activation of the degron is induced upon cleavage of the TEV protease (Jungbluth et al.,

2010). For this a synthetic cODC degron was investigated which is shorter than the original mODC. The cODC could be tested in *U. maydis* by integrating a TEV cleavage site in between the cODC and the 2A peptide. Another possibility is based on the usage of the rapamycin analog shield-1. It binds to a degron domain (DD) which either prevents or induces degradation by the proteasome (Banaszynski et al., 2006; Bonger et al., 2011). This system was already successfully implemented in mammalian cells as well as in plants (Su et al., 2013; Wang et al., 2015). However, a recent study showed that rapamycin influences cell morphology of sporidia of *U. maydis*, leading to the formation of several septa, several nuclei, big vacuoles and large lipid droplets (Romero-Aguilar et al., 2020). This can be attributed to the inhibition of the conserved serine/threonine kinase TOR by rapamycin (Romero-Aguilar et al., 2020). It has to be analyzed whether usage of shield-1 results in similar morphological defects. An upcoming possibility of degrading proteins or controlling the expression is based on optogenetic tools. For this, the light-reactive LOV2 domain of *Arabidopsis thaliana* is combined with parts of the mODC degron. The part of the mODC degron is masked by a Jα helix of the LOV2 domain. Upon irradiation with blue light, the mODC degron is exposed and induces degradation by the proteasome (Renicke et al., 2013). The functionality of this degron was proven in *S. cerevisiae*. Unfortunately, the establishment in *U. maydis* was not feasible up to now (Bachelor thesis, Christine Höwner, 2016). However, the usage of the LOV2 domain to regulate gene expression in *U. maydis* was recently demonstrated (Hüsemann and Heucken, manuscript in preparation). Whether the LOV2 domain can be used to degrade GCN4^{24} has to be shown in further experiments. In summary, the efficiencies of degradation identified in this project can be scored as followed: d1 > d2 > d1-L > d2-L > G1-L > G1. These results led to a number of degradation sequences of varying strength, which can be used for further applications in *U. maydis*.

3.3.2 P2A exhibits high separation rates to generate polycistronic mRNAs in *U. maydis*

2A peptides were first discovered in the foot-and-mouth disease virus (FMDV, F2A peptide) (Ryan et al., 1991). Later on, several 2A peptide sequences were found in several viruses (Luke et al., 2008). The ‘stop and carry on‘ mechanism of the ribosome at the C-terminal glycine and proline is not functional in prokaryotes (Donnelly et al., 1997), but it is widely used in eukaryotes for different applications. 2A peptides were for example used for the production of carotenoids in plants (Ha et al., 2010) or of the production of monoclonal antibodies in mammalian cell culture (Chng et al., 2015). Also in fungi, 2A peptides are increasingly used to express heterologous proteins or to control the expression of clusters by combining them in a polycistronic mRNA. In *S. cerevisiae*,

carotenoids were produced by generating a polycistronic construct of three carotene biosynthesis genes from the ascomycete *Xanthophyllomyces dendrorhous* (Beekwilder et al., 2014). The psychotropic mushroom alkaloid psilocybin was produced in high amounts by heterologous expression of the entire biosynthetic gene cluster in one polycistronic mRNA in *Aspergillus nidulans* (Hoefgen et al., 2018). Besides, the expression of gene clusters from *A. fumigatus* was conducted in *A. nidulans* using 2A peptides (Stroe et al., 2020). The applicability of 2A peptides for the expression of natural products in fungi was further demonstrated in *Aspergillus niger* (Schuetze and Meyer, 2017).

For the further analysis of 2A peptides in *U. maydis*, the same reporter construct was used which was established for the analysis of the combination of PEST sequences and F2A. Two fluorescence proteins were already successfully used as reporters to analyze the separation efficiencies of different 2A peptides in mammalian cells and in *S. cerevisiae* (Liu et al., 2017; Souza-Moreira et al., 2018). It was already reported that short linker sequences upstream of 2A peptides influence the expression of ORFs and improve the separation efficiency (Holst et al., 2006; Gao et al., 2012; Souza-Moreira et al., 2018). Therefore, first of all different linker sequences varying in their length were tested (Figure 2.21 B). In combination with the PEST sequences the separation efficiency within F2A was low. However, for the linker study the well-studied F2A was chosen, because a linker might increase the separation efficiency. An increase in the expression levels of mKate2^{HA} as well as Gfp was observed, which was associated with an increasing length of the tested linker sequences (Figure 2.21 C). Thus, the usage of a linker sequence upstream of the F2A also elevates the expression of mKate2^{HA} and Gfp in *U. maydis*. Hence, the longest tested linker (L2) should be used for further experiments to ensure high expression rates of ORFs which are combined by 2A peptides. However, a weak separation efficiency was observed within the F2A peptide. It was reported in several organisms that the separation efficiency can vary between different 2A peptides (Table 3.1). The best investigated 2A peptides are F2A from FMDV, E2A from the *Equine rhinitis* A virus (ERAV), T2A from *Thosea asigna* virus (TaV) and P2A from Porcine teschovirus-1 (PTV). The separation efficiencies in mammalian cells as well as in *D. melanogaster* vary from the worst separation efficiency in F2A, through E2A and T2A to an efficiency of almost 100% in P2A (Kim et al., 2011; Daniels et al., 2014). In the silkworm *Bombyx mori* F2A, E2A, T2A and P2A exhibit comparable separation efficiencies (Wang et al., 2015). In *S. cerevisiae* as well as in *A. fumigatus*, the highest separation efficiencies were achieved using P2A (Souza-Moreira et al., 2018; Manfiolli et al., 2019). In contrast to this, a high separation efficiency of nearly 100% was observed using F2A in *Trichoderma reesei* (Table 3.1; Subramanian

et al., 2017). In *Pichia pastoris*, separation efficiencies of 50-60% were observable for both F2A and P2A (Table 3.1; Geier et al., 2015). This shows a high diversity within the separation efficiencies of different 2A peptides in various organisms. Therefore, it was important to analyze several 2A peptides and their separation efficiencies in *U. maydis* to find the most efficient one. Western blot analysis as well as fluorescence microscopy revealed that P2A showed the highest separation efficiency, followed by E2A, T2A, Po2A and F2A (Figure 2.22 and Figure 2.23). Using FRET it could be confirmed that P2A had the highest separation efficiency of almost 100% (Figure 2.23 B). The other tested 2A peptides had separation rates of 20% (F2A), 30% (Po2A), 40% (T2A) and 60% (E2A; Table 3.1) and were comparable to previously determined rates conducted in mammalian cells (Kim et al., 2011). By confirming that 2A peptides have different separation efficiencies, it was shown that it is important to test different 2A peptides in the organism in which they will be used. Nevertheless, it can generally be said that P2A is the 2A peptide that most commonly exhibits nearly 100% separation efficiency (Table 3.1). In *U. maydis*, P2A in combination with the L2 linker was used for further applications.

Table 3.1: Comparison of 2A peptide separation efficiencies in different organisms; modified according to (Müntjes et al., 2020);Fungal organisms shaded in orange; other organisms shaded in gray

2A peptide	Organism	Seperation efficiency [%]	Reference
F2A	HEK293T; HT1080; HeLa	~50	(Kim et al., 2011)
	Zebrafish embryo	~40	(Kim et al., 2011)
	Mouse liver	~30	(Kim et al., 2011)
	Silkworm B. mori	91-98	(Wang et al., 2015)
	D. melanogaster	~65	(Daniels et al., 2014)
	T. reesei	~100	(Subramanian et al., 2017)
	P. pastoris	~50	(Geier et al., 2015)
	U. maydis	20	This study
E2A	HEK293T; HT1080; HeLa	~60	(Kim et al., 2011)
	Zebrafish embryo	~60	(Kim et al., 2011)
	Mouse liver	~50	(Kim et al., 2011)
	Silkworm *B. mori*	99-100	(Wang et al., 2015)
	D. melanogaster	~70	(Daniels et al., 2014)
	S. cerevisiae	~45	(Souza-Moreira et al., 2018)
	U. maydis	60	This study
T2A	HEK293T; HT1080; HeLa	~70	(Kim et al., 2011)
	Zebrafish embryo	~80	(Kim et al., 2011)
	Mouse liver	~50	(Kim et al., 2011)
	Silkworm *B. mori*	90-97	(Wang et al., 2015)
	D. melanogaster	~85	(Daniels et al., 2014)
	S. cerevisiae	~55	(Souza-Moreira et al., 2018)
	U. maydis	40	This study

P2A	HEK293T; HT1080; HeLa	~90	(Kim et al., 2011)
	Zebrafish embryo	~100	(Kim et al., 2011)
	Mouse liver	~90	(Kim et al., 2011)
	Silkworm *B. mori*	100	(Wang et al., 2015)
	D. melanogaster	~95	(Daniels et al., 2014)
	S. cerevisiae	~85	(Souza-Moreira et al., 2018)
	A. nidulans	~100	(Unkles et al., 2014)
	P. pastoris	~60	(Geier et al., 2015)
	A. niger	~100	(Schuetze and Meyer, 2017)
	A. fumigatus	~100	(Manfiolli et al., 2019)
	U. maydis	100	This study
Po2A	*U. maydis*	30	This study

To illustrate applicability of P2A, regulated gene expression was monitored. For this, a bi-cistronic mRNA was generated in which the *Photinus pyralis* firefly luciferase (FLuc) was combined with the RBP Rrm4 fused to Gfp. The combination of Rrm4-Gfp and FLuc enabled the visualization of the expression of Rrm4-Gfp by fluorescence microscopy on the one hand and the measurement of the FLuc activity by addition of luciferin on the other hand. The transcription of the construct was controlled by the inducible P_{crg} promoter (deriving from the arabinase gene *crg1*; Brachmann, 2001). Thus, expression of the bi-cistronic construct was inducible by switching the carbon source from glucose to arabinose (Bottin et al., 1996; Brachmann, 2001). Luciferases were already used to monitor the expression of genes and exhibit an excellent dynamic range and sensitivity (Qureshi, 2007; Grant et al., 2012). Furthermore, a luciferase was already successfully implemented to determine the activity of P2A in *A. niger* (Schuetze and Meyer, 2017). Additionally, it was already proven that the FLuc activity can be measured easily in *U. maydis* since the converted substrate luciferin is able to pass the cell wall (Hüsemann et al., manuscript in preparation). In general, monitoring gene expression is a powerful tool for studying the function of different genes in various environments as well as at different cell stages (Hong et al., 2011). Thus, the establishment of a robust system for tracking gene expression is extremely helpful and allows the analysis of the expression of various genes of *U. maydis*. It was shown that the fusion of Rrm4-Gfp to L2-P2A did not alter the activity of Rrm4 since bipolar growth of hyphae which was observable in medium containing glucose was rescued by the usage of arabinose as carbon source (Figure 2.24). Furthermore, the bi-cistronic construct seemed to be only expressed in the presence of arabinose as sole carbon source since FLuc activity as well as Rrm4-Gfp fluorescence were not detectable in medium which contained glucose (Figure 2.24). Thus, the promoter seemed to have no residual activity in the presence of glucose. This is consistent with other experiments where Rrm4 was expressed under the control of the P_{crg} promoter (personal communication Srimeenakshi Sankaranarayanan). In contrast, a residual activity of the P_{crg} promoter could be detected when genes responsible for the

activation of the signaling cascade for the formation of hyphae in *U. maydis* were controlled by this promoter (Brachmann, 2001). To monitor the expression of Rrm4-Gfp as well as FLuc, hyphal cells were shifted at different time points to medium which contains arabinose. FLuc activity as well as endosomal shuttling of Rrm4-Gfp were detected two hours after induction of the expression of the bi-cistronic construct (Figure 2.25). This showed that the measurement of FLuc activity was related to the expression of Rrm4-Gfp. It furthermore emphasized the robustness of the construct used in this project for monitoring gene expression and corroborates the literature describing luciferases as a robust read-out for monitoring gene expression (Qureshi, 2007; Grant et al., 2012). P2A was further used to enhance the production of biosurfactants and to uncouple the production of the glycolipids mannosylerythritol lipid (MEL) from nitrogen starvation in *U. maydis* (Müntjes et al., 2020). In summary, the P2A peptide which was established in this project can be successfully used in basic and applied science. Furthermore, it is likely that it can be successfully used to separate GCN4^{24} which should be degraded by a degron from downstream ORFs which will be analyzed for subcellular translational activity *in vivo*

3.4 Future directions

In this project, it was possible to establish different building blocks which are crucial to visualize a nascent peptide chain during translation. These can also be used in future projects and other applications. Furthermore, a new locus for the expression of heterologous proteins was tested, which possesses comparable expression rates as the well-studied *ip^S* locus. Together with other recently tested loci, it expands the repertoire at possible integration sites within the genome of *U. maydis* and facilitates expression of heterologous proteins.

mKate2 was successfully established as a new Rfp in *U. maydis* for labeling proteins and mRNAs within their 3´UTRs. The latter enables not only the simultaneous labeling of mRNAs and their corresponding nascent peptides but also various other experimental set-ups. It is known that all septin proteins are transported within mRNP complexes and that their localization to early endosomes is dependent on each other (Zander et al., 2016). However, up to now it was not feasible to analyze whether mRNAs encoding septin proteins are also co-transported on the same endosome. Together with the previous establishment of several systems for labeling of 3'UTRs of mRNAs (Zander et al., 2018), it is now possible to analyze two mRNAs and their transport through hyphae of *U. maydis*. This could lead to further insights whether mRNAs encoding for proteins which interact with each other are transported together.

The successful establishment of P2A with nearly 100% separation efficiencies provides the opportunity for various other applications in both basic and applied research. *U. maydis* potentially serves as a great production host for many industrial products (Bölker et al., 2008; Sarkari et al., 2014; Terfrüchte et al., 2014; Terfrüchte et al., 2017; Stoffels et al., 2020). It could already be shown that the establishment of P2A enabled the production of MELs independent of nitrogen starvation by the expression of a tri-cistronic mRNA (Müntjes et al., 2020). This can be further extended, for example to reduce the expression of different gene clusters to one mRNA. This decreases the number of loci required for the expression of heterologous proteins and allows a narrow and simultaneous expression of these proteins. Furthermore, the usage of the P2A enabled a simple and reliable monitoring of gene expression. For this, the recently established FLuc was used (Hüsemann, et al., manuscript in preparation). For future applications, FLuc can be used in combination with P2A to study protein stabilities and turnover rates or the expression of different mRNAs.

The hypothetical protein UMAG_00933 was identified to be able to interact with three tested antibodies. Furthermore, this protein seems to be associated to early endosomes and shuttles through hyphae in a bidirectional manner in dependency of the microtubule-cytoskeleton. Interestingly, UMAG_00933 seems to hitchhike on mRNP complexes transporting endosomes. In further experiments, it has to be clarified why UMAG_00933 seems to be associated with early endosomes. This may provide further information on the structure of the mRNPs, as some associated proteins are still unknown. Moreover, it is possible that future investigations of UMAG_00933 will provide new insights into the general transport of endosomes. Since UMAG_00933 appears to interact with antibodies, deletion may improve the expression level of antibodies expressed for biotechnological application (Terfrüchte et al., 2017). This could also be tested and examined in the future. Whether UMAG_00933 is generally capable of binding to antibodies or if the antibodies examined here were bound by chance must be verified by further experiments. If UMAG_00933 is an antibody-binding protein, this could be used for an artificial recruitment of proteins which can be fused to antibodies.

Unfortunately, in this project no degron was found that can be combined with P2A to degrade GCN4^{24} and reduce the background during fluorescence microscopy of nascent polypeptide chains. Further sequences and methods that induce protein degradation should be tested. In general, it could be possible to localize GCN4^{24} to the nucleus via a fusion to an NLS sequence. If this is successful, first experiments could be performed to visualize the translation of well-studied mRNAs, such as the *cdc3* mRNA. If the visualization of the translation with GCN4-scFv-sfGfp and GCN4^{24} is not feasible, the interaction of a fluorescently labeled antibody that binds to the FLAG tag could be used

(Morisaki et al., 2016). This has already been successfully applied to study translation in mammalian cells. With this antibody, experiments would also have to be carried out in order to determine whether it binds to UMAG_00933.

In general, the establishment of a method for the analysis of translational sites *in vivo* provides further insights to where and when translation occurs in hyphae of *U. maydis*. If translation can be verified on mRNP-transporting endosomes, this will underline the co-localization studies which were carried out previously (Baumann et al., 2014) and demonstrate a possible conservation of this mechanism (Cioni et al., 2019). Furthermore, the visualization of the translation can provide information on whether Rrm4 plays a regulatory role during translation. Rrm4 binds nine out of 17 subunits of the F_0F_1 ATP synthase at the stop codon (Olgeiser et al., 2019). Together with earlier experiments (Koepke et al., 2011), this suggests an important role of Rrm4 in mitochondrial functionality. Whether a translation in close proximity of mitochondria, as described in neurons, also occurs in *U. maydis* can be investigated with the method whose establishment was started in this project. In summary, this project has laid the groundwork for the establishment of an antibody-based labeling of the nascent polypeptide chain for the analysis of translationally active sites within the cell.

4 Materials and Methods

4.1 Materials

4.1.1 Chemicals, enzymes, kits

4.1.1.1 Chemicals

The chemicals used in this study (degree of purity: p.a.) were mainly ordered by the following companies unless specified otherwise: Carl Roth (Karlsruhe), Difco (Augsburg), Merck (Darmstadt), Sigma-Aldrich (Deisenhofen), Applichem (Darmstadt), VWR (West Chester, Caelo (Hilden), Thermo Fisher Scientific (Schwerte), Biorad (Feldkirchen), GE Healthcare (Solingen) and Fluka (Buchs).

4.1.1.2 Enzymes and kits

The following tables list the enzymes, protease inhibitors and various kits used in this study.

Table 4.1: Enzymes used in this study

Name	Application	Company
Lysozyme	Plasmid isolation	Thermo Fisher Scientific
Glucanex	Protoplasting of *U. maydis*	Merck
Phusion-HF-DNA-Polymerase	Amplification of DNA molecules	New England Biolabs
Restriction enzymes	Restriction of DNA molecules	New England Biolabs
RNAse A	Plasmid isolation; genomic DNA isolation	Boehringer Ingelheim
T4 DNA-ligase	Ligation of DNA molecules	Roche
Quick-ligase	Ligation of DNA molecules	New England Biolabs
T5 exonuclease	Gibson cloning	New England Biolabs
Taq DNA ligase	Gibson cloning	New England Biolabs

Table 4.2: Protease inhibitors used in this study

Name	Application	Company
Benzamidine	Preparation of cell extracts	Sigma-Aldrich
cOmplete™ EDTA-free Protease Inhibitor Cocktail	Preparation of cell extracts	Sigma-Aldrich
Phenylmethylsulfonylfluorid (PMSF)	Preparation of cell extracts	Sigma-Aldrich
Dithiothreitol (DTT)	Preparation of cell extracts	Thermo Scientific

Table 4.3: Kits used in this study

Name	Application	Company
Monarch® PCR and DNA Cleanup Kit	Purification of DNA and PCR products	New England Biolabs
Monarch DNA Gel Extraction Kit	Elution and purification of DNA fragments from agarose gels	New England Biolabs
Plasmid Mini Kit	Large scale plasmid preparation	Qiagen
PCR DIG Labeling Mix	Digoxigenin labeling of PCR products for generating Southern blot probes	Roche
CDP Star ®	Chemiluminescent substrate for alkaline phosphatase in Southern	Roche

	blot analysis	
AceGlow™	Chemiluminescent substrate for horseradish peroxidase in Western blot analysis	PeqLab
SureClean	Purification of DNA fragments and PCR products	Bioline

Table 4.4: Protein- and DNA size standards used in this study

Name	Application	Company
GeneRuler™ 1 kb DNA Ladder	DNA Gel electrophoresis	Thermo Fisher Scientific
GeneRuler™ 50 bp DNA Ladder	DNA Gel electrophoresis	Thermo Fisher Scientific
λ*PstI* (*PstI* digested entherophage λDNA)	DNA Gel electrophoresis	In house preparation
PageRuler™ Prestained Protein Ladder (10-180 kDa)	SDS-Page	Thermo Fisher Scientific
PageRuler™ Plus Prestained Protein Ladder (10-250 kDa)	SDS-Page	Thermo Fisher Scientific

4.1.2 Solutions and media

The solutions and buffers utilized were mainly generated as described in (Sambrook, 1989). Solutions or buffers of special composition are described in the sections of the corresponding part. If it was necessary, solutions or buffers were autoclaved by 121 °C or sterile filtered.

4.1.2.1 *E. coli* cell cultivation

E. coli cells were cultivated either in dYT liquid medium at 37 °C and 200 rpm or on YT agar plates at 37 °C. Required antibiotics are listed in Table 4.5.

Table 4.5: Concentrations of used antibiotics for the cultivation of *E. coli*

Antibiotics	Concentration
Ampicillin	100 µg/ml
Kanamycin	50 µg/ml

dYT liquid medium:
1.6% (w/v) Tryptone (Difco)
1.0% (w/v) Yeast extract (Difco)
0.5% (w/v) NaCl
Fill with ddH_2O and autoclave

dYT medium plates:
0.8% (w/v) Tryptone (Difco)
1.0% (w/v) Yeast extract (Difco)
0.5% (w/v) NaCl
1.3% (w/v) Bacto agar (Roth)
Fill with ddH_2O and autoclave

4.1.2.2 *U. maydis* cell cultivation

To cultivate *U. maydis* cells, complete medium (CM) was used and carbon sources (glucose or arabinose) were added. In liquid medium *U. maydis* cells were incubated at 28 °C and 200 rpm. To generate a liquid culture, a pre-culture (3ml of CM medium supplemented with 1% glucose) was incubated overnight. For a main culture, 10-50 µl of the pre-culture were added to 30 ml of CM (supplemented with glucose or arabinose) and incubated overnight afterwards. To cultivate *U. maydis* cells on solid media CM glucose or arabinose plates were used. Required antibiotics and their corresponding concentrations are listed in Table 4.6. For sterilization, media were either autoclaved for 5 min at 121 °C or filter-sterilized with a 0.22 µm Fitropur BT50 bottle filter (Sarstedt).

Table 4.6: Concentrations of used antibiotics for the cultivation of *U. maydis* in liquid medium or on plates

Antibiotics	Concentration medium	Concentration regeneration agar (Bottom)
Hygromycin	200 µg/ml	400 µg/ml
Nourseothricin	150 µg/ml	300 µg/ml
Carboxin	2 µg/ml	4 µg/ml
Geneticin	500 µg/ml	1000 µg/ml

Vitamin solution (Holliday, 1974):

0.05‰ (w/v) Folic acid
0.05‰ (w/v) Pyridoxin
0.2‰ (w/v) Pantothenic acid calcium salt
0.05‰ (w/v) 4-Aminobenzoic acid
0.2‰ (w/v) Nicotinic acid
0.2‰ (w/v) Choline chloride
1.0‰ (w/v) myo-Inositol
Fill with ddH_2O and sterile filter,
store at -20 °C

Salt solution (Holliday, 1974):

16.0‰ (w/v) KH_2PO_4
4.0‰ (w/v) Na_2SO_4
8.0‰ (w/v) KCl
1.32‰ (w/v) $CaCl_2*2H_2O$
2.0‰ (w/v) $MgSO_4$
Fill with ddH_2O and sterile filter

Trace element solution: (Holliday, 1974)	0.06‰ (w/v) H_3BO_3 0.14‰ (w/v) $MnCl*4H_2O$ 0.4‰ (w/v) $ZnCl_2$ 0.4 ‰ (w/v) $Na_2MoO_4*2H_2O$ 0.1‰ (w/v) $FeCl_3*6H_2O$ 0.04‰ (w/v) $CuSO_4*5H_2O$ Fill with ddH_2O and sterile filter
Complete medium (CM) (Holliday, 1974):	0.25% (w/v) Casaminoacids (Difco) 0.1% (w/v) Yeast extract (Difco) 1.0% (v/v) Vitamin solution 6.25% (v/v) Salt solution 0.05% (w/v) Salmon sperm 0.15% (w/v) NH_4NO_3 Fill with ddH_2O and adjust pH with 5M NaOH to 7. Autoclave and add 1% (w/v) of carbon source and needed antibiotic afterwards
Nitrate minimal medium (NM) (Scherer et al., 2006)	0.3% (w/v) KNO_3 6.25% (v/v) Salt solution Fill with ddH_2O and adjust pH with 5M KOH to 7. Autoclave and add 1% (w/v) of carbon source afterwards
Charcoal containing NM plates:	0.3% (w/v) KNO_3 6.25% (v/v) Salt solution Fill with ddH_2O and adjust pH with 5M KOH to 7. Autoclave and add 1% (w/v) of carbon source and 1% (w/v) charcoal afterwards
Regeneration agar:	Top: 1.0% (w/v) Yeast extract 0.4% (w/v) Bacto™-Peptone 0.4% (w/v) Sucrose 18.22% (w/v) Sorbitol 1.5% (w/v) Agar Fill with ddH_2O and autoclave

	Bottom: same as top plus antibiotics (see above)
NSY glycerin	0.8% (w/v) Nutrient Broth (Difco) 0.1% (w/v) Yeast-Extract (Difco) 0.5% Succrose (Roth) 80% (v/v) 87% Glycerin (f.c. 69.6%) Prepare with ddH_2O

4.1.3 Centrifuges

Samples of 1.5 or 2 ml sample volume where centrifuged in a Heraeus™ Biofuge™ Pico™ or a Heraerus™ Biofuge™ Fresco™ (Heraeus, Thermo Fisher Scientific). Larger samples with a volume of 15 or 30 ml were centrifuged in a Heraeus™ Biofuge™ Stratos™.

4.1.4 Oligonucleotides, plasmids and strains

4.1.4.1 Oligonucleotides

The oligonucleotides were synthesized by Metabion GmbH (Martinsried) or Integrated DNA Technologies Inc. (Coralville). The sequences were designed in a 5'-3' orientation. All oligonucleotides had a concentration of 100 µM. In Table 4.7 the designed and used oligonucleotides are listed. Oligonucleotides which are used for sequencing are excluded from this list.

Table 4.7: Cloning oligonucleotides used in this study

Name	Nucleotide sequence 5´-3´
AB14	CAATTGATGTACAAAGCTCGCGCGCTCTACG
AB15	ACCGGTTAGGAGCTGCATGTAGTTGC
AB325	ACCGGTGAAGAACTTTTGAGCAAGAA
AB326	AGCGGCCGCTAATGACCCG
AB603	TGTACAAACACGGCTTCCCGCCGGCGGTG
AB604	CAATTGGGGACCGGGGTTCTCCTCGAC
MB656	GATGAATTCATGCGCAAGGGCGAGGAGC
MB657	CTAGGGGCGCGCCTTACTTGTAGAGCTCGTCC
MB660	CATCCCTGCAGGGAGCAGCTGAAGCTATTCG
MB661	CAGTCCATGGCCCGTGGATGATGTTGTCTG
MB670	CCATGGTGTCGGAGCTCATC
MB671	GATGGCGCGCCGGCGTAGTCGGGCACGTCG
MB988	GGCGCGCCAAAGCTTAGCCACGG
MB989	CCATGGTCGGGACCTTTCTCTTCTTTTTTGGAGGCGCTTTCGTGAATTCTGCAGGT CCAGGATTTGATTCCACGTCGCCG
UM16	GGTCTCGCCTGCCATTTAAATCAGATGTTGTCAG
UM17	GGTCTCCAGGCAAGCTTATGACACAGCTTCAG
UM18	GGTCTCCGGCCGGCCTGAGTGGCCGTTACTTCG
UM19	GGTCTCGCTGCATTTAAATGCGCGAACTGCC
UM20	GTATACCCTGCAGGCTAGAACTAGTG
UM21	GTATACGCGATCGCGGGATCGAATTCCTGCAGCC
UM22	GTATACCAATTGATGGACGGAGGTTCTCACG

UM23	GTATACCCTAGGTTAGTTTCGCAGTGAGAAACC
UM24	GTATATCGCTAGCAAGAGCTCAACTCTTTCTTGG
UM25	GTATACCTTAAGTGCTCTCGGCGATTGCTGGG
UM31	GATATCCCATGGCACAAACACAGCCAC
UM32	GATATCGGCCGCGTGGGCCCCATTCGATAAACTGCTTGAAC
UM206	CAGACAACATCATCCACGGCAATTGCATGGCGGCCCATCACCA
UM207	TTCCCGAGCCCGACGAGACGGTGACCGTCGACGAGACGGTGACCTGG
UM404	AGCTGTCAAACATGAGAATTGCGGCGCTCGGTCTCGGCCTAGATG
UM405	ACGGCCACTCAGGCCTATTAATGCGTGCAGTCGACGGTCTCCG
UM406	CGCATTAATAGGCCTGAG
UM407	GCCGCAATTCTCATGTTTG
UM487	CCTGCAGGTTGGCCGCCATGGTGAGCAAGG
UM488	GCGGCCGCCGCCGGCCGCTTTACTTGTAC
UM848	GCCGCTCTTCCGTGCAATATTGGCCCTGGTGTCTTTG
UM849	GCCGCTCTTCCGGCCCTTGACTAGTTCGTAAACC
UM850	GCCGCTCTTCCCCTAATATTGAGGAGCGCCTCAAACAAATG
UM851	GCCGCTCTTCCGACAATATTCTCCAATCTCTTGCTTG
UM852	GGTCTCGCCTGCAATATTCGCAAATCGCACGCTGATG
UM853	GGTCTCCTGGCCTGCTCATCACGTTCGGCGCGG
UM854	GGTCTCCGGCCCTCAGGAACAAGAAGAGGTCG
UM855	GGTCTCGCTGCAATATTGACGTGATGCCAGTTCG
UM959	GGTCTCGCCTGCCCTGCAGGCTAGAACTAGTG
UM960	GGTCTCCAGGCCGGCCGGCGTAGTCGGGCACGTCGTAAGG
UM961	GGTCTCCGCCTGCGAGAGAGAGAGCTCAGCCCATGGTGAGCAAGGGCGAGG
UM962	GGTCTCGCTGCGGCGCGCCGGCCGCTAGATC
UM963	GGCCGGCCTGGCTCGGGCCCCGTGAAACAGCTGCTCAAC
UM964	GCTGAGCAGGTCCAGGATTTGATTCC
UM965	GGCCGGCCTCACGGCTTCCCGCCGGCGGTGGCGGCGCAGGATGATGGCACGCT GGTCCCCGTGAAACAGCTGCTCAAC
UM967	GCTGAGCGGGACCGGGGTTCTCCTCGAC
UM968	GGCCGGCCTCACGGCTTCCCGCCGGCGGTGGCGGCGCAGGATGATGGCACGCT GGTCGCCATGACCGTCATGGCCTTC
UM969	GGCCGGCCTGGCTCGGGCCGCCACAAGTTCCCCACCAAC
UM970	GCTGAGCGGGACCGGGGTTCGACTCGAC
UM971	GGCCGGCCTCACGGCTTCCCGCCGGCGGTGGCGGCGCAGGATGATGGCACGCT GGTCCGCCACAAGTTCCCCACCAAC
UM973	GGCCGGCCTGGCTCGGGCCGTGGTCCTCGTCCCCAGAAC
UM974	GCTGAGCGGGACCGGGGTTCTCCTCGAC
UM975	GGCCGGCCTCACGGCTTCCCGCCGGCGGTGGCGGCGCAGGATGATGGCACGCT GGTCCGTGGTCCTCGTCCCCAGAAC
UM976	GGCCGGCCTGGCTCGGGCGGCAACGGCAACCCGCTCATC
UM977	GCTGAGCGGGACCGGGGTTGAGCTCG
UM979	GGCCGGCCTGGCTCGGGCGGTCAGCGCACCACCGAGC
UM980	GCTGAGCGGGACCGGGGTTCGACTCG
UM982	GGCCGGCCTGGCTCGGGCCCCGTGAAACAGCTGCTCAAC
UM983	GCTGAGCTCCAGGATTTGATTCCACG
UM983	GCTGAGCTCCAGGATTTGATTCCACG
UM984	GGCCGGCCTCACGGCTTCCCGCCGGCGGTGGCGGCGCAGGATGATGCAGCTGGT CCCCGTGAAACAGCTGCTCAAC
UP75	GGTCTCGCCTGCATTTAAATCGTCGAGATCTGCAAGAGGCCGAGC
UP76	GGTCTCCTGGCCGACTTGGCATACTCTTCGGCACG
UP77	GGTCTCGGGCCGGCGTAACCACACCATCCCACC
UP78	GGTCTCGCTGCATTTAAATCCGAGGGAAATATCGTGAATATTG
UP79	GCATCCATGGCCGAGGTCG
UP80	CGGGAATTCGCGACTAGTCTTGATCTCGAGC
UP83	GGTCTCCGGCCTAGAGCCGCCCCGATTCGAGTTTC
UP84	GGTCTCGCTGCAATATTATCGCGCCCCTTTCGCCGGCTG
UP85	GGTCTCGCCTGAATATTCGGGATTTGTGAGTGATAATC
UP86	GGTCTCCAGGCGATGCAGAGATTAGCTCGTCTG
UP248	GGTCTCGCCTGCAATATTGTTGGCTATGCTGGCACTTTCG
UP249	GGTCTCCAGGCCGAGTGAAGCGTAATACCTAGC
UP250	GGTCTCCGGCCACCGTAGATCATGCCTGATG
UP251	GGTCTCGCTGCAATATTCGATGTGCATACAGCAAACCGCC
UP252	GGTCTCGGGGGACGGAACCATAACATCGTAGAG

UP253	GGTCTCGCCCCGTTCTCTTTTAGTCACACGTAGTC
UP375	CAATGTACAGGTACCGCAATGCCGGTGCAGTAGCCC
UP376	CAAGGCGCGCCTTACGAAGAAGGCATGGGCACAG
UP377	CATGGCGCGCCCTACACATTGATCCTAGCAG
UP378	ACTTGTACAGGAAGCTTAGCCATGGCTTCCC
UP379	CATTGTACAGGAAGCTTAGCCATGGCTTCC
UP380	TAAGGCGCGCCCTACACATTGATCCTAGCAGAAG
UP381	CAAGGCGCGCCTTACCCGTGAAACAGCTGCTCAACTTCCGAAGAAGGCATGGGC ACAG
UP382	CATGGCGCGCCCTACCCGTGAAACAGCTGCTCAACTTCCACATTGATCCTAGC AGAAG
UP383	TAAGGCGCGCCCTACCCGTGAAACAGCTGCTCAACTTCCACATTGATCCTAGCAGA AGCAC

4.1.4.2 Plasmids

Plasmid generation was performed by standard molecular cloning methods as described in (Sambrook, 1989), the Golden Gate cloning procedure described in (Terfrüchte et al., 2014) or the Gibson cloning method which is described in (Gibson et al., 2009). Oligonucleotides used for cloning are listed in Table 4.7. Plasmids containing synthetic genes were synthesized by Integrated DNA Technologies (Coralville). All heterologous sequences were designed according to the context-dependent codon usage for *U. maydis* (Zarnack et al., 2006; Zhou et al., 2018; http://dicodon-optimization.appspot.com). Sequencing of all constructs was performed at the Sequencing Service of the Genomics Service Unit at Ludwig Maximilians University Munich or at Eurofins Genomics (Ebersberg). The plasmids for gene expression in *U. maydis* are integrative vectors, derived from p123 (Aichinger et al., 2003). The plasmids carry sequences for homologous recombination at different loci. The sequence for homologous recombination at the ip^S-locus enables stable genomic integration and selection on carboxin containing media (CbxR; Brachmann, 2001). The expression locus for each construct is indicated in the plasmid descriptions following below. In Table 4.8 the used and in Table 4.9 the generated plasmids are listed, respectively.

Table 4.8: Plasmids used in this study, AmpR = Ampicillin resistance, KanR = Kanamycin resistance, HygR = Hygromycin resistance, G418R = Geneticin resistance, NatR = Nourseothricin resistance, CbxR = Carboxin resistance

Name		Construct description	Locus for integration in *U. maydis*	Resistance *E. coli*	Resistance *U. maydis*	Reference/ Producer
pCR®II-Topo		Vector which was used for the storage and cloning of PCR products with help of the type I Topoisomerase; possibility of blue-white selection for correct insertion.	-	AmpR/KanR	-	Life Technologies
pMF1hs	pUMa194	Vector contains the coding sequence for a 1884 bp *Sfi*I/*Sfi*I hygromycin resistance cassette with the constitutive promoter P_{hsp70}, the coding gene *hph* from *E. coli* (Wang et al., 1988) and the terminator T_{nos} deriving from *Agrobacterium tumefaciens* (Bevan, 1983).	-	AmpR	-	(Brachmann et al., 2004)
pMF1n	pUMa262	Vector contains the coding sequence for a 1437 bp *Sfi*I/*Sfi*I nourseothricin resistance cassette with the *gap1* promoter, the coding gene *nat* and the terminator T_{cyc1} from *Saccharomyces cerevisiae.*	-	AmpR	-	(Brachmann et al., 2004)
pRrm4-Gfp	pUMa496	Vector contains the coding sequence for a C-terminal fusion of Rrm4 to Gfp. Expression is under control of the native promoter of *rrm4* and is terminated via T_{nos}. The cassette is flanked by an 830 bp UF and a 1.9 kb DF for homologous recombination. The expression of the construct is driven by the native promoter of *rrm4.*	*rrm4*	AmpR	-	(Becht et al., 2006)
pP_{crg}-λN22-3xGfp	pUMa1044	Vector contains the coding sequence for the inducible P_{crg} promoter which controls the expression of the 22 aa RNA-binding protein λN (λN*) from the phage λ fused to a triple Gfp. Expression is terminated via T_{nos} terminator. Homologous recombination is feasible due to an ip^R gene.	ip^S	AmpR	CbxR	(Baumann et al., 2012)
pMF1g	pUMa1057	Vector contains the coding sequence for a 2073 bp *Sfi*I/*Sfi*I geneticin resistance cassette with the constitutive promoter P_{otef}, the coding gene *neo* and the terminator T_{cyc1} from S. cerevisiae.	-	AmpR	-	(Baumann et al., 2012)
pP_{otef}-*cdc12*-BoxB^{16}-3´UTR	pUMa1449	Vector contains the coding sequence for a constitutively expressed construct of the *cdc12* (UMAG_03599) gene in which 16 boxB binding sites for the RNA-binding protein λN are integrated in the 3´UTR. Expression is terminated via T_{nos}.	*cdc12*	AmpR	NatR	(Zander et al., 2016)
p*kin3*Δ	pUMa1231	Vector contains a *kin3* gene (UMAG_06251) deletion	*kin3*	AmpR	CbxR	(Baumann et

		construct which is flanked by a 1 kb upstream and 6 kb downstream flank for homologous recombination in *U. maydis* and the *ip*^{R} gene for selection.				al., 2012)
P$_{otef}$-mCherry[3]	pUMa1353	Vector contains the coding sequence for a constitutively expressed triple mCherry for cytosolic localization. Expression is driven with constitutive P$_{otef}$ promoter and terminated with T$_{nos}$. Vector contains the *ip*^{R} gene for homologous recombination in the *ip*^{S} locus.	*ip*^{S}	AmpR	CbxR	Carl Haag
pMK-scFv-myc	pUMa1465	Vector contains the coding sequence for a single chain variable fragment against the myc epitope. It was codon optimized for dicodon usage in *U. maydis* and custom ordered from GeneART.	-	AmpR	-	Parveen Sarkari
pDestI	pUMa1467	pUC57 derivative used in Golden Gate cloning as a destination vector for the final ligation construct. It contains a multiple cloning site including *Bsa*I restriction sites.	-	AmpR	-	(Terfrüchte et al., 2014)
pStorI	pUMa1545	Vector used in Golden Gate Cloning with *Bsa*I which contains the *Sfi*I/*Sfi*I geneticin resistance cassette from pUMa1057.	-	KanR	G418R	(Terfrüchte et al., 2014)
pStorII	pUMa1546	Vector used in Golden Gate Cloning with *Bsa*I which contains the *Sfi*I/*Sfi*I hygromycin resistance cassette from pUMa194.	-	KanR	HygR	(Terfrüchte et al., 2014)
p*upp2*Δ	pUMa1549	Vector contains an *upp2* gene (UMAG_00064) deletion construct which is flanked by a 1 kb upstream and 1.7 kb downstream flank for homologous recombination in *U. maydis.*	*upp2*	AmpR	HygR	(Sarkari et al., 2014)
p*upp3*Δ	pUMa1556	Vector contains an *upp3* gene (UMAG_11908) deletion construct which is flanked by a 1.4 kb upstream and 1.8 kb downstream flank for homologous recombination in *U. maydis.*	*upp3*	AmpR	HygR	(Sarkari et al., 2014)
pP$_{crg}$-MTS-sfGfp	pUMa1604	Vector contains the coding sequence for a heterologously expressed fusion of a mitochondrial localization signal (MTS) to superfolder Gfp (sfGfp). sfGfp was codon optimized for dicodon usage in *U. maydis* and custom ordered from IDT. Expression is under the control of the inducible P$_{crg}$ promoter and is terminated with T$_{nos}$. Vector contains the *ip*^{R} gene for homologous recombination.	*ip*^{S}	AmpR	CbxR	Thorsten Langner
PStorIII	pUMa1694	Vector used in Golden Gate Cloning with *Bsa*I which contains the *Sfi*I/*Sfi*I nourseothricin resistance cassette from pUMa262.	-	KanR	NatR	Carl Haag

pP_{tef}-mCherry-Rab5a	pUMa1806	Vector contains the coding sequence for an ectopic N-terminal fusion of mCherry to Rab5a (UMAG_10615). Expression is under control of the constitutive P_{tef} promoter and is terminated with T_{nos}.	*ip^S*	AmpR	CbxR	(Pohlmann et al., 2015)
pDestII	pUMa2074	pUC57 derivative used in Golden Gate cloning as a destination vector for the final ligation construct. It contains a multiple cloning site including *Sap*I restriction sites.	-	AmpR	-	(Müntjes, 2013)
pRrm4-mEos2	pUMa2086	Vector contains the coding sequence for a C-terminal fusion of the RNA-binding protein Rrm4 (UMAG_10836) and the photoswitchable protein mEos2. Expression is under control of the native promoter of *rrm4* and is terminated via T_{nos}. The cassette is flanked by an 830 bp UF and a 1.9 kb DF for homologous recombination. The expression of the construct is driven by the native promoter of *rrm4.*	*rrm4*	AmpR	NatR	Kira Müntjes
PStorIV	pUMa2242	Vector used in Golden Gate Cloning with *Sap*I which contains the *Sfi*I/*Sfi*I hygromycin resistance cassette from pUMa194.	-	KanR	HygR	(Müntjes, 2013)
p*cdc10*-BoxB^{16}-3´UTR	pUMa2288	Vector contains a construct of the *cdc10* (UMAG_10644) gene in which 16 boxB binding sites for the RNA-binding protein λN* are integrated in the 3´UTR. Expression is driven with native promoter and terminated with T_{nos}.	*cdc10*	AmpR	NatR	(Zander et al., 2016)
p*cdc11*-BoxB^{16}-3´UTR	pUMa2292	Vector contains a construct of the *cdc11* (UMAG_03449) gene in which 16 boxB binding sites for the RNA-binding protein λN* are integrated in the 3´UTR. Expression is driven with native promoter and terminated with T_{nos}.	*cdc11*	AmpR	NatR	(Zander et al., 2016)
pP_{otef}-mCherry-*cdc3*-PBS^{12}-3´UTR	pUMa2492	Vector contains a construct in which 12 copies of PP7 binding sites for the PP7 RNA-binding protein from the phage PP7 were integrated in the 3´UTR of *cdc3*. In addition, Cdc3 is N-terminally tagged with mCherry. The construct is under the control of the constitutive Promoter P_{otef}. Termination takes place with the T_{nos} terminator.	*cdc3*	AmpR	NatR	(Müntjes, 2015)
p*pep4*Δ::P_{otef}-Gfp-T_{nos}	pUMa2580	Vector contains a cassette for the constitutive expression of eGfp. The expression is driven by the P_{otef} promoter and terminated by the T_{nos}. The cassette is flanked by an 800 bp UF and 700 bp DF for homologous recombination at the *pep4* locus (UMAG_04926).	*pep4*	AmpR	NatR	Kai Hussnätter
p*vps60*Δ	pUMa2692	Vector contains a *vps60* gene (UMAG_05282) deletion construct which is flanked by a 700 bp UF and 900 bp DF for homologous recombination in the desired locus.	*vps60*	AmpR	G418R	Carl Haag

pP$_{oma}$-10xHis-UmciA-H7 Nb-TEV-3xHA-Cts1	pUMa2863	Vector contains the coding sequence for a fusion of a nanobody against a part of the botulinum toxin, 10 times His-tag for purification, a TEV protease cleavage site and the chitinase protein Cts1 fused to three times HA-tag. The expression of the construct is under the control of the strong P$_{oma}$ promoter. Terminated is the expression with help of T$_{nos}$.	*ip*^{S}	AmpR	CbxR	(Terfrüchte et al., 2017)
pP$_{otef}$-phox-Gfp	pUMa2931	Vector contains the coding sequence for an N-teminal fusion of Gfp to the phox domain from the endosomal t-SNARE protein Yup1 (UMAG_05406). Expression is driven by constitutive P$_{otef}$ promoter and terminated by T$_{nos}$. Vector contains *ip*^{R} gene for homologous recombination.	*ip*^{S}	AmpR	CbxR	Thomas Pohlmann
pPab1mCherry	pUMa2963	Vector contains the coding sequence for a C-terminal fusion of the Poly(A)-binding protein Pab1 (UMAG_03494) to mCherry. The construct is flanked by 1 kb UF and 900 bp DF for homologous recombination in desired locus.	*pab1*	AmpR	NatR	Silke Jankowski
pCdc3mCherry	pUMa3099	Vector contains the coding sequence for an N-terminal fusion of the septin protein Cdc3 (UMAG_10503) to mCherry. The expression is driven by the native promoter of *cdc3*. The construct is flanked by 1.7 kb UF and 1 kb DF for homologous recombination in the desired locus.	*cdc3*	AmpR	NatR	Silke Jankowski
pHRdSV40-NLS-dCas9-24xGCN4_v4-NLS-P2A-BFP-dWPRE	pUMa3162	dCas9 fused to 24 copies of the GCN4 peptide v4, which is part of the Suntag system.	-	AmpR	-	designed by Ron Vale (Addgene plasmid # 60910)(Tanenbaum et al., 2014)
pHR-scFv-GCN4-sfGFP-GB1-NLS-dWPRE	pUMa3163	The plasmid encodes an antibody that binds to the GCN4 peptide from the Suntag system, and is fused to sfGFP and an NLS for imaging.	-	AmpR	-	designed by Ron Vale (Addgene plasmid # 60906)(Tanenbaum et al., 2014)
pP$_{otef}$-Gfp	pUMa3440	Vector contains a constitutively and cytosolically expressed eGfp. Expression is terminated with T$_{nos}$. Vector contains the *ip*^{R} gene for homologous recombination in *ip* locus.	*ip*^{S}	AmpR	CbxR	Markus Tulinski

pP_{otef}-FLuc^{HA}	pUMa3797	Vector contains a constitutively and cytosoliccaly expressed firefly luciferase (FLuc) from *Photinus pyralis*. The *firefly* gene was optimized for dicdon usage of *U. maydis*. Expression is terminated with T_{nos}. Vector contains UF and DF for integration into *upp3* locus.	*upp3*	AmpR	NatR	Lisa Hüsemann/Nicole Heucken
pP_{crg}-Rrm4-Gfp	pUMa3981	Vector contains a fusion construct of Rrm4 and Gfp for an expression in the ip^S locus. Expression is under the control of the inducible P_{crg} promoter and is terminated with $T_{nos.}$	ip^S	AmpR	CbxR	Srimeenakshi Sankaranarayanan

Table 4.9: Plasmids generated in this study, AmpR = Ampicillin resistance, KanR = Kanamycin resistance, HygR = Hygromycin resistance, G418R = Geneticin resistance, NatR = Nourseothricin resistance, CbxR = Carboxin resistance

Name		Construct and cloning description	Locus for integration in *U. maydis*	Resistance *E. coli*	Resistance *U. maydis*	Reference
pRrm4-mOrange2	pUMa2958	Vector for the expression of a C-terminal fusion of Rrm4 (UMAG_10836) to mOrange2. mOrange2 was codon optimized for dicodon usage in *U. maydis* and custom ordered from IDT. mOrange2 was inserted via *Sfi*I and *Asc*I into pUMa2086. Expression is driven with the native promoter of *rrm4* and terminated with T_{nos}. The coding sequence for the fusion protein is flanked by an 830 bp UF and a 1.9 kb DF for homologous recombination.	*rrm4*	AmpR	NatR	This study
p*pep4*Δ::P_{otef}-mOrange2	pUMa2984	Vector endcodes for a constitutively and cytosolically expressed mOrange2. mOrange2 was codon optimized for dicodon usage in *U. maydis* and custom ordered from IDT. mOrange2 was inserted into pUMa2580 via *Asc*I and *Nco*I. The expression is driven by the P_{otef} promoter and terminated by the T_{nos}. The cassette is flanked by 800 bp UF and 700 bp DF for homologous recombination at the *pep4* locus (UMAG_04926).	*pep4*	AmpR	NatR	This study
pRrm4-mKate2	pUMa2985	Vector for the expression of a C-terminal fusion of Rrm4 (UMAG_10836) to mKate2. mKate2 was codon optimized for dicodon usage in *U. maydis* and custom ordered from IDT. mKate2 was inserted via *Sfi*I and *Asc*I into pUMa2086. Expression is driven with the native promoter of *rrm4* and terminated with T_{nos}. The coding sequence for the fusion protein is flanked by an 830 bp UF and a 1.9 kb DF for homologous recombination.	*rrm4*	AmpR	NatR	This study
p*pep4*Δ::P_{otef}-	pUMa2986	Vector contains a constitutively and cytosolically expressed	*pep4*	AmpR	NatR	This study

mKate2		mKate2. mKate2 was codon optimized for dicodon usage in *U. maydis* and custom ordered from IDT. mKate2 was inserted into pUMa2580 via *Asc*I and *Nco*I. The expression is driven by the P_{otef} promoter and terminated by the T_{nos}. The cassette is flanked by 800 bp UF and 700 bp DF for homologous recombination at the *pep4* locus (UMAG_04926)				
p*upp2*Δ::P_{otef}-Gfp	pUMa3131	Vector for targeted ectopic expression of Gfp in the *upp3* locus (UMAG_11908). For pUMa3131, a 3370 bp fragment containing the constitutive P_{otef} promoter, the eGfp coding sequence and the T_{nos} terminator from pUMa2580 were cloned into pUMa1549, using the restriction endonuclease *Sfi*I. Thereby, the expression cassette was inserted in between flanking regions of 800 bp for homologous recombination	*upp2*	AmpR	NatR	This study
p*upp3*Δ::P_{otef}-Gfp	pUMa3132	Vector for targeted ectopic expression of Gfp in the *upp3* locus (UMAG_11908). For pUMa3132, a 3370 bp fragment containing the constitutive P_{otef} promoter, the eGfp coding sequence and the T_{nos} terminator from pUMa2580 were cloned into pUMa1556, using the restriction endonuclease *Sfi*I. Thereby, the expression cassette was inserted in between flanking regions of 800 bp for homologous recombination	*upp3*	AmpR	NatR	This study
pP_{crg}-λN*-mKate2^2	pUMa3137	Vector for targeted ectopic expression of the modified λN* RNA-binding protein C-terminally fused to double mKate2 in the ip^S locus. For pUMa3137, a 1413 bp fragment containing two times mKate2 from pUMa3181 was cloned into pUMa1044, using the restriction endonuclease *Asc*I and *Not*I. Thereby λN* was fused to mKate2^2.	ip^S	AmpR	CbxR	This study
pP_{otef}-mKate2-HA-PEST-F2A	pUMa3169	Intermediate vector for cloning of pUMa3170. The coding region of mKate2 is fused to an HA-tag, a PEST sequence and the F2A peptide. The PEST sequence is a degron sequence from the ornithine decarboxylase from mouse which is also recognized in *U. maydis* (Brachmann, 2001). The F2A peptide derives from the foot-and-mouth disease virus 18 (Liu et al., 2017). The fusion of PEST sequence and F2A was custom ordered from IDT. mKate2-HA was PCR amplified from pUMa2986 with oligonucleotides MB670/MB671. The PCR product was cloned into pUMa1353 with the restriction endonucleases *Asc*I and *Nco*I in combination with the PEST-F2A construct which	ip^S	AmpR	CbxR	This study

		was cloned with the restriction endonucleases *Asc*I and *BsrG*I.				
pP_{otef}-mKate2-HA-PEST-F2A-Gfp^{NLS}	pUMa3170	Vector contains the final construct of a fusion of mKate2-HA, PEST-F2A, eGfp and an NLS. The nuclear localization sequence (NLS) (Pohlmann et al., 2015) and the Gfp were PCR amplified with oligonucleotides MB988/MB989 from pUMa496 and cloned into pUMa3169 via *BsrG*I and *Sfi*I.	*ip^S*	AmpR	CbxR	This study
p*upp3*Δ::P_{tef}- Gfp	pUMa3212	Vector contains a heterologously expressed Gfp under the control of the P_{tef} promoter in the *upp3* locus. Expression is terminated via T_{nos}. To generate pUMa3212 P_{tef} was amplified via PCR with oligonucleotides MB660/MB661 from pUMa1806 and stored in pCR®II-Topo. It was cloned with the restriction endonucleases *Nco*I and *Sbf*I into pUMa3132. Thereby the expression cassette was inserted in between flanking regions of 800 bp for homologous recombination.	*upp3*	AmpR	NatR	This study
p*upp3*Δ::P_{tef}- Gfp	pUMa3213	Same as pUMa3212 but the resistance cassette was exchanged for hygromycin. For this, the resistance cassette from pUMa194 was cloned into pUMa3212 using the restriction endonuclease *Not*I. For cloning, the backbone of pUMa3212 was dephosphorylated with Antarctic phosphatase.	*upp3*	AmpR	HygR	This study
p*upp3*Δ::P_{tef}-GCN4-scFv-Gfp	pUMa3214	Vector contains a fusion of the single chain variable fragment (scFv) of the GCN4 transcription factor of *S. cerevisiae*, which is used in the Suntag method (Tanenbaum et al., 2014), to Gfp. ScFv-GCN4 was codon optimized for dicodon usage in *U. maydis* and custom ordered from IDT. It was cloned into pUMa3213 with the restriction endonucleases *Asc*I and *Nco*I.	*upp3*	AmpR	HygR	This study
p*upp3*Δ::P_{tef}-GCN4-scFV-sfGfp	pUMa3215	Same as pUMa3214, but Gfp was exchanged for superfolder Gfp (sfGfp). To generate pUMa3215, sfGfp was amplified via PCR with oligonucleotides MB656/MB657 using pUMa1604 as template and stored in pCR®II-Topo. It was cloned with the restriction endonucleases *Asc*I and *EcoR*I into pUMa3134.	*upp3*	AmpR	HygR	This study
pP_{crg}-λN*-2xGfp	pUMa3232	Vector contains the inducible P_{crg} promoter which controls the expression of an improved version of the RNA-binding protein λN (λN*) from the phage λ fused to a double Gfp. The expression is terminated by T_{nos}. The vector contains the *ip^R* gene for integration into the *ip^S* locus via homologous recombination.	*ip^S*	AmpR	CbxR	This study

pTea1-Gfp	pUMa3299	Vector contains a C-terminal fusion of Gfp to the protein Tea1 (UMAG_15019). Cloned via *Bsa*I Golden Gate Cloning into pUMa1467 and pUMa1546. The resistance cassette and the Gfp are flanked by regions 1 kb upstream and downstream of *tea1*. The regions were amplified by PCR with oligonucleotides UP75/UP76 and UP77/UP78 using genomic DNA from the *U. maydis* wild type strain UM521 as template.	*tea1*	AmpR	HygR	This study
pStorV	pUMa3300	Vector used in Golden Gate Cloning with *Bsa*I which contains a cassette expressing recyclable hygromycin resistance. The recycling hygromycin cassette is based upon the Flp/FRT system (Park et al., 2011)	-	KanR	-	This study
p*upp3*Δ::P$_{tef}$-myc-scFv-sfGfp	pUMa3302	Same as pUMa3215, but the scFv-GCN4 was exchanged with scFv against the myc epitope. For this, the ScFv was amplified via PCR with the oligonucleotides UP79/UP80 from pUMa1465 and stored in pCR®II-Topo. It was cloned into pUMa3215 via *EcoR*I/*Nco*I.	*upp3*	AmpR	HygR	This study
p*kin7a*Δ	pUMa3304	Vector contains a construct for the deletion of *kin7a* (UMAG_00896). Cloned via *Bsa*I Golden Gate Cloning into pUMa1467 and pUMa3300. The resistance cassette is flanked by regions 1 kb upstream and 500 bp downstream of *kin7a*. The regions were amplified by PCR with oligonucleotides UP85/UP86 and UP83/UP84 using genomic DNA from wild type strain UM521 as template.	*kin7a*	AmpR	HygR	This study
p*upp3*Δ::P$_{tef}$-GCN4-scFV-sfGfp	pUMa3310	Same as pUMa3215. Exchange of resistance cassette for better strain design. pUMa2692 was cut with *Not*I to get the geneticin resistance gene. This was inserted into pUMa3215.	*upp3*	AmpR	G418R	This study
pP$_{otef}$-*cdc3*-PBS^{12}-3´UTR	pUMa3359	Same as pUMa3736. Resistance cassette was exchanged for recyclable hygromycin. For this the Gibson assembly was used. The resistance cassette (2883 bp) was amplified via PCR from pUMa3300 with oligonucleotides UM404/UM405. The backbone from pUMa3736 (9919 bp) was amplified via PCR with oligonucleotides UM406/UM407. In the Gibson mix both fragments were ligated to generate pUMa3359.	*cdc3*	AmpR	HygR	This study
p*upp3*Δ::P$_{otef}$-mKate2^{HA}-F2A-Gfp^{NLS}	pUMa3407	Vector contains a fusion of mKate2^{HA} and Gfp^{NLS}. In between an F2A peptide ensures expression of two proteins from one open reading frame (F2A originally from the foot-and-mouth disease virus 18). Expression is driven by the constitutive P$_{otef}$ and terminated by T$_{nos}$. Flanking	*upp3*	AmpR	NatR	This study (in cooperation with Lisa Hüseman

		regions of 800 bp ensure homologous recombination at *upp3* locus.				n/ Nicole Heucken)
p*upp3*Δ::P$_{otef}$-mKate2^{HA}-Eo2A-Gfp^{NLS}	pUMa3408	Vector contains a fusion of mKate2^{HA} and Gfp^{NLS}. In between an Eo2A peptide ensures expression of two proteins from one open reading frame (Eo2A originally from inflavirus (Luke et al., 2008). Expression is driven by the constitutive P$_{otef}$ and terminated by T$_{nos}$. Flanking regions of 800 bp ensure homologous recombination at *upp3* locus.	*upp3*	AmpR	NatR	This study (in cooperation with Lisa Hüseman n/ Nicole Heucken)
p*upp3*Δ::P$_{otef}$-mKate2^{HA}-Po2A-Gfp^{NLS}	pUMa3409	Vector contains the coding sequence for a fusion of mKate2^{HA} and Gfp^{NLS}. In between a Po2A peptide ensures expression of two proteins from one open reading frame (Po2A originally from rotavirus). Expression is driven by the constitutive P$_{otef}$ and terminated by T$_{nos}$. Flanking regions of 800 bp ensure homologous recombination at *upp3* locus.	*upp3*	AmpR	NatR	This study (in cooperation with Lisa Hüseman n/ Nicole Heucken)
p*upp3*Δ::P$_{otef}$-mKate2^{HA}-P2A-Gfp^{NLS}	pUMa3410	Vector contains the coding sequence for a fusion of mKate2^{HA} and Gfp^{NLS}. In between a P2A peptide ensures expression of two proteins from one open reading frame (P2A originally from porcine teschovirus-1 2A). Expression is driven by the constitutive P$_{otef}$ and terminated by T$_{nos}$. Flanking regions of 800 bp ensure homologous recombination at *upp3* locus.	*upp3*	AmpR	NatR	This study (in cooperation with Lisa Hüseman n/ Nicole Heucken)
p*upp3*Δ::P$_{otef}$-mKate2^{HA}-E2A-Gfp^{NLS}	pUMa3411	Vector contains the coding sequence for a fusion of mKate2^{HA} and Gfp^{NLS}. In between an E2A peptide ensures expression of two proteins from one open reading frame (E2A originally from ERAV virus; (Kim et al., 2011)). Expression is driven by the constitutive P$_{otef}$ and terminated by T$_{nos}$. Flanking regions of 800 bp ensure homologous recombination at *upp3* locus.	*upp3*	AmpR	NatR	This study (in cooperation with Lisa Hüseman n/ Nicole Heucken)
p*upp3*Δ::P$_{otef}$-mKate2^{HA}-T2A-Gfp^{NLS}	pUMa3415	Vector contains the coding sequence for a fusion of mKate2^{HA} and Gfp^{NLS}. In between a T2A peptide ensures expression of two proteins from one open reading frame (T2A originally from Tetraviridae; (Geier et al., 2015)). Expression is driven by the constitutive P$_{otef}$ and terminated	*upp3*	AmpR	NatR	This study (in cooperation with Lisa

		by T_{nos}. Flanking regions of 800 bp ensure homologous recombination at *upp3* locus.				Hüseman n/ Nicole Heucken)
p*upp3*Δ::P$_{otef}$-mKate2^{HA}-F2AΔP-Gfp^{NLS}	pUMa3435	Same as pUMa3407. Here, the last proline within the F2A is deleted to prevent cleavage within the peptide.	*upp3*	AmpR	NatR	This study (in cooperatio n with Lisa Hüseman n/ Nicole Heucken)
p*upp3*Δ::P$_{otef}$-Gfp-G1-PEST	pUMa3441	Vector for targeted ectopic expression of Gfp in fusion with a degron sequence (PEST) deriving from the G1 cyclin (UMAG_04791) of *U. maydis* in the *upp3* locus. For pUMa3441, a 259 bp fragment was amplified with oligonucleotides UP375/UP376 using genomic DNA from wild type strain UM521 as template. The PCR fragment was cloned into pUMa3132 with the restriction endocucleases *BsrG*I and *Asc*I.	*upp3*	AmpR	NatR	This study
p*upp3*Δ::P$_{otef}$-Gfp-d1-PEST	pUMa3442	Same as pUMa3441. Here, the PEST sequence from ornithine decarboxylase from mouse with a half-life of one hour was integrated. PCR was done with oligonucleotides UP377/UP378	*upp3*	AmpR	NatR	This study
p*upp3*Δ::P$_{otef}$-Gfp-d2-PEST	pUMa3443	Same as pUMa3441. Here, the PEST sequence from ornithine decarboxylase from mouse with a half-life of two hours was integrated. PCR was done with oligonucleotides UP379/UP380.	*upp3*	AmpR	NatR	This study
p*upp3*Δ::P$_{otef}$-Gfp-G1-PEST-Linker	pUMa3444	Same as pUMa3441. Here, an 8 aa linker (EVEQLFHG) was integrated downstream of the PEST sequence. The linker sequence was integrated into oligonucleotide UP381 which was used instead of UP376 for PCR amplification	*upp3*	AmpR	NatR	This study
p*upp3*Δ::P$_{otef}$-Gfp-d1-PEST-Linker	pUMa3445	Same as pUMa3442. Here, an 8 aa linker (EVEQLFHG) was integrated downstream of the PEST sequence. The linker sequence was integrated into oligonucleotide UP382 which was used instead of UP377 for PCR amplification.	*upp3*	AmpR	NatR	This study
p*upp3*Δ::P$_{otef}$-Gfp-d2-PEST-Linker	pUMa3446	Same as pUMa3443. Here, an 8 aa linker (EVEQLFHG) was integrated downstream of the PEST sequence. The linker sequence was integrated into oligonucleotide UP383 which was used instead of UP380 for PCR amplification.	*upp3*	AmpR	NatR	This study
pP$_{otef}$-phox-	pUMa3726	Vector contains the coding sequence for a heterologous	*ip^{S}*	AmpR	CbxR	This study

mKate2-BC2^{12}		fusion of the phox domain from Yup1, mKate2 and 12 copies of the BC2 epitope which is recognized by the BC2 nanobody (Nb) (Virant et al., 2018). A construct containing 12 copies of the BC2 epitope was codon optimized for dicodon usage in *U. maydis* and custom ordered from IDT. It was cut with *Nde*I and *Not*I for cloning. The phox domain was amplified via PCR with oligonucleotides UM31/UM32 from pUMa2931. Together with the mKate2 which was cut from the IDT vector with *Nde*I and *Sfi*I it was inserted in pUMa2931.				
pP_{otef}-phox-mKate2-BC2^{24}	pUMa3727	Same as pUMa3726. 24 copies of the BC2 epitope were cloned with *Nde*I and *Not*I into pUMa3726.	*ip^{S}*	AmpR	CbxR	This study
p*upp3*Δ::P_{tef}-BC2-Nb-sfGfp	pUMa3728	Same as pUMa3310. The GCN4-ScFv was exchanged to the BC2-Nb which is usually used for dSTORM microscopy (Virant et al., 2018). For this the BC2-Nb was codon optimized for dicodon usage in *U. maydis* and custom ordered from IDT. It was cut with *EcoR*I and *Sbf*I and the fragment was inserted in pUMa3310.	*upp3*	AmpR	G418R	This study
pUF+DF	pUMa3732	This vector is the first one for the generation of a cassette system for RNA live imaging and visualization of local translation. Here, the UF and DF of the *cdc3* gene where inserted in pUMa1467 via *Bsa*I Golden Gate cloning. For this, 1.6 kb UF and 1.2 kb DF were amplified via PCR with oligonucleotides UM16/UM17 and UM18/UM19. The UF and DF can be used for homologous recombination at the desired locus.	*cdc3*	AmpR	-	This study
pUF-P_{otef}-DF	pUMa3733	In this vector, the constitutive promoter P_{otef} was inserted into pUMa3732. For this, the P_{otef} was amplified via PCR with oligonucleotides UM20/UM21 from pUMa2580 and was stored in pCR®II-Topo. It was cloned with *Asi*SI/*Sbf*I into pUMa3732.	*cdc3*	AmpR	-	This study
pUF-P_{otef}-cdc3-DF	pUMa3734	In this vector the *cdc3* gene was inserted into pUMa3733. For this *cdc3* was amplified via PCR with oligonucleotides UM22/UM23 from pUMa3285 and was stored in pCR®II-Topo. It was cloned with *Avr*II/*Mfe*I into pUMa3733.	*cdc3*	AmpR	-	This study
pUF-P_{otef}-*cdc3*-PBS^{12}-3´UTR-DF	pUMa3735	In this vector, the 3´UTR of *cdc3* including 12 copies of PBS was inserted into pUMa3734. For this the 3´UTR and PBS^{12} was amplified via PCR with oligonucleotides UM24/UM25 from pUMa2492 and was stored in pCR®II-Topo. It was cloned with *Afl*II/*Nhe*I into pUMa3734.	*cdc3*	AmpR	-	This study
pP_{otef}-*cdc3*-PBS^{12}	pUMa3736	Final vector of the cassette system for RNA live imaging	*cdc3*	AmpR	NatR	This study

		and visualization of local translation. Here the nourseothricin resistance cassette with the *gap1* promoter, the coding gene *nat* and the terminator T_{cyc1} was cloned into pUMa3735. For this, pUMa2580 was digested with *Asc*I and *Sfi*I and the 1713 bp fragment was inserted into pUMa3735 upstream of the DF.				
p*upp3*Δ::P_{tef}-sfGfp	pUMa3872	Same as pUMa3728. For pUMa3872 the antibody was removed to get an expression of sfGfp in the *upp3* locus under the control of the constitutive P_{tef}. For this pUMa3728 was cut twice: Firstly with *AlwN*I and *Mfe*I to generate a 3652 bp fragment, secondly with *AlwN*I and *EcoR*I to generate a 5771 bp fragment. Both fragments were ligated to get the final plasmid.	*upp3*	AmpR	G418R	This study
p*upp3*Δ::P_{tef}-Bot-Nb-sfGfp	pUMa3873	Same as pUMa3728. The antibody was exchanged to a nanobody against a part of the botulinum toxin (Bot-Nb).For this Gibson cloning was used. pUMa3728 was cut with the restriction endonucleases *BstE*II and *Mfe*I. The coding sequence for the Bot-Nb was amplified via PCR with oligonucleotides UM206/UM207 from pUMa2863.	*upp3*	AmpR	G418R	This study
p*upp3*Δ::P_{tef}-Moontag-Nb-sfGfp	pUMa4042	Same as pUMa3728. Antibody was exchanged to the Moontag-Nb (Boersma et al., 2019). The coding sequence for the Moontag-Nb was codon optimized for dicodon usage in *U. maydis* and custom ordered from IDT. The 399 bp Nb sequence was cloned into pUMa3728 using the restriction endonucleases *Age*I and *Mfe*I.	*upp3*	AmpR	G418R	This study
p*UMAG_00933*Δ	pUMa4173	Vector contains a deletion construct for UMAG_00933. Cloned via *SapI*I Golden Gate Cloning into pUMa2242 and pUMa2074. The resistance cassette is flanked by regions 1 kb upstream and 1.1 kb downstream of UMAG_00933. The regions were amplified by PCR with oligonucleotides UM848/UM849 and UM850/UM851 using genomic DNA from wild type strain UM521 as template.	*UMAG_00933*	AmpR	HygR	This study
p*UMAG_00933*-Gfp	pUMa4174	Vector contains the coding sequence for a C-terminal fusion of Gfp to the protein UMAG_00933. Cloned via *Bsa*I Golden Gate Cloning into pUMa1467 and pUMa1694. The resistance cassette and the Gfp coding sequence are flanked by regions 1 kb upstream and downstream of *UMAG_00933*. The regions were amplified by PCR with oligonucleotides UM8525/UM853 and UM854/UM855 using genomic DNA from wild type strain UM521 as template.	*UMAG_00933*	AmpR	NatR	This study
p*upp3*Δ::P_{otef}-	pUMa4197	Same as pUMa4260. In addition a linker sequence	*upp3*	AmpR	NatR	This study

mKate2^{HA}-L2-F2AΔP-Gfp^{NLS}		(KLSHGFPPAVAAQDDGTLV) and the F2A peptide in which the last proline is deleted were integrated in between the mKate2^{HA} and the Gfp. For this, F2AΔP was amplified via PCR with oligonucleotides UM984/UM983 from pUMa3435 and stored in pCR®II-Topo. The linker sequence was integrated in one oligonucleotide. The fragment was cloned into pUMa4260 with the restriction endonucleases *Blp*I and *Fse*I				
p*upp3*Δ::P$_{otef}$-mKate2^{HA}-L2-F2A-Gfp^{NLS}	pUMa4198	Same cloning strategy as pUMa4197. Here, F2A was integrated. The linker-F2A was codon optimized for dicodon usage in *U. maydis* and custom ordered from IDT.	*upp3*	AmpR	NatR	This study
p*upp3*Δ::P$_{otef}$-mKate2^{HA}-L2-P2A-Gfp^{NLS}	pUMa4199	Same cloning strategy as pUMa4197. Here, P2A was integrated. Used oligonucleotides: UM965/UM964. Template: pUMa3410.	*upp3*	AmpR	NatR	This study
p*upp3*Δ::P$_{otef}$-mKate2^{HA}-L2-E2A-Gfp^{NLS}	pUMa4200	Same cloning strategy as pUMa4197. Here, E2A was integrated. Used oligonucleotides: UM970/UM971. Template: pUMa3411	*upp3*	AmpR	NatR	This study
p*upp3*Δ::P$_{otef}$-mKate2^{HA}-L2-T2A-Gfp^{NLS}	pUMa4202	Same cloning strategy as pUMa4197. Here, T2A was integrated. Used oligonucleotides: UM974/UM975. Template: pUMa3415.	*upp3*	AmpR	NatR	This study
p*upp3*Δ::P$_{otef}$-mKate2^{HA}-L2-Eo2A-Gfp^{NLS}	pUMa4203	Same cloning strategy as pUMa4197. Here, Eo2A was integrated. The linker-Eo2A was codon optimized for dicodon usage in *U. maydis* and custom ordered from IDT.	*upp3*	AmpR	NatR	This study
p*upp3*Δ::P$_{otef}$-mKate2^{HA}-L2-Po2A-Gfp^{NLS}	pUMa4204	Same cloning strategy as pUMa4197. Here Po2A was integrated. The linker-Po2A was codon optimized for dicodon usage in *U. maydis* and custom ordered from IDT.	*upp3*	AmpR	NatR	This study
pP$_{otef}$-mKate2^{HA}-Gfp^{NLS}	pUMa4259	Intermediate vector to analyze 2A peptides. Vector contains the coding sequence for a fusion of mKate2, an HA-tag and Gfp fused to a nuclear localization sequence (NLS). Cloned via *Bsa*I Golden Gate cloning into pUMa1467. The fragment P$_{otef}$-mKate2 was amplified via PCR with oligonucleotides UM959/UM960. The fragment containing Gfp-NLS was amplified with UM961/UM962. In both cases pUMa3410 serves as template.	-	AmpR	-	This study
p*upp3*Δ::P$_{otef}$-mKate2^{HA}-Gfp^{NLS}	pUMa4260	Vector contains the same construct which was built in pUMa4259. This construct was inserted into pUMa4259 for expression in the *upp3* locus. For this, pUMa4259 was cut with *Asc*I and *Sbf*I and the 2495 bp fragment was cloned into pUMa3410.	*upp3*	AmpR	NatR	This study
p*upp3*Δ::P$_{otef}$-mKate2^{HA}-GSG-	pUMa4261	Same cloning strategy as pUMa4197. Here, F2A was integrated. Instead of inserting a longer linker, the short	*upp3*	AmpR	NatR	This study

F2A-Gfp^{NLS}		linker GSG was integrated upstream of F2A. Used oligonucleotides: UM963/UM964. Template: pUMa3407.				
p*upp3*Δ::P$_{otef}$-mKate2^{HA}-L1-P2A-Gfp^{NLS}	pUMa4263	Same cloning strategy as pUMa4197. Here, P2A was integrated. Instead of inserting a longer linker the short linker GSG was integrated upstream of P2A. Used oligonucleotides: UM967/UM968. Template: pUMa3410.	*upp3*	AmpR	NatR	This study
p*upp3*Δ::P$_{otef}$-mKate2^{HA}-L1-F2AΔP-Gfp^{NLS}	pUMa4273	Same cloning strategy as pUMa4197. Here, F2A with a deletion of the last proline was integrated. Instead of inserting a longer linker the short linker GSG was integrated upstream of F2AΔP. Used oligonucleotides: UM969/UM970. Template: pUMa3411.	*upp3*	AmpR	NatR	This study
pP$_{otef}$-Phox-mKate2-GCN4-epitop^{24}	pUMa4438	Same as pUMa3726. The binding sites from the BC2-Nb were exchanged with 12 copies of binding sites for the GCN4-Nb. For this, the binding sites were amplified via PCR with oligonucleotides AB325/AB326 from pUMa3162 and stored in pCR®II-Topo. The 1748 bp fragment was cloned into pUMa3726 via *Age*I and *Not*I.	*ip^S*	AmpR	CbxR	This study
pP$_{crg}$-Rrm4-Gfp-L2-P2A-FLuc^{HA}	pUMa4565	The vector contains the coding sequence for a fusion of Rrm4-Gfp and FLuc^{HA} separated by L2-P2A. The L2-P2A was amplified with AB603/AB604 from pUMa4276 and stored in pCR®II-Topo. The 161 bp fragment was cloned into pUMa3981 with *BsrG*I and *Mfe*I. The FLuc^{HA} was cloned into pUMa3987 via *Asc*I and *Mfe*I. The vector contains the *ip^R* gene for homologous recombination.	*ip^S*	AmpR	CbxR	This study

4.1.4.3 *E. coli* strains

The Top10 *E. coli* strain (Grant et al., 1990), Invitrogen) was used for all cloning steps in this study. The strain has the following genotype: *F-mcrA Δ(mrr-hsdRMS-mcrBC)φ80lacZΔM15 ΔlacX74 recA1 araD139 Δ(araleu)7697 galU galK rpsL endA1 nupG.*

4.1.4.4 *U. maydis* strains

Table 4.10 shows the *U. maydis* strains which were used in this study. They were used as progenitor and control strains, respectively. Table 4.11 shows the *U. maydis* strains generated in this study.

Table 4.10: *U. maydis* strains used in this study, all strains are derivatives of AB33 and have the additional genotype a2 P_{nar}:bW2bW1.

Strain	Relevant genotype	UMa	Reference
AB33	*a2 Pnar:bWebE1*	133	(Brachmann, 2001)
AB33*rrm4*Δ	*rrm4Δ*	273	(Becht et al., 2006)
AB33Rrm4-Gfp	*rrm4-Gfp*	274	(Becht et al., 2006)
AB33*grp1*Δ	*grp1Δ*	380	(Olgeiser et al., 2019)
AB33Pab1-Gfp	*pab1-Gfp*	389	(König et al., 2009)
AB33Gfp-Cdc3	*gfp-cdc3*	421	(Baumann et al., 2014)
AB33P_{otef}Gfp	*gfp*	486	(Baumann et al., 2014)
AB33Pab1-mCherry-3xMyc	*gab1-mCherry-3xmyc*	578	Thomas Pohlmann
AB33*kin3*Δ	*kin3Δ*	662	Thomas Pohlmann
AB33P_{otef}-*cdc3*-boxB^{16}-3'UTR	*cdc3B^{16}*	773	Sebastian Baumann
AB33P_{crg}λN*Gfp^3/ P_{otef}*cdc3*-boxB^{16}-3´UTR	*λN*Gfp^{3}cdc3B^{16}*	779	Sebastian Baumann
AB33Rrm4-mCherry	*rrm4-mCherry*	830	(Baumann et al., 2014)
AB33*upa1*Δ	*upa1Δ*	859	(Pohlmann et al., 2015)
AB33P_{crg}λN*G^2/ P_{otef}cdc3CnB^{16}	*λN*G^{3}cdc3CnB^{16}*	1002	(Baumann et al., 2014)
AB33P_{crg}mCherry	*mCherry*	1203	Thorsten Langner
AB33*upa2*Δ	*upa2Δ*	1505	(Jankowski et al., 2019)
AB33*pep4*Δ::P_{otef}Gfp	*pep4ΔP_{otef}Gfp*	1569	Julius Wierichs
AB33Rrm4-TagRfp	*rrm4-TagRfp*	1317	(Müntjes, 2015)
AB33P_{otef}PCP-GfpG^{2}NLS/ P_{otef}*cdc3*-mCherry-PBS^{12}-3´UTR	*PCP*G^{2}NLScdc3*PBS^{12}	1735	(Müntjes, 2015)
AB33*pep4*Δ:P_{otef}ProtA-TagRfp	*pep4ΔprotA-TagRfp*	1747	(Müntjes, 2015)

Table 4.11: Description of *U. maydis* strains generated in this study, all strains are derivatives of AB33 and have the additional genotype a2 P_{nar}:bW2bW1.

Strain	relevant genotype	UMa	integrated plasmid (pUMa)	Locus	Progenitor	Reference
AB33Rrm4-mOrange2	*rrm4-mOrange2*	1984	2958	*rrm4*	UMa273	This study
AB33Rrm4-mKate2	*rrm4-mKate2*	1985	2985	*rrm4*	UMa273	This study
AB33*pep4*Δ::P_{otef}-	*mOrange*	1986	2984	*pep4*	UMa1569	This

mOrange2						study
AB33*pep4*Δ::P$_{otef}$-mKate2	*mKate2*	1987	2986	*pep4*	UMa1569	This study
AB33*upp2*Δ	*upp2*Δ	2147	1549	*upp2*	UMa133	This study
AB33*upp3*Δ	*upp3*Δ	2148	1556	*upp3*	UMa133	This study
AB33*upp2*Δ:P$_{otef}$-Gfp	*gfp*	2178	3131	*upp2*	UMa2147	This study
AB33*upp3*Δ:P$_{otef}$-Gfp	*gfp*	2179	3132	*upp3*	UMa2148	This study
AB33P$_{otef}$-*cdc3*-boxB^{16}-3'UTR/P$_{crg}$-λN*-mKate2^{2}	*λN*mKate22/ cdc3B^{16}*	2218	3137	*ip^{S}*	UMa773	This study
AB33Tea1-Gfp	*tea1-gfp*	2268	3299	*tea1*	UMa133	This study
AB33P$_{otef}$-mKate2-d1-F2A-Gfp	*mKate2-d1-F2A-gfp*	2277	3283	*ip^{S}*	UMa133	This study
AB33*upp3*Δ::P$_{tef}$-GCN4-scFv-sfGfp	*GCN4-scFv-sfgfp*	2278	3310	*upp3*	UMa133	This study
AB33*upp3*Δ::P$_{tef}$-GNC4-scFv-sfGfp/kin7aΔ	*GCN4-scFv-sfGfp/kin7a*Δ	2279	3304	*kin7a*	UMa2279	This study
AB33P$_{crg}$-λN*-mKate2^{2}	*λN*mKate2^{2}*	2345	3137	*ip^{S}*	UMa133	This study
AB33*upp3*Δ::Pt$_{ef}$-Myc-scFv-sfGfp	*Myc-scFv-sfgfp*	2395	3302	*upp3*	UMa2179	This study
AB33*upp3*Δ:P$_{otef}$-Gfp-G1-PEST	*gfp-G1-PEST*	2421	3441	*upp3*	UMa2148	This study
AB33*upp3*Δ::P$_{otef}$-Gfp-G1-PEST-linker	*gfp-G1-PEST-Linker*	2422	3444	*upp3*	UMa2148	This study
AB33*upp3*Δ::P$_{otef}$-Gfp-d1	*gfp-d1-PEST*	2423	3442	*upp3*	UMa2148	This study
AB33_*upp3*Δ::P$_{otef}$-Gfp-d2	*gfp-d2-PEST*	2425	3443	*upp3*	UMa2148	This study
AB33_*upp3*Δ::P$_{otef}$-Gfp-d1-linker	*gfp-d1-PEST-Linker*	2426	3445	*upp3*	UMa2148	This study
AB33_*upp3*Δ::P$_{otef}$-Gfp-d2-linker	*gfp-d2-PEST-Linker*	2427	3446	*upp3*	UMa2148	This study
AB33_*upp3*Δ::P$_{tef}$-BC2-Nb-sfGFP	*BC2-Nb-sfgfp*	2634	3728	*upp3*	UMa2148	This study
AB33*upp3*Δ::P$_{tef}$-GCN4-scFc-sfGFP-upa1Δ	*GCN4-scFv-sfgfp/upa1*Δ	2679	3728	*upa1*	UMa1505	This study
AB33*upp3*Δ::P$_{tef}$-GCN4-scFv-sfGFP-upa2Δ	*GCN4-scFv-sfGfp/upa2*Δ	2680	3728	*upa2*	UMa859	This study
AB33*upp3*Δ::P$_{tef}$-GCN4-ScFv-sfGFP-rrm4Δ	*GCN4-scFv-sfgfp/rrm4*Δ	2681	3728	*upp3*	UMa273	This study
AB33*upp3*Δ::P$_{tef}$-sfGFP	*sfgfp*	2683	3872	*upp3*	UMa2148	This study
AB33*upp3*Δ::P$_{tef}$-Bot-Nb-sfGFP	*BC2-Nb-sfgfp*	2684	3873	*upp3*	UMa2148	This study
AB33*upp3*Δ::P$_{tef}$-Moontag-Nb-sfGFP	*Moontag-Nb-sfgfp*	2799	4042	*upp3*	Uma2148	This study
AB33*upp3*Δ:P$_{tef}$-GCN4-scFv-sfGfp/*UMAG_00933*Δ	*GCN4-scFv-sfGfp/UMAG_00933*Δ	3029	4173	*UMAG_00933*	UMa2278	This study
AB33*UMAG_00933*-Gfp	*UMAG_00933-gfp*	3030	4174	*UMAG_00933*	AB33	This study
AB33*upp3*Δ::P$_{otef}$-	*mKate2-GSG-F2A-*	3116	4261	*upp3*	UMa2148	This

mKate2^{HA}-L1-F2A-Gfp^{NLS}	*gfp-^{NLS}*					study
AB33*upp3*Δ::P$_{otef}$-mKate2^{HA}-L2-E2A-Gfp^{NLS}	*mKate2-L2-E2A-gfp-^{NLS}*	3117	4200	*upp3*	UMa2148	This study
AB33*upp3*Δ::P$_{otef}$-mKate2-^{HA}-L2-Eo2A-Gfp-^{NLS}	*mKate2-L2-Eo2A-gfp-^{NLS}*	3118	4203	*upp3*	UMa2148	This study
AB33*upp3*Δ::P$_{otef}$-mKate2^{HA}-Linker-F2AΔP-Gfp^{NLS}	*mKate2-L2-F2AΔP-gfp-^{NLS}*	3119	4197	*upp3*	UMa2148	This study
AB33*upp3*Δ::P$_{otef}$-mKate2^{HA}-L2-T2A-Gfp^{NLS}	*mKate2-L2-T2A-gfp-^{NLS}*	3120	4202	*upp3*	UMa2148	This study
AB33*upp3*Δ::P$_{otef}$-mKAte2-^{HA}-L1-P2A-Gfp-^{NLS}	*mKate2-L1-P2A-gfp-^{NLS}*	3121	4263	*upp3*	UMa2148	This study
AB33*upp3*Δ::P$_{otef}$-mKAte2^{HA}-GSG-F2AΔP-Gfp^{NLS}	*mKate2-GSG-F2AΔIP-gfp-^{NLS}*	3122	4273	*upp3*	UMa2148	This study
AB33*upp3*Δ::P$_{otef}$-mKate2^{HA}-L2-P2A-Gfp^{NLS}	*mKate2-L2-P2A-gfp-^{NLS}*	3123	4199	*upp3*	UMa2148	This study
AB33*upp3*Δ::P$_{tef}$-GCN4-scFv-sfGfp/UMAG_00933Δ/Rrm4-mKate2	*GCN4-scFv-sfgfp/UMAG_00933Δ/rrm4mKate2*	3126	2985	*rrm4*	UMa3029	This study
AB33*upp3*Δ::P$_{tef}$-GCN4-ScFv-sfGfp/UMAG_00933Δ/mCherry-Cdc3	*GCN4-scFv-sfgfp/UMAG_00933Δ/mCherry-cdc3*	3127	3099	*cdc3*	UMa3029	This study
AB33*upp3*Δ::P$_{tef}$-Bc2-Nb-sfGfp/UMAG_00933Δ	*BC2-Nb-sfgfp/UMAG_00933Δ*	3130	4173	*UMAG_00933*	UMa2634	This study
AB33*upp3*Δ::P$_{otef}$-mKate2^{HA}-L2-F2A-eGFP^{NLS}	*mKate2-L2-F2A-Gfp^{NLS}*	3144	4198	*upp3*	UMa2278	This study
AB33*upp3*Δ::P$_{otef}$-mKate2^{HA}-L2-Po2A-Gfp^{NLS}	*mKate2-L2-Po2A-Gfp^{NLS}*	3145	4204	*upp3*	UMa2278	This study
AB33*upp3*Δ::P$_{tef}$-GCN4-scFv-sfGfp/UMAG_00933Δ/P$_{otef}$-phox-mKate2-GCN4^{24}	*GCN4-scFv-sfGfp/UMAG_00933Δ/rphox-mKate2-GCN4^{24}*	3163	4438	*ip^{S}*	UMa3029	This study
AB33_*upp3*Δ::P$_{tef}$-GCN4-scFv-sfGfp/kin3Δ	*GCN4-scFv-sfGfp/kin3Δ*	3164	1231	*kin3*	UMa2278	This study
AB33*rrm4*Δ/P$_{crg}$-Rrm4-Gfp-L2-P2A-FLuc^{HA}	*Rrm4Δ/rrm4-gfp-L2-P2A-fluc*	3212	4565	*ip^{S}*	Uma273	This study

4.2 Microbiological methods

4.2.1 *E. coli*

4.2.1.1 Cultivation of *E. coli* cells

E. coli cells were mostly grown on solid or liquid dYT medium, supplemented with antibiotics in concentrations shown in Table 4.5. Cultivation was performed overnight in glass tubes on a rotary wheel at 37 °C and 200 rpm.

4.2.1.2 Preparation of chemically competent *E. coli* cells

Chemically competent *E. coli* cells were prepared with help of a modified protocol of (Cohen et al., 1972). They are stored at -80 °C and free for usage.

4.2.1.3 *E. coli* transformation

To introduce foreign DNA into *E. coli* cells, plasmid DNA was transformed into competent cells using a heat shock method. For this, 2-20 µl of each construct were added to 50 µl of competent cells. This mixture was incubated on ice for 30 min and a heat shock (42 °C for 45 s) step was performed afterwards. Following an additional incubation for approximately 2 min on ice, 150 µl sterile dYT medium without antibiotics were added to the cell suspension and the cells were incubated for 30 min at 37 °C and 200 rpm. After incubation, the cell suspension was streaked onto YT agar plates containing ampicillin. The plates were incubated overnight at 37 °C.

4.2.2 *U. maydis*

4.2.2.1 Cultivation of *U. maydis* cells

U. maydis cells were mostly grown on solid or liquid CM medium, supplemented with carbon source. Cultivation was performed in glass tubes on a rotary wheel or in baffled shaking flasks. Cultivation of the cells was always performed at 28 °C and 200 rpm. For induction of filamentous growth (section 4.2.2.3), the cells were shifted to liquid or solid NM medium. If necessary, solid CM-medium was supplemented with antibiotics in concentrations listed in Table 4.6. For long term storage, *U. maydis* cells were mixed with NSY-glycerin and stored at -80 °C.

4.2.2.2 Preparation of chemically competent *U. maydis* cells (protoplasts)

To prepare chemically competent *U. maydis* cells, a modified version of the protocols of (Gillissen et al., 1992) and (Schulz et al., 1990) was used. The desired strains for competent *U. maydis* cells were streaked out onto CM plates and incubated for at least 2 days at 28 °C. The cells were inoculated in CM liquid medium at 28 °C and 200 rpm,

afterwards. The pre-cultures were then diluted (1:100) in 50 ml fresh CM and incubated at 28 °C and 200 rpm until an OD_{600} of 0.6-1 was reached. Subsequently the cultures were centrifuged for 5 min at 3.000 rpm. The cell pellets were resuspended in 20 ml SCS buffer and centrifuged again for 5 min at 3.000 rpm. The cell pellets were resuspended in a novozyme containing solution (7 mg/2 ml SCS; sterile filtered) or a glucanex solution (12.5 mg/ml SCS; sterile filtered) and incubated for 5-15 min at RT. The cells were checked under a light microscope every 5 min to control the cells (30-40% should be round or pinhead-like). The following steps were all performed on ice. By adding 10 ml of cold (4 °C) SCS buffer to the novozyme or glucanex suspension and performing a centrifugation step for 5 min at 2,400 rpm the reaction was stopped. To wash the cell pellet, this step was repeated twice. Subsequently, the pellets were resuspended in 10 ml of cold STC buffer and centrifuged again for 5 min at 2,400 rpm. Finally the cell pellets were resuspended in 1 ml of cold STC buffer and 100 µl aliquots were made. The aliquots were kept frozen at -80 °C.

SCS buffer:	1st Solution: 20 mM tri-Na-Citrate*2H_2O 1 M Sorbitol 2nd Solution: 20 mM Citric acid*H_2O 1 M Sorbitol Fill with ddH_2O. Adjust the pH of the first solution to 5.8 with help of the second solution and autoclave.
STC buffer:	50% (v/v) 2 M Sorbitol 1% (v/v) 1 M Tris-HCl pH 7.5 10% (v/v) 1 M $CaCl_2$ Fill with ddH_2O and sterile filter

4.2.2.3 *U. maydis* transformation

The chemically competent *U. maydis* cells were thawed on ice for 10 minutes. 1 µl heparin (15 mg/ml) and previously linearized plasmid-DNA (3-4 µg) were added and the cells were incubated on ice for 15 minutes. Subsequently, 500 µl STC/PEG were added and mixed with the cells. The suspension was incubated on ice for 15 min. The suspension was streaked out onto two plates and incubated for 7-14 days at 28 ˚C or RT. The plates used for the transformation consisted of two layers of agar: The top

layer contained only Reg-light medium contrary to the bottom layer which also contained antibiotics.

STC/PEG:	60% (v/v) STC buffer
	40% (v/v) PEG
	Sterile filtration

4.2.2.4 Shifting of *U. maydis* cultures in NM for induction of hyphal growth

To analyze hyphae of *U. maydis,* a lab strain (AB33, *a2* P_{nar}:*bW2*,*bE1*;(Brachmann, 2001)) was used. This strain contains the *nar1* promoter upstream of a synthetic *b* fusion coding sequence (Banks et al., 1993). This promoter drives the expression of the bW/bE heterodimer and allows an induction of hyphal growth by switching the nitrogen source. To shift the cells to a nitrate minimal medium (NM), a pre-culture of 3 ml CM medium was inoculated overnight at 28 °C and 200 rpm. On the next day, a main culture of 30 ml CM and approximately 20-30 µl of pre-culture was inoculated for an additional night at 28 °C and 200 rpm. In the next morning, the OD_{600} of the cultures was measured and the corresponding volume for an OD_{600} of 0.5 in 20 ml was centrifuged for 3 min at 5000 rpm. The supernatant was removed completely and the cell pellet was resuspended in 20 ml of NM to wash the cells. Another centrifugation step of 3 min and 5000 rpm was performed. The supernatant was discarded and the cells were resuspended again in 20 ml NM containing carbon source. The culture was then agitated at 28 ˚C and 200 rpm for typically 6-8 h.

4.2.2.5 Determination of density of bacterial and fungal cell cultures

To determine the density of cell cultures, photometric measurements with a Novaspec II photometer (Pharmacia Biotech) at a wavelength of 600 nm were performed. For measurements, cultures were diluted to a maximum OD_{600} of 0.8 to ensure the linear dependency of the measurement. An OD_{600} of 1 of an *U. maydis* culture corresponds to 1-5 x 10^7 and of *E. coli* to 10^9 cells, respectively.

4.2.2.6 Analysis of growth NM plates containing charcoal

For the analysis of the hyphal growth, 2 µl of sporidial cells were dropped on NM plates containing charcoal. The plates were incubated for 2 days at 28 °C. The colony morphology was analyzed with the stereomicroscope Zeiss Stemi 2000C equipted with the light source Zeiss KL1500 LCD (Zeiss). The morphology was documanted using a Canan PowerShot A650 IS-camera (Canon GmbH, Krefeld, Germany).

4.2.2.7 Monitor the cell density of sporidial cells with Biolector I system

To monitor the cell density over time, the Biolector I system (m2lab GmbH; Baesweiler, Germany) was used. For this, the desired strains were streaked out onto CM plates and incubated for at least 2 days at 28 °C. The cells were inoculated in CM liquid medium at 28 °C and 200 rpm, afterwards. The pre-cultures were then diluted (1:100) in 20 ml fresh CM and incubated at 28 °C and 200 rpm until an OD_{600} of 0.5 was reached. The cells were diluted to an OD_{600} of 0.1 and 1,500 µl of this dilution were transferred to a 48 well plate. For the measurement three biological as well as three technical replicates were included. Within the Biolector I, the cell density was measured every 30 min for 24 h. The data analysis was conducted with the provided software BioLection 2.4.5. The biomass was measured with excitation and emission of 620 nm and a gain of 30. Here, the scattered light is measured in contrast to the transmitted light which is measured with spectrophotometry (Ladner et al., 2016).

Parameters for measurement:

Temperature:	28 °C
Humidity:	85 rH
O_2:	20.95%
Shaker frequency:	1,000 rmp

4.2.2.8 Analysis of growth behavior of *U. maydis* under stress conditions

To analyze the influence of different temperatures on *U. maydis*, sporidia were dropped on CM plates. For this, 2 µl of a main culture (OD_{600}0.5) were dropped in serial dilution (10^1-10^5) and the plates were incubated for 2 days at 28 °C and 37 °C, and for 4 days at 16 °C. The cell morphology was documented using the imaging system LAS4000 (Fujifilm). For the analysis of growths of deletion mutants in the presence of different agents, an agar diffusion test (halo test) was performed. For this, 500 µl of a main culture of sporidia as well as hyphal cells (OD_{600}0.5) were streaked out on square-shaped agar plates (120 mm). For the test, filter paper was cut, soaked with different stress inducing agents and placed on the plates. The plates were incubated for 2 days at 28 °C. Afterwards, zones of growth inhibition (halo formation) were analyzed and compared in between the different strains.

Tested agents and concentrations:

Calcofluore White:	2 mg/ml solved in H_2O
H_2O_2:	30% solved in H_2O

SDS:	20% solved in H_2O
Tunicamycin:	5 mg/ml solved in DMSO
Olegomycin:	6 mM solved in DMSO
Cycloheximide:	100 mg/ml solved in DMSO
Benomyl:	2 mM solved in DMSO
Latrunculin A:	1 mM solved in DMSO
Hydroxyurea:	3 mg/ml solved in H_2O

4.3 Molecular biological methods

4.3.1 Isolation of nucleic acids

4.3.1.1 Isolation of plasmid DNA from *E. coli*

To elute transformed plasmid DNA from *E. coli* a modified protocol for the boiling preparation (Sambrook, 1989) was used. Different transformants were inoculated in 1 ml dYT medium supplemented with ampicillin and cultivated overnight at 37 °C at 200 rpm. On the next day, the culture was centrifuged at 13,000 rpm for 2 min. The supernatant was removed and 200 µl STET as well as 20 µl of lysozyme were added. After resuspending the cell pellet, it was incubated at 90 °C for 1 min and centrifuged for 10 min at 13,000 rpm. The remaining pellet was removed and 20 µl NaOAc (3 M) and 500 µl isopropyl alcohol were added to the supernatant. The tube was inverted a few times and then centrifuged again for 10 min at 13,000 rpm. The supernatant was discarded and the pellet was washed with 200 µl 70% ethanol and then subsequently centrifuged for 3 min at 13,000rpm. To remove the ethanol, the pellet was dried for 10-15 min at 50 °C. To dissolve the DNA pellet, 100 µl TE-RNAse was added and the tube was agitated for 10 min at 50 °C and 650 rpm.

STET buffer:	0.1 M NaCl 10 mM Tris/HCl pH 8.0 1 mM EDTA 5% Triton-X-100 Fill with ddH_2O and autoclave
Lysozyme:	1.0% (w/v) Lysozyme (Muraminidase) 10 mM Tris- HCl (pH 8.0) Sterile filtration
TE-RNAse:	8.69 mM Tris- HCl (pH 8.0) 10 mM Na_2-EDTA*$2H_2O$

1.31 mM Tris Base
Fill with ddH_2O and autoclave
After autoclaving: add RNAseA (10 mg/ml) in 50 ml TE buffer

4.3.1.2 Isolation of genomic DNA from *U. maydis*

To isolate genomic DNA from *U. maydis,* a modified protocol from (Bosch et al., 2016) was used. For this, single colonies were inoculated in 3 ml CM for two days at RT and 200 rpm. 2 ml of these cultures were centrifuged for 3 min at 13,000 rpm. The supernatant was discarded and approximately 200 µl of glass beads were added to the cell pellet. Subsequently, 500 µl lysis buffer (50:50 diluted with TE buffer) was added and the mixture was agitated for 15 min at 1,500 rpm followed by heating the samples for 20 min at 65 °C in a thermoblock. After adding potassium acetate (8 M), the suspension was inverted to grain the proteins. Then a centrifugation step of 15 min and 13,000 rpm was performed. Approximately 400 µl of the resulting supernatant were transferred to a new tube and mixed with 500 µl isopropyl alcohol. After inverting the tube, it was centrifuged for 15 min at 13,000 rpm. The supernatant was discarded and the DNA pellet was washed by adding 200 µl 70% ethanol and another centrifugation for 10 min at 13,000 rpm. After removing the ethanol completely, 50 µl TE-RNAse were added and the pellet was dissolved by agitating for 30 min at 50 °C and 900 rpm.

U. maydis lysis buffer:
10 mM Tris/HCl pH 8.0
100 mM NaCl
1% (w/v) SDS
2% (w/v) Triton X-100
1 mM EDTA
Solve in ddH_2O

4.3.2 *In vitro* nuclease modifications

4.3.2.1 Measurement of the concentration and purity of DNA

The concentration and purity of isolated nucleic acid was measured with the help of the NanoDrop ND-2000c (Thermo Scientific) at OD_{260}. The purity was analyzed by the quotient of OD_{260}/OD_{280}.

4.3.2.2 Restriction analysis

For restriction of DNA, different restriction enzymes were used. All enzymes and used buffers were ordered from the company New England Biolabs (NEB). The restriction

digests were inoculated for 2-12 h at enzyme specific temperatures and buffers containing BSA. The restrictions were analyzed on agarose gels.

Example for a typical restriction:

DNA (Plasmid):	1.0-5.0 µl
Enzyme specific buffer (5x):	4.0 µl
Restriction enzyme:	0.2-0.5 µl
	Add ddH_2O to a total volume of 20 µl.

4.3.2.3 Dephosphorylation

To prevent re-ligation events of cut backbone DNA, the Antarctic phosphatase with the according buffer from the company NEB was used. For dephosphorylation, the preparation was incubated for 1 h at 37 °C. To stop the reaction, the mixture was incubated for 5 min at 80 °C.

Preparation of dephosphorylation:

Restriction digest:	30 µl
Phosphatase buffer (10x):	7 µl
Antarctic phosphatase:	3 µl
	Add ddH_20 to a total volume of 70 µl

4.3.2.4 Polymerase chain reaction (PCR)

PCRs were used on one hand for the amplification of desired fragments and on the other hand to verify the correctness of transformants from *U. maydis* in a so called diagnostic PCR. To amplify DNA fragments, different linearized plasmids were used as templates. In the case of a diagnostic PCR, a colony was resuspended in 20 mM NaOH and incubated for 30 min at RT. 1 µl of this suspension was used for the PCR. For the amplification of DNA fragments, the PTC-200 Peltier Thermal Cyclerfrom MJ Research was used. In order to optimize the concentration and purity of the PCR fragments, different elongation times and annealing temperatures were used. The Phusion polymerase needs 15-30 s for the amplification of 1 kb. For the amplification of DNA fragments, the Phusion polymerase provided by NEB was used. Diagnostic PCRs were performed with a self-made Phusion.

Exemplary preparation of a PCR:

Template DNA:	0.5 µl (10-50 ng)
dNTPs:	0.5 µl (200 µM)
5x Phusion buffer:	10 µl
Oligonucleotide 1:	0.25 µl (0.5 µM)
Oligonucleotide 2:	0.25 µl (0.5 µM)
Phusion polymerase:	0.5 µl (1 U)
DMSO:	1.5 µl
	Add ddH_20 to a total volume of 50 µl

Exemplary PCR program:

98 °C	1 min	
98 °C	10 s	
55-70 °C	20 s	
72 °C	20-30 s	↑ x34 Cycles
72 °C	8 min	
4 °C	∞	

4.3.2.5 Detection und separation of nucleic acids

The analysis of DNA fragments was performed by agarose gel electrophoresis with varying agarose concentrations (0.8-2%). Agarose ordered by Biozym was dissolved in 1x tris-EDTA-acetate-buffer (TAE buffer) by boiling in a microwave. For the detection of DNA under UV light, 0.01% (w/v) ethidium bromide was added to the gel. A constant voltage of about 10 V per cm gel was applied. To estimate the size of the separated fragments a 1 kb DNA ladder from the company Fermentas was loaded simultaneously.

50x TAE buffer:	2 mM Tris-Base
	2 mM Acetic acid (>99.7 % Roth)
	10% (v/v) 0.5 M EDTA pH 8.0
	Fill with ddH_2O

4.3.2.6 Purification from an agarose gel

To purify DNA from an agarose gel, the fragments were visualized on a UV light table (TCP-20.LM, Vilber Lourmat Deutschland GmbH) after gel electrophoresis. The desired product was cut out from the gel and the JetQuick Gel Extraction Kit (Genomed) or the Monarch Kit (NEB) was used to isolate DNA. The isolation was conducted according to the manufacturer's instructions.

4.3.2.7 Ligation

To ligate different DNA fragments, the T4 DNA ligase (Roche) or the Quick ligase (NEB) and the related buffers from the companies were used. Different insert to backbone ratios were used (1:1, 1:3, 1:5). The ligation reactions were incubated for 4 h at RT or 12 h at 16 °C in case of the T4 and 15 min at RT for the quick ligase, respectively.

Exemplary preparation for a ligation:

Backbone-DNA:	n mol
Insert-DNA:	5x n mol
T4 DNA ligase-buffer (10x):	2 µl
T4 DNA ligase:	1 µl
	Add dd$H_2$0 to a total volume of 20 µl

4.3.2.8 Golden Gate Cloning

In addition to standard restriction and ligation steps, Golden Gate cloning was used to generate plasmids. Here, restriction and ligation takes place in one tube in so called One-pot reaction (Terfrüchte et al., 2014). For this, the restriction enzymes *Bsa*I (Engler et al., 2009) as well as *Sap*I and the T4 DNA ligase were used. In addition, storage vectors containing resistance cassettes for *U. maydis* and different destination vectors were mixed with the other components to make an integration of PCR fragments into a new vector possible.

Exemplary preparation for the One-pot reaction:

Storage vector DNA:	75 ng	
Destination vector DNA:	75 ng	
Insert DNA:	40 ng	
Ligase buffer (10x):	1.5 µl	
T4 DNA ligase:	0.75 µl	
Restriction enzyme *Bsa*I-HF/SapI:	0.5 µl	
	Add ddH_2O to a total volume of 15 µl	
PCR program GOGATE:	37 °C	2 min
	16 °C	5 min ↑ x50 Cycles
	37 °C	5 min
	50 °C	5 min

80 °C	5 min
16 °C	∞

4.3.2.9 Gibson Cloning

To generate plasmids in this study, also the Gibson cloning (Gibson et al., 2009) was used. With this, PCR products were inserted into a vector backbone by overlapping sequences. The vector backbone was either cut with restriction endonucleases or amplified via PCR. The inserts were amplified via PCR with oligonucleotides containing overlapping sequences of 25 nt to the vector backbone. The PCR products were gel purified before their addition to the reaction. The PCR products and the vector backbone were added to 15 µl of an assembly mix. A total of 0.02–0.5 pmols of PCR products was used. The whole mixture was incubated for 60 min at 50 °C. 10 µl of the assembly mix were transformed in chemically competent *E. coli* cells.

5x isothermal reaction buffer (6 ml):	3 ml of 1 M Tris-HCl pH 7.5
	150 µl of 2 M MgCl2
	60 µl of 100 mM dGTP
	60 µl of 100 mM dATP
	60 µl of 100 mM dTTP
	60 µl of 100 mM dCTP
	300 µl of 1 M DTT
	1.5 g PEG-8000
	300 µl of 100 mM NAD
Assembly master mix:	320 µl 5x isothermal reaction buffer
	6.4 µl of 1 U T5 Exonuclease
	20 µl of 2 U Phusion DNA polymerase
	160 µl of 40 U Taq DNA ligase
	Add ddH_2O to a total volume of 1.2 µl
	Aliquots à 15 µl and store at -20 °C

4.3.3 Sequencing

4.3.3.1 Sequencing at Genomics Service Unit (Ludwig Maximilians University Munich)

To verify the correctness of the generated plasmids, they were sent for sequencing. For this purpose, 250 ng of purified plasmid DNA and 3.2 pmol oligonucleotide were mixed with 10 mM Tris/HCl, pH 8.5, to a final volume of 7 µl. The sequencing was

performed by the LMU service in Munich. The subsequent analysis of the raw data was performed using Clone Manager 9 software.

4.3.3.2 Overnight sequencing at Eurofins Genomics (Ebersberg)

For urgent sequencing purposes, 15 µl of 50-100 ng/µl of purified plasmid DNA were mixed with 2 µl of 1 µM respective sequencing oligonucleotide. The subsequent analysis of the raw data was performed using Clone Manager 9 software.

4.3.4 Southern Blot verification

To confirm positive transformants which were identified via a diagnostic PCR, a Southern blot with a modified protocol of (Southern, 1975) was performed. This allows direct visualization of the integrated constructs and makes it possible to verify the correct integration by homologous recombination.

4.3.4.1 Capillary blotting

First, the genomic DNA was digested with restriction enzymes and separated on an agarose gel. The gel was washed firstly with 0.25 M HCl, secondly with DENAT, and finally with RENAT solution. With the help of capillary blotting, the DNA was then transferred to a nylon membrane (Hybond-N+ nylon membrane, GE-Healthcare). For this, a Whatman paper was dampened with 20xSSC solution and placed across a glass with both ends in contact with the buffer. The gel was placed upside-down on the Whatman paper and the membrane was placed on top of the gel. Two additional Whatman papers, which were the size of the gel, were placed on top of the membrane. Finally a small stack of paper towels as well as a weight were placed on top to increase the undertow. After 4 h the whole DNA was transferred to the membrane.

0.25M HCl:	3.26% (v/v) HCl (25%) Add ddH_2O
DENAT solution:	1.5 M NaCl 0.4 M NaOH Add ddH_2O
RENAT solution:	1.5 M NaCl 282 mM Tris-HCl 218 mM Tris Base Add ddH_2O

SSC buffer (20x):	3 M NaCl
	3 M $Na_3C_6H_5O_7$* 2 H_2O
	Add ddH_2O
	Adjust pH with NaOH to 7.4

4.3.4.2 Detection of immobilized DNA via DIG-labeling

To secure the DNA onto the membrane a UV-crosslinking at 120 mJ was used. The membrane was prehybridized with hybridization buffer for 30 min at 65 °C, and then hybridized with boiled probes (5 min at 95 °C) over night at 65 °C. Hybridization was performed using probes which were generated with digoxigenin (DIG)-labeled dNTPs via PCR on plasmid DNA. The probes could bind to the complementary DNA strand and could be detected due to the DIG-labeling using DIG antibodies. After hybridization, three washing steps were conducted using Southern wash buffer I, II and III at 65 °C. Further incubation and washing steps took place at RT. First the membrane was washed with DIG wash buffer for 5 min, followed by 30 min incubation in DIG-2 blocking solution. Subsequently, the membrane was incubated in α-DIG antibody (Roche; 1:10000 dilution in DIG-2) for at least 1 h. To get rid of unbound antibody, the membrane was washed with DIG wash buffer twice. Before adding CDP-Star (Roche; 1:100 dilution in DIG-3), the membrane was equilibrated in DIG-3 for 5 min. According to a 5 min incubation step with CDP-Star, chemiluminescence was detected with the imaging system LAS4000 (Fujifilm).

Southern hybridization buffer:	26% (v/v) SSPE (20x)
	5% (v/v) Denhardt solution
	5% (v/v) SDS (10%)
	Add ddH_2O
Southern wash buffer I:	10% (v/v) SSPE (20x)
	1% (v/v) SDS (10%)
	Add ddH_2O
Southern wash buffer II:	5% (v/v) SSPE (20x)
	1% (v/V) SDS (10%)
	Add ddH_2O
Southern wash buffer III:	0.5% (v/v) SSPE (20x)
	1% (v/v) SDS (10%)
	Add ddH_2O

DIG-1:	0.1 M Maleic acid 0.15 M NaCl
DIG-2:	90% (v/v) DIG-1 10% (w/v) milk powder
DIG-3:	0.1 M Tris-HCl 0.1 M NaCl Adjust pH with NaOH to 9.5
DIG wash buffer:	0.3% (v/v) Tween-20 99.7% (v/v) DIG-1
SSPE buffer (20x):	3 M NaCl 200 mM Na_2-HPO_4 20 mM Na_2-EDTA Adjust pH to 7.4
Denhardt solution:	2% (w/v) BSA fraction V 2% (w/v) Ficoll 2% (w/v) PVP (Polyvinyl Pyrrolidone)

4.4 Protein biochemistry

4.4.1 Disruption *of U. maydis* cells

To isolate total protein extracts from *U. maydis* cells, first a culture of 50 ml CM was grown up to an OD_{600} of 0.8. If protein extracts of filaments were needed, this culture was then shifted to nitrate minimal medium (NM) containing a carbon source to an OD_{600} of 0.5 and incubated for at least 6 h at 28 °C. The cultures were centrifuged for 5 min at 3000 rpm and subsequently resuspended in 1-2 ml lysis buffer (either lysis buffer, urea buffer or native lysis buffer), to which protease inhibitors were freshly added. Then glass beads were added to the resuspended cells. The cells were disrupted in 1.5 ml Eppendorf tubes with the help of the Mixer Mill MM400 (Retsch) and were agitated for 10 min at 30 Hz. For filaments, the cells were agitated three times with cooling steps in between. After disrupting the cells, the tubes were centrifuged for 3 min at 13,000 rpm and 4 °C. The supernatant was decanted into a fresh tube and another centrifugation step for 30 min at 13,000 rpm and 4 °C were performed. The resulting supernatant was decanted in a fresh tube and the protein extract was stored at -80 °C.

Lysis buffer:	50 mM Tris-HCl pH 7.4 (stored at 4 °C) 150 mM NaCl 0.5 M EDTA pH 8 0.5% Nonidet P-40 Fill with dH_2O
Urea buffer:	9.61 g Urea 1 ml Tris-HCl, pH 8.0 Add 20 ml ddH_2O Protease inhibitors added freshly: 1 mM DTT 1 mM PMSF 2.5 mM Benzamidine 1x cOmplete™ Protease Inhibitor Cocktail (Roche)
Lysis buffer (native):	50 ml 1xPBS 1 mM PMSF 2.5 mM Benzamidine 1x cOmplete™ Protease Inhibitor Cocktail (Roche)

4.4.2 Determination of protein concentration

The Bradford assay (Bradford, 1976) was used to determine the total protein concentration. First the sample was diluted 1:10 in H_2O. Different concentrations of BSA as a standard were used to create a calibration curve for calculation of the protein concentration of the protein extracts. 10 µl of each standard and protein sample were mixed with 200 µl diluted (1:5 in H_2O) Bradford reagent (Bio-Rad). The mixture was incubated for 5 min at RT. During incubation a color reaction occurs. The staining increases with higher protein concentrations. It was measured with the Safire Microplate Reader (Tecan) at 595 nm. For the calculation of the sample concentrations, their absorbance was plugged into the equation of the calibration curve.

4.4.3 Sodium dodecyl sulfate polyacrylamide gel electrophoresis (SDS-PAGE)

Sodium dodecyl sulfate polyacrylamide gel electrophoresis (SDS-PAGE) (Laemmli, 1970) is a method to determine the molecular weight of proteins by separating them in an electric field. In contrast to an agarose gel electrophoresis where the negative charge of the DNA's phosphate backbone leads to the migration to the anode, proteins are treated with sodium dodecyl sulfate (SDS), an anionic and amphipathic detergent masking their intrinsic charge. In addition, SDS denatures the protein structure. 10 µg of the protein sample were supplied with 15 µl 1x loading buffer. The mixture was incubated for 7 min at 95 °C and afterwards centrifuged with 13,000 rpm for 2 min. The gel was loaded with 15-25 µl of the prepared protein sample (5-10 µg). 8 µl of the PageRuler™ Prestained Protein Ladder (Thermo Fisher) was loaded on each gel to estimate the molecular weight of the proteins. Separation was carried out in 1x Tris glycine running buffer with constant amperage of 40 mA per gel. After the electrophoresis run, the SDS-PAGE gel was incubated in Coomassie brilliant blue (CBB) staining solution to visualize protein bands (4.4.4). For the specific detection of proteins, the SDS gel was subjected to Western blot analysis (4.4.5-4.4.6).

Loading buffer:	6% (v/v) SDS
	15% (w/v) β-Mercaptoethanol
	50 mM Tris-HCl pH 6.8
	30% (v/v) Glycerol
	0.003% (w/v) Bromophenol blue
10x Tris-glycine running buffer:	25mM Tris pH 8.4
	192 mM Glycine
	0.1% (v/v) SDS

Table 4.12: Compounds of the separating and stacking gel

Compounds	Separating gel	Stacking gel
Acrylamide (30:0.8)	7.5-15%	5%
Tris-HCl pH 8.8	0.375 M	-
Tris-HCl pH 6.8	-	0.125 M
SDS	0.1%	0.1%
APS	0.05%	0.05%
TEMED	0.1%	0.1%
Glycerol	1.25%	-

4.4.4 Protein staining using Coomassie brilliant blue

To visualize the proteins separated by SDS-PAGE, the SDS gel or a western blot membrane were stained with Coomassie brilliant blue by incubating them for 15 min in the staining solution. Gels and membranes were de-stained using a de-stainer solution and an additional incubation step for 30 min. De-staining was repeated 2-3 times.

Coomassie staining solution:	0.05% (w/v) Coomassie brilliant blue R250 45% (v/v) Methanol 9% (v/v) Glacial acetic acid
Coomassie de-staining solution:	10% (v/v) Glacial acetic acid 10% (v/v) Methanol 80% dH_2O

4.4.5 Western blotting

To specifically detect different proteins, the separated proteins were transferred and immobilized on a PVDF membrane by semi-dry blotting. Two Whatman papers were soaked in anode I, one in anode II and three in cathode buffer, respectively. The PVDF membrane was incubated in absolute methanol for 1 min before equilibration in anode buffer I. To setup the blot, two Whatman papers, soaked with anode buffer I, followed by one Whatman paper soaked with anode buffer II are prepared. The membrane was placed on the last Whatman paper soaked with anode buffer II, followed by the SDS-gel and the three Whatman papers, soaked with cathode buffer. The transfer was carried out at constant amperage of 80 mA per gel for 1 h.

Cathode buffer:	25 mM Tris-HCl pH 9.4 40 mM ε-Aminocaprone acid 15% (v/v) Methanol Fill with ddH_2O
Anode buffer I:	300 mM Tris-HCl pH 10.4 15% (v/v) Methanol Fill with dH_2O
Anode buffer II:	30 mM Tris-HCl pH 10.4 15% (v/v) Methanol Fill with ddH_2O

4.4.6 Western blot detection

To detect the expressed proteins, specific antibodies were used. For the preparation of the Western blot detection a blocking solution was added to the membrane to block unspecific binding sites. It was incubated for 1 h. The primary antibody solution was added for an additional incubation of 1 h at room temperature or at 4 °C overnight (Table 4.13). After incubation, the antibody solution was removed. The membrane was washed three times for 10 min with 1x Tris-buffered saline with Tween20 (TBS-T). Afterwards the membrane was incubated in the secondary antibody solution for 1 h at room temperature (Table 4.14) and subsequently washed three times with TBS-T for 10 min. For the detection reaction, 500 µl HRP Substrate Peroxide Solution and 500 µl HRP Substrate Luminol Reagent (Millipore, Darmstadt, Germany) were mixed and spread over the membrane. The measurement was taken according to the manual's instructions at a luminescence image analyzer, LAS4000 (GE Healthcare, Solingen, Germany).

10x TBS buffer:	0.1% (w/v) Tris Base 0.6% (w/v) Tris-HCl 0.9% (w/v) NaCl Fill with dH_2O
1x TBS-T buffer:	10% (v/v) 10x TBS buffer 0.05% (v/v) Tween20 Fill with dH_2O
Blocking buffer:	3% (w/v) milk powder Dissolve in TBS buffer
Antibody solution:	3% (w/v) milk powder Dissolve in TBS buffer Primary antibody: see Tab.11.4. Secondary antibody: see Tab.12.4

Table 4.13: Used primary antibodies and dilutions

Antibody	Origin	Company	Dilution
α-Gfp (monoclonal)	Mouse	Roche	1:1000
α-HA (monoclonal)	Mouse	Roche	1:4000
α-Gfp (polyclonal)	Rabbit	Chromotek	1:1000

Table 4.14: Used secondary antibodies and dilutions

Antibody	Origin	Company	Dilution
α-Mouse IgG, HRP conjugate	Horse	Promega	1:10.000
α-rabbit IgG, HRP conjugate	Goose	NEB	1:10.000

4.4.1 Far-Western blot analysis for analyzing interaction of GCN4-scFV-sfGFP to proteins

To analyze the binding of GCN4-scFv fused to sfGfp, the scFv was natively isolated from *U. maydis* cells. 10 µg of total cell extract of different test strains were run on an SDS-PAGE followed by blotting on a PVDF membrane. The membrane was blocked as described before. To detect possible interactions of GCN4-scFv-sfGfp to proteins from *U. maydis*, the native purified cell extract from the strain expressing the scFv was used as primary antibody. As a control, cell extracts from a strain only expressing sfGfp was used. For this, the membranes were incubated overnight at 4 °C with the cell extracts mixed with blocking solution. On the next day, the membranes were washed three times with TBS-T buffer and α-Gfp antibody originally deriving from mouse (Table 4.13) was used as secondary antibody. This was again incubated overnight at 4 °C. Afterwards, the standard Western blot detection protocol was followed.

4.5 Microscopy and image processing

4.5.1 Microscopy setup

Microscopy was performed as described in (Baumann et al., 2012). The wide-field microscopes 1) Zeiss (Oberkochen Germany) Axio Observer.Z1 provided with CoolSNAP HQ2 CCD (Photometrics, Tuscon, AZ, USA), Orca Flash4.0 camera (Hamamatsu, Japan) and objective lenses Plan Neofluar (40x, NA 1.3), Plan Apochromat (63x, NA 1.4), Plan-Neofluar (100x, NA 1.3) and α-Plan Apochromat (100x, NA 1.46) and 2) Zeiss Axio Imager.M1 provided with a Spot Pursuit CCD camera (Diagnostic Instruments, Sterling Heights, MI, USA) and objective lenses Plan Neofluar (40x and 100x, NA 1.3; 63x, NA 1.25) were used. Excitation of fluorescently-labeled proteins was carried out using an HXP metal halide lamp (LEj, Jena, Germany) in combination with filter sets for Gfp (ET470/40BP, ET495LP, ET525/50BP), for Rfp/mCherry (ET560/40BP, ET585LP, ET630/75BP) and for DAPI (AT350/50BP, ET400LP, ET460/50BP; Chroma, Bellow Falls, VT, USA). For detection of weak signals, a laser-based epifluorescence-microscopy was used. A VS-LMS4 Laser Merge-System (Visitron Systems) combines solid state lasers for the excitation of Gfp (488 nm/100 mW) and Rfp/mCherry (561 nm/150 mW). All parts of the microscope systems were controlled by the software package MetaMorph (Molecular Devices,

version 7) or VisiView (Visitron). This was also used for image processing including the modification of brightness and contrast as well as measurements, quantifications, kymographs and maximum projections of z-stacks.

4.5.2 RNA live imaging

RNA live imaging was performed as described in (Zander et al., 2018). Cells expressing different systems for RNA live imaging were analyzed with regards to mRNA movement through hyphae of *U. maydis*. For excitation of Gfp, the laser line was set to 20% and for mCherry to 30%, respectively. Hyphae were observed with the 63x Plan-Apochromat in combination with a Spot Pursuit CCD or an Orca Flash4.0 camera. Each movie was recorded with 150 ms/frame and contained 150 frames. For quantification of moving mRNAs, kymographs were generated to study the number, velocity and distance of particles (only distances > 5 µm were scored). To determine the average number of particles per 100 µm of hypha, the total length of hyphae was measured, divided by the number of particles and calculated to 100 µm.

4.5.3 Co-localization studies

To analyze co-localization events, a VS-LMS4 Laser Merge-System (Visitron Systems) was used in combination with the CoolSNAP HQ2 CCD camera. A dichroic beam splitter (dcxr565) is combined with an excitation filter for Gfp and Rfp and a special emission filter (Gfp ET520/40; Rfp ET632/60). For the simultaneous detection of two fluorescent proteins, a two-channel imager was used. The imager splits green and red emission lights and detects them on separate regions of the CCD camera chip.

4.5.4 Analysis of phenotypes, subcellular localizations and moving particles

To analyze subcellular localizations, phenotypes and moving particles, a minimum of 30 cells from three independent experiments were analyzed per strain. Hyphae were observed with the 63x Plan-Apochromat in combination with a Spot Pursuit CCD or an Orca Flash4.0 camera. Each movie was recorded with 150 ms/frame and contained 150 frames. For quantification of moving mRNAs, kymographs were generated to study the number, velocity and distance of particles (only distances > 5 µm were scored). To determine the average number of particles per 100 µm of hypha, the total length of hyphae was measured, divided by the number of particles and calculated to 100 µm.

4.5.5 FRET-APB measurements

To measure the efficiency of the cleavage within the 2A peptides, fluorescence resonance energy transfer after acceptor photobleaching (FRET-APB) was performed.

This is a tool to detect molecular interactions between proteins, which was measured in the present work in between Gfp and mKate2. The FRET-APB was quantified by measuring the intensity increase of the donor fluorophore after bleaching of the acceptor according to the following formula:

$$FRET\ efficiency\ E = \frac{Intensity_{Donor\ after} - Intensity_{Donor\ before}}{Intensity_{Donor\ after}} * 100$$

The formula does not include any corrections for background fluorescence or effects like fluorescence recovery of the donor fluorophore during bleaching time of the acceptor. Therefore a control strain harboring only Gfp was included in each set of experiment. In total three independent experiments with 10 cells each were conducted. FRET-APB was measured using a Zeiss LSM780 laser-scanning microscope and a C-Apochromat 40x/1,20 korr M27 water objective (Carl Zeiss, Jena). GFP was excited with a 488 nm argon laser with a power of 0.3% and emission detection using a filter at 490 to 552 nm. mKate2 was excited using a 561 nm diode laser with a power of 5% and emission detection using filter at 588 to 686 nm. In total, 20 frames (256 x 256 pixels) at a pixel time of 3.15 µs/pixel were measured with no line averaging. After the 5th frame, the nucleus and the surrounding area was bleached at 100% laser power of the 561 nm laser, for 50-100 iterations. After the bleaching, 15 more frames were recorded.

4.5.6 Cell Tracker™ Blue (CMAC) staining

For the visualization of vacuoles in hyphae, cells were incubated with Cell Tracker™ Blue (CMAC, Invitrogen). CMAC is a fluorescent chloromethyl derivative (7-amino-4-chloromethylcoumarin) that freely diffuses through the membranes of living cells. Once inside the cell, it is converted into a membrane-impermeant dye which accumulates in vacuoles due to the fact that 7-amino-4-methylcoumarin derivatives are known to be substrates for vacuolar enzymes (Molecular probes handbook (www.probes.com), chapter 12, page 521). For staining, 500 µl of hyphae suspension were labeled with 13 µM CMAC. After 30–60 s of incubation at RT, samples were microscopically analyzed.

4.5.7 FM4-64 staining

For the visualization of endocytic components in hyphae, cells were incubated with the lipophilic dye FM4-64 (Invitrogen). The styryl dye FM4-64 visualizes vacuolar organelle morphology and dynamics as well as endocytic pathway components like early and late endosomes and multivesicular bodies. For staining, 1 ml of hyphae suspension was

incubated with 0.8 µM FM4-64. After 30–60 s of incubation at room temperature, samples were microscopically analyzed (Baumann et al., 2012).

4.5.8 Benomyl treatment

To inhibit the tubulin polymerization and analyze the impact of defective microtubules on moving particles in hyphae, they were incubated with benomyl (Sigma Aldrich). Benomyl is a benzimidazole fungicide which binds to microtubules. To inhibit polymerization, cells were incubated with 50 µM of benomyl for 1 h at 28 °C and 200 rpm (Becht et al., 2006).

4.6 Mass spectrometry analysis

4.6.1 Immunoprecipitation

To enrich proteins which potentially interact with expressed antibodies in *U. maydis* an immunoprecipitation (IP) was performed (Bonifacino et al., 2016). The antibodies of interest were fused to sfGfp. The usage of magnetic agarose beads coated with α-Gfp antibodies (Chromotek) enables the specific purification of proteins which interact with the expressed antibodies. For the IP, cell extracts from 50 ml of hyphal culture were generated as described in section 4.4.1. 30 µl of the magnetic agarose beads were pre-washed with wash buffer and subsequently added to the cell extracts. The mixture was incubated for 1 h at 4 °C and the beads were collected using a magnetic rack beads separator afterwards. The supernatant was discarded and the beads on which the proteins bound were washed three times with the wash buffer. Each time the beads were collected using the separator. To remove the proteins from the beads 50 µl loading buffer, which is described in section 4.4.3, were added and the mixture was incubated for 6 min at 95 °C. Last, the beads were separated from the mixture using the separator and the supernatant was handed over for mass spectrometry analysis.

4.6.2 Mass spectrometry sample preparation

Liquid chromatography and mass spectrometric analysis were performed in collaboration with the Molecular Proteomics Laboratory (BMFZ, Heinrich-Heine-University Düsseldorf, Dr. Gereon Poschmann and Prof. Dr. Kai Stühler). Eluted protein samples were processed for mass spectrometric analysis by in-gel digestion essentially as described (Grube et al., 2018). Briefly, samples were separated (~5 mm running distance) in Bis-Tris buffered 4-12% acrylamide gels (Thermo Fisher). After silver staining and de-staining of the gel, protein containing lanes were washed 3 times alternating with 10 mM ammonium hydrogen carbonate and a 1:1 (v/v) solution of 10 mM ammonium hydrogen carbonate and acetonitrile. Proteins were reduced by

adding 50 µl of an aqueous solution of 10 mM DTT and 50 mM ammonium hydrogen carbonate on dried gel pieces and incubation at 56 °C for 45 min. Afterwards, proteins were alkylated by adding 50 µl of an aqueous solution of 55 mM iodoacetamide and 50 mM ammonium hydrogen carbonate and 30 min incubation at RT. The gel pieces were washed as indicated above, dried and digested with 0.1 µg trypsin in 50 mM ammonium hydrogen carbonate overnight at 37 °C. Peptides were extracted from the gel by adding two times 40 µl of 1:1 (v/v) acetonitrile and 0.1% trifluoroacetic acid (in water) followed by 15 min incubation in an ultrasonic bath. Peptides were dried and finally resuspended in 17 µl of 0.1% trifluoroacetic acid.

4.6.3 Mass spectrometry run

Next, peptide samples were separated on an Ultimate 3000 rapid separation liquid chromatography system (RSLS, Thermo Fisher). First, peptides were trapped on a trapping column (Acclaim PepMap100, 3 µm C18 particle size, pore size 100 Å, inner diameter 75 µm, 2 cm length, Thermo Fisher) using 0.1% (v/v) trifluoroacetic acid (in water) as mobile phase. After 10 min, peptides were separated at 60 °C on an analytical column (Acclaim PepMapRSLC, 2 µm C18 particle size, 100 Å pore size, 75 µm inner diameter, 25 cm length, Thermo Fisher) for 1 h (gradient from 4 to 40% solvent (0.1% (v/v) formic acid, 84% (v/v) acetonitrile in water). Separated peptides were directly analyzed by an online coupled QExactive plus quadrupole/orbitrap mass spectrometer (Thermo Fisher). Peptides were sprayed into the mass spectrometer via an online coupled nano source equipped with distally coated emitters (New Objective) at a spray voltage of 1.4 kV. The mass spectrometer was operated in data dependent positive mode: First survey scans were carried out in the obitrap and subsequently, precursors were isolated by the build in quadrupole and fragmented via higher-energy collisional dissociation. Fragment spectra were recorded at a resolution of 17500.

4.6.4 Mass spectrometry data anaylsis

Raw data was further processed using the MaxQuant (version 1.6.0.16) software environment with standard parameters. Searches were carried out with tryptic cleavage specificity considering two potential missed cleavage sites, carbamidomethyl at cysteines and methionine oxidation as well as protein N-terminal acetylation as variable modification. Sequences used as search-basis were p3_t237631_Ust_maydi_v2GB_MkT_v1.fasta UMa2278 protein.fasta UMa2684 protein.fasta. The ‘match between runs’ option was enabled as well as the label-free quantification. Only proteins identified with at least two peptides were reported and

proteins showing valid LFQ-intensity values in three replicates of at least one group used for further calculations.

4.7 Computer programs and bioinformatics

4.7.1 Nucleic and amino acid analysis

Clone manager 9 (Sci Ed Central Software)
PEDANT (http://pedant.helmholtz-muenchen.de/)
Ensemble Fungi (https://fungi.ensembl.org/index.html)
Blastn /Blastp (http://blast.ncbi.nlm.nih.gov/Blast.cgi)
ClustalX/ClustalW (http://www.clustal.org/)
GeneDoc 2.6 (https://genedoc.software.informer.com/2.6/)
SMART Database (http://smart.embl-heidelberg.de/)
NCBI CDD (https://www.ncbi.nlm.nih.gov/Structure/cdd/wrpsb.cgi)
PDB (https://www.rcsb.org/search/advanced/sequence)
Coot (https://www2.mrc-lmb.cam.ac.uk/personal/pemsley/coot/)
Pymol (https://pymol.org/2/)
Uniprot (https://www.uniprot.org/)

4.7.2 Operation of special devices

i-control™ Microplate Reader Software (Tecan Trading AG)
ImageQuant LAS4000 Control Software (GE Healthcare)
Metamorph 7 (Molecular Devices)
VisiView (Visitron)

4.7.3 Data analysis, writing and graphics

Microsoft Office 2010 (Microsoft Corporation)
Canvas 12 (ACDSee Systems)
GraphPad Prism 5 (GraphPad Software Inc.)

5 Appendix

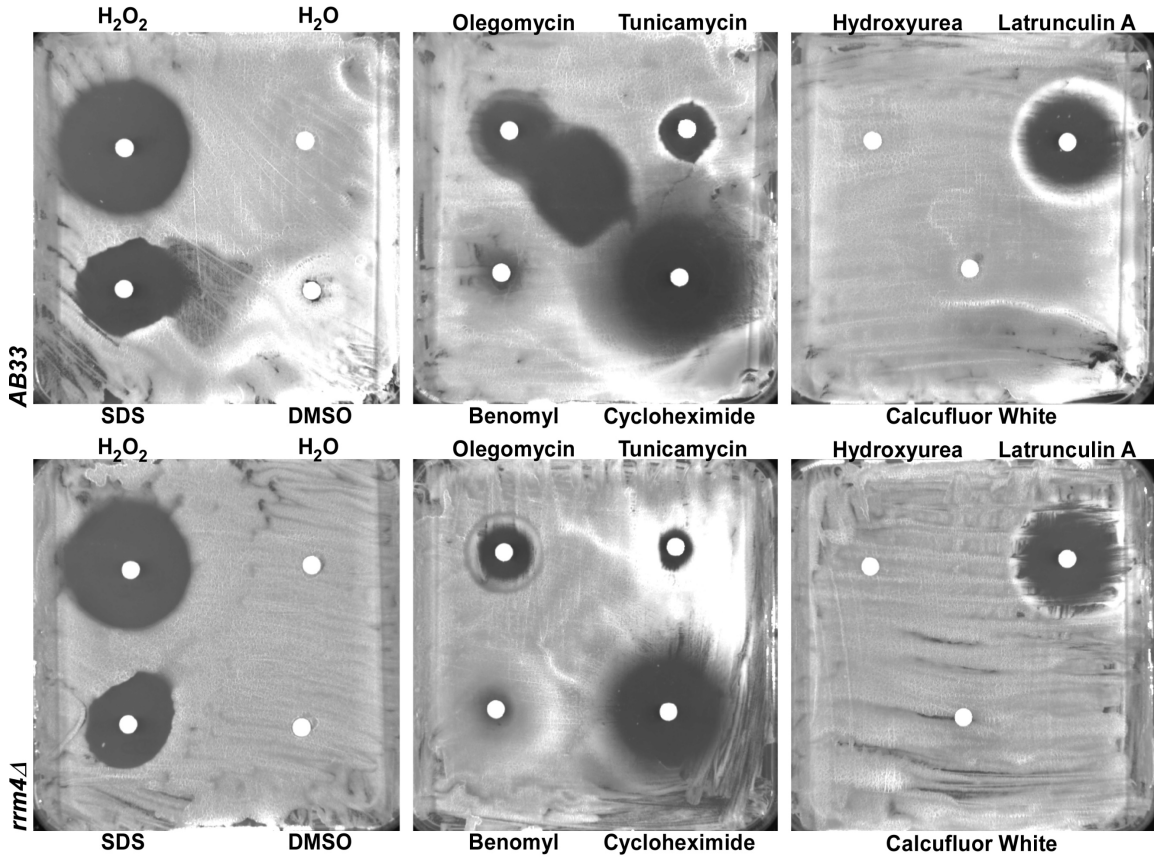

Figure 6.1: Halo test of AB33 and *rrm4*Δ strains as control to test the influence of UMAG_00933 in stress response. Sporidial cells were plated on CM-plates containing glucose. For agar diffusion test, filter paper was cut and soaked with different stress inducing reagents. Halo formation was analyzed after 48 h of incubation.

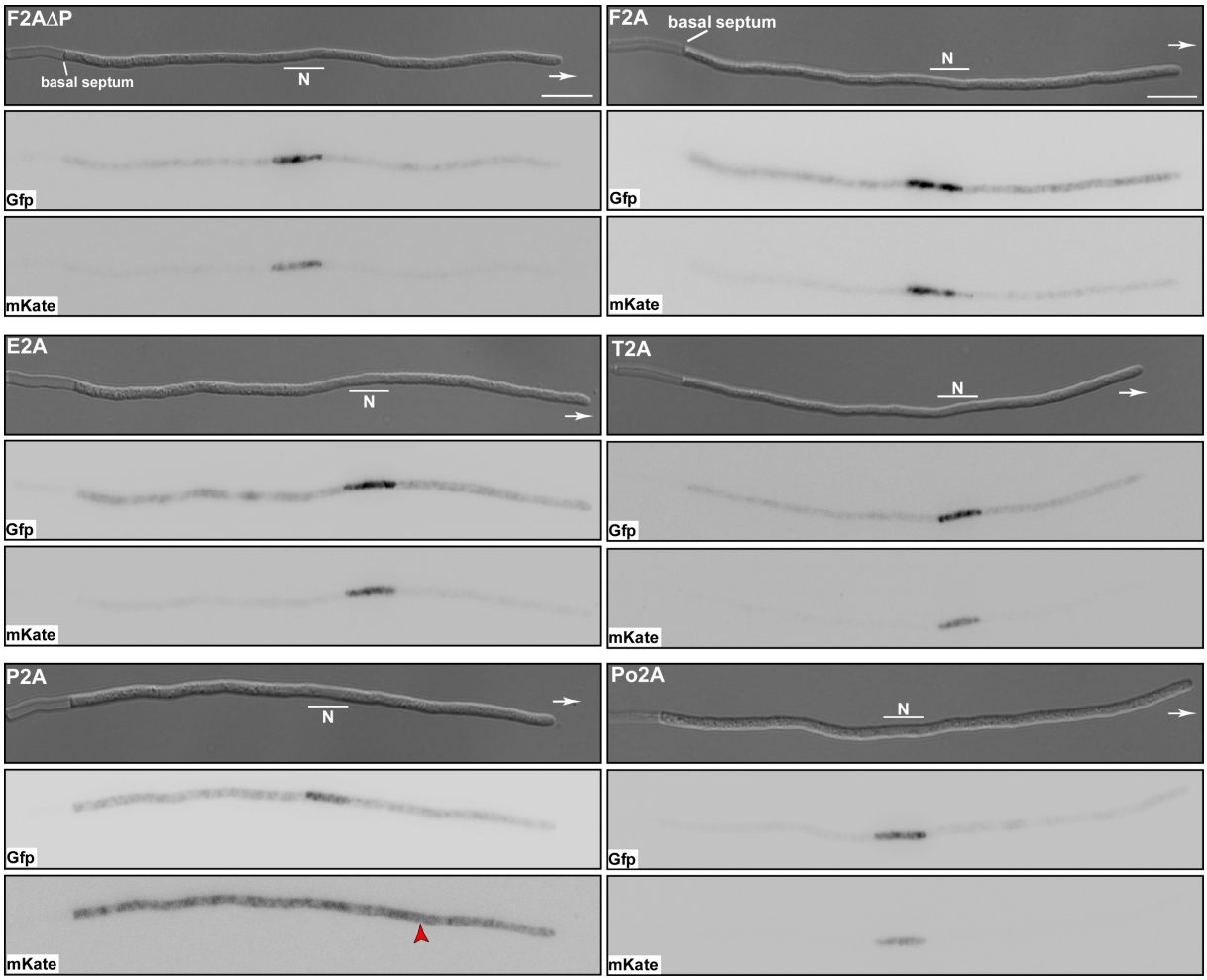

Figure 6.2: Separation efficiencies of F2AΔP, F2A, E2A, T2A, P2A and Po2A peptides analyzed in hyphae of *U. maydis*. Morphology and fluorescence microscopy of hyphal cells expressing reporter constructs for analysis of 2A peptide separation efficiency (inverted picture; N, nucleus; scale bar 10 µm; for hyphal cells: 6 h.p.i.; growth direction is indicated by arrow).

6 Authors contribution

Parts of this dissertation were submitted for publication to the Frontier in Microbiology journal, section Fungi and Their Interactions (Müntjes K., Philipp M., Hüsemann L., Heucken N., Weidtkamp-Peters S., Schipper K., Zurbriggen M.D. and Feldbrügge M., Establishing polycistronic expression in the model microorganism *Ustilago maydis* (DOI: 10.3389/fmicb.2020.01384).

Kira Müntjes, Magnus Phillip, Lisa Hüsemann, Nicole Heucken, Kerstin Schipper, Matias D. Zurbriggen and Michael Feldbrügge designed and planned the study. Lisa Hüsemann and Nicole Heucken designed and cloned pre-vectors, which were needed for the establishment of 2A peptides. Kira Müntjes generated the plasmids and strains and performed the Western blot analysis as well as the fluorescence microscopy which were needed for the establishment of the 2A peptides (section 2.3.3 and 2.3.4). Kira Müntjes and Stefanie Weidtkamp-Peters performed the FRET analysis (section 2.3.4). Kira Müntjes performed the analysis of the promoter induction (section 2.3.5). Magnus Phillip generated the plasmids and strains and performed Western blot analysis as well as thin layer chromatography to optimize the production of the MELs. Kira Müntjes, Kerstin Schipper and Michael Feldbrügge analysed the data. Kira Müntjes, Kerstin Schipper, Matias D. Zurbriggen and Michael Feldbrügge designed and revised the manuscript.

List of modified or directly used figures derived from the publication:

This Thesis	**Publication**
Figure 2.2 A	Figure 1 C
Figure 2.19 B	Figure 1 A
Figure 2.21	Figure 1 D
Figure 2.22	Figure 2
Figure 2.23	Figure 3 A and C
Figure 2.24	Figure 4 A - D
Figure 2.25	Figure 4 E and F
Figure 6.2	Figure 3 B and Figure S1

7 References

Ahmad ZA, Yeap SK, Ali AM, Ho WY, Alitheen NB, Hamid M. 2012. scFv antibody: principles and clinical application. Clin Dev Immunol 2012:980250.

Aichinger C, Hansson K, Eichhorn H, Lessing F, Mannhaupt G, Mewes W, Kahmann R. 2003. Identification of plant-regulated genes in Ustilago maydis by enhancer-trapping mutagenesis. Mol Genet Genomics 270:303-314.

Akerström B, Bjorck L. 1986. A physicochemical study of protein G, a molecule with unique immunoglobulin G-binding properties. J Biol Chem 261:10240-10247.

Albrecht G, Mosch HU, Hoffmann B, Reusser U, Braus GH. 1998. Monitoring the Gcn4 protein-mediated response in the yeast Saccharomyces cerevisiae. J Biol Chem 273:12696-12702.

Amm I, Sommer T, Wolf DH. 2014. Protein quality control and elimination of protein waste: the role of the ubiquitin-proteasome system. Biochim Biophys Acta 1843:182-196.

Andreassi C, Riccio A. 2009. To localize or not to localize: mRNA fate is in 3'UTR ends. Trends Cell Biol 19:465-474.

Atkins JF, Wills NM, Loughran G, Wu CY, Parsawar K, Ryan MD, Wang CH, Nelson CC. 2007. A case for "StopGo": reprogramming translation to augment codon meaning of GGN by promoting unconventional termination (Stop) after addition of glycine and then allowing continued translation (Go). RNA 13:803-810.

Austin RJ, Xia T, Ren J, Takahashi TT, Roberts RW. 2002. Designed arginine-rich RNA-binding peptides with picomolar affinity. J Am Chem Soc 124:10966-10967.

Aviner R, Geiger T, Elroy-Stein O. 2013. PUNCH-P for global translatome profiling: Methodology, insights and comparison to other techniques. Translation (Austin) 1:e27516.

Bailey-Elkin BA, Knaap RCM, Kikkert M, Mark BL. 2017. Structure and Function of Viral Deubiquitinating Enzymes. J Mol Biol 429:3441-3470.

Balch WE, Morimoto RI, Dillin A, Kelly JW. 2008. Adapting proteostasis for disease intervention. Science 319:916-919.

Banaszynski LA, Chen LC, Maynard-Smith LA, Ooi AG, Wandless TJ. 2006. A rapid, reversible, and tunable method to regulate protein function in living cells using synthetic small molecules. Cell 126:995-1004.

Banks GR, Shelton PA, Kanuga N, Holden DW, Spanos A. 1993. The Ustilago maydis nar1 gene encoding nitrate reductase activity: sequence and transcriptional regulation. Gene 131:69-78.

Bauer KE, Segura I, Gaspar I, Scheuss V, Illig C, Ammer G, Hutten S, Basyuk E, Fernandez-Moya SM, Ehses J, Bertrand E, Kiebler MA. 2019. Live cell imaging reveals 3'-UTR dependent mRNA sorting to synapses. Nat Commun 10:3178.

Baumann S, Komissarov A, Gili M, Ruprecht V, Wieser S, Maurer SP. 2020. A reconstituted mammalian APC-kinesin complex selectively transports defined packages of axonal mRNAs. Sci Adv 6:eaaz1588.

Baumann S, Konig J, Koepke J, Feldbrugge M. 2014. Endosomal transport of septin mRNA and protein indicates local translation on endosomes and is required for correct septin filamentation. EMBO Rep 15:94-102.

Baumann S, Pohlmann T, Jungbluth M, Brachmann A, Feldbrugge M. 2012. Kinesin-3 and dynein mediate microtubule-dependent co-transport of mRNPs and endosomes. J Cell Sci 125:2740-2752.

Becalska AN, Gavis ER. 2009. Lighting up mRNA localization in Drosophila oogenesis. Development 136:2493-2503.

Becht P, Konig J, Feldbrugge M. 2006. The RNA-binding protein Rrm4 is essential for polarity in Ustilago maydis and shuttles along microtubules. J Cell Sci 119:4964-4973.

Becht P, Vollmeister E, Feldbrugge M. 2005. Role for RNA-binding proteins implicated in pathogenic development of Ustilago maydis. Eukaryot Cell 4:121-133.

Beekwilder J, van Rossum HM, Koopman F, Sonntag F, Buchhaupt M, Schrader J, Hall RD, Bosch D, Pronk JT, van Maris AJ, Daran JM. 2014. Polycistronic expression of a beta-carotene biosynthetic pathway in Saccharomyces cerevisiae coupled to beta-ionone production. J Biotechnol 192 Pt B:383-392.

Bertrand E, Chartrand P, Schaefer M, Shenoy SM, Singer RH, Long RM. 1998. Localization of ASH1 mRNA particles in living yeast. Mol Cell 2:437-445.

Besse F, Ephrussi A. 2008. Translational control of localized mRNAs: restricting protein synthesis in space and time. Nat Rev Mol Cell Biol 9:971-980.

Bethune J, Jansen RP, Feldbrugge M, Zarnack K. 2019. Membrane-Associated RNA-Binding Proteins Orchestrate Organelle-Coupled Translation. Trends Cell Biol 29:178-188.

Bevan MWF, R.B.; Chilton, M. D. . 1983. A chimaeric antibiotic resistance gene as a selectable marker for plant cell transformation. Nature 304:184-187.

Bhattacharyya S, Yu H, Mim C, Matouschek A. 2014. Regulated protein turnover: snapshots of the proteasome in action. Nat Rev Mol Cell Biol 15:122-133.

Bielska E, Schuster M, Roger Y, Berepiki A, Soanes DM, Talbot NJ, Steinberg G. 2014. Hook is an adapter that coordinates kinesin-3 and dynein cargo attachment on early endosomes. J Cell Biol 204:989-1007.

Bindels DS, Haarbosch L, van Weeren L, Postma M, Wiese KE, Mastop M, Aumonier S, Gotthard G, Royant A, Hink MA, Gadella TW, Jr. 2017. mScarlet: a bright monomeric red fluorescent protein for cellular imaging. Nat Methods 14:53-56.

Björck L. 1988. Protein L. A novel bacterial cell wall protein with affinity for Ig L chains. J Immunol 140:1194-1197.

Boersma S, Khuperkar D, Verhagen BMP, Sonneveld S, Grimm JB, Lavis LD, Tanenbaum ME. 2019. Multi-Color Single-Molecule Imaging Uncovers Extensive Heterogeneity in mRNA Decoding. Cell 178:458-472 e419.

Bölker M. 2001. Ustilago maydis--a valuable model system for the study of fungal dimorphism and virulence. Microbiology 147:1395-1401.

Bölker M, Basse CW, Schirawski J. 2008. Ustilago maydis secondary metabolism-from genomics to biochemistry. Fungal Genet Biol 45 Suppl 1:S88-93.

Bonger KM, Chen LC, Liu CW, Wandless TJ. 2011. Small-molecule displacement of a cryptic degron causes conditional protein degradation. Nat Chem Biol 7:531-537.

Bonifacino JS, Gershlick DC, Dell'Angelica EC. 2016. Immunoprecipitation. Curr Protoc Cell Biol 71.

Bosch K, Frantzeskakis L, Vranes M, Kamper J, Schipper K, Gohre V. 2016. Genetic Manipulation of the Plant Pathogen Ustilago maydis to Study Fungal Biology and Plant Microbe Interactions. J Vis Exp.

Bostrom K, Wettesten M, Boren J, Bondjers G, Wiklund O, Olofsson SO. 1986. Pulse-chase studies of the synthesis and intracellular transport of apolipoprotein B-100 in Hep G2 cells. J Biol Chem 261:13800-13806.

Bottin A, Kamper J, Kahmann R. 1996. Isolation of a carbon source-regulated gene from Ustilago maydis. Mol Gen Genet 253:342-352.

Bouvet JP, Pires R, Lunel-Fabiani F, Crescenzo-Chaigne B, Maillard P, Valla D, Opolon P, Pillot J. 1990. Protein F. A novel F(ab)-binding factor, present in normal liver, and largely released in the digestive tract during hepatitis. J Immunol 145:1176-1180.

Bouvet JP, Pires R, Quan C, Iscaki S, Pillot J. 1991. Non-immune VH-binding specificity of human protein Fv. Scand J Immunol 33:381-386.

Brachmann A. Die frühe Infektionsphase von Ustilago maydis: Genregulation durch das bW/bE-Heterodimer. 2001. In: Dissertation. Ludwig-Maximilians-University Munich.

Brachmann A, Konig J, Julius C, Feldbrugge M. 2004. A reverse genetic approach for generating gene replacement mutants in Ustilago maydis. Mol Genet Genomics 272:216-226.

Brachmann A, Weinzierl G, Kamper J, Kahmann R. 2001. Identification of genes in the bW/bE regulatory cascade in Ustilago maydis. Mol Microbiol 42:1047-1063.

Bradford MM. 1976. A rapid and sensitive method for the quantitation of microgram quantities of protein utilizing the principle of protein-dye binding. Anal Biochem 72:248-254.

Braselmann E, Wierzba AJ, Polaski JT, Chrominski M, Holmes ZE, Hung ST, Batan D, Wheeler JR, Parker R, Jimenez R, Gryko D, Batey RT, Palmer AE. 2018. A multicolor riboswitch-based platform for imaging of RNA in live mammalian cells. Nat Chem Biol 14:964-971.

Braun MB, Traenkle B, Koch PA, Emele F, Weiss F, Poetz O, Stehle T, Rothbauer U. 2016. Peptides in headlock--a novel high-affinity and versatile peptide-binding nanobody for proteomics and microscopy. Sci Rep 6:19211.

Bullock SL. 2007. Translocation of mRNAs by molecular motors: think complex? Semin Cell Dev Biol 18:194-201.

Busch KE, Hayles J, Nurse P, Brunner D. 2004. Tea2p kinesin is involved in spatial microtubule organization by transporting tip1p on microtubules. Dev Cell 6:831-843.

Buxbaum AR, Haimovich G, Singer RH. 2015. In the right place at the right time: visualizing and understanding mRNA localization. Nat Rev Mol Cell Biol 16:95-109.

Buxbaum AR, Wu B, Singer RH. 2014. Single beta-actin mRNA detection in neurons reveals a mechanism for regulating its translatability. Science 343:419-422.

Buxbaum AR, Yoon YJ, Singer RH, Park HY. 2015. Single-molecule insights into mRNA dynamics in neurons. Trends Cell Biol 25:468-475.

Cajigas IJ, Tushev G, Will TJ, tom Dieck S, Fuerst N, Schuman EM. 2012. The local transcriptome in the synaptic neuropil revealed by deep sequencing and high-resolution imaging. Neuron 74:453-466.

Castillo-Lluva S, Perez-Martin J. 2005. The induction of the mating program in the phytopathogen Ustilago maydis is controlled by a G1 cyclin. Plant Cell 17:3544-3560.

Chassin H, Muller M, Tigges M, Scheller L, Lang M, Fussenegger M. 2019. A modular degron library for synthetic circuits in mammalian cells. Nat Commun 10:2013.

Chekulaeva M, Landthaler M. 2016. Eyes on Translation. Mol Cell 63:918-925.

Chen X, Zhang D, Su N, Bao B, Xie X, Zuo F, Yang L, Wang H, Jiang L, Lin Q, Fang M, Li N, Hua X, Chen Z, Bao C, Xu J, Du W, Zhang L, Zhao Y, Zhu L, Loscalzo J, Yang Y. 2019. Visualizing RNA dynamics in live cells with bright and stable fluorescent RNAs. Nat Biotechnol 37:1287-1293.

Chng J, Wang T, Nian R, Lau A, Hoi KM, Ho SC, Gagnon P, Bi X, Yang Y. 2015. Cleavage efficient 2A peptides for high level monoclonal antibody expression in CHO cells. MAbs 7:403-412.

Chromotek. 2018. Chromotek - Spot Tag ChromoBlog. In.

Cioni JM, Lin JQ, Holtermann AV, Koppers M, Jakobs MAH, Azizi A, Turner-Bridger B, Shigeoka T, Franze K, Harris WA, Holt CE. 2019. Late Endosomes Act as mRNA Translation Platforms and Sustain Mitochondria in Axons. Cell 176:56-72 e15.

Cohen SN, Chang AC, Hsu L. 1972. Nonchromosomal antibiotic resistance in bacteria: genetic transformation of Escherichia coli by R-factor DNA. Proc Natl Acad Sci U S A 69:2110-2114.

Cook GP, Tomlinson IM. 1995. The human immunoglobulin VH repertoire. Immunol Today 16:237-242.

Crauwels M, Van Vaerenbergh N, Kulaya NB, Vincke C, D'Huyvetter M, Devoogdt N, Muyldermans S, Xavier C. 2020. Reshaping nanobodies for affinity purification on protein a. N Biotechnol 57:20-28.

Cui XA, Zhang H, Palazzo AF. 2012. p180 promotes the ribosome-independent localization of a subset of mRNA to the endoplasmic reticulum. PLoS Biol 10:e1001336.

Czaplinski K. 2014. Understanding mRNA trafficking: are we there yet? Semin Cell Dev Biol 32:63-70.

Daigle N, Ellenberg J. 2007. LambdaN-GFP: an RNA reporter system for live-cell imaging. Nat Methods 4:633-636.

Daniels RW, Rossano AJ, Macleod GT, Ganetzky B. 2014. Expression of multiple transgenes from a single construct using viral 2A peptides in Drosophila. PLoS One 9:e100637.

Darnell JC, Van Driesche SJ, Zhang C, Hung KY, Mele A, Fraser CE, Stone EF, Chen C, Fak JJ, Chi SW, Licatalosi DD, Richter JD, Darnell RB. 2011. FMRP stalls ribosomal translocation on mRNAs linked to synaptic function and autism. Cell 146:247-261.

Das S, Singer RH, Yoon YJ. 2019. The travels of mRNAs in neurons: do they know where they are going? Curr Opin Neurobiol 57:110-116.

Davidovic L, Jaglin XH, Lepagnol-Bestel AM, Tremblay S, Simonneau M, Bardoni B, Khandjian EW. 2007. The fragile X mental retardation protein is a molecular adaptor between the neurospecific KIF3C kinesin and dendritic RNA granules. Hum Mol Genet 16:3047-3058.

Day RN, Davidson MW. 2009. The fluorescent protein palette: tools for cellular imaging. Chem Soc Rev 38:2887-2921.

de Felipe P, Luke GA, Hughes LE, Gani D, Halpin C, Ryan MD. 2006. E unum pluribus: multiple proteins from a self-processing polyprotein. Trends Biotechnol 24:68-75.

Deisenhofer J. 1981. Crystallographic refinement and atomic models of a human Fc fragment and its complex with fragment B of protein A from Staphylococcus aureus at 2.9- and 2.8-A resolution. Biochemistry 20:2361-2370.

Derrick JP, Wigley DB. 1992. Crystal structure of a streptococcal protein G domain bound to an Fab fragment. Nature 359:752-754.

Dieterich DC, Hodas JJ, Gouzer G, Shadrin IY, Ngo JT, Triller A, Tirrell DA, Schuman EM. 2010. In situ visualization and dynamics of newly synthesized proteins in rat hippocampal neurons. Nat Neurosci 13:897-905.

Dieterich DC, Link AJ, Graumann J, Tirrell DA, Schuman EM. 2006. Selective identification of newly synthesized proteins in mammalian cells using bioorthogonal noncanonical amino acid tagging (BONCAT). Proc Natl Acad Sci U S A 103:9482-9487.

Donnelly ML, Gani D, Flint M, Monaghan S, Ryan MD. 1997. The cleavage activities of aphthovirus and cardiovirus 2A proteins. J Gen Virol 78 (Pt 1):13-21.

Doshi R, Chen BR, Vibat CR, Huang N, Lee CW, Chang G. 2014. In vitro nanobody discovery for integral membrane protein targets. Sci Rep 4:6760.

Dreyfuss G, Kim VN, Kataoka N. 2002. Messenger-RNA-binding proteins and the messages they carry. Nat Rev Mol Cell Biol 3:195-205.

Egan MJ, McClintock MA, Reck-Peterson SL. 2012. Microtubule-based transport in filamentous fungi. Curr Opin Microbiol 15:637-645.

Egea G, Izquierdo JM, Ricart J, San Martin C, Cuezva JM. 1997. mRNA encoding the beta-subunit of the mitochondrial F1-ATPase complex is a localized mRNA in rat hepatocytes. Biochem J 322 (Pt 2):557-565.

Elstner M, Andreoli C, Klopstock T, Meitinger T, Prokisch H. 2009. The mitochondrial proteome database: MitoP2. Methods Enzymol 457:3-20.

Engler C, Gruetzner R, Kandzia R, Marillonnet S. 2009. Golden gate shuffling: a one-pot DNA shuffling method based on type IIs restriction enzymes. PLoS One 4:e5553.

Estey MP, Kim MS, Trimble WS. 2011. Septins. Curr Biol 21:R384-387.

Fei J, Sharma CM. 2018. RNA Localization in Bacteria. Microbiol Spectr 6.

Feldbrügge M, Zarnack K, Vollmeister E, Baumann S, Koepke J, Konig J, Munsterkotter M, Mannhaupt G. 2008. The posttranscriptional machinery of Ustilago maydis. Fungal Genet Biol 45 Suppl 1:S40-46.

Femino AM, Fay FS, Fogarty K, Singer RH. 1998. Visualization of single RNA transcripts in situ. Science 280:585-590.

Ferrandon D, Elphick L, Nusslein-Volhard C, St Johnston D. 1994. Staufen protein associates with the 3'UTR of bicoid mRNA to form particles that move in a microtubule-dependent manner. Cell 79:1221-1232.

Flora P, Wong-Deyrup SW, Martin ET, Palumbo RJ, Nasrallah M, Oligney A, Blatt P, Patel D, Fuchs G, Rangan P. 2018. Sequential Regulation of Maternal mRNAs through a Conserved cis-Acting Element in Their 3' UTRs. Cell Rep 25:3828-3843 e3829.

Forsgren A, Sjoquist J. 1966. "Protein A" from S. aureus. I. Pseudo-immune reaction with human gamma-globulin. J Immunol 97:822-827.

Freitag J, Lanver D, Bohmer C, Schink KO, Bolker M, Sandrock B. 2011. Septation of infectious hyphae is critical for appressoria formation and virulence in the smut fungus Ustilago maydis. PLoS Pathog 7:e1002044.

Frenken LG, van der Linden RH, Hermans PW, Bos JW, Ruuls RC, de Geus B, Verrips CT. 2000. Isolation of antigen specific llama VHH antibody fragments and their high level secretion by Saccharomyces cerevisiae. J Biotechnol 78:11-21.

Fuchs U, Manns I, Steinberg G. 2005. Microtubules are dispensable for the initial pathogenic development but required for long-distance hyphal growth in the corn smut fungus Ustilago maydis. Mol Biol Cell 16:2746-2758.

Gao SY, Jack MM, O'Neill C. 2012. Towards optimising the production of and expression from polycistronic vectors in embryonic stem cells. PLoS One 7:e48668.

Garcia-Muse T, Steinberg G, Perez-Martin J. 2003. Pheromone-induced G2 arrest in the phytopathogenic fungus Ustilago maydis. Eukaryot Cell 2:494-500.

Garcia-Rodriguez LJ, Gay AC, Pon LA. 2007. Puf3p, a Pumilio family RNA binding protein, localizes to mitochondria and regulates mitochondrial biogenesis and motility in budding yeast. J Cell Biol 176:197-207.

Garcia JF, Parker R. 2015. MS2 coat proteins bound to yeast mRNAs block 5' to 3' degradation and trap mRNA decay products: implications for the localization of mRNAs by MS2-MCP system. RNA 21:1393-1395.

Garcia JF, Parker R. 2016. Ubiquitous accumulation of 3' mRNA decay fragments in Saccharomyces cerevisiae mRNAs with chromosomally integrated MS2 arrays. RNA 22:657-659.

Geier M, Fauland P, Vogl T, Glieder A. 2015. Compact multi-enzyme pathways in P. pastoris. Chem Commun (Camb) 51:1643-1646.

George RA, Heringa J. 2002. An analysis of protein domain linkers: their classification and role in protein folding. Protein Eng 15:871-879.

Gibson DG, Young L, Chuang RY, Venter JC, Hutchison CA, 3rd, Smith HO. 2009. Enzymatic assembly of DNA molecules up to several hundred kilobases. Nat Methods 6:343-345.

Gillissen B, Bergemann J, Sandmann C, Schroeer B, Bolker M, Kahmann R. 1992. A two-component regulatory system for self/non-self recognition in Ustilago maydis. Cell 68:647-657.

Glock C, Heumuller M, Schuman EM. 2017. mRNA transport & local translation in neurons. Curr Opin Neurobiol 45:169-177.

Glockshuber R, Malia M, Pfitzinger I, Pluckthun A. 1990. A comparison of strategies to stabilize immunoglobulin Fv-fragments. Biochemistry 29:1362-1367.

Gonsalvez GB, Little JL, Long RM. 2004. ASH1 mRNA anchoring requires reorganization of the Myo4p-She3p-She2p transport complex. J Biol Chem 279:46286-46294.

Graille M, Stura EA, Corper AL, Sutton BJ, Taussig MJ, Charbonnier JB, Silverman GJ. 2000. Crystal structure of a Staphylococcus aureus protein A domain complexed with the Fab fragment of a human IgM antibody: structural basis for recognition of B-cell receptors and superantigen activity. Proc Natl Acad Sci U S A 97:5399-5404.

Grant GD, Gamsby J, Martyanov V, Brooks L, 3rd, George LK, Mahoney JM, Loros JJ, Dunlap JC, Whitfield ML. 2012. Live-cell monitoring of periodic gene expression in synchronous human cells identifies Forkhead genes involved in cell cycle control. Mol Biol Cell 23:3079-3093.

Grant SG, Jessee J, Bloom FR, Hanahan D. 1990. Differential plasmid rescue from transgenic mouse DNAs into Escherichia coli methylation-restriction mutants. Proc Natl Acad Sci U S A 87:4645-4649.

Grate D, Wilson C. 1999. Laser-mediated, site-specific inactivation of RNA transcripts. Proc Natl Acad Sci U S A 96:6131-6136.

Griffiths AD, Duncan AR. 1998. Strategies for selection of antibodies by phage display. Curr Opin Biotechnol 9:102-108.

Grooms SY, Noh KM, Regis R, Bassell GJ, Bryan MK, Carroll RC, Zukin RS. 2006. Activity bidirectionally regulates AMPA receptor mRNA abundance in dendrites of hippocampal neurons. J Neurosci 26:8339-8351.

Grube L, Dellen R, Kruse F, Schwender H, Stuhler K, Poschmann G. 2018. Mining the Secretome of C2C12 Muscle Cells: Data Dependent Experimental Approach To Analyze Protein Secretion Using Label-Free Quantification and Peptide Based Analysis. J Proteome Res 17:879-890.

Gu W, Deng Y, Zenklusen D, Singer RH. 2004. A new yeast PUF family protein, Puf6p, represses ASH1 mRNA translation and is required for its localization. Genes Dev 18:1452-1465.

Guha P, Kaptan E, Gade P, Kalvakolanu DV, Ahmed H. 2017. Tunicamycin induced endoplasmic reticulum stress promotes apoptosis of prostate cancer cells by activating mTORC1. Oncotarget 8:68191-68207.

Ha SH, Liang YS, Jung H, Ahn MJ, Suh SC, Kweon SJ, Kim DH, Kim YM, Kim JK. 2010. Application of two bicistronic systems involving 2A and IRES sequences to the biosynthesis of carotenoids in rice endosperm. Plant Biotechnol J 8:928-938.

Haag C, Pohlmann T, Feldbrugge M. 2017. The ESCRT regulator Did2 maintains the balance between long-distance endosomal transport and endocytic trafficking. PLoS Genet 13:e1006734.

Hall RA. 2004. Studying protein-protein interactions via blot overlay or Far Western blot. Methods Mol Biol 261:167-174.

Halstead JM, Lionnet T, Wilbertz JH, Wippich F, Ephrussi A, Singer RH, Chao JA. 2015. Translation. An RNA biosensor for imaging the first round of translation from single cells to living animals. Science 347:1367-1671.

Hamers-Casterman C, Atarhouch T, Muyldermans S, Robinson G, Hamers C, Songa EB, Bendahman N, Hamers R. 1993. Naturally occurring antibodies devoid of light chains. Nature 363:446-448.

Hassler M, Shaltiel IA, Haering CH. 2018. Towards a Unified Model of SMC Complex Function. Curr Biol 28:R1266-R1281.

Heimel K, Scherer M, Vranes M, Wahl R, Pothiratana C, Schuler D, Vincon V, Finkernagel F, Flor-Parra I, Kamper J. 2010. The transcription factor Rbf1 is the master regulator for b-mating type controlled pathogenic development in Ustilago maydis. PLoS Pathog 6:e1001035.

Heinrich S, Sidler CL, Azzalin CM, Weis K. 2017. Stem-loop RNA labeling can affect nuclear and cytoplasmic mRNA processing. RNA 23:134-141.

Herskowitz I. 1988. Life cycle of the budding yeast Saccharomyces cerevisiae. Microbiol Rev 52:536-553.

Higuchi Y, Ashwin P, Roger Y, Steinberg G. 2014. Early endosome motility spatially organizes polysome distribution. J Cell Biol 204:343-357.

Hirokawa N. 2006. mRNA transport in dendrites: RNA granules, motors, and tracks. J Neurosci 26:7139-7142.

Hoefgen S, Lin J, Fricke J, Stroe MC, Mattern DJ, Kufs JE, Hortschansky P, Brakhage AA, Hoffmeister D, Valiante V. 2018. Facile assembly and fluorescence-based screening method for heterologous expression of biosynthetic pathways in fungi. Metab Eng 48:44-51.

Hogan DJ, Riordan DP, Gerber AP, Herschlag D, Brown PO. 2008. Diverse RNA-binding proteins interact with functionally related sets of RNAs, suggesting an extensive regulatory system. PLoS Biol 6:e255.

Holliday R. 1974. Molecular aspects of genetic exchange and gene conversion. Genetics 78:273-287.

Holliger P, Hudson PJ. 2005. Engineered antibody fragments and the rise of single domains. Nat Biotechnol 23:1126-1136.

Holst J, Vignali KM, Burton AR, Vignali DA. 2006. Rapid analysis of T-cell selection in vivo using T cell-receptor retrogenic mice. Nat Methods 3:191-197.

Holt CE, Bullock SL. 2009. Subcellular mRNA localization in animal cells and why it matters. Science 326:1212-1216.

Holt CE, Martin KC, Schuman EM. 2019. Local translation in neurons: visualization and function. Nat Struct Mol Biol 26:557-566.

Hong H, Yang Y, Cai W. 2011. Imaging gene expression in live cells and tissues. Cold Spring Harb Protoc 2011:pdb top103.

Howden AJ, Geoghegan V, Katsch K, Efstathiou G, Bhushan B, Boutureira O, Thomas B, Trudgian DC, Kessler BM, Dieterich DC, Davis BG, Acuto O. 2013. QuaNCAT: quantitating proteome dynamics in primary cells. Nat Methods 10:343-346.

Hoyt MA, Zhang M, Coffino P. 2003. Ubiquitin-independent mechanisms of mouse ornithine decarboxylase degradation are conserved between mammalian and fungal cells. J Biol Chem 278:12135-12143.

Huotari J, Helenius A. 2011. Endosome maturation. EMBO J 30:3481-3500.

Inganäs M. 1981. Comparison of mechanisms of interaction between protein A from Staphylococcus aureus and human monoclonal IgG, IgA and IgM in relation to the classical FC gamma and the alternative F(ab')2 epsilon protein A interactions. Scand J Immunol 13:343-352.

Ingolia NT, Ghaemmaghami S, Newman JR, Weissman JS. 2009. Genome-wide analysis in vivo of translation with nucleotide resolution using ribosome profiling. Science 324:218-223.

Irion U, St Johnston D. 2007. bicoid RNA localization requires specific binding of an endosomal sorting complex. Nature 445:554-558.

Ishii M, Kunimura JS, Jeng HT, Penna TC, Cholewa O. 2007. Evaluation of the pH- and thermal stability of the recombinant green fluorescent protein (GFP) in the presence of sodium chloride. Appl Biochem Biotechnol 137-140:555-571.

Jambhekar A, Derisi JL. 2007. Cis-acting determinants of asymmetric, cytoplasmic RNA transport. RNA 13:625-642.

Jan CH, Williams CC, Weissman JS. 2014. Principles of ER cotranslational translocation revealed by proximity-specific ribosome profiling. Science 346:1257521.

Jankowski S, Pohlmann T, Baumann S, Muntjes K, Devan SK, Zander S, Feldbrugge M. 2019. The multi PAM2 protein Upa2 functions as novel core component of endosomal mRNA transport. EMBO Rep 20:e47381.

Jaramillo AM, Weil TT, Goodhouse J, Gavis ER, Schupbach T. 2008. The dynamics of fluorescently labeled endogenous gurken mRNA in Drosophila. J Cell Sci 121:887-894.

Jastroch M, Divakaruni AS, Mookerjee S, Treberg JR, Brand MD. 2010. Mitochondrial proton and electron leaks. Essays Biochem 47:53-67.

Joosten V, Lokman C, Van Den Hondel CA, Punt PJ. 2003. The production of antibody fragments and antibody fusion proteins by yeasts and filamentous fungi. Microb Cell Fact 2:1.

Jordan A, Reichard P. 1998. Ribonucleotide reductases. Annu Rev Biochem 67:71-98.

Jungbluth M, Renicke C, Taxis C. 2010. Targeted protein depletion in Saccharomyces cerevisiae by activation of a bidirectional degron. BMC Syst Biol 4:176.

Kalderon D, Roberts BL, Richardson WD, Smith AE. 1984. A short amino acid sequence able to specify nuclear location. Cell 39:499-509.

Kamper J, Reichmann M, Romeis T, Bolker M, Kahmann R. 1995. Multiallelic recognition: nonself-dependent dimerization of the bE and bW homeodomain proteins in Ustilago maydis. Cell 81:73-83.

Kanai Y, Dohmae N, Hirokawa N. 2004. Kinesin transports RNA: isolation and characterization of an RNA-transporting granule. Neuron 43:513-525.

Kao DI, Aldridge GM, Weiler IJ, Greenough WT. 2010. Altered mRNA transport, docking, and protein translation in neurons lacking fragile X mental retardation protein. Proc Natl Acad Sci U S A 107:15601-15606.

Keon JP, White GA, Hargreaves JA. 1991. Isolation, characterization and sequence of a gene conferring resistance to the systemic fungicide carboxin from the maize smut pathogen, Ustilago maydis. Curr Genet 19:475-481.

Kikuchi N, Kolpashchikov DM. 2016. Split Spinach Aptamer for Highly Selective Recognition of DNA and RNA at Ambient Temperatures. Chembiochem 17:1589-1592.

Kim JH, Lee SR, Li LH, Park HJ, Park JH, Lee KY, Kim MK, Shin BA, Choi SY. 2011. High cleavage efficiency of a 2A peptide derived from porcine teschovirus-1 in human cell lines, zebrafish and mice. PLoS One 6:e18556.

King C, Sarabipour S, Byrne P, Leahy DJ, Hristova K. 2014. The FRET signatures of noninteracting proteins in membranes: simulations and experiments. Biophys J 106:1309-1317.

Koepke J, Kaffarnik F, Haag C, Zarnack K, Luscombe NM, Konig J, Ule J, Kellner R, Begerow D, Feldbrugge M. 2011. The RNA-binding protein Rrm4 is essential for efficient secretion of endochitinase Cts1. Mol Cell Proteomics 10:M111 011213.

Kolattukudy PE, Rogers LM, Li D, Hwang CS, Flaishman MA. 1995. Surface signaling in pathogenesis. Proc Natl Acad Sci U S A 92:4080-4087.

König J, Baumann S, Koepke J, Pohlmann T, Zarnack K, Feldbrugge M. 2009. The fungal RNA-binding protein Rrm4 mediates long-distance transport of ubi1 and rho3 mRNAs. EMBO J 28:1855-1866.

Kozak M. 1983. Comparison of initiation of protein synthesis in procaryotes, eucaryotes, and organelles. Microbiol Rev 47:1-45.

Kozlov G, Menade M, Rosenauer A, Nguyen L, Gehring K. 2010. Molecular determinants of PAM2 recognition by the MLLE domain of poly(A)-binding protein. J Mol Biol 397:397-407.

Kronvall G. 1973. A surface component in group A, C, and G streptococci with non-immune reactivity for immunoglobulin G. J Immunol 111:1401-1406.

Kruzel EK, Hull CM. 2010. Establishing an unusual cell type: how to make a dikaryon. Curr Opin Microbiol 13:706-711.

Kugler JM, Lasko P. 2009. Localization, anchoring and translational control of oskar, gurken, bicoid and nanos mRNA during Drosophila oogenesis. Fly (Austin) 3:15-28.

Ladner T, Held M, Flitsch D, Beckers M, Buchs J. 2016. Quasi-continuous parallel online scattered light, fluorescence and dissolved oxygen tension measurement combined with monitoring of the oxygen transfer rate in each well of a shaken microtiter plate. Microb Cell Fact 15:206.

Laemmli UK. 1970. Cleavage of structural proteins during the assembly of the head of bacteriophage T4. Nature 227:680-685.

Lakowicz JR. 2006. Principle of Fluorescence Spectroscopy. Springer, Boston, MA.

Langdon EM, Gladfelter AS. 2018. A New Lens for RNA Localization: Liquid-Liquid Phase Separation. Annu Rev Microbiol 72:255-271.

Langner T, Göhre V. 2016. Fungal chitinases: function, regulation, and potential roles in plant/pathogen interactions. Curr Genet 62:243-254.

Langner T, Ozturk M, Hartmann S, Cord-Landwehr S, Moerschbacher B, Walton JD, Göhre V. 2015. Chitinases Are Essential for Cell Separation in Ustilago maydis. Eukaryot Cell 14:846-857.

Lanker S, Valdivieso MH, Wittenberg C. 1996. Rapid degradation of the G1 cyclin Cln2 induced by CDK-dependent phosphorylation. Science 271:1597-1601.

Lanver D, Mendoza-Mendoza A, Brachmann A, Kahmann R. 2010. Sho1 and Msb2-related proteins regulate appressorium development in the smut fungus Ustilago maydis. Plant Cell 22:2085-2101.

Lanver D, Tollot M, Schweizer G, Lo Presti L, Reissmann S, Ma LS, Schuster M, Tanaka S, Liang L, Ludwig N, Kahmann R. 2017. Ustilago maydis effectors and their impact on virulence. Nat Rev Microbiol 15:409-421.

Larson DR, Zenklusen D, Wu B, Chao JA, Singer RH. 2011. Real-time observation of transcription initiation and elongation on an endogenous yeast gene. Science 332:475-478.

Lecuyer E, Yoshida H, Parthasarathy N, Alm C, Babak T, Cerovina T, Hughes TR, Tomancak P, Krause HM. 2007. Global analysis of mRNA localization reveals a prominent role in organizing cellular architecture and function. Cell 131:174-187.

Lehmler C, Steinberg G, Snetselaar KM, Schliwa M, Kahmann R, Bolker M. 1997. Identification of a motor protein required for filamentous growth in Ustilago maydis. EMBO J 16:3464-3473.

Lenz JH, Schuchardt I, Straube A, Steinberg G. 2006. A dynein loading zone for retrograde endosome motility at microtubule plus-ends. EMBO J 25:2275-2286.

Lesnik C, Golani-Armon A, Arava Y. 2015. Localized translation near the mitochondrial outer membrane: An update. RNA Biol 12:801-809.

Li X, Coffino P. 1993. Degradation of ornithine decarboxylase: exposure of the C-terminal target by a polyamine-inducible inhibitory protein. Mol Cell Biol 13:2377-2383.

Liao YC, Fernandopulle MS, Wang G, Choi H, Hao L, Drerup CM, Patel R, Qamar S, Nixon-Abell J, Shen Y, Meadows W, Vendruscolo M, Knowles TPJ, Nelson M, Czekalska MA, Musteikyte G, Gachechiladze MA, Stephens CA, Pasolli HA, Forrest LR, St George-Hyslop P, Lippincott-Schwartz J, Ward ME. 2019. RNA Granules Hitchhike on Lysosomes for Long-Distance Transport, Using Annexin A11 as a Molecular Tether. Cell 179:147-164 e120.

Lin MZ, McKeown MR, Ng HL, Aguilera TA, Shaner NC, Campbell RE, Adams SR, Gross LA, Ma W, Alber T, Tsien RY. 2009. Autofluorescent proteins with excitation in the optical window for intravital imaging in mammals. Chem Biol 16:1169-1179.

Lindahl G, Kronvall G. 1988. Nonimmune binding of Ig to Clostridium perfringens. Preferential binding of IgM and aggregated IgG. J Immunol 140:1223-1227.

Lindsey R, Momany M. 2006. Septin localization across kingdoms: three themes with variations. Curr Opin Microbiol 9:559-565.

Liu Z, Chen O, Wall JBJ, Zheng M, Zhou Y, Wang L, Ruth Vaseghi H, Qian L, Liu J. 2017. Systematic comparison of 2A peptides for cloning multi-genes in a polycistronic vector. Sci Rep 7:2193.

Long RM, Gu W, Lorimer E, Singer RH, Chartrand P. 2000. She2p is a novel RNA-binding protein that recruits the Myo4p-She3p complex to ASH1 mRNA. EMBO J 19:6592-6601.

Luke GA, de Felipe P, Lukashev A, Kallioinen SE, Bruno EA, Ryan MD. 2008. Occurrence, function and evolutionary origins of '2A-like' sequences in virus genomes. J Gen Virol 89:1036-1042.

Lutje Hulsik D, Liu YY, Strokappe NM, Battella S, El Khattabi M, McCoy LE, Sabin C, Hinz A, Hock M, Macheboeuf P, Bonvin AM, Langedijk JP, Davis D, Forsman Quigley A, Aasa-Chapman MM, Seaman MS, Ramos A, Poignard P, Favier A, Simorre JP, Weiss RA, Verrips CT, Weissenhorn W, Rutten L. 2013. A gp41 MPER-specific llama VHH requires a hydrophobic CDR3 for neutralization but not for antigen recognition. PLoS Pathog 9:e1003202.

Luzio JP, Parkinson MD, Gray SR, Bright NA. 2009. The delivery of endocytosed cargo to lysosomes. Biochem Soc Trans 37:1019-1021.

Ma L, Yang F, Zheng J. 2014. Application of fluorescence resonance energy transfer in protein studies. J Mol Struct 1077:87-100.

Macdonald PM, Luk SK, Kilpatrick M. 1991. Protein encoded by the exuperantia gene is concentrated at sites of bicoid mRNA accumulation in Drosophila nurse cells but not in oocytes or embryos. Genes Dev 5:2455-2466.

Mailfert S, Hamon Y, Bertaux N, He HT, Marguet D. 2017. A user's guide for characterizing plasma membrane subdomains in living cells by spot variation fluorescence correlation spectroscopy. Methods Cell Biol 139:1-22.

Manfiolli AO, Siqueira FS, Dos Reis TF, Van Dijck P, Schrevens S, Hoefgen S, Foge M, Strassburger M, de Assis LJ, Heinekamp T, Rocha MC, Janevska S, Brakhage AA, Malavazi I, Goldman GH, Valiante V. 2019. Mitogen-Activated Protein Kinase Cross-Talk Interaction Modulates the Production of Melanins in Aspergillus fumigatus. mBio 10.

Margeot A, Blugeon C, Sylvestre J, Vialette S, Jacq C, Corral-Debrinski M. 2002. In Saccharomyces cerevisiae, ATP2 mRNA sorting to the vicinity of mitochondria is essential for respiratory function. EMBO J 21:6893-6904.

Martin KC, Ephrussi A. 2009. mRNA localization: gene expression in the spatial dimension. Cell 136:719-730.

Mata J, Nurse P. 1997. tea1 and the microtubular cytoskeleton are important for generating global spatial order within the fission yeast cell. Cell 89:939-949.

McClintock MA, Dix CI, Johnson CM, McLaughlin SH, Maizels RJ, Hoang HT, Bullock SL. 2018. RNA-directed activation of cytoplasmic dynein-1 in reconstituted transport RNPs. Elife 7.

Merzlyak EM, Goedhart J, Shcherbo D, Bulina ME, Shcheglov AS, Fradkov AF, Gaintzeva A, Lukyanov KA, Lukyanov S, Gadella TW, Chudakov DM. 2007. Bright monomeric red fluorescent protein with an extended fluorescence lifetime. Nat Methods 4:555-557.

Mitchell LS, Colwell LJ. 2018. Comparative analysis of nanobody sequence and structure data. Proteins 86:697-706.

Mizuguchi H, Xu Z, Ishii-Watabe A, Uchida E, Hayakawa T. 2000. IRES-dependent second gene expression is significantly lower than cap-dependent first gene expression in a bicistronic vector. Mol Ther 1:376-382.

Mofatteh M, Bullock SL. 2017. SnapShot: Subcellular mRNA Localization. Cell 169:178-178 e171.

Moks T, Abrahmsen L, Nilsson B, Hellman U, Sjoquist J, Uhlen M. 1986. Staphylococcal protein A consists of five IgG-binding domains. Eur J Biochem 156:637-643.

Molina L, Kahmann R. 2007. An Ustilago maydis gene involved in H2O2 detoxification is required for virulence. Plant Cell 19:2293-2309.

Morisaki T, Lyon K, DeLuca KF, DeLuca JG, English BP, Zhang Z, Lavis LD, Grimm JB, Viswanathan S, Looger LL, Lionnet T, Stasevich TJ. 2016. Real-time quantification of single RNA translation dynamics in living cells. Science 352:1425-1429.

Morris J, Lehmann R. 1999. Drosophila oogenesis: versatile spn doctors. Curr Biol 9:R55-58.

Müller J, Pohlmann T, Feldbrugge M. 2019. Core components of endosomal mRNA transport are evolutionarily conserved in fungi. Fungal Genet Biol 126:12-16.

Müntjes K. 2013. Charakterisierung eines EMP70 verwandtenTransmembranproteins im ModellorganismusUstilago maydis. In: Bachelor´s Thesis. Heinrich-Heine-Universität, Düsseldorf.

Müntjes K. 2015. Optimization of RNA live imaging inUstilago maydis. In: Master´s thesis. Heinrich-Heine-Universität Düsseldorf.

Müntjes K, Philipp M, Hüsemann L, Heucken N, Weidtkamp-Peters S, Schipper K, Zurbriggen MD, Feldbrügge M. 2020. Establishing Polycistronic Expression in the Model Microorganism Ustilago maydis. Frontiers in Microbiology 11.

Murakami Y, Matsufuji S, Kameji T, Hayashi S, Igarashi K, Tamura T, Tanaka K, Ichihara A. 1992. Ornithine decarboxylase is degraded by the 26S proteasome without ubiquitination. Nature 360:597-599.

Muyldermans S, Cambillau C, Wyns L. 2001. Recognition of antigens by single-domain antibody fragments: the superfluous luxury of paired domains. Trends Biochem Sci 26:230-235.

Muyldermans S, Lauwereys M. 1999. Unique single-domain antigen binding fragments derived from naturally occurring camel heavy-chain antibodies. J Mol Recognit 12:131-140.

Narciso JETU, I.D.C; Cabang, A.B.; Chavez, J. F. C.; Pablo, J.L.B.; Padilla-Concepcion, G. P.; Padlan, E. . 2012. Anatomy of the antibody molecule: a continuing analysis based on high-resolution crystallographic structures. Phil Sci Letts 5:63-89.

Neriec N, Percipalle P. 2018. Sorting mRNA Molecules for Cytoplasmic Transport and Localization. Front Genet 9:510.

Niessing D, Jansen RP, Pohlmann T, Feldbrugge M. 2018. mRNA transport in fungal top models. Wiley Interdiscip Rev RNA 9.

Nilson BH, Solomon A, Bjorck L, Akerstrom B. 1992. Protein L from Peptostreptococcus magnus binds to the kappa light chain variable domain. J Biol Chem 267:2234-2239.

Nishiguchi A, Numoto N, Ito N, Azuma T, Oda M. 2019. Three-dimensional structure of a high affinity anti-(4-hydroxy-3-nitrophenyl)acetyl antibody possessing a glycine residue at position 95 of the heavy chain. Mol Immunol 114:545-552.

Nishimura K, Fukagawa T, Takisawa H, Kakimoto T, Kanemaki M. 2009. An auxin-based degron system for the rapid depletion of proteins in nonplant cells. Nat Methods 6:917-922.

Norvell A, Debec A, Finch D, Gibson L, Thoma B. 2005. Squid is required for efficient posterior localization of oskar mRNA during Drosophila oogenesis. Dev Genes Evol 215:340-349.

Olgeiser L, Haag C, Boerner S, Ule J, Busch A, Koepke J, Konig J, Feldbrugge M, Zarnack K. 2019. The key protein of endosomal mRNP transport Rrm4 binds translational landmark sites of cargo mRNAs. EMBO Rep 20.

Paradies MA, Steward O. 1997. Multiple subcellular mRNA distribution patterns in neurons: a nonisotopic in situ hybridization analysis. J Neurobiol 33:473-493.

Park YN, Masison D, Eisenberg E, Greene LE. 2011. Application of the FLP/FRT system for conditional gene deletion in yeast Saccharomyces cerevisiae. Yeast 28:673-681.

PDB. n.d. In. https://www.rcsb.org/search/advanced/sequence

Piatkevich KD, Efremenko EN, Verkhusha VV, Varfolomeev SD. 2010. Red fluorescent proteins and their properties. Russian Chemical Reviews 79:243-258.

Pichon X, Bastide A, Safieddine A, Chouaib R, Samacoits A, Basyuk E, Peter M, Mueller F, Bertrand E. 2016. Visualization of single endogenous polysomes reveals the dynamics of translation in live human cells. J Cell Biol 214:769-781.

Pilaz LJ, Lennox AL, Rouanet JP, Silver DL. 2016. Dynamic mRNA Transport and Local Translation in Radial Glial Progenitors of the Developing Brain. Curr Biol 26:3383-3392.

Pohlmann T, Baumann S, Haag C, Albrecht M, Feldbrugge M. 2015. A FYVE zinc finger domain protein specifically links mRNA transport to endosome trafficking. Elife 4.

Pokrywka NJ, Meng L, Debiec K, Stephenson EC. 2004. Identification of hypomorphic and null alleles of swallow via molecular and phenotypic analyses. Dev Genes Evol 214:185-192.

Pymol. n.d. In. https://pymol.org/2/

Quilis I, Igual JC. 2017. A comparative study of the degradation of yeast cyclins Cln1 and Cln2. FEBS Open Bio 7:74-87.

Qureshi SA. 2007. Beta-lactamase: an ideal reporter system for monitoring gene expression in live eukaryotic cells. Biotechniques 42:91-96.

Rahman MM, Kipreos ET. 2010. The specific roles of mitotic cyclins revealed. Cell Cycle 9:22-23.

Ram AF, Klis FM. 2006. Identification of fungal cell wall mutants using susceptibility assays based on Calcofluor white and Congo red. Nat Protoc 1:2253-2256.

Rechsteiner M. 1990. PEST sequences are signals for rapid intracellular proteolysis. Semin Cell Biol 1:433-440.

Rechsteiner M. 1991. Natural substrates of the ubiquitin proteolytic pathway. Cell 66:615-618.

Rechsteiner M, Rogers SW. 1996. PEST sequences and regulation by proteolysis. Trends Biochem Sci 21:267-271.

Reineke G, Heinze B, Schirawski J, Buettner H, Kahmann R, Basse CW. 2008. Indole-3-acetic acid (IAA) biosynthesis in the smut fungus Ustilago maydis and its relevance for increased IAA levels in infected tissue and host tumour formation. Mol Plant Pathol 9:339-355.

Renicke C, Schuster D, Usherenko S, Essen LO, Taxis C. 2013. A LOV2 domain-based optogenetic tool to control protein degradation and cellular function. Chem Biol 20:619-626.

Ricart J, Egea G, Izquierdo JM, San Martin C, Cuezva JM. 1997. Subcellular structure containing mRNA for beta subunit of mitochondrial H+-ATP synthase in rat hepatocytes is translationally active. Biochem J 324 (Pt 2):635-643.

Roberts TM, Rudolf F, Meyer A, Pellaux R, Whitehead E, Panke S, Held M. 2016. Identification and Characterisation of a pH-stable GFP. Sci Rep 6:28166.

Rogers S, Wells R, Rechsteiner M. 1986. Amino acid sequences common to rapidly degraded proteins: the PEST hypothesis. Science 234:364-368.

Romero-Aguilar L, Guerra-Sanchez G, Tenorio EP, Tapia-Rodriguez M, Matus-Ortega G, Flores-Herrera O, Gonzalez J, Pardo JP. 2020. Rapamycin induces morphological

and physiological changes without increase in lipid content in Ustilago maydis. Arch Microbiol 202:1211-1221.

Rook MS, Lu M, Kosik KS. 2000. CaMKIIalpha 3' untranslated region-directed mRNA translocation in living neurons: visualization by GFP linkage. J Neurosci 20:6385-6393.

Roulston C, Luke GA, de Felipe P, Ruan L, Cope J, Nicholson J, Sukhodub A, Tilsner J, Ryan MD. 2016. '2A-Like' Signal Sequences Mediating Translational Recoding: A Novel Form of Dual Protein Targeting. Traffic 17:923-939.

Rusche LN, Rine J. 2010. Switching the mechanism of mating type switching: a domesticated transposase supplants a domesticated homing endonuclease. Genes Dev 24:10-14.

Ryan MD, King AM, Thomas GP. 1991. Cleavage of foot-and-mouth disease virus polyprotein is mediated by residues located within a 19 amino acid sequence. J Gen Virol 72 (Pt 11):2727-2732.

Saint-Georges Y, Garcia M, Delaveau T, Jourdren L, Le Crom S, Lemoine S, Tanty V, Devaux F, Jacq C. 2008. Yeast mitochondrial biogenesis: a role for the PUF RNA-binding protein Puf3p in mRNA localization. PLoS One 3:e2293.

Sambrook JFERMT. 1989. Molecular Cloning: A Laboratory Manual (2nd ed.). . Cold Spring Harbor, NY: Cold Spring Harbor Laboratory Press

Sarkari P, Reindl M, Stock J, Muller O, Kahmann R, Feldbrugge M, Schipper K. 2014. Improved expression of single-chain antibodies in Ustilago maydis. J Biotechnol 191:165-175.

Saville BJD, M.E.; Doyle, C.E. 2012. Investigating Host Induced Meiosis in a Fungal Plant Pathogen. In: Swan A, editor. Meiosis. Molecular mechanisms and cytogenetic diversit. Rijeka, Croatia.

Scherer M, Heimel K, Starke V, Kamper J. 2006. The Clp1 protein is required for clamp formation and pathogenic development of Ustilago maydis. Plant Cell 18:2388-2401.

Schmid M, Jaedicke A, Du TG, Jansen RP. 2006. Coordination of endoplasmic reticulum and mRNA localization to the yeast bud. Curr Biol 16:1538-1543.

Schmidt EK, Clavarino G, Ceppi M, Pierre P. 2009. SUnSET, a nonradioactive method to monitor protein synthesis. Nat Methods 6:275-277.

Schneider-Poetsch T, Ju J, Eyler DE, Dang Y, Bhat S, Merrick WC, Green R, Shen B, Liu JO. 2010. Inhibition of eukaryotic translation elongation by cycloheximide and lactimidomycin. Nat Chem Biol 6:209-217.

Schuchardt I, Assmann D, Thines E, Schuberth C, Steinberg G. 2005. Myosin-V, Kinesin-1, and Kinesin-3 cooperate in hyphal growth of the fungus Ustilago maydis. Mol Biol Cell 16:5191-5201.

Schuetze T, Meyer V. 2017. Polycistronic gene expression in Aspergillus niger. Microb Cell Fact 16:162.

Schulz B, Banuett F, Dahl M, Schlesinger R, Schafer W, Martin T, Herskowitz I, Kahmann R. 1990. The b alleles of U. maydis, whose combinations program pathogenic development, code for polypeptides containing a homeodomain-related motif. Cell 60:295-306.

Schuster M, Kilaru S, Fink G, Collemare J, Roger Y, Steinberg G. 2011. Kinesin-3 and dynein cooperate in long-range retrograde endosome motility along a nonuniform microtubule array. Mol Biol Cell 22:3645-3657.

Schwanhausser B, Gossen M, Dittmar G, Selbach M. 2009. Global analysis of cellular protein translation by pulsed SILAC. Proteomics 9:205-209.

Schwer B, Schneider S, Pei Y, Aronova A, Shuman S. 2009. Characterization of the Schizosaccharomyces pombe Spt5-Spt4 complex. RNA 15:1241-1250.

Shaner NC, Campbell RE, Steinbach PA, Giepmans BN, Palmer AE, Tsien RY. 2004. Improved monomeric red, orange and yellow fluorescent proteins derived from Discosoma sp. red fluorescent protein. Nat Biotechnol 22:1567-1572.

Shaner NC, Lin MZ, McKeown MR, Steinbach PA, Hazelwood KL, Davidson MW, Tsien RY. 2008. Improving the photostability of bright monomeric orange and red fluorescent proteins. Nat Methods 5:545-551.

Sharma P, Yan F, Doronina VA, Escuin-Ordinas H, Ryan MD, Brown JD. 2012. 2A peptides provide distinct solutions to driving stop-carry on translational recoding. Nucleic Acids Res 40:3143-3151.

Shcherbo D, Merzlyak EM, Chepurnykh TV, Fradkov AF, Ermakova GV, Solovieva EA, Lukyanov KA, Bogdanova EA, Zaraisky AG, Lukyanov S, Chudakov DM. 2007. Bright far-red fluorescent protein for whole-body imaging. Nat Methods 4:741-746.

Shcherbo D, Murphy CS, Ermakova GV, Solovieva EA, Chepurnykh TV, Shcheglov AS, Verkhusha VV, Pletnev VZ, Hazelwood KL, Roche PM, Lukyanov S, Zaraisky AG, Davidson MW, Chudakov DM. 2009. Far-red fluorescent tags for protein imaging in living tissues. Biochem J 418:567-574.

Shepard KA, Gerber AP, Jambhekar A, Takizawa PA, Brown PO, Herschlag D, DeRisi JL, Vale RD. 2003. Widespread cytoplasmic mRNA transport in yeast: identification of 22 bud-localized transcripts using DNA microarray analysis. Proc Natl Acad Sci U S A 100:11429-11434.

Shumway SD, Maki M, Miyamoto S. 1999. The PEST domain of IkappaBalpha is necessary and sufficient for in vitro degradation by mu-calpain. J Biol Chem 274:30874-30881.

Sil A, Herskowitz I. 1996. Identification of asymmetrically localized determinant, Ash1p, required for lineage-specific transcription of the yeast HO gene. Cell 84:711-722.

Silverman GJ, Roben P, Bouvet JP, Sasano M. 1995. Superantigen properties of a human sialoprotein involved in gut-associated immunity. J Clin Invest 96:417-426.

Song MS, Moon HC, Jeon JH, Park HY. 2018. Neuronal messenger ribonucleoprotein transport follows an aging Levy walk. Nat Commun 9:344.

Southern EM. 1975. Detection of specific sequences among DNA fragments separated by gel electrophoresis. J Mol Biol 5:503-517.

Souza-Moreira TM, Navarrete C, Chen X, Zanelli CF, Valentini SR, Furlan M, Nielsen J, Krivoruchko A. 2018. Screening of 2A peptides for polycistronic gene expression in yeast. FEMS Yeast Res 18.

Spellig T, Bolker M, Lottspeich F, Frank RW, Kahmann R. 1994. Pheromones trigger filamentous growth in Ustilago maydis. EMBO J 13:1620-1627.

Spellig T, Bottin A, Kahmann R. 1996. Green fluorescent protein (GFP) as a new vital marker in the phytopathogenic fungus Ustilago maydis. Mol Gen Genet 252:503-509.

Spieth J, Brooke G, Kuersten S, Lea K, Blumenthal T. 1993. Operons in C. elegans: polycistronic mRNA precursors are processed by trans-splicing of SL2 to downstream coding regions. Cell 73:521-532.

St Johnston D. 2005. Moving messages: the intracellular localization of mRNAs. Nat Rev Mol Cell Biol 6:363-375.

Steinberg G, Schliwa M, Lehmler C, Bolker M, Kahmann R, McIntosh JR. 1998. Kinesin from the plant pathogenic fungus Ustilago maydis is involved in vacuole formation and cytoplasmic migration. J Cell Sci 111 (Pt 15):2235-2246.

Steinberg G, Wedlich-Soldner R, Brill M, Schulz I. 2001. Microtubules in the fungal pathogen Ustilago maydis are highly dynamic and determine cell polarity. J Cell Sci 114:609-622.

Stenmark H. 2009. Rab GTPases as coordinators of vesicle traffic. Nat Rev Mol Cell Biol 10:513-525.

Stoffels P, Muller MJ, Stachurski S, Terfruchte M, Schroder S, Ihling N, Wierckx N, Feldbrugge M, Schipper K, Buchs J. 2020. Complementing the intrinsic repertoire of Ustilago maydis for degradation of the pectin backbone polygalacturonic acid. J Biotechnol 307:148-163.

Stroe MC, Netzker T, Scherlach K, Kruger T, Hertweck C, Valiante V, Brakhage AA. 2020. Targeted induction of a silent fungal gene cluster encoding the bacteria-specific germination inhibitor fumigermin. Elife 9.

Su L, Li A, Li H, Chu C, Qiu JL. 2013. Direct modulation of protein level in Arabidopsis. Mol Plant 6:1711-1714.

Subramanian V, Schuster LA, Moore KT, Taylor LE, 2nd, Baker JO, Vander Wall TA, Linger JG, Himmel ME, Decker SR. 2017. A versatile 2A peptide-based bicistronic protein

expressing platform for the industrial cellulase producing fungus, Trichoderma reesei. Biotechnol Biofuels 10:34.
Swetha P, Fan Z, Wang F, Jiang JH. 2020. Genetically encoded light-up RNA aptamers and their applications for imaging and biosensing. J Mater Chem B 8:3382-3392.
Szymczak AL, Workman CJ, Wang Y, Vignali KM, Dilioglou S, Vanin EF, Vignali DA. 2004. Correction of multi-gene deficiency in vivo using a single 'self-cleaving' 2A peptide-based retroviral vector. Nat Biotechnol 22:589-594.
Takeuchi J, Chen H, Hoyt MA, Coffino P. 2008. Structural elements of the ubiquitin-independent proteasome degron of ornithine decarboxylase. Biochem J 410:401-407.
Tanenbaum ME, Gilbert LA, Qi LS, Weissman JS, Vale RD. 2014. A protein-tagging system for signal amplification in gene expression and fluorescence imaging. Cell 159:635-646.
Tatebe H, Shimada K, Uzawa S, Morigasaki S, Shiozaki K. 2005. Wsh3/Tea4 is a novel cell-end factor essential for bipolar distribution of Tea1 and protects cell polarity under environmental stress in S. pombe. Curr Biol 15:1006-1015.
Teis D, Saksena S, Emr SD. 2009. SnapShot: the ESCRT machinery. Cell 137:182-182 e181.
Terfrüchte M, Joehnk B, Fajardo-Somera R, Braus GH, Riquelme M, Schipper K, Feldbrugge M. 2014. Establishing a versatile Golden Gate cloning system for genetic engineering in fungi. Fungal Genet Biol 62:1-10.
Terfrüchte M, Reindl M, Jankowski S, Sarkari P, Feldbrugge M, Schipper K. 2017. Applying Unconventional Secretion in Ustilago maydis for the Export of Functional Nanobodies. Int J Mol Sci 18.
Tian L, Doroshenk KA, Zhang L, Fukuda M, Washida H, Kumamaru T, Okita TW. 2020. Zipcode RNA-binding Proteins and Membrane Trafficking Proteins Cooperate to Transport Glutelin mRNAs in Rice Endosperm. Plant Cell.
Tiruchinapalli DM, Oleynikov Y, Kelic S, Shenoy SM, Hartley A, Stanton PK, Singer RH, Bassell GJ. 2003. Activity-dependent trafficking and dynamic localization of zipcode binding protein 1 and beta-actin mRNA in dendrites and spines of hippocampal neurons. J Neurosci 23:3251-3261.
Tom Dieck S, Muller A, Nehring A, Hinz FI, Bartnik I, Schuman EM, Dieterich DC. 2012. Metabolic labeling with noncanonical amino acids and visualization by chemoselective fluorescent tagging. Curr Protoc Cell Biol Chapter 7:Unit7 11.
Tool C. n.d. In. https://www2.mrc-lmb.cam.ac.uk/personal/pemsley/coot/
Tutucci E, Vera M, Biswas J, Garcia J, Parker R, Singer RH. 2018. An improved MS2 system for accurate reporting of the mRNA life cycle. Nat Methods 15:81-89.
Tyagi S. 2009. Imaging intracellular RNA distribution and dynamics in living cells. Nat Methods 6:331-338.
Unkles SE, Valiante V, Mattern DJ, Brakhage AA. 2014. Synthetic biology tools for bioprospecting of natural products in eukaryotes. Chem Biol 21:502-508.
Valencia-Burton M, McCullough RM, Cantor CR, Broude NE. 2007. RNA visualization in live bacterial cells using fluorescent protein complementation. Nat Methods 4:421-427.
Villasenor R, Kalaidzidis Y, Zerial M. 2016. Signal processing by the endosomal system. Curr Opin Cell Biol 39:53-60.
Virant D, Traenkle B, Maier J, Kaiser PD, Bodenhofer M, Schmees C, Vojnovic I, Pisak-Lukats B, Endesfelder U, Rothbauer U. 2018. A peptide tag-specific nanobody enables high-quality labeling for dSTORM imaging. Nat Commun 9:930.
Vollmeister E, Schipper K, Baumann S, Haag C, Pohlmann T, Stock J, Feldbrugge M. 2012. Fungal development of the plant pathogen Ustilago maydis. FEMS Microbiol Rev 36:59-77.
Vollmeister E, Schipper K, Feldbrugge M. 2012. Microtubule-dependent mRNA transport in the model microorganism Ustilago maydis. RNA Biol 9:261-268.
Wang C, Han B, Zhou R, Zhuang X. 2016. Real-Time Imaging of Translation on Single mRNA Transcripts in Live Cells. Cell 165:990-1001.
Wang J, Holden DW, Leong SA. 1988. Gene transfer system for the phytopathogenic fungus Ustilago maydis. Proc Natl Acad Sci U S A 85:865-869.

Wang JT, Medress ZA, Vargas ME, Barres BA. 2015. Local axonal protection by WldS as revealed by conditional regulation of protein stability. Proc Natl Acad Sci U S A 112:10093-10100.

Wang S, Beattie GM, Hayek A, Levine F. 1996. Development of a VSV-G protein pseudotyped retroviral vector system expressing dominant oncogenes from a lacO-modified inducible LTR promoter. Gene 182:145-150.

Wang Y, Wang F, Wang R, Zhao P, Xia Q. 2015. 2A self-cleaving peptide-based multi-gene expression system in the silkworm Bombyx mori. Sci Rep 5:16273.

Wannier TM, Gillespie SK, Hutchins N, McIsaac RS, Wu SY, Shen Y, Campbell RE, Brown KS, Mayo SL. 2018. Monomerization of far-red fluorescent proteins. Proc Natl Acad Sci U S A 115:E11294-E11301.

Weatheritt RJ, Gibson TJ, Babu MM. 2014. Asymmetric mRNA localization contributes to fidelity and sensitivity of spatially localized systems. Nat Struct Mol Biol 21:833-839.

Wedlich-Soldner R, Bolker M, Kahmann R, Steinberg G. 2000. A putative endosomal t-SNARE links exo- and endocytosis in the phytopathogenic fungus Ustilago maydis. EMBO J 19:1974-1986.

Wedlich-Söldner R, Straube A, Friedrich MW, Steinberg G. 2002. A balance of KIF1A-like kinesin and dynein organizes early endosomes in the fungus Ustilago maydis. EMBO J 21:2946-2957.

Weil TT, Forrest KM, Gavis ER. 2006. Localization of bicoid mRNA in late oocytes is maintained by continual active transport. Dev Cell 11:251-262.

Weirich CS, Erzberger JP, Barral Y. 2008. The septin family of GTPases: architecture and dynamics. Nat Rev Mol Cell Biol 9:478-489.

Wideman JG, Leung KF, Field MC, Dacks JB. 2014. The cell biology of the endocytic system from an evolutionary perspective. Cold Spring Harb Perspect Biol 6:a016998.

Williams CC, Jan CH, Weissman JS. 2014. Targeting and plasticity of mitochondrial proteins revealed by proximity-specific ribosome profiling. Science 346:748-751.

Woraratanadharm T, Kmosek S, Banuett F. 2018. UmTea1, a Kelch and BAR domain-containing protein, acts at the cell cortex to regulate cell morphogenesis in the dimorphic fungus Ustilago maydis. Fungal Genet Biol 121:10-28.

Worn A, Auf der Maur A, Escher D, Honegger A, Barberis A, Pluckthun A. 2000. Correlation between in vitro stability and in vivo performance of anti-GCN4 intrabodies as cytoplasmic inhibitors. J Biol Chem 275:2795-2803.

Wu B, Eliscovich C, Yoon YJ, Singer RH. 2016. Translation dynamics of single mRNAs in live cells and neurons. Science 352:1430-1435.

Yan X, Hoek TA, Vale RD, Tanenbaum ME. 2016. Dynamics of Translation of Single mRNA Molecules In Vivo. Cell 165:976-989.

Yano T, Lopez de Quinto S, Matsui Y, Shevchenko A, Shevchenko A, Ephrussi A. 2004. Hrp48, a Drosophila hnRNPA/B homolog, binds and regulates translation of oskar mRNA. Dev Cell 6:637-648.

Zander S, Baumann S, Weidtkamp-Peters S, Feldbrugge M. 2016. Endosomal assembly and transport of heteromeric septin complexes promote septin cytoskeleton formation. J Cell Sci 129:2778-2792.

Zander S, Muntjes K, Feldbrugge M. 2018. RNA Live Imaging in the Model Microorganism Ustilago maydis. Methods Mol Biol 1649:319-335.

Zappulo A, van den Bruck D, Ciolli Mattioli C, Franke V, Imami K, McShane E, Moreno-Estelles M, Calviello L, Filipchyk A, Peguero-Sanchez E, Muller T, Woehler A, Birchmeier C, Merino E, Rajewsky N, Ohler U, Mazzoni EO, Selbach M, Akalin A, Chekulaeva M. 2017. RNA localization is a key determinant of neurite-enriched proteome. Nat Commun 8:583.

Zarnack K, Maurer S, Kaffarnik F, Ladendorf O, Brachmann A, Kamper J, Feldbrugge M. 2006. Tetracycline-regulated gene expression in the pathogen Ustilago maydis. Fungal Genet Biol 43:727-738.

Zhou L, Obhof T, Schneider K, Feldbrugge M, Nienhaus GU, Kamper J. 2018. Cytoplasmic Transport Machinery of the SPF27 Homologue Num1 in Ustilago maydis. Sci Rep 8:3611.

Zimyanin VL, Belaya K, Pecreaux J, Gilchrist MJ, Clark A, Davis I, St Johnston D. 2008. In vivo imaging of oskar mRNA transport reveals the mechanism of posterior localization. Cell 134:843-853.

Acknowledgments

Zunächst möchte ich mich bei Michael bedanken, der mich seit meiner Bachelorarbeit immer unterstützt, motiviert und gefordert hat und der mein wissenschaftliches Arbeiten stark geprägt hat.

Bei Prof. Dr. Lutz Schmitt möchte ich mich ausdrücklich für die Annahme des Zweitgutachtens und die konstruktiven Diskussionen während meiner Doktorarbeit bedanken.

Der Graduiertenschule „MB Train“ möchte ich danken, dass ich als assoziiertes Mitglied an zahlreichen Veranstaltungen teilnehmen durfte.

Bei Silke möchte ich mich ausdrücklich bedanken. Du bist einfach die Allerbeste und ohne dich wäre ich während meiner Doktorarbeit ganz bestimmt verloren gegangen. Ich vermisse unsere gemeinsame Zeit auf der Terrasse, unsere Pausen und die gemeinsamen Arbeiten an der Cleanbench, die für einen Außenstehenden sicherlich nach purem Chaos aussahen (was es natürlich nicht war!!), jetzt schon unfassbar. Ich freue mich wahnsinnig, in dir nicht nur eine gute Arbeitskollegin, sondern auch eine unfassbar wichtige Freundin gefunden zu haben. Danke auch, dass du dir meine Arbeit durchgelesen und mir mit Rat und Tat zur Seite gestanden hast!!

Ich möchte mich hier natürlich auch bei allen RabLab-Angehörigen bedanken. Carl, Thomas und Lilli: Danke, dass ihr immer ein offenes Ohr hattet und mir mit Rat und Tat zu Seite standet! Thomas und Sebastian: Auch wenn ihr nicht mehr Teil des RabLab-Teams seid, vielen Dank, dass ihr meine Arbeit gelesen und korrigiert habt!! Nina, danke, dass auch du einfach immer für mich da warst und bist und ich immer auf dich zählen kann. Arbeiten mit einer Freundin macht einfach noch mehr Spaß! Senthil, Markus, Sri und Woogie: Thanks a lot for all the nice hours in the lab and the gossip times we had together! Ein besonderes Dank gilt natürlich auch Sachiko. Du hast meine riesigen Stapel an pUMa- und UMa-Sheets hingenommen und abgearbeitet und mir unfassbar geholfen. Simone, auch du hast mir die letzte Zeit zur Seite gestanden und mir Luft verschafft, alle Experimente unter einen Hut zu bekommen. Ute, du hattest immer ein offenes Ohr und hast mir immer ausgeholfen, wenn du konntest!

Magnus, Pesto und Kai: mit euch macht Ballspielen im Office am meisten Spaß! Danke für die vielen lustigen Stunden die wir zusammen hatten! Michele, vielen Dank, dass du immer ein offenes Ohr für mich hattest. Wir haben es geschafft. Ist das zu fassen? Ich werde nie vergessen, wie wir zusammen im Bachelor-Modul unseres Instituts daran gezweifelt haben, ob wir jemals da durchkommen.

Ich möchte mich natürlich auch bei allen anderen Feldi-Angehörigen für die Hilfsbereitschaft, die Unterstützung und die tolle Arbeitsatmosphäre bedanken!

Ein großes Dank gilt auch meinen Freunden außerhalb des Labors. Isi, Jo, Lauri, Caro und Martin, ihr habt mich immer ertragen, mich abgelenkt und mich durch diese Zeit begleitet. Lennart, vielen Dank, dass du das gesamte Studium für mich da warst und mich aus dem einen oder anderen Loch geholt hast!

Ohne meine Familie hätte ich das Ganze hier nicht geschafft. Ihr seid immer für mich da und ertragt all meine Launen, wie schlecht sie auch sein mögen. Mama, Arndt und Omid: Vielen Dank für die Aufmunterungen, wenn mal wieder etwas nicht geklappt hat! Die jährlich wiederkehrenden Auszeiten vom Labor in Griechenland haben sehr gut getan! Mama, ohne dich wäre ich sicher nicht so weit gekommen und ich danke dir von Herzen, dass du immer für mich da bist! Omid, vielen Dank, dass du mich immer erträgst und mich von einem noch so schlechten Tag im Labor abgelenkt hast! Und „hier ne so Dings, L.“.